IRE Transactions on ANTENNAS and PROPAGATION

Volume AP-9 SEPTEMBER, 1961 Number 5

Published Bimonthly

In This Issue

Dipole Antennas Coupled to a Two-Wire Transmission Line

Mutual-Coupling Effects in Scanning Dipole Arrays

Optimum Feeds for All Three Modes of a Monopulse Antenna I: Theory

Optimum Feeds for All Three Modes of a Monopulse Antenna II: Practice

A New Way of Solving Maxwell's Equations

Correlation of Wind Shear with Tropospheric Scatter Signals

Coherent and Incoherent Scattering of Microwaves from the Ocean

Electromagnetic Propagation in an Exponential Ionization Density

Propagation Characteristics of High UHF Signals

Scatter Propagation and Meteorological Conditions in the Caribbean

PUBLISHED BY THE

Professional Group on Antennas and Propagation

IRE TRANSACTIONS® PGAP IS A PUBLICATION DEVOTED TO EXPERIMENTAL AND THEORETICAL PAPERS ON RADIO ANTENNAS, ON GUIDED OR UNGUIDED PROPAGATION OF RADIO WAVES, AND ON ALLIED FIELDS OF RADIO PHYSICS SUCH AS RADIO ASTRONOMY

MANUSCRIPTS should be submitted to Sidney A. Bowhill, *Editor,* 222 Electrical Engineering, Pennsylvania State University, University Park, Pa. Manuscripts should be original typewritten copy, double-spaced, plus one carbon copy and two sets of copies of illustrations. Original illustrations will be called for if the paper is accepted. References should appear as footnotes and include author's name, title, journal, volume, initial and final page numbers, and date.

CONTRIBUTIONS, which should average 15 double-spaced typewritten pages in length, are subjected to review by the *Associate Editors* and their readers. Each paper must have a summary of less than 200 words.

COMMUNICATIONS should not exceed five double-spaced typewritten pages in length, together with not more than three illustrations. Accepted at the Editor's discretion, they appear in the first available issue.

NEWS ITEMS concerning PGAP members and group activities should be sent to the *News Editor,* R. C. Hansen, Aerospace Corp., Box 95085, Los Angeles 45, Calif.

ORIGINAL ILLUSTRATIONS should be submitted as follows: All line drawings (graphs, charts, block diagrams, cutaways, etc.) should be inked uniformly and ready for reproduction. If commercially printed grids are used in graph drawings, author should be sure printer's ink is of a color that will reproduce. Photographs should be glossy prints. Call-outs or labels should be marked on a registered tissue overlay, not on the illustration itself. No illustration should be larger than 8 x 10 inches. Lettering on illustrations must have height at least two per cent of the illustration width.

Copies can be purchased from **the INSTITUTE OF RADIO ENGINEERS, 1 East 79 St., New York 21, N.Y.** Individual copies of this issue, and all available back issues, except Vols. AP-5, No. 1; AP-6, No. 1; AP-7, Special Supplement, may be purchased at the following prices: IRE members (one copy) $2.25, libraries and colleges $3.25, all others $4.50. Yearly subscription rate: non-members $17.00; colleges and public libraries $10.00. IRE TRANSACTIONS ON ANTENNAS AND PROPAGATION. Printed in U.S.A. Printed by George Banta Co., Inc., Curtis Reed Plaza, Menasha, Wisconsin.

Second-class postage paid at MENASHA, WISCONSIN, and additional mailing offices under the act of August 24, 1912. Acceptance for mailing at a special rate of postage is provided for in the act of February 28, 1925, embodied in Paragraph 4, Section 412, P. L. & R., authorized October 26, 1927.

IRE Transactions on Antennas and Propagation

Volume AP-9 SEPTEMBER, 1961 Number 5
Published Bimonthly

TABLE OF CONTENTS

CONTRIBUTIONS

Philip S. Carter 1897–1961 424

Dipole Antennas Coupled Electromagnetically to a Two-Wire Transmission Line ..... *K.-M. Chen and R. W. P. King* 425

Mutual-Coupling Effects in Scanning Dipole Arrays ..... *L. A. Kurtz, R. S. Elliott, S. Wehn, and W. L. Flock* 433

Optimum Feeds for All Three Modes of a Monopulse Antenna I: Theory ..... *Peter W. Hannan* 444

Optimum Feeds for All Three Modes of a Monopulse Antenna II: Practice ..... *Peter W. Hannan* 454

A New Way of Solving Maxwell's Equations ..... *V. H. Rumsey* 461

Correlation of Wind Shear with Tropospheric Scatter Signals ..... *Louis H. Bauer* 466

Coherent and Incoherent Scattering of Microwaves from the Ocean ..... *C. I. Beard* 470

Electromagnetic Propagation in an Exponential Ionization Density ..... *Leonard S. Taylor* 483

Some Propagation Characteristics of High UHF Signals in the Immediate Vicinity of Trees ..... *A. H. LaGrone and C. W. Chapman* 487

Tropospheric Scatter Propagation and Meteorological Conditions in the Caribbean ..... *R. E. Gray* 492

COMMUNICATIONS

Comments on "Scatter Communications with Radar Chaff" ..... *E. S. Cassedy, J. Fainberg, and R. A. Hessemer, Jr.* 497

Calculated Equatorial Plane Radiation Patterns Produced by a Circumferential Slot on a Cylinder ..... *C. M. Knop and A. R. Battista* 498

Dielectric Lens for Second-Mode Spiral ..... *J. H. Craven* 499

Comments on "Diffraction of Scalar Waves by a Circular Aperture" ..... *J. Bazer and A. Brown* 499

On the Determination of the Disk Temperature and the Flux Density of a Radio Source Using High-Gain Antennas ..... *H. C. Ko* 500

Operators for Wave Equations in General Linear Media ..... *I. Sugai* 501

On the Transposed Radiating Systems in an Anisotropic Medium ..... *Chen To Tai* 502

Contributors 503

Papers to be Published in Future Issues ..... *Inside Back Cover*

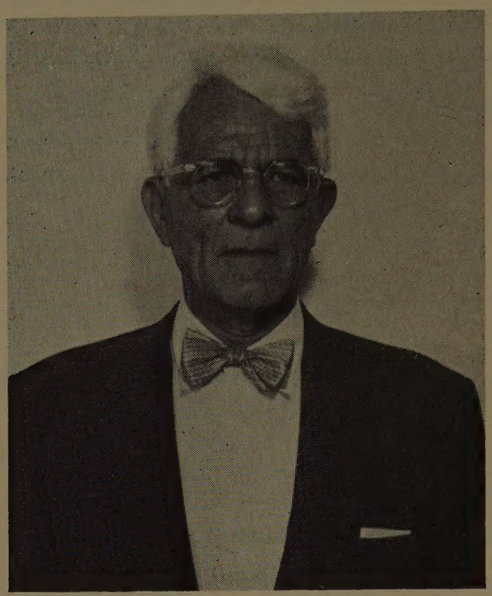

Philip S. Carter
1897–1961

On April 20, 1961, the field of antennas lost one of its senior practitioners, and the Professional Group on Antennas and Propagation one of its elder statesmen. On that day Philip S. Carter died at his home in Port Jefferson, New York, after an extended illness. Phil Carter has been sorely missed at the PGAP meetings, where he long has contributed to the solution of major problems and to the fun.

He was born in Glastonbury, Connecticut, on July 22, 1897, and graduated in Mechanical Engineering from Stanford University, California, in 1918. He served in the Signal Corps in World War I, was employed by the General Electric Company, and in 1920 transferred to RCA, where he remained. He worked during these years with Alexanderson, Beverage and Hansell.

He contributed to the development of the Wave Antenna, participated in the invention of many directive antennas using long wires, and himself invented the very popular folded-dipole antenna. In the course of this work he obtained 100 patents.

In his many published papers in the IRE PROCEEDINGS, he established an international reputation as an antenna expert and a brilliant analyst. He served on many IRE Committees, including the Antenna and Waveguides Technical Committee and the Administrative Committee of PGAP.

Those of us who worked so closely with Phil Carter on PGAP problems share our loss with his many other associates in the IRE and at RCA.

L. C. V. A.

contributions

Dipole Antennas Coupled Electromagnetically to a Two-Wire Transmission Line*

K.-M. CHEN† AND R. W. P. KING‡, FELLOW, IRE

Summary—**The circuit properties of a dipole antenna coupled electromagnetically to a two-wire transmission line are studied theoretically and experimentally. Some arrays constructed of a number of dipole antennas coupled electromagnetically to a two-wire line are considered and the radiation patterns are found.**

INTRODUCTION

An antenna array consisting of dipole antennas coupled electromagnetically to a single two-wire transmission line was first proposed by Sletten [1]. Since then, experimental studies of this array have been made by several authors [2], but their results are neither comprehensive nor entirely consistent. The research reported in this paper is intended to provide a reasonably complete theoretical and experimental picture of the properties of such arrays.

The array consists of several dipole antennas situated in a plane parallel to that of a two-wire transmission line. The centers of these dipole antennas are located opposite positions of voltage maximum along the transmission line. When the axis of a typical dipole antenna is parallel to the direction of the line, no currents are excited, since the antenna is in the neutral plane of the transmission line. However, when the antenna is rotated from that neutral position, the antenna is excited by the charges on and currents in the line. The magnitude of the excitation which induces currents in each antenna varies with 1) the angle of rotation of the antenna from its neutral position, 2) the length of the antenna, 3) the distance between the antenna and the line, and 4) the spacing of the transmission line. It is the dependence of the antenna current on these many parameters that makes the problem both difficult and interesting.

Some features of an antenna system of this type are:

1) In constructing a high-gain antenna array for high-power VHF-UHF communication purposes in a conventional manner, numerous transmission lines must be used to feed the antenna elements with voltages of proper amplitude and phase. In such an arrangement the transmission lines are easily unbalanced owing to interactions between them. This causes difficulty in adjusting the feeding system and makes the realization of a predetermined field pattern difficult. The proposed antenna system sidesteps this difficulty by having only a single two-wire transmission line.

* Received by the PGAP, November 3, 1960; revised manuscript received, February 27, 1961. This research was supported by the U. S. Air Force under Contract No. AF19(604)4118.

† Rad. Lab., University of Michigan, Ann Arbor, Mich. Formerly at Gordon McKay Lab., Harvard University, Cambridge, Mass.

‡ Gordon McKay Lab., Harvard University, Cambridge, Mass.

2) An antenna array of the proposed type can be designed to radiate more power than a slot array fed by a waveguide. The simplicity of the construction is another convenience.

In the analysis the antenna current induced by the near-zone field of the two-wire line is obtained first, and then the equivalent input impedance of the antenna as seen from the line. In the last part of the paper, several antenna arrays with different properties are suggested and the corresponding radiation patterns are obtained. The theoretical results are compared with experiment and found to be in good agreement.

Antenna Current[1]

The first topic to be investigated is the current induced in a dipole antenna when it is coupled to a two-wire line. Before the dipole is coupled to the line, which is short-circuited at one end, the distributions of charge per unit length and current along the line have a standing-wave pattern. After the dipole is coupled to the line, the wave pattern on the line tends to change from a standing wave to a traveling wave since the line transfers power to the antenna.

In general, the distribution of the charge per unit length on the line can be written as

$$q(z) = [q_1 \cos \beta_0 z - jq_2 \sin \beta_0 z]e^{j\omega t}. \tag{1}$$

From the equation of continuity of charge, the corresponding distribution of current in the line is expressed as

$$I(z) = [-jv_0 q_1 \sin \beta_0 z + v_0 q_2 \cos \beta_0 z]e^{j\omega t}. \tag{2}$$

For the TEM mode, these charges and currents maintain a transverse electric field in the transverse plane perpendicular to the axis of the line. If the geometry of the assembly of the dipole antenna and the line is as shown in Fig. 1, the tangential electric field at the surface of the antenna can be found [3] to be

$$E_t(s) = \frac{-d}{\pi\epsilon_0} \frac{[b^2 + d^2 - s^2 \sin^2 \theta]}{[(s \sin \theta + d)^2 + b^2][(s \sin \theta - d)^2 + b^2]} \times [q_1 \cos (\beta_0 s \cos \theta) \sin \theta - jq_2 \sin (\beta_0 s \cos \theta) \sin \theta], \tag{3}$$

where s is the distance measured from the center along the dipole antenna, θ is the angle which the antenna made with the axis of the line, b is the distance between the dipole antenna and the line, and $2d$ is the spacing of the two-wire line. Also shown in Fig. 1 are the charge and the current distributions when $q_2 = 0$ and the configuration of the transverse electric field.

$E_t(s)$ may be resolved into symmetrical and antisymmetrical components with respect to $s = 0$ as follows:

[1] The details of this part are available in a previous work of Chen [3].

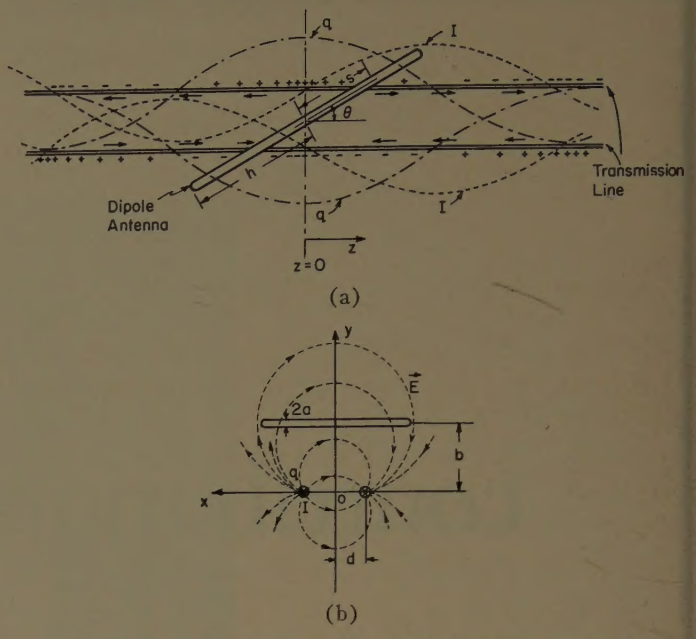

Fig. 1—Geometry of antenna assembly (transmission line has a standing wave pattern).

$$E_t^s(s) = \frac{-dq_1}{\pi\epsilon_0} \frac{[b^2 + d^2 - s^2 \sin^2 \theta]}{[(s \sin \theta + d)^2 + b^2][(s \sin \theta - d)^2 + b^2]} \cdot \cos (\beta_0 s \cos \theta) \sin \theta; \tag{4}$$

$$E_t^a(s) = \frac{jdq_2}{\pi\epsilon_0} \frac{[b^2 + d^2 - s^2 \sin^2 \theta]}{[(s \sin \theta + d)^2 + b^2][(s \sin \theta - d)^2 + b^2]} \cdot \sin (\beta_0 s \cos \theta) \sin \theta. \tag{5}$$

$E_t^s(s)$ induces a symmetrical current, $E_t^a(s)$ an antisymmetrical current in the antenna. In the following analysis, the symmetrical and antisymmetrical parts of the antenna current are found separately.

Since the tangential component of the electric field at the surface of the perfectly-conducting antenna vanishes, a differential equation governing the symmetrical vector potential at the surface and in the direction of the antenna as maintained by the symmetrical current in the antenna [4] is

$$\frac{\partial^2 A_s^s}{\partial s^2} + \beta_0^2 A_s^s = -j \frac{\beta_0^2}{\omega} E_t^s(s). \tag{6}$$

A_s^s is defined as

$$A_s^s(s) = \frac{\mu_0}{4\pi} \int_{-h}^{h} \frac{e^{-j\beta_0 \sqrt{(s-s')^2 + a^2}}}{\sqrt{(s-s') + a^2}} I_s^s(s')ds',$$

where h is the half length and a is the radius of the dipole antenna. The general solution for $A_s^s(s)$ is found with symmetry condition $A_s^s(s) = A_s^s(-s)$. It is

$$A_s^s(s) = \frac{-j}{v_0} [C_s \cos \beta_0 s - \theta_s(s)], \tag{7}$$

where

$$\theta_s(s) = -\int_0^s E_t^s(w)\sin\beta_0(s-w)dw$$

$$= \frac{q_1 d\sin\theta}{\pi\epsilon_0}\int_0^s \frac{[b^2+d^2-w^2\sin^2\theta]}{[(w\sin\theta+d)^2+b^2][(w\sin\theta-d)^2+b^2]} \cdot\cos(\beta_0 w\cos\theta)\sin\beta_0(s-w)dw. \quad (8)$$

The constant C_s is to be determined by the boundary condition $I_s^s(s=\pm h)=0$.

In the antenna of length $2h$, with $\beta_0 h$ near $\pi/2$, it is reasonable to assume the zeroth-order distribution of the symmetrical current to be given by

$$[I_s^s(s)]_0 = \frac{-j4\pi}{\zeta_0\psi_s}C_s(\cos\beta_0 s-\cos\beta_0 h). \quad (9)$$

The substitution of (9) in (7) with $s=h$ leads to

$$A_s^s(h) = \frac{-j}{v_0}[C_s\cos\beta_0 h-\theta_s(h)]$$

$$= \frac{-j}{v_0\psi_s}\int_{-h}^{h} C_s(\cos\beta_0 s-\cos\beta_0 h)\frac{e^{-j\beta_0\sqrt{(h-s)^2+a^2}}}{\sqrt{(h-s)^2+a^2}}ds.$$

After rearrangement, C_s is found to be

$$C_s = \frac{\psi_s\theta_s(h)}{\cos\beta_0 h\psi_s - C_a(h,h)+\cos\beta_0 hE_a(h,h)}. \quad (10)$$

The expansion parameter ψ_s is taken as the ratio of the maximum vector potential to the maximum current at $s=0$ on the surface of the antenna. It is found to be

$$\psi_s = \frac{C_a(h,0)-\cos\beta_0 hE_a(h,0)}{1-\cos\beta_0 h}. \quad (11)$$

The constants which appear above are defined as

$$C_a(h,w) = \int_{-h}^{h}\frac{e^{-j\beta_0\sqrt{(s-w)^2+a^2}}}{\sqrt{(s-w)^2+a^2}}\cdot\cos\beta_0 s\,ds,$$

$$E_a(h,w) = \int_{-h}^{h}\frac{e^{-j\beta_0\sqrt{(s-w)^2+a^2}}}{\sqrt{(s-w)^2+a^2}}ds,$$

with $\zeta_0\doteq 120\pi$ ohms.

In the case $\beta_0 h=\pi/2$, which is of particular interest, the symmetrical antenna current is

$$[I_s^s(s)]_0 = \frac{j4\pi}{\zeta_0 C_a(h,h)}\theta_s(h)\cos\beta_0 s. \quad (12)$$

Note that the first-order current is available in a previous work of Chen [3].

Following the method used in the analysis of the symmetrical current, the antisymmetrical current is found as follows:

The antisymmetrical vector potential at the surface and in the direction of the antenna as maintained by the antisymmetrical current in one antenna is

$$\frac{\partial^2 A_s^a}{\partial s^2}+\beta_0^2 A_s^a = -j\frac{\beta_0^2}{\omega}E_t^a(s). \quad (13)$$

With the symmetry condition $A_s^a(s)=-A_s^a(-s)$, the general solution of $A_s^a(s)$ is found to be

$$A_s^a(s) = \frac{-j}{v_0}[C_a\sin\beta_0 s-\theta_a(s)], \quad (14)$$

where

$$\theta_a(s) = -\int_0^s E_t^a(w)\sin\beta_0(s-w)dw$$

$$= \frac{-jq_2 d\sin\theta}{\pi\epsilon_0}\int_0^s \frac{[b^2+d^2-w^2\sin^2\theta]}{[(w\sin\theta+d)^2+b^2][(w\sin\theta-d)^2+b^2]} \cdot\sin(\beta_0 w\cos\theta)\sin\beta_0(s-w)dw. \quad (15)$$

From the boundary condition $I_s^a(s=\pm h)=0$, the antisymmetrical current in an antenna with $\beta_0 h=\pi/2$ can be found to be

$$[I_s^a(s)]_0 = \frac{-j4\pi}{\zeta_0\psi_a}[\theta_a(h)\sin\beta_0 s-\theta_a(s)], \quad (16)$$

where

$$\psi_a \doteq \frac{1}{0.707\theta_a(h)-\theta_a\left(\frac{h}{2}\right)}\int_{-h}^{h}[\theta_a(h)\sin\beta_0 s - \theta_a(s)]K\left(\frac{h}{2},s\right)ds$$

$$K\left(\frac{h}{2},s\right) = \frac{e^{-j\beta_0\sqrt{\left(\frac{h}{2}-s\right)^2+a^2}}}{\sqrt{\left(\frac{h}{2}-s\right)^2+a^2}}.$$

The resultant current in the dipole antenna with $\beta_0 h=\pi/2$ is obtained by adding up the symmetrical and the antisymmetrical currents as follows:

$$[I_s(s)]_0 = [I_s^s(s)]_0+[I_s^a(s)]_0$$

$$= \frac{j4\pi}{\zeta_0}\left[\frac{\theta_s(h)}{C_a(h,h)}\cos\beta_0 s - \frac{1}{\psi_a}(\theta_a(h)\sin\beta_0 s-\theta_a(s))\right]. \quad (17)$$

The ratio of the amplitudes of $[I_s^s(s)]_0$ and $[I_s^a(s)]_0$ is

$$\frac{[I_s^s(s)]_{0\max}}{[I_s^a(s)]_{0\max}} \doteq \frac{\frac{\theta_s(h)}{C_a(h,h)}}{\frac{0.707\theta_a(h)}{\psi_a}} > 5 \qquad \text{for } \beta_0 h=\frac{\pi}{2}.$$

It can be shown that $[I_s^s(s)]_0$ and $[I_s^a(s)]_0$ are approximately 90° out of phase. The magnitude is

$$|I_s(s)| = \sqrt{|I_s^s(s)|^2+|I_s^a(s)|^2}.$$

A dipole antenna with $\beta_0 h = \pi/2$ carries both symmetrical and antisymmetrical currents, but the latter is usually much smaller than the former. Therefore, in practice, only the symmetrical current needs to be considered.

Fig. 2 shows the theoretical and the experimental distributions of current along the antenna. The latter were measured with a small loop protruding from a slot in the antenna. The distribution is very close to a cosine curve. Figs. 3 and 4 show the theoretical and the experimental variations of the antenna current at the center of the antenna with the rotation of the antenna. In Fig. 3, the distance between the antenna and the line is 6.5 cm and the distribution pattern on the line is essentially a standing wave. In Fig. 4, the distance from the antenna to the line is 0.75 cm and the distribution of current along the line is maintained as a traveling wave in the course of the antenna rotation by loading the line with another antenna coupled to the line a wavelength away. The optimum orientation of the antenna at which the maximum antenna current is obtained depends greatly on the distance between the antenna and the line. Figs. 5 and 6 show the theoretical and the experimental variations of the antenna current with the length of the antenna. The resonant length at which the antenna current reaches its maximum is found to be slightly shorter than a half wavelength [5]. Figs. 7 and 8 show the theoretical and experimental variations of the antenna current with the distance between the antenna and the line. It is interesting to observe that when the orientation of the antenna is great, the antenna current decreases quite slowly when the separation is increased. Fig. 9 shows the theoretical and the experimental variations of the antenna current with the spacing of the line. The antenna current is increased as the spacing of the line is increased. It is to be noted that the power loss due to radiation from the line is also increased by an increase in the line spacing.

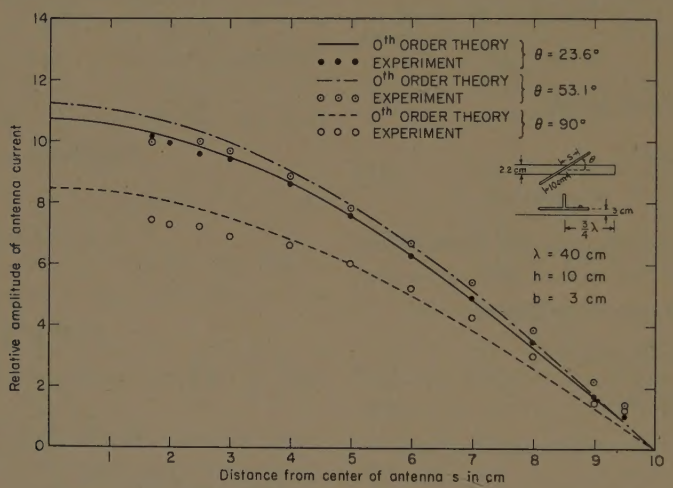

Fig. 2—Current distribution along the dipole antenna.

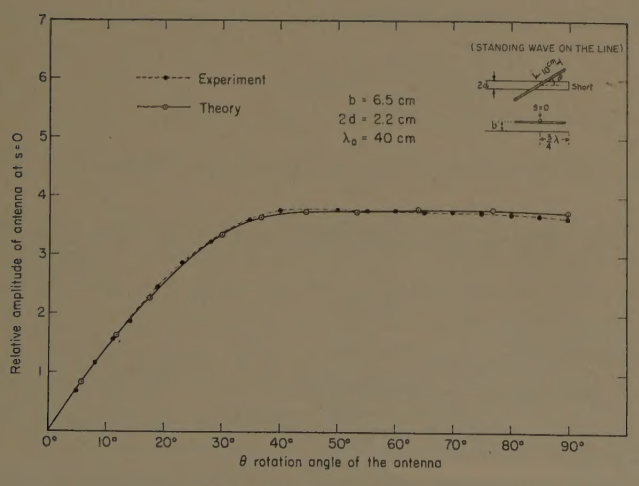

Fig. 3—Variation of antenna current $I(s=0)$ with the rotation of the antenna.

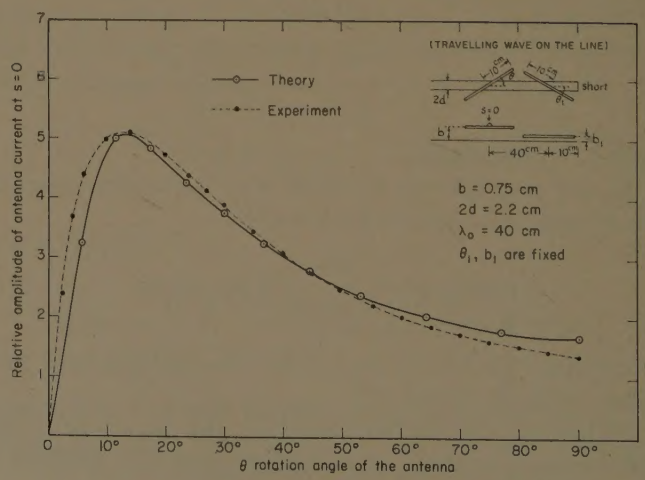

Fig. 4—Variation of antenna current $I(s=0)$ with the rotation of the antenna.

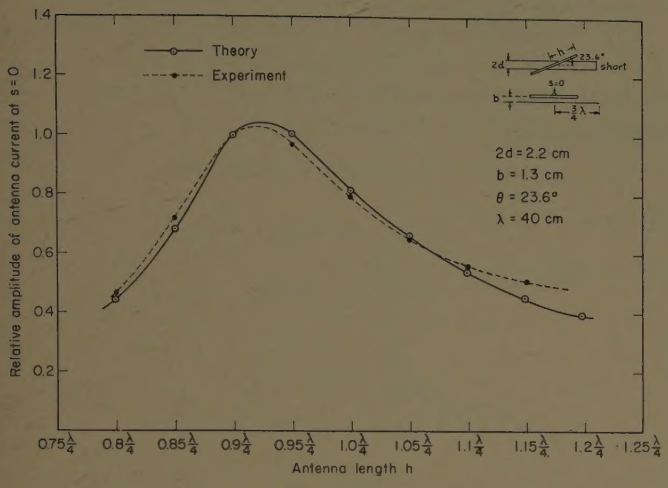

Fig. 5—Variation of antenna current $I(s=0)$ with the length of the antenna.

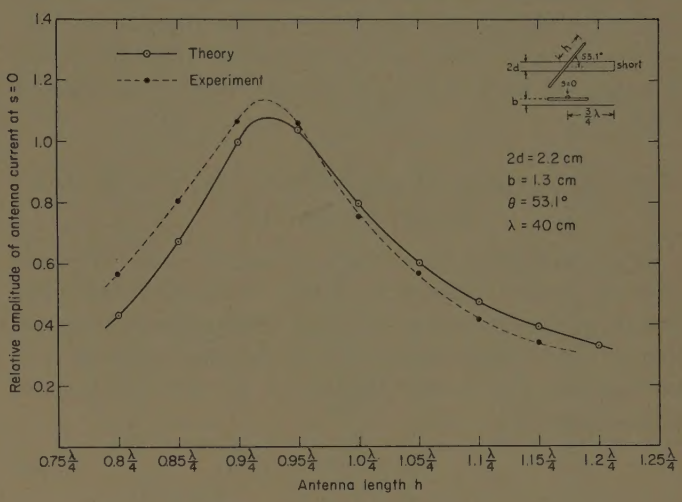

Fig. 6—Variation of antenna current $I(s=0)$ with the length of the antenna.

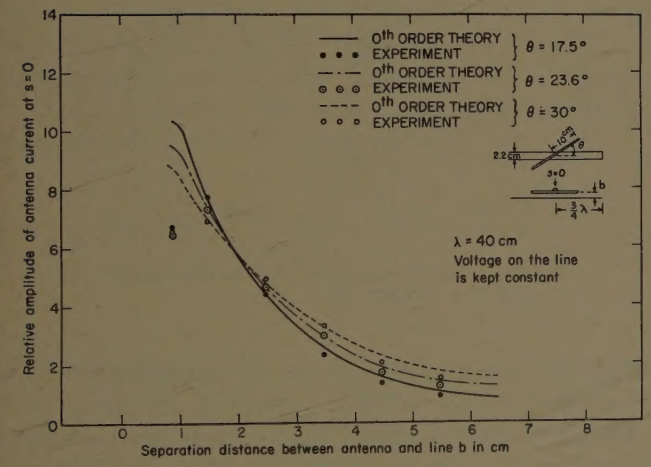

Fig. 7—Variation of antenna current with the separation distance when the voltage on the line is kept constant.

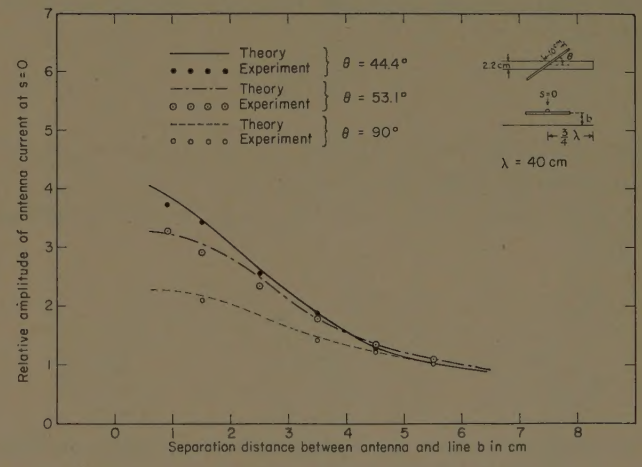

Fig. 8—Variation of antenna current with the separation distance when the voltage on the line is kept constant.

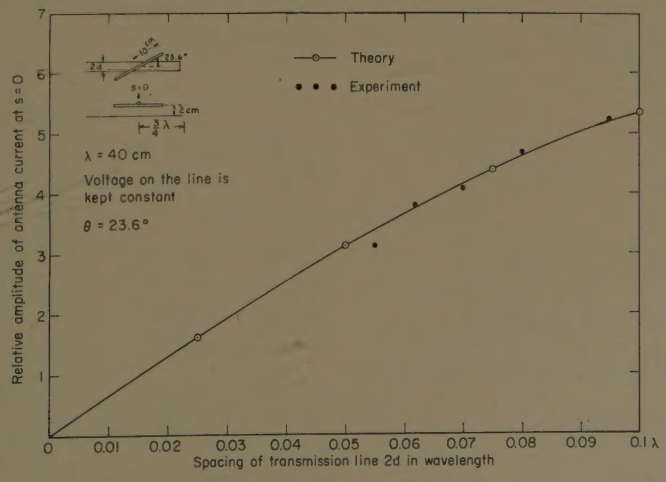

Fig. 9—Variation of antenna current with the spacing of the transmission line.

An important problem relating to the antenna current is the significance and effect of the unbalanced current in the line. Since the discussion is rather involved, it is omitted here. It may be found in a previous work of Chen [3].

Equivalent Input Conductance of a Dipole as a Load for the Line

When a dipole antenna is coupled to a two-wire line with its center opposite a voltage maximum along the line, it is equivalent to a shunt admittance across the line at that voltage maximum. If the line is assumed to be lossless, the power dissipated in that equivalent admittance is

$$P = \text{Re}\,(\tfrac{1}{2}VI^*) = \tfrac{1}{2}V^2G, \tag{18}$$

where V is the line voltage across the equivalent admittance and G is the equivalent conductance. This power dissipated in the equivalent admittance must be equal to the power radiated from the dipole antenna. That is,

$$P = \tfrac{1}{2}I_0^2R_0, \tag{19}$$

where I_0 is the input current and R_0 is the input resistance [6] of a dipole antenna.

I_0 is found in (9) as a function of q_1. V can be related to q_1 as

$$V = \frac{q_1}{C} = q_1\frac{\ln\dfrac{2d}{R}}{\pi\epsilon_0}.$$

C is the capacitance per unit length of a two-wire line and R is the radius of the line wire.

When (18) and (19) are set equal to each other, an expression for G is obtained as follows:

$$G = \frac{K^2}{\left(\ln\dfrac{2d}{R}\right)^2}\left(\frac{\pi}{\zeta_0}\right)^2R_0, \tag{20}$$

where

$$K = \frac{4(1-\cos\beta_0h)}{[\psi_s\cos\beta_0h - C_a(h,h) + \cos\beta_0hE_a(h,h)]} \times d\sin\theta\int_0^h \frac{[b^2+d^2-w^2\sin^2\theta]}{[(w\sin\theta+d)^2+b^2][(w\sin\theta-d)^2+b^2]} \cdot\cos(\beta_0w\cos\theta)\sin\beta_0(h-w)dw.$$

The theoretical results are compared to the experimental results in [1]. The agreement is quite satisfactory.

Radiation Pattern[2]

The fundamental unit of the antenna array described in this paper is a pair of tilted dipoles as shown in Fig. 10. In a dipole antenna with $\beta_0h=\pi/2$, the current can be assumed to be given approximately by

$$I(s) = I_0\cos\beta_0s + jI_a\sin 2\beta_0s, \tag{21}$$

where

$$I_0 = \frac{j4\pi}{\zeta_0C_a(h,h)}\theta_s(h),$$

$$I_a = \frac{-2\pi}{\zeta_0\psi_a}\theta_a(h) < \frac{1}{5}I_0.$$

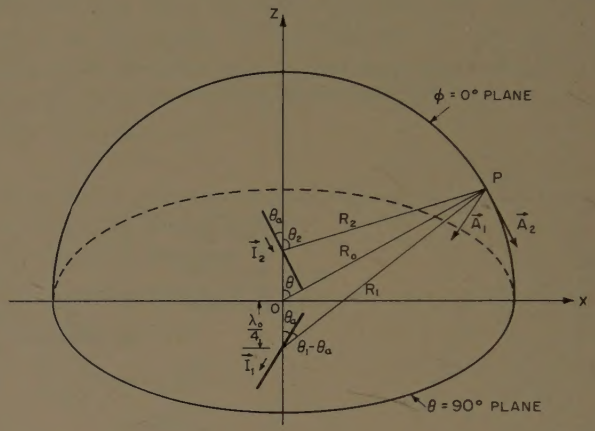

Fig. 10—Coordinate system for determination of radiation pattern.

With this antenna current the radiation pattern of a pair of tilted dipoles may be evaluated. In the interest of simplicity and practical design, only the radiation patterns in the E plane (or $\phi=0°$ plane) and in the H plane (or $\theta=90°$ plane) are presented here.

Let the pair of dipoles be located in the plane $\phi=0°$ with the tilt angle θ_a. The radiation function in the E plane maintained by the symmetrical antenna current is found to be

$$F_s(\theta,\theta_a) = \frac{\cos\left[\dfrac{\pi}{2}\cos(\theta-\theta_a)\right]}{\sin(\theta-\theta_a)}e^{-j(\pi/2)\cos\theta} + \frac{\cos\left[\dfrac{\pi}{2}\cos(\theta+\theta_a)\right]}{\sin(\theta+\theta_a)}e^{j(\pi/2)\cos\theta}, \tag{22}$$

and

$$E_\theta^r(\theta,\theta_a) = \frac{-j\zeta_0I_0}{2\pi}\frac{e^{-j\beta_0R_0}}{R_0}F_s(\theta,\theta_a). \tag{23}$$

[2] The details of this part are available in a previous work of Chen [7].

The antisymmetrical antenna current maintains a radiation field as follows:

$$F_a(\theta, \theta_a) = \frac{\cos\left[\frac{\pi}{2}\cos(\theta - \theta_a)\right]}{[4 - \cos^2(\theta - \theta_a)]} \sin(\theta - \theta_a) e^{-j(\pi/2)\cos\theta} + \frac{\cos\left[\frac{\pi}{2}\cos(\theta + \theta_a)\right]}{[4 - \cos^2(\theta + \theta_a)]} \sin(\theta + \theta_a) e^{j(\pi/2)\cos\theta},$$

and

$$E_{\theta_a}{}^r(\theta, \theta_a) = \frac{\zeta_0 I_a}{\pi} \frac{e^{-j\beta_0 R_0}}{R_0} F_a(\theta, \theta_a).$$

However, since $I_a \ll I_0$, $E_{\theta_a}(\theta, \theta_a)$ may be ignored so that $E_\theta{}^r(\theta, \theta_a)$ alone, as given in (23), is adequate in practice.

From (22), it is observed that the E plane radiation pattern has four major lobes; two along the line $\theta = 90°$ (the broadside effect), the other two along the line $\theta = 0°$ (the end-fire effect). Therefore, it is clear that this arrangement of antennas functions as a combined broadside and end-fire array. The following formula expresses the ratio of these two effects:

$$\frac{F_s(90°, \theta_a)}{F_s(0°, \theta_a)} = \tan\theta_a \left[\frac{\cos\left(\frac{\pi}{2}\sin\theta_a\right)}{\cos\left(\frac{\pi}{2}\cos\theta_a\right)}\right]. \quad (24)$$

It is seen from (24) that when θ_a is small, this ratio is large and the broadside effect is predominant; while when θ_a is large, the ratio becomes small and the end-fire effect becomes significant. When $\theta_a = 45°$, the ratio is unity and the two effects are equal.

The H plane radiation pattern is found to be:

$$G(\phi, \theta_a) = \left[\frac{\cos\left[\frac{\pi}{2}\sin\theta_a\cos\phi\right]}{1 - \sin^2\theta_a\cos^2\phi}\right]\cos\theta_a, \quad (25)$$

and the corresponding electric field is

$$E_\theta{}^r(\phi, \theta_a) = \frac{-j\zeta_0 I_0}{\pi} \frac{e^{-j\beta_0 R_0}}{R_0} G(\phi, \theta_a). \quad (26)$$

From (25), it is found that the pattern is nearly independent of ϕ when the tilt angle θ_a of the antenna is small. In practical application, θ_a is usually set to be small (say 20°) so that the radiation pattern in the H plane is nearly omnidirectional.

Radiation Patterns of Arrays

Certain antenna arrays which are composed of a number of dipole antennas coupled electromagnetically to a two-wire line are shown in Figs. 11 and 12. By an

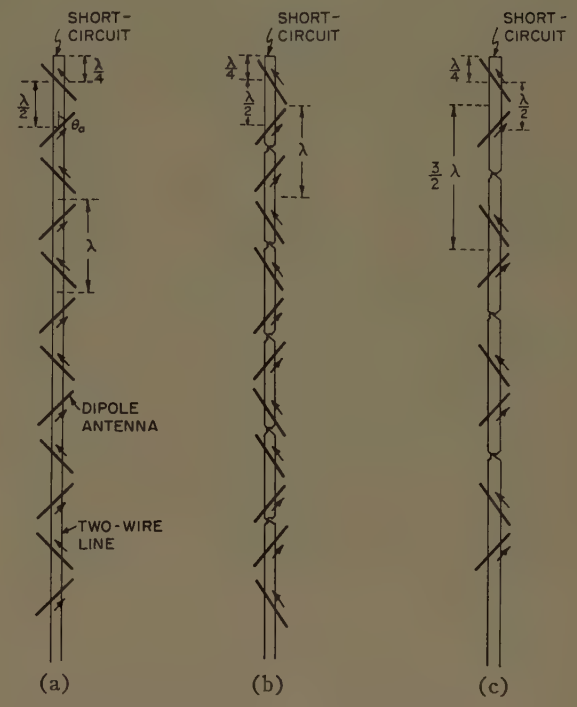

Fig. 11—Broadside arrays. (a) Broadside and end-fire array.

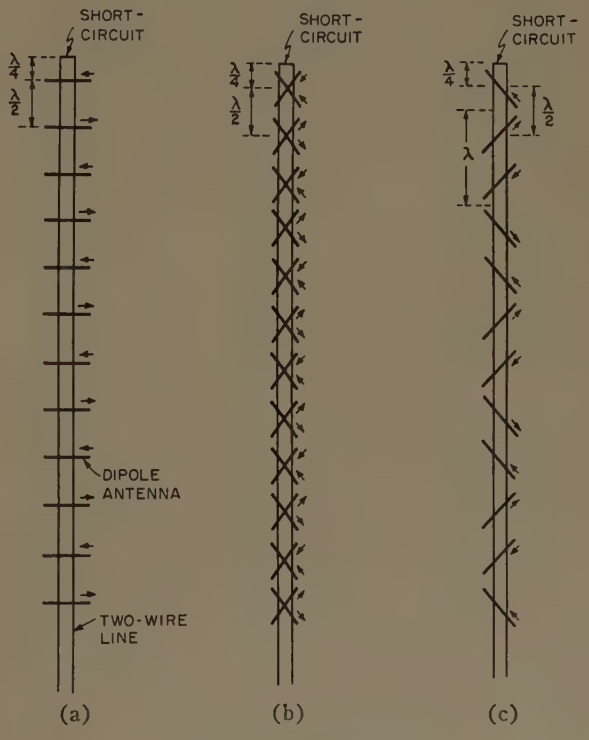

Fig. 12—End-fire arrays.

appropriate arrangement of the dipole antennas coupled to the line, an antenna array can be made to function as 1) a combined broadside and end-fire array, 2) a broadside array, or 3) an end-fire array. The radiation pattern for each array is found as follows:

1) An array with broadside and end-fire properties as shown in Fig. 11(a). The radiation pattern in the E plane is

$$F(\theta, \theta_a) = F_s(\theta, \theta_a)\left[\frac{\sin\left(\frac{N}{2}\pi\cos\theta\right)}{\sin(\pi\cos\theta)}\right], \tag{27}$$

where $F_s(\theta, \theta_a)$ is expressed in (22), and N is the total number of the dipole antennas.

2) A broadside array as shown in Fig. 11(b). The radiation pattern in the E plane is

$$F(\theta, \theta_a) = f_x(\theta, \theta_a)\left[\frac{\sin\left(N\frac{\pi}{2}\cos\theta\right)}{\sin\left(\frac{\pi}{2}\cos\theta\right)}\right] + f_x(\theta, \theta_a)2\sin\left(\frac{\pi}{2}\cos\theta\right)\cdot\left[\frac{\sin\left[\frac{N\pi}{2}\left(\frac{1}{2}-\cos\theta\right)\right]}{\cos(\pi\cos\theta)}\right], \tag{28}$$

where

$$f_x(\theta, \theta_a) = \left[\frac{\cos\left(\frac{\pi}{2}\cos\theta_a\cos\theta\right)}{1-\cos^2\theta_a\cos^2\theta}\right]\cos\theta_a\sin\theta \tag{29}$$

$$f_x(\theta, \theta_a) = \left[\frac{\cos\left(\frac{\pi}{2}\sin\theta_a\sin\theta\right)}{1-\sin^2\theta_a\sin^2\theta}\right]\sin\theta_a\cos\theta. \tag{30}$$

3) A broadside array as shown in Fig. 11(c). The E plane radiation pattern is

$$F(\theta, \theta_a) = F_s(\theta, \theta_a)\left[\frac{\sin\left(N\frac{3\pi}{4}\cos\theta\right)}{\sin\left(\frac{3\pi}{2}\cos\theta\right)}\right]. \tag{31}$$

4) An end-fire array as shown in Fig. 12(a). The E plane radiation pattern is

$$F(\theta, \theta_a) = \left[\frac{\cos\left(\frac{\pi}{2}\sin\theta\right)}{\cos\theta}\right]\cdot\left[\frac{\sin\left(N\frac{\pi}{2}(1-\cos\theta)\right)}{\cos\left(\frac{\pi}{2}\cos\theta\right)}\right]. \tag{32}$$

5) An end-fire array as shown in Fig. 12(b). The E plane radiation pattern is

$$F(\theta, \theta_a) = 2f_x(\theta, \theta_a)\left[\frac{\sin\left(N\frac{\pi}{4}(1-\cos\theta)\right)}{\cos\left(\frac{\pi}{2}\cos\theta\right)}\right]. \tag{33}$$

6) An end-fire array as shown in Fig. 12(c). The E plane radiation pattern is

$$F(\theta, \theta_a) = -2\cos\left(\frac{\pi}{2}\cos\theta\right) = f_x(\theta, \theta_a)\left[\frac{\sin\left[N\frac{\pi}{4}(1-2\cos\theta)\right]}{\cos(\pi\cos\theta)}\right] + f_x(\theta, \theta_a)\left[\frac{\sin\left[N\frac{\pi}{2}(1-\cos\theta)\right]}{\cos\left(\frac{\pi}{2}\cos\theta\right)}\right]. \tag{34}$$

The H plane radiation patterns for these arrays are assumed to be nearly omnidirectional.

References

[1] C. J. Sletten, "A New Antenna Radiator for VHF-UHF Communications," AFCRC, Cambridge, Mass., Tech. Rept. No. 57-114; 1957.

[2] S. R. Seshadri and K. Iizuka, "A Dipole Antenna Coupled Electromagnetically to a Two-Wire Line," Cruft Lab., Harvard University, Cambridge, Mass., SR No. 21; 1958.

[3] K.-M. Chen, "A Dipole Antenna Coupled Electromagnetically to a Two-Wire Transmission Line," Cruft Lab., Harvard University, Cambridge, Mass., SR No. 6, Ser. 2; 1960.

[4] R. W. P. King, "Theory of Linear Antennas," Harvard University Press, Cambridge, Mass., p. 72; 1956.

[5] *Ibid.*, p. 168.

[6] *Ibid.*, pp. 168–179 or pp. 232–238.

[7] K.-M. Chen, "Radiation patterns of antenna arrays consisting of dipoles coupled to a two-wire line," Cruft Lab., Harvard University, Cambridge, Mass., SR No. 8, Ser. 2; 1960.

Mutual-Coupling Effects in Scanning Dipole Arrays*

L. A. KURTZ†, MEMBER, IRE, R. S. ELLIOTT‡, FELLOW, IRE, S. WEHN†, STUDENT MEMBER, IRE, AND W. L. FLOCK||, MEMBER, IRE

Summary—**The perturbations in mutual coupling due to finiteness of a dipole array and its ground plane have been studied. Experimental procedures were evolved to measure these perturbations and their influence on antenna performance as a function of beam position. Data for one- and two-dimensional dipole arrays are presented and interpreted, particularly with reference to edge effects.**

Introduction

ELECTRONICALLY scanned antenna arrays have been receiving increasingly favorable attention in recent years because of several claimed advantages. These include capabilities to achieve rapid scanning and to create a pattern with a very low side-lobe level. Some workers have questioned the validity of this latter claim, pointing to the feeding difficulties caused by the changing influence of mutual coupling on aperture distribution as the beam is scanned. This paper reports the results of an investigation of the effect of mutual coupling in various scanning dipole arrays. This investigation was conducted in conjunction with a theoretical study on the same topic carried out at the Massachusetts Institute of Technology Lincoln Laboratories.[1,2] Another theoretical study on mutual coupling effects was undertaken at about the same time at the Stanford Research Institute.[3]

The term mutual coupling as used in the present context needs some elaboration. Imagine a uniformly-spaced array of identical radiators, each fitted with a pair of terminals. Let the impedance as seen at one pair of terminals be measured with all other terminals open-circuited. We shall call this impedance the self-impedance of the element. Next, let the impedance be remeasured with currents flowing at all other terminals. The result, called the active impedance, will differ from the self-impedance because the currents flowing in the other radiators create electromagnetic fields which induce voltages in the radiator being measured. It is obvious that the phases and amplitudes of these induced voltages will depend on the phases and amplitudes of the currents flowing in the other radiators. Thus, the active impedance is a function of the aperture distribution and will vary with scan. Since all spacings in the array, considered as fractions of a wavelength, are frequency-sensitive, it follows that the active impedance also varies with frequency.

If the array and its ground plane were *infinite* in extent and if the elements were excited with a common amplitude and a uniform progressive phase, symmetry conditions would require that the active impedance of all elements be the same. These active impedances would vary with scan angle and frequency, but always in synchronism.

Because the array and its ground plane are *finite*, conditions are somewhat different. The finiteness of the ground plane alters the image of each element, the alteration being greatest for elements near the edge. The finiteness of the array alters the total mutual coupling to an element, this effect being greatest for elements near the periphery of the array, since they are closest to the elements missing from the infinite array. Further, the finiteness of the array and its ground plane influence the coupling between an element and a distant antenna used to measure the array pattern. Here again, the edge elements are most affected.

These edge effects combine to cause the active impedances of the array elements to differ from each other and to vary unequally with frequency and scan angle. If the edge effects are ignored and the harness which feeds the array is provided with network compensation based on the assumed behavior of an *infinite* array, perturbations in the aperture distribution will result, and pattern performance will be affected. Admittedly, the larger the array, the smaller the perturbations, because the edge elements then comprise a smaller fraction of the total elements. But the larger the array, the greater the potential for extremely low side-lobe levels. A small perturbation has more effect on a 60-db side-lobe level design than it does on a 40-db design. Thus, the need arises to assess the seriousness of the edge effects and the limitations they put on pattern design. It is to the attention of this problem that the present study has been directed.

* Received by the PGAP, November 8, 1960; revised manuscript received, May 3, 1961. The work reported in this paper was performed by Rantec Corp. under subcontract to Lincoln Laboratories, Mass. Inst. Tech., Lexington, Mass., with the support of the U. S. Air Force.

† Rantec Corp., Calabasas, Calif.

‡ University of California at Los Angeles. Consultant to Rantec Corp., Calabasas, Calif.

|| University of Alaska, College, Alaska. Formerly consultant to Rantec Corp., Calabasas, Calif.

[1] S. Edelberg and A. A. Oliner, "Mutual coupling effects in large antenna arrays: Part I—Slot arrays," IRE TRANS. ON ANTENNAS AND PROPAGATION, vol. AP-8, pp. 286–297; May, 1960.

[2] S. Edelberg and A. A. Oliner, "Mutual coupling effects in large antenna arrays: Part II—compensation effects," IRE TRANS. ON ANTENNAS AND PROPAGATION, vol. AP-8, pp. 360–367; July, 1960.

[3] P. S. Carter, Jr., "Mutual impedance effects in large beam scanning arrays," IRE TRANS. ON ANTENNAS AND PROPAGATION, vol. AP-8, pp. 276–285; May, 1960.

Analysis

Assume an array of N radiating elements, not necessarily identical, arbitrarily spaced. Let N cross sections be taken in the transmission lines which connect to the elements, far enough back from each radiating element to assure that, at each cross section, a pure, single transmission-line mode exists. In addition to the array, assume a distant antenna, also fed by a transmission line, at some cross section of which a single transmission-line mode can be identified. Then a simple extension of a proof given by Silver[4,5] shows that an equivalent multi-mesh circuit is a valid representation for the array plus distant antenna. The terminals of the circuit correspond to the cross sections in the transmission lines, and the voltages and currents active in the circuit correspond to the voltages and currents of the transmission-line modes as they exist at the cross sections.[6] Such a formulation avoids the gap problem,[7] and since a knowledge of conditions in the gap is not needed for network compensation, this is a desirable simplification.

The mesh equations for the equivalent circuit can be written

$$\begin{aligned} V_0 &= I_0Z_{00} + I_1Z_{01} + \cdots + I_NZ_{0N} \\ V_1 &= I_0Z_{10} + I_1Z_{11} + \cdots + I_NZ_{1N} \\ &\vdots \\ V_N &= I_0Z_{N0} + I_1Z_{N1} + \cdots + I_NZ_{NN}. \end{aligned} \tag{1}$$

where V_0 and I_0 are the voltage and current at the terminals of the distant antenna; V_n and I_n ($n=1, 2, \cdots, N$) are the voltage and current at the terminals of the nth element of the array; Z_{nn} is the self-impedance of the nth element, and Z_{nm} is the mutual impedance between the nth and mth elements. By reciprocity, $Z_{nm}=Z_{mn}$.

For a *transmitting* array, $V_0=-I_0Z_{0L}$, in which Z_{0L} is the load placed across the terminals of the distant antenna. Then, from (1),

$$I_0 \sim \sum_{n=1}^{N} I_nZ_{0n}. \tag{2}$$

As the distant antenna is moved over the surface of a sphere whose center lies at the array, the current I_0 traces out the transmitting pattern of the array through the dependence of the impedances Z_{0n} on angular position of the distant antenna relative to the array. The currents I_n which appear in (2) can be found by solving (1). In any practical case, the terms I_0Z_{n0} which appear in this solution can be neglected, giving

$$I_n = \frac{\begin{vmatrix} Z_{11} & \cdots & Z_{1,n-1} & V_1 & \cdots & Z_{1N} \\ \vdots & & & \vdots & & \\ Z_{N1} & \cdots & Z_{N,n-1} & V_n & \cdots & Z_{NN} \end{vmatrix}}{\begin{vmatrix} Z_{11} & \cdots & Z_{1,n-1} & Z_{1n} & \cdots & Z_{1n} \\ \vdots & & & \vdots & & \\ Z_{N1} & \cdots & Z_{N,n-1} & Z_{Nn} & \cdots & Z_{NN} \end{vmatrix}}. \tag{3}$$

By appropriately varying the voltages V_k, the currents I_n in (3) can be made to vary in such a way as to make the pattern (2) scan. Eqs. (2) and (3) point up the fact that the transformations which connect the pattern current I_0 to the array currents I_n, and these currents in turn to the driving voltages V_k, depend upon the mutual impedances between each array element and the distant antenna, upon the self-impedances of the array elements, and upon their mutual impedances with each other.

As an illustration of what this implies, consider the case of a linear array of identical elements, uniformly spaced and backed by a ground plane. If the array were *infinite* in extent, then by symmetry,

$$Z_{0n} = \zeta(\theta)e^{in\psi(\theta)}, \tag{4}$$

in which ζ and ψ would be factors dependent on scan angle θ, but independent of n. Further by symmetry,

$$Z_{mn} = Z_{m+p,n+p}, \tag{5}$$

in which m, n, and p would be any integers. Thus, the manner in which the currents I_n differed from each other would be totally dependent on the voltages V_k. So, too, would the pattern be controlled entirely by the voltages V_k.[8] Indeed, this is the assumption which is normally made in designing the aperture distribution of a uniform linear array. The *finiteness* of the array invalidates (4) and (5) in three distinct ways:

1) $Z_{0n} \neq \zeta e^{in\psi}$ for ζ and ψ independent of n. The departure is most pronounced for elements near the edge. It is due to the finiteness of the ground plane which provides only partial images and to the fact that an element is no longer immersed in a sequence of similar elements extending infinitely in both directions.

2) $Z_{mn} \neq Z_{m+p,n+p}$ $\quad m = 1, \cdots, N \quad n = 1, \cdots, N$ $\quad 1 \leq m+p \leq n \quad 1 \leq n+p \leq N.$

This departure is also most pronounced for elements near the edge, and for the same reasons.

3) $Z_{m+p,n+p}$ does not exist for

$$\begin{aligned} m &= 1, \cdots, N \quad n = 1, \cdots, N \\ m+p &< 1 \quad \text{or} \quad m+p > N \\ \text{and/or } n+p &< 1 \quad \text{or} \quad n+p > N. \end{aligned}$$

[4] S. Silver, "Microwave Antenna Theory and Design," Mass. Inst. Tech. Radiation Lab. Ser., vol. 12, pp. 53–60; McGraw-Hill Book Co., Inc., New York, N. Y.; 1949.

[5] R. S. Elliott, "A Critical Review of the Reciprocity Theorem," Rantec Tech. Memo. No. P183-1; September, 1957.

[6] P. S. Carter, Sr., "Circuit relations in radiating systems and applications to antenna problems," Proc. IRE, vol. 20, pp. 1004–1041; June, 1932.

[7] R. W. P. King, "Theory of Linear Antennas," Harvard University Press, Cambridge, Mass., pp. 844–848; 1956.

[8] For example, if $V_k=e^{ik\Omega}$ (uniform amplitude, uniform progressive phase), then solving (3) would yield $I_n \cong e^{in\Omega}$, and solving (2) would yield a conical pattern of zero beamwidth at the scan angle θ for which $\psi(\theta)+\Omega=0$.

These three types of deviation will be called jointly the edge effects. Referring to (2), we see that the first edge effect imposes a need to compensate the array curents I_n in order to achieve the desired pattern. Total compensation may not be possible, since ζ and ψ may depend on scan angle and the index n in a manner which prevents it.

Turning to (3), we see that all three edge effects impose a need to compensate the driving voltages V_k via the array impedances Z_{mn} (through their appearance or nonappearance in the determinants), and via the impedances Z_{0n} (through their implicit effect on the currents I_n). These conclusions are obviously equally valid for two-dimensional transmitting arrays.

If the array and its harness are reciprocal, everything which has been said is equally applicable to a receiving array. If the harness is nonreciprocal, one can still draw these same conclusions about the array and sub-harness consisting of that part of the harness extending back from the array elements to the positions of the nonreciprocal elements. Thus, the need for compensation of the edge effects appears to be a real one which cannot be avoided. What remains to be determined is its importance.

Antenna Range

The problem of providing a suitable antenna range for the experimental determination of the importance of the edge effects was a perplexing one. The measurements were to be made at UHF on arrays of dipoles with the practical restriction that the array dimensions were never larger than 10 λ by 10 λ. A conventional approach for taking patterns would be to mount the array vertically and rotate it. To remove the effects of the earth and the mounting structure, a high tower of awkward shape would be required. The resulting inaccessibility of the array elements seemed too great a disadvantage. Thus it was decided to mount the arrays horizontally and use a "sky hook" antenna as the other end of the range.

An 18-foot square ground plane, elevated six feet off the ground and rotatable about a vertical axis, was therefore constructed to accommodate a variety of arrays. Forty feet to the west of the ground plane, a tower 120 feet tall was erected, and 125 feet to the east of the ground plane, a pulley was attached to an imbedded concrete stanchion. A traveling rope was installed over this pulley and two others were located at the base and top of the tower. Thus, the rope formed a triangle with a sagging hypotenuse and vertices defined by the three pulleys. The plane of the rope bisected the ground plane. The shortest distance from the center of the ground plane to the sagging hypotenuse was 60 feet.

A battery-operated transmitter could be secured to the traveling rope and equipped with either a dipole or loop. This assured a uniform pattern in the plane of the rope for either polarization. A motor drive attached to the pulley at the tower base, with a synchro takeoff to a pattern recorder, completed the range.

The rotating feature of the ground plane permitted patterns to be taken through any principal plane of the array and also permitted conical cuts. Placing the ground plane six feet off the ground allowed the impedance-measuring bridge and operating personnel to be under the ground plane, which proved to be essential.

Mutual Coupling in One-Dimensional Dipole Arrays

A variety of dipole arrays, mounted on the 18-foot square ground plane, were studied at the single frequency 592 Mc and at the single interelement spacing of one-half wavelength. The dipole element common to all these arrays is sketched in Fig. 1. It is constructed of one-half-inch diameter tubing and is fed from a conventional balun composed of the same tubing. The shorting plate of the balun is used to mount the dipole a quarter wavelength off the ground plane.

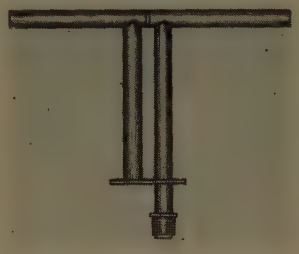

Fig. 1—Basic dipole element.

In the first experiment, a one-by-ten array was arranged along one centerline of the ground plane with one end element a half wavelength from the edge. This caused the other end element to be practically in the middle of the ground plane and permitted separation of the various edge effects. With the elements oriented parallel, then 45° echelon, then colinear, a bridge and slotted line were used to measure Z_{nn}, Z_{nm}, and Z_{n0} for the elements of the array.[9] The complete data for all these experiments is too voluminous to be included in this paper but is available elsewhere.[10] Significant excerpts of the data under discussion are shown in Tables I and II.

Interpretation of this data can be simplified by returning to the discussion of the edge effects in the analysis section. For the one-by-ten arrays described by the data in Tables I and II, we see that dipole No. 1 experiences edge effects due to the proximity of the ground-plane edge and due to being an end element in the array, whereas dipole No. 10 does not experience edge effects due to the proximity of the ground-plane edge, but only due to being an end element. Yet for parallel and echelon orientation, Z_{nn} for the two end

[9] The reader is reminded that the zero subscripts refer to the distant antenna; all other subscripts refer to elements in the array.

[10] "Study of Mutual and Self-Impedance Problems in Large Scanning Arrays," Rantec Corp., Final Rept. P183; September, 1959.

TABLE I

MUTUAL-IMPEDANCE DATA FOR VARIOUS 1×10 DIPOLE ARRAYS

n	Z_{nn}			$Z_{n,n+1}$			$Z_{n,n+2}/Z_{n,n+1}$			$Z_{n,n+3}/Z_{n,n+1}$			$Z_{n,n+4}/Z_{n,n+1}$		
	Parallel	45° Echelon	Colinear	Parallel	45° Echelon	Colinear	Parallel	45° Echelon	Colinear	Parallel	45° Echelon	Colinear	Parallel	45° Echelon	Colinear
1	2.32∠19°	2.12∠16°	2.23∠19°	0.87∠65°	0.74∠45°	1.14∠32°	0.34∠154°	0.23∠151°	*	0.16∠327°	0.09∠323°	*	0.095∠499°	0.05∠508°	*
2	2.32∠19°	2.10∠15°	2.14∠20°	*	*	1.14∠33°	*	*	0.13∠150°	0.17∠324°	0.09∠322°	0.03∠312°	*	0.05∠513°	0.01∠479°
3	2.34∠20°	2.11∠16°	2.16∠20°	0.87∠63°	0.74∠38°	1.17∠35°	0.35∠154°	0.23∠151°	0.13∠150°	0.17∠324°	0.09∠321°	0.03∠308°	0.095∠504°	0.05∠506°	0.01∠479°
4	2.29∠20°	2.09∠16°	2.10∠22°	*	*	1.15∠38°	*	0.23∠150°	0.13∠151°	0.16∠321°	0.09∠331°	0.03∠310°	*	*	0.01∠480°
5	2.30∠20°	2.10∠16°	2.07∠23°	0.88∠64°	0.76∠41°	1.18∠42°	0.35∠152°	0.23∠150°	0.13∠148°	0.16∠324°	*	0.03∠311°	0.095∠498°	0.05∠507°	0.01∠478°
6	2.32∠19°	2.10∠15°	2.08∠23°	*	*	1.07∠37°	*	0.23∠154°	0.13∠153°	0.16∠324°	0.09∠327°	*	0.098∠501°	0.05∠509°	0.01∠479°
7	2.36∠18°	2.15∠15°	2.08∠23°	0.82∠63°	0.77∠40°	1.02∠34°	0.35∠152°	*	*	*	0.08∠325°	0.03∠311°			
8	2.29∠18°	2.12∠15°	2.07∠23°	*	*	1.19∠42°	0.35∠152°	0.22∠154°	0.14∠149°						
9	2.30∠20°	2.13∠16°	2.08∠23°	0.87∠64°	0.75∠40°	1.03∠35°									
10	2.34∠19°	2.13∠15°	2.18∠22°												

* Data not taken at these points.

$Z_0 = 50$ ohms

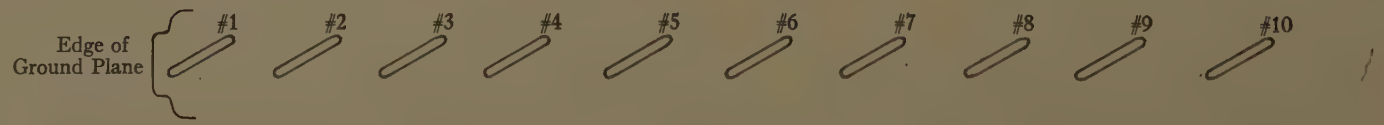

TABLE II

Z_{n0} vs Scan Angle for a 1×10 Parallel Dipole Array*

n	Beam Tilt Angle in Degrees†						
	0°	10°	20°	30°	40°	50°	60°
1	1.01|4°	0.99|20°	1.02|11°	0.95|5°	0.91|6°	0.90|18°	0.82|17°
2	0.98|4°	0.97|13°	1.01|9°	1.03|1°	1.01|2°	0.97|14°	0.86|14°
3	0.96|6°	0.97|11°	1.00|8°	1.02|1°	1.04|0°	1.02|10°	0.92|10°
4	0.97|3°	0.98|1°	1.03|2°	1.01|1°	0.98|5°	1.01|7°	0.93|5°
5	0.96|4°	0.98|3°	1.03|4°	1.05|1°	1.04|3°	1.03|4°	1.01|1°
6	1.00|0°	1.00|0°	1.00|0°	1.00|0°	1.01|0°	1.01|0°	1.03|0°
7	0.98|1°	1.02|3°	1.05|2°	1.03|0°	1.02|0°	0.99|3°	1.02|6°
8	0.99|3°	1.02|10°	1.05|9°	1.03|5°	1.01|0°	0.98|6°	1.00|13°
9	0.98|1°	1.02|12°	1.07|13°	1.06|3°	1.05|2°	1.01|10°	1.04|17°
10	1.00|2°	1.01|5°	1.08|17°	1.06|5°	1.04|9°	1.03|15°	1.06|24°

* Uniform progressive phase suppressed.
† Beam tilts toward element 1.

elements is about the same and only slightly higher than Z_{nn} for a central element. Some variance is seen for the colinear case, but a positive interpretation is clouded by the variability of tip-to-tip spacing between ends of adjacent colinear elements. It was found that as little as a sixteenth-inch variation in this spacing could cause a considerable change in Z_{11} and Z_{12}. In any event, even for the colinear case, the effect of the ground-plane edge on Z_{nn} seems to be quite small. This was borne out by later experiments on two-dimensional arrays.

The above remarks apply also for $Z_{n,n+1}$. By the time one gets to $Z_{n,n+2}$, even the colinear data have settled down to a steady value, supporting the idea that tip-to-tip variability is accountable in the colinear case.

The effect of the finiteness of the array itself shows up in the Z_{nn} and $Z_{n,n+1}$ data for all three orientations, but appears negligible for $Z_{n,n+2}$ and beyond. It appears greatest for the colinear case but in general does not cause more than a few per cent variation in the impedance values.

Z_{n0} is only slightly affected by the edge at broadside, but develops more and more unbalance as the beam is scanned further off broadside. The variation is great enough to require compensation by the time the beam is out to 60°.

A suitably terminated parasitic dipole was placed beyond dipole No. 1, and even though the parasite was not in contact with the ground plane, its presence caused the impedance data for dipole No. 1 to approach closely to that of a central dipole, thus enforcing the idea that the finiteness of the array itself is the most important edge effect.

The meaning of these edge effects can be appreciated from a discussion of the active impedance. For a one-dimensional array, this can be written

$$Z_{\text{active}} = Z_{11} + \frac{I_2}{I_1} Z_{12} + \frac{I_3}{I_1} Z_{13} + \cdots \qquad (6)$$

We can see from Table I that for a colinear array, $Z_{12}/Z_{11} \cong 1/2$, $Z_{13}/Z_{11} \cong -1/16$, etc. Therefore, if $I_1 = I_2 = I_3$, etc., (a good assumption in a small segment of a large array), it follows that Z_{active} ranges roughly from $2Z_{11}$ down to an almost negligible value for an element with neighbors on both sides, as the beam is scanned from broadside to endfire. However, for an element with a neighbor on only one side, the variation is only from $1.5Z_{11}$ down to $0.5Z_{11}$. This effect on Z_{active} is therefore much greater than the effect caused by the variations in Z_{nn} and Z_{nm} noted in Table I. However, until we relate effect on pattern to variations in mutual coupling, it is not fair to conclude that the variations seen in Table I are small enough to be ignored. This is a point which shall be discussed further, after the data on two-dimensional dipole arrays has been presented.

At this juncture in the experimental program, the Lincoln computer was supplied with smoothed data taken from Table I, plus idealized data for Z_{n0}, for the case of the colinear array. Calculations were made, using (1), of the receiving currents in a ten-element linear dipole array in which each element was terminated in a matched load. Concomitantly, the receiving currents were measured vs scan angle for the one-by-ten colinear array. The comparison of computed and measured values is shown in Table III. The agreement is quite good, close to broadside, becoming poorer as the beam is scanned further out. This is attributed to the fact that the variations in Z_{n0} data were not included and suggests this correction cannot be ignored in wide-angle scanning designs.

Concerning the amplitudes displayed in Table III, one can conclude that the variations are chiefly confined to the two elements closest to each end, even out to 50° scan. Even the phase errors are not too bad in the middle six elements.

Mutual Coupling in Two-Dimensional Dipole Arrays

Five-by-five and five-by-ten dipole arrays of various element orientations were tested. Only two of these arrays will be discussed, since the conclusions drawn from the others are in complete agreement.

Five linear arrays of ten parallel dipoles each were mounted on a small ground plane, such that all fifty dipoles were a half wavelength on centers and all edge dipoles were a half wavelength from the corresponding ground-plane edge. Measurements yielded data of which the sample in Table IV is typical. Interestingly, the corresponding Z_{nm} data, when normalized to the respective self-impedances, compare quite closely. This was found to be true for all fifteen sets of data and indicates that the edge effects alter the mutual impedances in much the same ratio that they alter the self-impedances.

The bridge and "sky hook" range were used to measure Z_{n0} and I_k for all fifty dipoles as a function of scan angle. Once again, the case of all elements terminated in a matched load was used in determining I_k. Samples of this data are shown in Tables V and VI.

Comparing the data in Tables I and IV, we see that mutual impedance between parallel dipoles in a common row is essentially unaffected by whether there is a single row or several rows. In the 45° direction, the comparison must be inferred by interpolation because the spacing is $\sqrt{2}$ greater in the two-dimensional array than it was in the corresponding one-dimensional array. When the interpolation is made, it is found that the mutual-impedance values for the one- and two-dimensional arrays agree quite closely.

It is a little unfair to compare rows of colinear dipoles in the two cases of Tables I and IV, because such a row is only five elements long in the two-dimensional case. However, the agreement is fairly good. This same

TABLE III

RELATIVE VALUES OF RECEIVING CURRENT I_k FOR A TEN-ELEMENT COLINEAR DIPOLE ARRAY

Dipole No.	$\theta=0°$		$\theta=10°$		$\theta=20°$		$\theta=30°$		$\theta=40°$		$\theta=50°$	
	Meas.	Calc.	Meas.	Calc.	Meas.	Calc.	Meas.	Calc.	Meas.	Calc.	Meas.	Calc.
1	1.25 ⌊16.8°	1.25 ⌊5°	1.18 ⌊15°	1.18 ⌊11°	1.02 ⌊22°	1.20 ⌊16°	0.86 ⌊65°	0.94 ⌊17°	0.69 ⌊83°	0.78 ⌊16°	0.72 ⌊108°	0.68 ⌊8°
2	0.91 ⌊23.2	0.94 ⌊6	0.98 ⌊5	1.05 ⌊6	1.07 ⌊1	1.14 ⌊1	0.93 ⌊31	1.10 ⌊4	0.87 ⌊49	0.97 ⌊8	0.87 ⌊71	0.88 ⌊5
3	1.04 ⌊13.9	1.01 ⌊3	0.93 ⌊2	0.94 ⌊0	0.95 ⌊5	1.00 ⌊4	0.91 ⌊14	1.06 ⌊2	0.94 ⌊22	1.06 ⌊4	0.97 ⌊39	0.97 ⌊3
4	1.01 ⌊14.0	1.01 ⌊2	1.03 ⌊1	1.01 ⌊1	1.00 ⌊3	0.98 ⌊1	0.91 ⌊9	1.01 ⌊3	1.00 ⌊8	1.05 ⌊2	1.02 ⌊19	1.00 ⌊1
5	1.03 ⌊0.9	1.00 ⌊0	0.98 ⌊0	0.99 ⌊0	1.05 ⌊4	1.02 ⌊1	0.93 ⌊3	0.99 ⌊2	1.05 ⌊1	1.04 ⌊1	1.04 ⌊4	1.01 ⌊0
6	1.00 ⌊0.7	1.00 ⌊0	1.00 ⌊0	1.00 ⌊0	1.01 ⌊0	1.00 ⌊0	1.01 ⌊0	1.00 ⌊0	1.00 ⌊0	1.00 ⌊0	1.00 ⌊0	1.00 ⌊0
7	1.02 ⌊5.8	1.01 ⌊2	1.01 ⌊3	0.97 ⌊0	1.07 ⌊2	1.03 ⌊2	1.02 ⌊6	1.01 ⌊2	0.97 ⌊3	0.96 ⌊1	0.98 ⌊3	1.01 ⌊1
8	1.04 ⌊5.5	1.01 ⌊3	1.02 ⌊1	1.05 ⌊1	1.10 ⌊6	1.01 ⌊3	0.97 ⌊4	0.95 ⌊1	1.00 ⌊8	0.97 ⌊5	1.03 ⌊6	1.07 ⌊2
9	0.96 ⌊8.7	0.94 ⌊6	0.98 ⌊2	0.88 ⌊1	1.15 ⌊6	0.96 ⌊7	1.20 ⌊1	1.06 ⌊5	1.23 ⌊9	1.11 ⌊4	1.13 ⌊24	1.14 ⌊4
10	1.24 ⌊24.5	1.25 ⌊5	1.26 ⌊4	1.25 ⌊1	1.44 ⌊4	1.25 ⌊6	1.49 ⌊22	1.17 ⌊12	1.32 ⌊19	1.08 ⌊13	1.06 ⌊50	1.00 ⌊18

TABLE IV

Z_{nm} DATA FOR FIVE BY TEN DIPOLE ARRAY

0.019 | 683°	0.039 | 526	0.043 | 584	0.039 | 526	0.019 | 683
1.00 | 0	0.54 | 9	0.074 | 133	0.014 | 283	0.004 | 533
0.023 | 524	0.059 | 443	0.071 | 406	0.059 | 443	0.023 | 524
0.380 | 95	0.179 | 115	0.031 | 205	0.004 | 318	0.005 | 606
0.020 | 379	0.074 | 283	0.155 | 245	0.074 | 283	0.020 | 379
0.133 | 246	0.083 | 269	0.023 | 380	0.008 | 559	0.008 | 694
0.035 | 197	0.156 | 101	0.380 | 95	0.156 | 101	0.035 | 197
0.068 | 416	0.046 | 439	0.025 | 530	0.017 | 667	0.010 | 787
0.090 | 142	0.549 | 17	1.00 | 0	0.549 | 17	0.090 | 142
0.038 | 587	0.030 | 611	0.022 | 683	0.017 | 793	0.010 | 911
0.035 | 197	0.156 | 101	0.380 | 95	0.156 | 101	0.035 | 197
0.024 | 770	0.022 | 787	0.017 | 848	0.014 | 931	0.010 | 1033
0.020 | 379	0.074 | 283	0.155 | 245	0.074 | 283	0.020 | 379
0.016 | 953	0.014 | 965	0.013 | 1014	0.011 | 1085	0.008 | 1179
0.023 | 524	0.059 | 443	0.071 | 406	0.059 | 443	0.023 | 524
0.011 | 1135	0.010 | 1146	0.010 | 1180	0.008 | 1243	0.007 | 1334
0.019 | 683	0.039 | 526	0.043 | 584	0.039 | 526	0.019 | 683
0.007 | 1319	0.007 | 1320	0.008 | 1347	0.007 | 1412	0.006 | 1491
0.016 | 850	0.024 | 778	0.030 | 756	0.024 | 778	0.016 | 850
0.005 | 1499	0.006 | 1493	0.006 | 1531	0.005 | 1586	0.004 | 1654

Upper values: WRT central element.
$Z_{SELF} = 2.20 \angle 14°$

Lower values: WRT corner element
$Z_{SELF} = 2.30 \angle 13°$

TABLE V

Z_{n0} AND I_k DATA FOR FIVE-BY-TEN DIPOLE ARRAY

1.05 | 5°	1.05 | 10	1.03 | 6	1.03 | 15	1.07 | 8
1.18 | 31	0.97 | 41	0.95 | 26	0.90 | 44	1.22 | 31
1.04 | 5	1.04 | 10	1.03 | 7	1.02 | 12	1.04 | 8
1.29 | 16	1.12 | 30	1.07 | 18	1.12 | 31	1.29 | 19
1.05 | 6	1.02 | 8	1.01 | 5	1.01 | 9	1.03 | 7
1.15 | 15	1.02 | 27	1.01 | 10	1.00 | 30	1.21 | 18
1.01 | 2	1.04 | 11	0.99 | 7	1.01 | 8	1.01 | 5
1.19 | 10	1.05 | 28	0.99 | 12	1.02 | 28	1.23 | 15
1.02 | 1	1.02 | 5	1.02 | 3	0.89 | 7	1.01 | 4
1.19 | 4	1.02 | 23	1.05 | 5	1.00 | 23	1.26 | 12
1.04 | 0	1.04 | 6	1.00 | 0	1.01 | 6	1.04 | 4
1.18 | 3	1.02 | 21	1.00 | 0	1.02 | 25	1.23 | 10
1.00 | 0	1.04 | 6	1.04 | 2	1.00 | 4	1.02 | 1
1.23 | 1	1.08 | 18	1.05 | 3	1.02 | 22	1.22 | 6
1.02 | 2	1.06 | 7	1.02 | 2	1.03 | 2	1.05 | 2
1.16 | 3	1.05 | 16	0.98 | 3	1.02 | 16	1.23 | 1
1.03 | 4	1.07 | 2	1.03 | 1	1.03 | 0	1.06 | 3
1.25 | 6	1.16 | 10	1.08 | 2	1.12 | 9	1.28 | 3
1.04 | 6	1.05 | 1	1.03 | 2	1.03 | 1	1.04 | 7
1.19 | 2	0.98 | 19	0.93 | 4	0.98 | 21	1.17 | 2

$\theta = 0°$.
Upper values: Z_{n0}.
Lower values: I_k.

TABLE VI
Z_{n0} AND I_k DATA FOR FIVE-BY-TEN DIPOLE ARRAY

0.93|15°	1.00|16	0.98|19	1.00|17	0.93|15
2.26|31	1.87|23	1.78|34	1.91|26	2.26|34
0.86|15	0.96|15	0.93|16	0.96|17	0.88|16
1.90|15	1.52|0	1.39|13	1.46|1	1.94|20
0.83|12	0.95|14	0.96|12	0.94|11	0.88|14
1.77|4	1.38|9	1.27|10	1.37|15	1.77|8
0.82|12	0.96|10	0.99|8	0.96|7	0.88|10
1.64|3	1.30|17	1.17|7	1.26|26	1.67|33
0.88|11	1.00|6	1.03|1	1.01|1	0.94|4
1.73|5	1.30|20	1.08|2	1.25|29	1.59|10
0.89|10	1.01|6	1.02|0	1.01|7	0.91|8
1.60|6	1.26|28	1.02|0	1.25|35	1.65|20
0.92|3	0.97|4	1.00|9	1.02|10	0.93|12
1.58|16	1.23|33	0.96|7	1.18|39	1.63|29
0.88|6	0.98|13	0.98|15	1.01|15	0.92|17
1.55|21	1.23|38	0.96|10	1.15|44	1.62|33
0.93|8	1.00|14	1.03|18	1.03|23	0.96|24
1.51|25	1.17|41	1.00|10	1.14|51	1.67|38
0.92|20	1.03|26	1.12|29	1.03|30	0.96|29
1.50|25	1.04|37	1.22|14	1.03|46	1.56|37

$\theta = 60°$.
Upper values: Z_{n0}.
Lower values: I_k

five-by-ten array was also tested with all dipoles rotated 90°, and the colinear data agrees even more closely with the one-dimensional data. Thus, we can conclude that one-dimensional measurements of the mutual impedance between dipoles will give a good indication of the mutual-impedance relationships in a two-dimensional array.

Comparing Table II with Tables V and VI reveals little difference between the one- and two-dimensional arrays. For a broadside beam, Z_{n0} is essentially the same for the two cases. With the beam scanned off 60°, the average agreement in Z_{n0} values is not quite so good, but this effect is insignificant, because neither set of Z_{n0} values has departed drastically from unity. However, the disagreement in I_k values *is* significant. We cannot compare Table III with Tables V and VI because the latter deal with scan in the H plane. However, tables similar to V and VI can be constructed from I_k data taken on the five-by-ten array with all dipoles rotated 90°. When this is done,[11] the one-dimensional I_k values do agree with the two-dimensional values out to 30° scan. However, beyond 30° scan, the disagreement between the two cases becomes marked. This is evident when Table III is compared with Table VII wherein the I_k data for 45° scan is listed. Table VII shows a depression in I_k magnitude extending in all directions from the central elements, whereas Table III shows a tilted distribution in the direction of scan. The difference can be attributed to the additional mutual-impedance terms which are present in the two-dimensional case.

The slotted line was used to measure the active impedance vs scan of a central element in the five-by-ten dipole array. This was done by recording a sequence of partial-reflection coefficients and summing the data with proper regard for phase. The procedure is somewhat equivalent to measuring the terms in (6) one by one. The interested reader can find the details of this procedure elsewhere.[10] The results are shown in Table VIII. Scanning in the E plane causes an increase in the real component and a decrease in the imaginary component, whereas scanning in the H plane causes a decrease in the real component along with a decrease in the imaginary component of the active impedance. As a consequence of this, compensation causes diagonal scanning to affect the active impedance relatively little. Thus, a 45° echelon array, scanned in either principal plane, is attractive from the point of view of active impedance. Two crossed 45° echelon arrays, used for polarization diversity, with one-dimensional scanning, are much to be preferred over the conventional combination of horizontal and vertical dipoles. Experiments have confirmed these assertions.

[11] "Study of Mutual and Self-Impedance Problems in Large Scanning Arrays," Rantec Corp., Progress Rept. No. 17; July, 1959.

TABLE VII

I_k DATA FOR TEN-BY-FIVE DIPOLE ARRAY

0.53∠12°	0.50∠3°	0.54∠1°	0.54∠0°	0.56∠10°
0.67∠17°	0.60∠5°	0.65∠9°	0.60∠7°	0.68∠15°
0.75∠21°	0.64∠6°	0.68∠10°	0.59∠1°	0.76∠18°
0.81∠21°	0.69∠0°	0.82∠2°	0.66∠1°	0.83∠19°
0.87∠26°	0.78∠6°	1.00∠0°	0.77∠2°	0.86∠24°
0.83∠30°	0.69∠16°	0.95∠6°	0.69∠13°	0.84∠28°
0.72∠27°	0.47∠9°	0.73∠2°	0.47∠11°	0.74∠28°
0.72∠17°	0.61∠14°	0.90∠25°	0.60∠13°	0.70∠16°
0.92∠23°	0.86∠11°	1.20∠5°	0.83∠6°	0.96∠18°
0.86∠57°	0.75∠46°	0.79∠33°	0.74∠44°	0.88∠67°

E-plane scan $\theta = 45°$.

TABLE VIII

NORMALIZED ACTIVE IMPEDANCE VS INTERELEMENT PHASE SHIFT FOR CENTRAL ELEMENT OF A FIVE-BY-TEN DIPOLE ARRAY
$Z_0 = 50$ ohms

	E-Plane Scan→							
←H-Plane Scan	0°	30°	60°	90°	120°	150°	180°	
0°	0.80+j0.77	0.78+j0.64	0.80+j0.42	1.16+j0.30	2.95+j0.12	15 −j40	Negative	
30°	0.83+j0.78	0.81+j0.66	0.81+j0.47	1.15+j0.37	2.8 +j0.40	28 +j10	Negative	
60°	0.77+j0.67	0.80+j0.68	0.70+j0.45	0.96+j0.36	2.15+j0.33	10 −j1.00	Negative	
90°	0.70+j0.52	0.67+j0.50	0.60+j0.36	0.73+j0.25	1.49+j0.13	4.40−j1.30	3−j10	
120°	0.68+j0.42	0.60+j0.45	0.46+j0.30	0.50+j0.13	1.0 −j0.20	2.30−j2.10	Negative	
150°	0.43+j0.38	0.33+j0.36	0.22+j0.17	0.25−j0.05	0.66−j0.43	1.53−j2.35	Negative	
180°	0.26+j0.37	0.21+j0.24	0.12+j0.03	0.21−j0.15	0.79−j0.57	2.0 −j3.8	Negative	

It is interesting to note from Table VIII that for far out E-plane scanning, the real part of the active impedance becomes negative. This agrees with the independent calculations of Blasi.[12]

Assessement of Edge Effects in Dipole Arrays

From a study of Tables III, V, VI and VII and the parallel discussions, one can reach the conclusion that, except for wide-angle E-plane scanning, the errors in receiving currents are principally confined to the first few dipoles near the edges of the array. Furthermore, these errors in receiving currents do not, in the range quoted, exceed one hundred per cent, and reach that value only in the end elements. Accordingly, one can make an estimate of the effect these errors might have on the antenna pattern. The procedure adopted was to assume a 100 per cent error in the receiving current in each end element, a 75 per cent error in the penultimate elements, a 50 per cent error in the next elements in, a 25 per cent error in the next elements in, and no errors in all remaining internal elements. One-dimensional arrays of various numbers of elements were considered, always with half-wavelength spacing. A perfect network attached to the array, which would convert a uniform amplitude distribution in the array to a Dolph-Tchebycheff pattern of desired sidelobe level, was also assumed. It was further assumed that the eight error currents, in the four elements at each end of the array, had such phases as to cause the greatest sidelobe level distortion after being operated on by the network. The results of the ensuing calculations are shown in Fig. 2. A twelve-element array designed for 20-db sidelobes gives only 7-db sidelobes, whereas a 144-element array designed for 20-db sidelobes gives 15-db sidelobes. However, a 144-element array designed for 40-db sidelobes gives only 32-db sidelobes.

It should be emphasized that this is the most pessimistic case and would not be expected to occur over more than a small segment of the total scan range. It is evident that the larger the array, the smaller the effect. This is consonant with earlier results on random errors[13] and leads to the important conclusion that all sources of error in antenna arrays become less significant as the array size is increased.

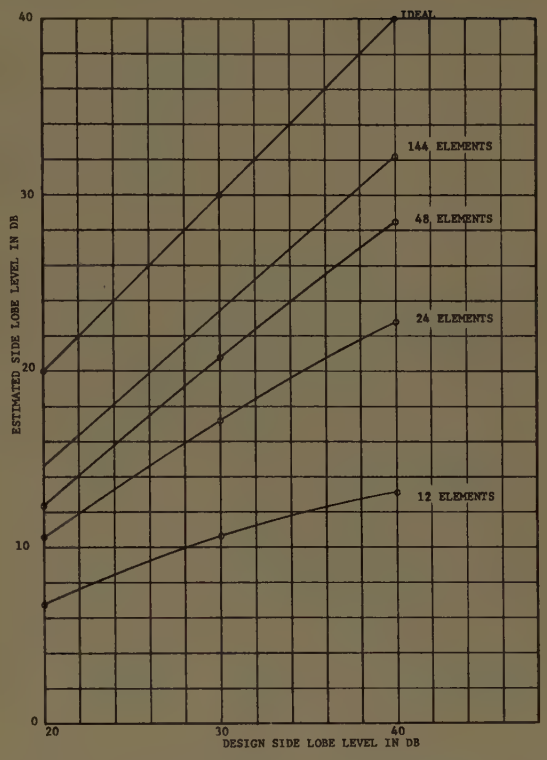

Fig. 2—Worst possible degradation in sidelobe level for a dipole array with tapered current errors in the four elements on each end.

In applications where the edge effect must be taken into account, we conclude that the effect of missing mutual-impedance terms is the most important, that Z_{n0} variations are unimportant except at wide scan angles, and that unbalances between the values of $Z_{n,n+k}$ and $Z_{n,n-k}$ are insignificant.

Other element types have been studied for edge effects in arrays, notably helices and log-periodic elements. Though the data amassed was not so extensive as for dipoles, the conclusions drawn were the same, and there is thus strong evidence to believe that these conclusions about edge effects have general applicability.

Acknowledgment

The authors gratefully acknowledge the helpful technical counsel of Drs. S. Edelberg and A. Oliner. They also wish to thank their colleagues who cheerfully performed many tedious tasks in this program, and are especially grateful to I. Baker, L. Madill, and V. Gardner.

[12] E. A. Blasi and R. S. Elliott, "Scanning antenna arrays of discrete elements," IRE Trans. on Antennas and Propagation, vol. AP-7, pp. 435–436; October, 1959.

[13] R. S. Elliott, "Mechanical and electrical tolerances for two-dimensional scanning antenna arrays," IRE Trans. on Antennas and Propagation, vol. AP-8, pp. 114–120; January, 1958.

Optimum Feeds for All Three Modes of a Monopulse Antenna I: Theory*

PETER W. HANNAN†, SENIOR MEMBER, IRE

Summary—**In a monopulse antenna for use in a tracking radar, the requirements for the sum and difference modes are not the same. For the amplitude-comparison type of monopulse having an antenna whose main aperture is illuminated by a feed, these independent requirements can be met by a feed designed to fulfill two conditions. One is that excitation of the feed aperture in the difference modes be effectively about twice as wide as in the sum mode. The other is that the shapes of all the feed excitations be free of any avoidable irregularities.**

The amount of improvement available when these conditions are met depends on the optimization point desired for each mode, as well as the design of the reference antenna. In a typical case, the gains and slopes in the difference modes should increase by several db. Furthermore, the near sidelobes and the spillover radiation in the difference modes should decrease by an order of magnitude. A small increase of gain in the sum mode is also available, and finally, the criticalness of positioning the feed may be appreciably reduced.

I. Introduction

IN THE FIELD of tracking radars, the need for antennas of increased angular accuracy has led from sequential lobing and conical scan to simultaneous lobing or monopulse. As the requirements become even more demanding, it becomes necessary to incorporate advances in the design of monopulse antennas to more fully realize their potentialities. One such advance is possible in the amplitude-monopulse type of antenna consisting of a reflector or lens illuminated by a feed.

For an ordinary single-mode antenna, the optimum design of a simple feed for maximum antenna gain is well known [1], [2]. In the case of a monopulse antenna, there are usually a sum and two difference modes, and it has not been customary to design a feed for simultaneous optimum performance in all three of these modes. The particular compromise that is made may depend on the system requirements, and the relative importance of the various modes. One choice often made involves a "crossover level" which maximizes a certain product of sum gain and difference slope [3], [4]; in this case, neither of these quantities achieves its optimum value. In addition, some of the other antenna characteristics, such as sidelobe levels, spillover radiations, and criticalness to misalignment, are considerably poorer than they need be with an optimum design in every mode.

It is the purpose of this paper to discuss in detail the limitations involved in the usual compromise design, and to describe the degree of improvement available if each mode can be optimized independently. In a companion paper, means to achieve this independent optimization in all three modes will be presented.

II. Description of Monopulse Antenna

It is assumed that the reader has some familiarity with monopulse [5], [6]; however, it is desirable to describe the basic monopulse antenna system which is considered in this paper. This is shown in Fig. 1, together with the terminology to be used. The essential components are a comparator, a feed, and a focusing element.

There are three regions of the antenna system which are of special interest. When signals are provided to the feed by the comparator, there exists a field across the aperture of the feed which is herein termed the *feed excitation*. This, in turn, creates a field across the aperture of the focusing element which is called the *main aperture illumination*. The resulting field at a large distance from the antenna may be described by its distribution as a function of angle; this is the *antenna pattern*.

A. Modes of Operation

In describing the operation of a monopulse antenna, there are two different concepts which are commonly employed. One concept considers the signals which may exist within the comparator that would excite different portions of the feed aperture and create antenna patterns consisting of simple lobes displaced from the antenna axis. This may be called the *lobe* concept; it stems from sequential-lobing and conical-scanning antennas. The lobe concept is helpful in understanding the properties of a monopulse antenna, and for the ordinary monopulse antenna it is often employed as the principal means of analysis. However, it does not provide a convenient basis for the optimization discussed in this paper. In addition, the lobe signals represent an intermediate stage in the system, and do not have as direct an operational significance as may be desired.

The concept which is employed in this paper considers the signals existing in the three channels at the input of the comparator. Since these three channels cor-

* Received by the PGAP, November 22, 1960; revised manuscript received, March 27, 1961. The material in this paper is the result of antenna development work for the Bell Telephone Laboratories on Army Ordnance Corps projects. Preparation of this paper has been supported mainly by a subcontract with BTL in connection with prime contract No. DA-30-069-ORD-1955.

† Wheeler Labs., Inc., Smithtown, N. Y.

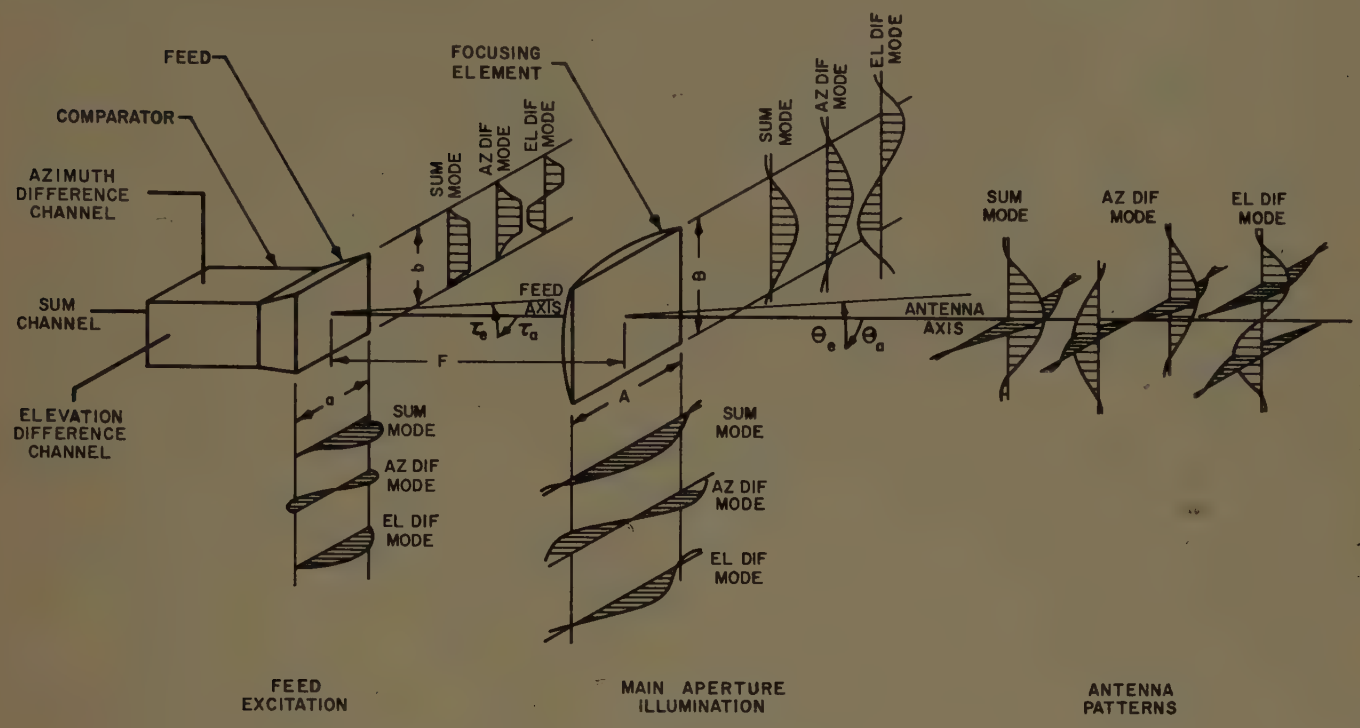

Fig. 1—Monopulse antenna system.

respond to three distinct modes of operation, this viewpoint may be referred to as the *mode* concept. These modes are called the *sum mode*, the *azimuth difference mode*, and the *elevation difference mode*, in accordance with the type of action occurring within the comparator during reception.

When coupled to the transmitter of a radar system, the sum mode provides illumination of the distant target; when coupled to a receiver it provides range information and a reference signal. The azimuth and elevation difference modes are coupled to receivers whose signals, when combined with the reference sum signal, provide azimuth and elevation angle information, respectively. Although only the sum mode actually exists in transmission, it is common practice to consider all three modes in transmission for ease of analysis; by reciprocity the antenna patterns are the same whether obtained in transmission or reception. Shown in Fig. 1 are a sample set of field distributions during transmission for the sum, azimuth, and elevation modes, in each of the three regions of interest.

B. Assumptions and Limitations

A number of assumptions are made in this paper which simplify the calculations and presentation. As shown in Fig. 1, the feed and main apertures are rectangular, and each field distribution is assumed to be separable into the product of a horizontal and a vertical distribution. In the sum mode, both the horizontal and the vertical distributions are of the even type. In each of the difference modes, the distribution in one direction is of the odd type while in the other direction it is of the even type. The antenna is, of course, assumed to be free of any dissipation losses. It is also assumed that both the feed aperture and the main aperture are large compared with a wavelength, and that the feed is much smaller than the main aperture. As a result of all these assumptions, both the main illumination and the antenna patterns are relatively easy to calculate, and can be presented in a single dimensionless form. Many practical antennas do not correspond exactly to the assumptions made, and in these cases the numerical results obtained herein are applicable only as approximations; however, the basic concepts and trends are generally valid.

The analysis presented in this paper is specifically developed for the *amplitude-comparison* type of monopulse, as typified by the antenna shown in Fig. 1. A similar approach could be applied to the phase-comparison type [7]. However, in a phase-comparison antenna of the kind involving a feed and a focusing element, improvements analogous to those suggested in this paper are difficult to implement, and are beyond the scope of this presentation.

III. Need for Different Widths of Feed Excitation in Sum and Difference Modes

One of the requirements for optimizing a monopulse feed in all three modes is that the width of feed excitation be different in the sum and difference modes. This can be shown in several ways, each furnishing a different insight into the basic processes involved in ob-

taining good antenna performance. In each case, the sum and one difference mode will be investigated; the other difference mode would have the same requirement as the one considered.

A. Focal Field

The first viewpoint is shown in Fig. 2, which illustrates the region around a feed during reception. When a plane wave is incident on the focusing element, it is focused to a compact area [8] which allows a relatively small feed to capture most of the available power. It can be seen intuitively (as well as proven rigorously) that for maximum signal, the size of the feed aperture should be about equal to the size of the main lobe of the focused wave, when the power in the sidelobes of the focused wave is intentionally wasted in the interests of a practical design. For the sum mode, indicated in Fig. 2(a), this situation corresponds to the standard design of a simple single-mode antenna for maximum gain.

In the difference mode, the antenna pattern has two main peaks of opposite polarity which are displaced equal amounts off the antenna axis. When a wave is incident on the antenna from the direction of one peak, it is focused to an area off the center of the feed, as indicated in Fig. 2(b); a similar area on the opposite side would correspond to a wave incident from the direction of the other peak. To obtain the proper signal from each wave, the feed aperture may be divided into two halves, connected to the symmetrical arms of a hybrid junction. It can be seen that for maximum signal at each peak, each half aperture should be about equal to the size of the main lobe of one focused wave, just as it is in the case of the sum mode. Thus the over-all feed-aperture dimension in the odd plane of the difference mode should be about twice as great as that for maximum sum gain, and in the even plane it should be about equal to that for maximum sum gain. It is also interesting to note that, upon analysis of the output from the complete circuit including the hybrid junction, the maximum difference gain should be about 3 db below the maximum sum gain.

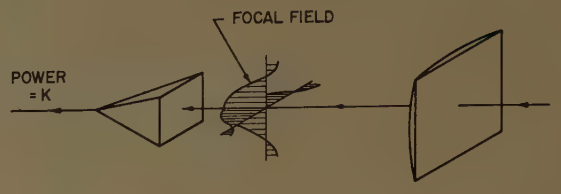

(a) Sum mode.

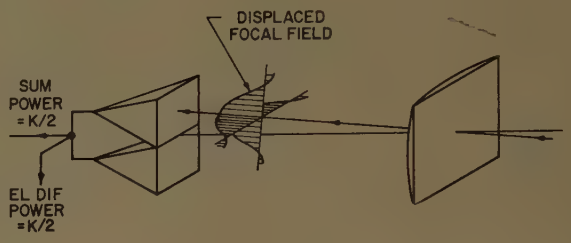

(b) Difference mode.

Fig. 2—Optimum feed sizes; focal-field viewpoint.

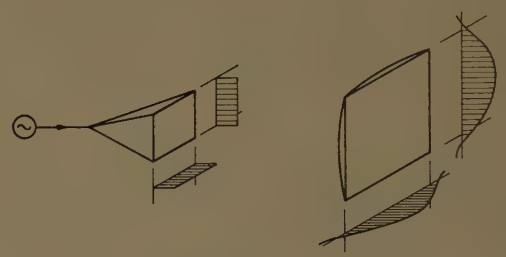

(a) Sum mode.

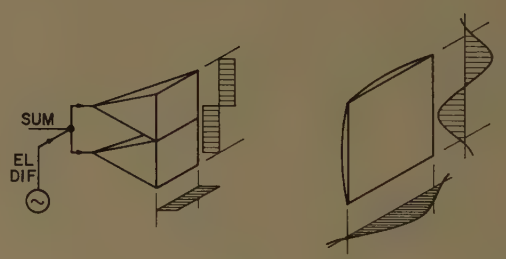

(b) Difference mode.

Fig. 3—Optimum feed sizes; illumination viewpoint.

B. Main Aperture Illumination

Another viewpoint considers the illumination of the main aperture by the feed during transmission; this is illustrated in Fig. 3 for a hypothetical feed having "constant" excitation in both planes. In order to obtain maximum gain in the sum mode, the feed size should be such that the illumination is tapered down at the edge of the main aperture by about 10 db, as shown in Fig. 3(a). This is the well-known [1], [2] optimum taper which balances excessive spillover loss against excessive waste of the main aperture, to achieve maximum gain in a simple, single-mode antenna. In some designs, the illumination is tapered further down so that the discontinuity at the edge of the main aperture is reduced: this lowers the level of the sidelobes in the antenna pattern, at the expense of a small reduction of gain.

For the case of the difference mode, the considerations of maximum gain and low sidelobes lead to a similar conclusion: namely, the illumination of the main aperture should be appreciably tapered down at the edge. In addition, some of the special problems of the difference mode, such as criticalness to feed tilt and edge asymmetries, place a premium on low illumination at the edge of the main aperture. For simplicity, it may be assumed that the difference illumination should be tapered down by about the same amount as the sum illumination, say 10 db, as shown in Fig. 3(b). How-

ever, in the odd plane of the difference mode, the feed is only about half as directive as in the sum mode; therefore the feed aperture dimension in this odd plane should be about twice as great as it is for the sum mode. In the even plane, the feed aperture dimensions for the two modes should be about equal. This conclusion is, of course, the same as that reached previously.

It is instructive to consider the situation in which the feed size is optimized for the sum mode, but cannot be increased for the difference mode. Under these circumstances the difference illumination reaches a maximum close to the edge of the main aperture, as shown in Fig. 4(a), and the large discontinuity at this location creates high sidelobes in the corresponding antenna pattern. At least half of the power in the difference mode goes into spillover, so that there is about 3-db loss in the difference signal compared with the optimum condition; thus, the difference peak gain would be about 6 db below the sum gain. The high illumination of the edge of the main aperture makes the difference mode sensitive to antenna misalignment and edge asymmetries, and the large amount of spillover is likely to contribute to additional sidelobes. These "spillover sidelobes" may be especially offensive in permitting spurious signals to enter the difference channel; examples of this are coherent signals such as those caused by reflection from the ground and reflection from asymmetrical antenna surfaces, or incoherent signals such as thermal radiation from the ground.

If the feed size were optimized for a difference mode without decreasing it for the sum mode, the sum illumination would be too narrow. As indicated in Fig. 4(b), optimization in one difference mode causes about half the main aperture to be wasted in the sum mode; thus a reduction of about 3 db in sum gain would result. Attempting to optimize the feed size in both difference modes would create additional losses.

While it is true that a feed size might be utilized which strikes a compromise between optimum sum-mode and optimum difference-mode performance, the defects mentioned above would still be present to a large degree. Thus, it is evident that the ordinary feed design having the same effective size in the sum and difference modes imposes a limitation which degrades the antenna performance in a number of ways, many of which are likely to have a significant effect on system performance.

C. Antenna Pattern Characteristics

Up to this point, the viewpoints chosen have merely illustrated the need for different feed-aperture sizes in the sum and difference modes, and have not yielded quantitative estimates of antenna performance. The final viewpoint to be presented is one whereby numerical values are obtained for a number of significant characteristics of the antenna pattern. These values are plotted

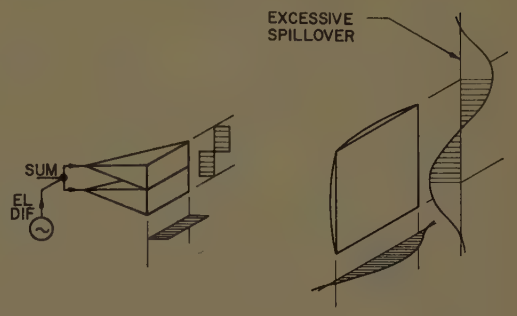

(a) Difference mode when feed is optimized for sum mode.

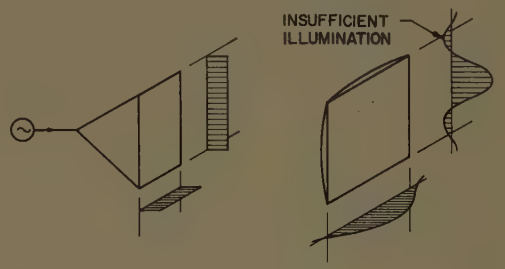

(b) Sum mode when feed is optimized for one difference mode.

Fig. 4—Non-optimum feed sizes; illumination viewpoint.

in Figs. 5–8 (pp. 448–449) as a function of normalized feed aperture size, for the case of "constant" shapes of excitation of the feed aperture. As will be discussed in Section IV, these are not the best shapes for the feed excitation. However, they are relatively simple to calculate, and provide a typical case for study of the effect of feed aperture size on the antenna patterns; in addition, the useful concept of effective aperture is ordinarily related to a "constant" shape.

For the exact definitions of the various antenna pattern characteristics, the reader is referred to Section VII. The curves themselves are drawn as accurately as possible, because they are likely to be helpful during the design of an antenna. Each curve originates from an explicit formula; these formulas appear in the report [9] from which this paper stems. A few of the formulas also appear in [10] and [11].

Sum Mode: In Fig. 5, a set of curves are shown for several characteristics of the antenna pattern in the sum mode. These characteristics include gain ratio (efficiency), sidelobe ratios, and beamwidth ratio. A curve for spillover power ratio is also presented; since the spillover cannot be included in a general calculation of sidelobes, some indication of the "spillover sidelobe" effect is desirable. Also shown for reference is a dashed curve of edge taper voltage ratio for the illumination of the main aperture.

It should be understood that all of these quantities are determined on the basis of a one-dimensional geometry. However as mentioned in Section II-B, the field strength of the antenna radiation is separable into the product of a horizontal and a vertical distribution, in the usual manner for a large rectangular aperture. As

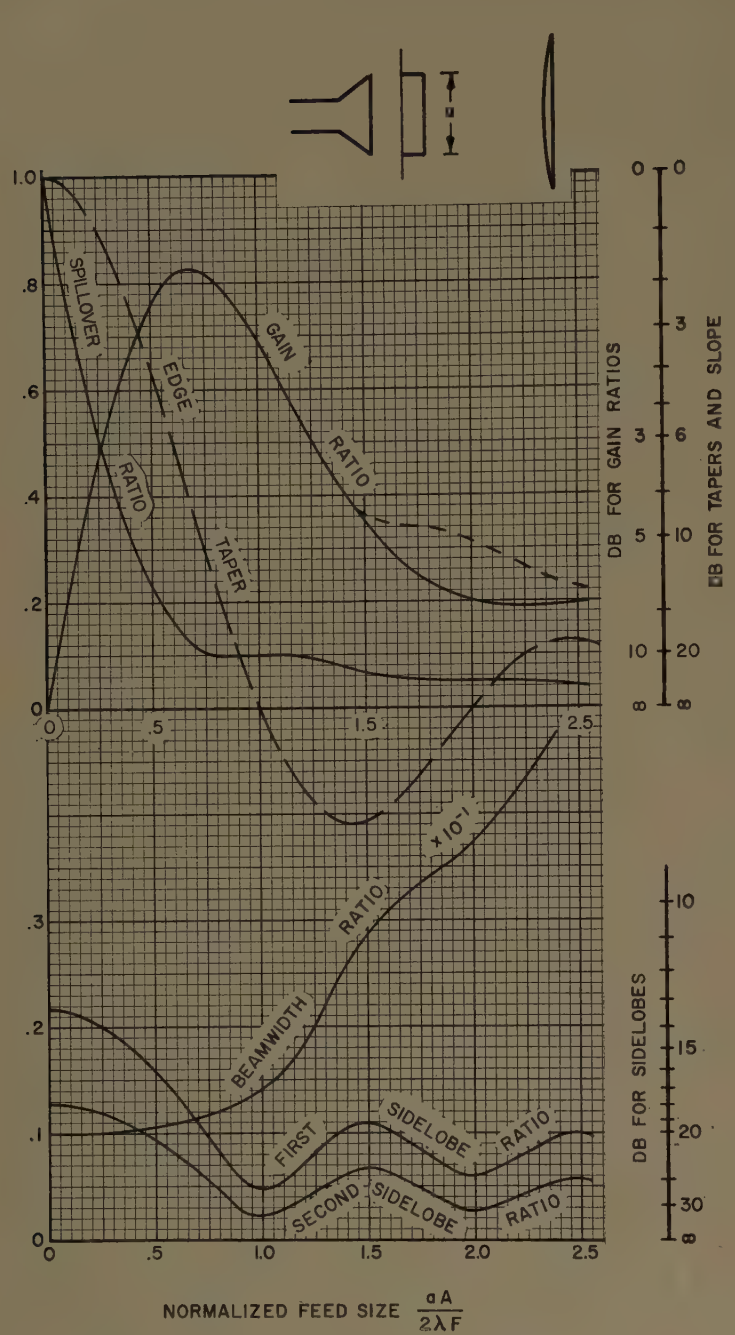

Fig. 5—Sum-pattern characteristics vs feed size.

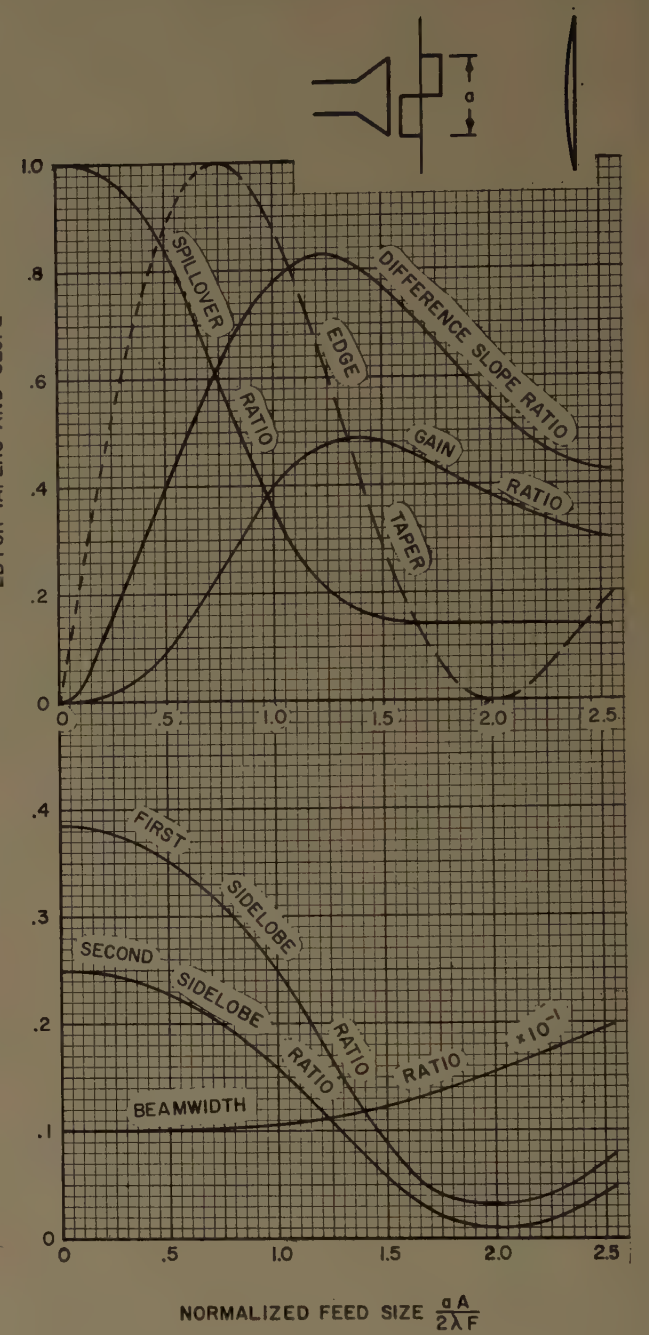

Fig. 6—Difference-pattern characteristics vs feed size.

a result, the two-dimensional sum-mode value for gain ratio may be obtained by multiplying together the appropriate one-dimensional sum-mode values for each of the two planes involved. In the case of spillover, this multiplication rule applies instead to the fraction of power not spilled over, *i.e.*, one minus the spillover ratio. The other pattern characteristics given in Fig. 5 are also valid for the two-dimensional case, when restricted to the appropriate cardinal plane.

It may be seen that the curve of gain ratio reaches a maximum at a normalized feed size of 0.68, while the curves for the relative levels of both the first and second sidelobes reach a minimum at a normalized feed size of 1.00. If one were to define an optimum feed size for the sum mode in terms of the best combination of these two properties, then an intermediate size, say about 0.80, would be chosen. Assuming that the antenna requirements are the same for both planes of the sum mode, the same result would apply to both dimensions of the feed aperture.

Difference Mode: In Fig. 6, all but one of the curves show properties for the difference mode which are similar to those properties given in Fig. 5 for the sum mode. As before, these are given for a one-dimensional geometry; in this case, only the odd plane of the difference mode is considered. The two-dimensional difference-mode values for gain ratio (difference peak efficiency) and one-minus-spillover-ratio are obtainable by mul-

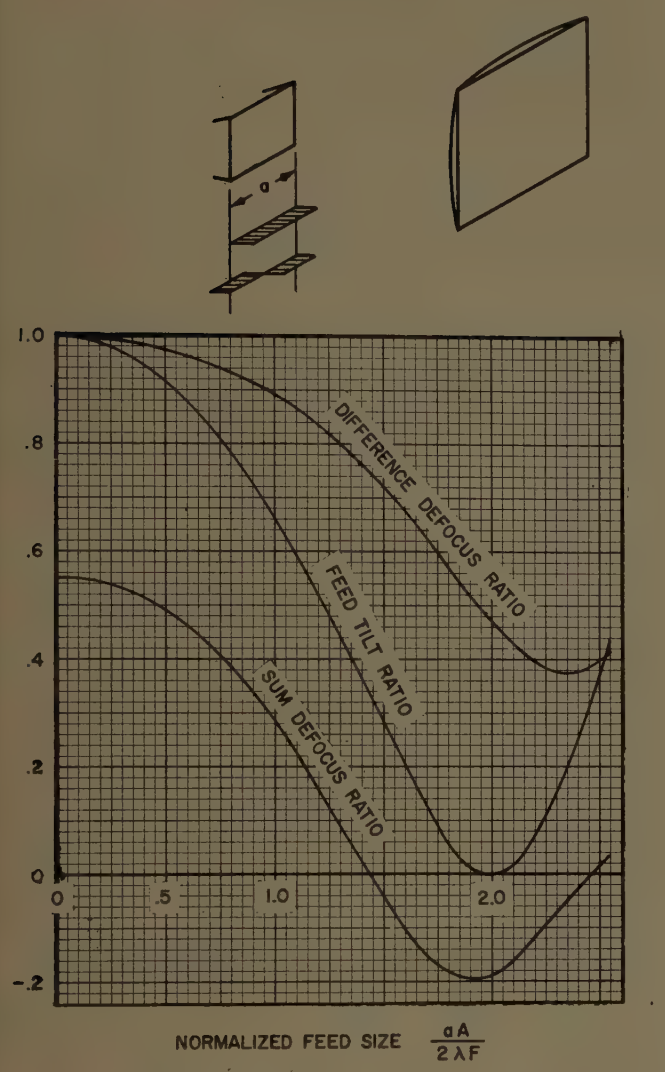

Fig. 7—Effects of misalignment on patterns vs feed size.

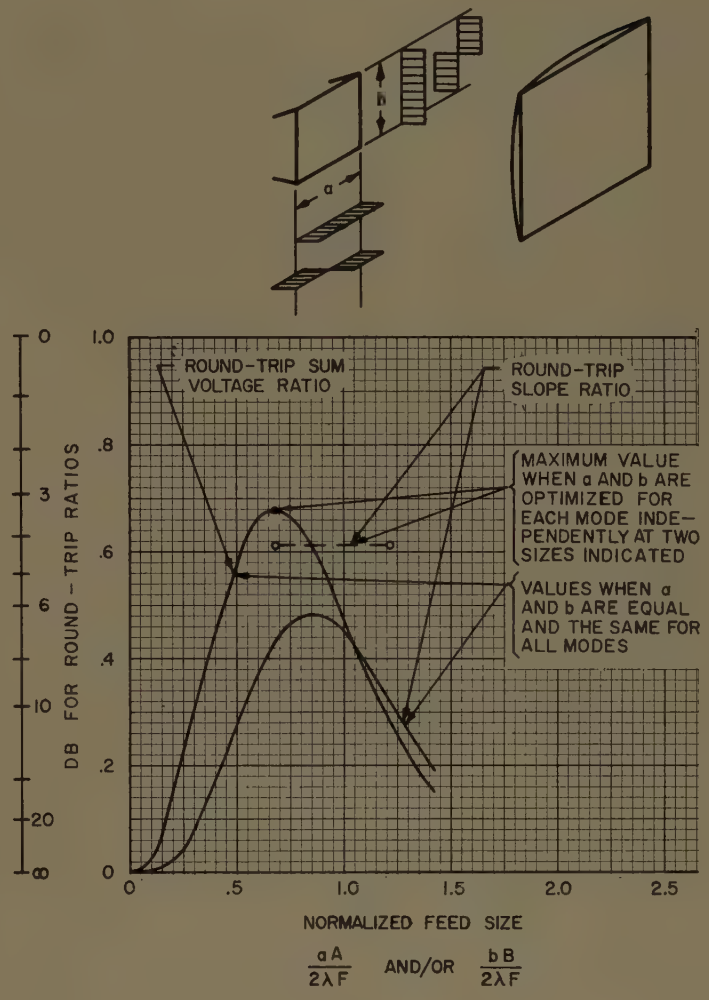

Fig. 8—Round-trip pattern characteristics vs feed size.

tiplying the one-dimensional difference-mode value in the odd plane (Fig. 6) by the appropriate one-dimensional sum-mode value in the even plane (Fig. 5). The beamwidth ratio, sidelobe ratios, and edge taper are valid for the two-dimensional case when restricted to the odd plane of the difference mode.

The curve of gain ratio reaches a maximum at a normalized feed aperture size in the difference plane of about 1.37, which is approximately twice the size for maximum sum gain. The first and second sidelobe ratios are minimum at a normalized feed size of 2.00, so an optimum size in the difference plane, considering both gain and sidelobe level, might be at about 1.60; these feed sizes also are twice those obtained for the sum mode. In the other plane, the feed aperture size would be optimized on the basis of the sum-mode curves, and would be about equal to the size obtained previously for the sum mode.

As mentioned in Section III-B, spillover may be an important contribution to sidelobes in the difference mode. It may be seen from the curve of spillover ratio that at a normalized feed size of 1.60 the spillover power is less than 1/3 of its value at a feed size of 0.80, and has been reduced to an approximate, practical minimum. Actually, as will be discussed in Section IV, a more ideal shape for the feed excitation would permit a further reduction in spillover.

There is one additional characteristic of the antenna pattern in the difference mode which is shown in Fig. 6; this is the difference slope, or the slope of the difference pattern on the axis of the antenna. This characteristic is of fundamental importance in a monopulse antenna because it determines the angle sensitivity, or the ability to accurately track the angle of a distance source under conditions in which errors may be caused by spurious signals of either an incoherent nature (receiver noise, antenna noise, etc.) or a coherent nature (plumbing asymmetries, antenna asymmetries, ground reflections, etc.). The difference slope is presented in Fig. 6 as a voltage ratio, normalized with respect to the maximum possible difference slope (see Section VII). As before, it is given for a one-dimensional geometry; the two-dimensional case may be determined for the odd plane of the difference mode by multiplying the difference

slope ratio by the square root of the sum-mode gain ratio in the other plane. It may be observed from the curve that the difference slope reaches a maximum for a normalized feed aperture size of about 1.23 in the odd plane. This is somewhat smaller than the size for maximum gain at the difference peak, but is still considerably larger than that for maximum sum gain.

Misalignment Factors: In Fig. 7 some quantities are shown which are concerned with the degradation of the monopulse characteristics caused by certain misalignments or misadjustments within the antenna. While these do not have the basic significance of the characteristics discussed so far, they are, nevertheless, of great interest to the antenna designer. One of these quantities is called the feed-tilt ratio, and indicates the amount by which the central null of the difference pattern is filled in when the feed is tilted away from the direction of the center of the main aperture. The difference-signal component thus created is in quadrature with the normal signal and does not shift the angular position of the central minimum of the difference patterns; however, as has been described elsewhere [12], it can combine with a phase difference between the channels of the plumbing or IF circuits to cause a boresight error. The feed-tilt ratio is presented here as the rate of change of spurious difference voltage with feed-tilt angle for a small amount of tilt, normalized with respect to the maximum possible value (see Section VII). Under the assumptions of Section II-B, this ratio is applicable to both a one-dimensional and a two-dimensional geometry without any reference to the other plane. In the two-dimensional case, the tilt angle to be considered is the component (see Fig. 1) in the odd plane of the particular difference mode of interest.

It is apparent from the curve of feed-tilt ratio that if the feed aperture dimension in the difference plane is small, the feed-tilt ratio is large and the feed may have to be carefully aligned to obtain good performance. However, if the normalized feed size increases to a value of 2.00, the feed-tilt ratio is zero and the alignment becomes noncritical. This is a consequence of the zero in amplitude of illumination at the edge of the main aperture; under this condition a small sideways shift of the illumination causes no significant change. (The second-order shape of the curve at this point corresponds to the second-order shape of the illumination curve, and the latter is an unusual property of the "constant" shape of difference excitation assumed at the feed aperture. A more customary shape would be predominantly first-order and would go through a reversal of sign at this point, but the noncritical property would still exist.) In many ordinary monopulse antennas, it is necessary to provide a feed-tilt adjustment because tolerances cannot be held tight enough to rely on proper alignment of the feed. If the feed aperture were enlarged toward the noncritical point, it might be possible to eliminate the feed-tilt adjustment. On the other hand, one should remember that certain errors in the comparator may also be compensated by a feed-tilt adjustment; if this is eliminated, another type of compensation may be required.

The other quantities shown in Fig. 7 describe an effect of defocusing the antenna, or of moving the feed toward or away from the main aperture. The particular effect of interest is the change of phase between the on-axis sum and difference signals. In a pure amplitude-comparison monopulse antenna, an incoming wave creates sum and difference signals which are in-phase or out-of-phase with each other at the output of an idealized comparator. If the antenna is then defocused, this phase relationship is modified, and the monopulse system becomes a mixture of amplitude-comparison and phase-comparison. As described elsewhere [13], it is desirable to keep this phase change, called the hybrid-monopulse angle, within limits. In Fig. 7, two curves are shown which are labeled difference defocus ratio and sum defocus ratio, respectively. These ratios yield the rate of a phase change with axial feed displacement for small departures from the focal point, normalized with respect to the maximum possible rate of change in the difference mode (see Section VII). The difference between the two phase changes is the hybrid-monopulse angle. Under the assumptions of Section II-B, this is applicable to both a one-dimensional and a two-dimensional geometry, without any reference to the other plane. It may be seen that by choosing certain feed aperture dimensions in the sum and difference modes, the values for the difference and sum defocus ratios can be made equal, and therefore the hybrid-monopulse angle can be made noncritical to small amounts of defocusing. The ratio of feed sizes is, however, appreciably greater than two; for instance, a sum size of 0.68 would require a difference size of about 2.09.

The properties shown in Fig. 7 may be considered together with all of those of Fig. 6 in determining an optimum size for the feed aperture in the difference mode. The size chosen will, of course, depend on the relative importance of the various properties in any particular application. In a typical case, a consideration of all the properties might give the same result as that obtained with only the first six properties in Fig. 6. Thus, the normalized feed size in the odd plane would have an optimum value of about 1.60 for the difference mode, roughly twice as great as the optimum value for the sum mode.

Round-Trip Performance: Earlier in this paper, mention was made of a compromise feed size which would provide the best performance for the ordinary situation in which the sizes cannot be different in the sum and difference modes. It is instructive to examine such a design, in order to compare it with the more ideal one in which the size for each mode may be optimized independently. For the sake of simplicity and correlation with other investigations of this subject, the optimization will be confined to two particular quantities; one is the on-axis round-trip sum voltage (sum

voltage squared) and the other is the on-axis round-trip slope (sum voltage times difference slope). Fig. 8 shows curves of these two quantities in normalized form, as a function of normalized feed aperture size, for a two-dimensional case in which the sizes are the same for the sum and both difference modes, and the hypothetical "constant" excitation is assumed for both planes.

A feed size midway between the peaks of these two curves may be chosen as representing the best compromise, and it appears that only a small degradation is obtained [3]. However, in the case of the round-trip slope curve, one factor is the one-way one-dimensional difference slope, and the latter is far from its true optimum value.

The values which the two round-trip quantities would attain when the feed size is optimized independently in the sum and difference modes are indicated in Fig. 8, by means of the black dot and the dashed horizontal line. For the round-trip slope a significant increase is thereby obtained; the actual amount is approximately 2.5 db. There would also be, of course, a marked improvement in other properties discussed previously, such as sidelobes and spillover in the difference modes. Furthermore, these latter benefits could be considerably greater if the feed size were optimized with all of these quantities in mind.

IV. Need for Efficient Shapes of Feed Excitation in Sum and Difference Modes

The preceding section has shown the desirability of allowing the feed aperture *size* to be different for the sum and difference modes. There is another aspect of the feed excitation which has an important effect on antenna performance: namely, the *shape* of the excitation. This will be illustrated by the same three viewpoints employed previously.

A. Focal Field

In Fig. 9, the field of an incoming wave in the focal region near the feed is shown. The shape of the major lobe of this field is smooth and tapers in a simple manner to zero on each side. It is natural to expect that for high gain, the shape as well as the size of the feed excitation should be similar to that of the focused field. (As a matter of interest, the "matched filter" criterion [14] could probably be employed to prove that the greatest signal is received when the shapes are identical.) By way of example, two simple hypothetical shapes of feed excitation may be considered. In Fig. 9(a), cosine and sine shapes are shown for the sum and difference modes, respectively. Since these closely approximate the shape of the major lobe of the focal field, the gain should be close to the maximum obtainable by complete utilization of this major lobe. In Fig. 9(b), double-cosine shapes are shown; here the gain should be significantly reduced because of the dissimilarity in the region of the "holes" between the double cosines. It might also be added that this situation is characterized by an inherent reflection of the incoming wave by the feed, and the reflected power is capable of causing additional deficiencies in the performance of the antenna [15].

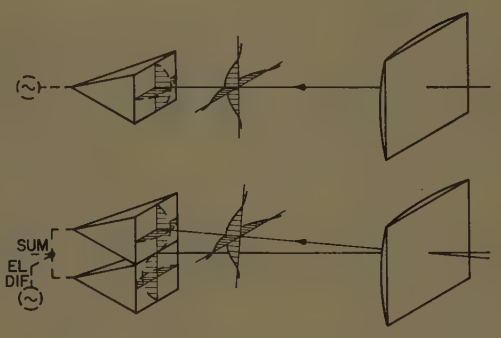

(a) An efficient set of shapes.

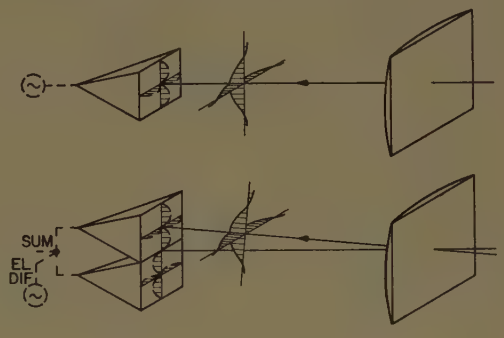

(b) An inefficient set of shapes.

Fig. 9—Comparison of feed-excitation shapes; focal-field viewpoint.

B. Main Aperture Illumination

Fig. 10 presents the viewpoint which evaluates the illumination of the main aperture, and the same examples of feed-excitation shapes are considered. With the cosine and sine shapes illustrated in Fig. 10(a), the radiation pattern of the feed has low sidelobes, and the power wasted in spillover beyond the edges of the main aperture is minimized. With the double-cosine shapes illustrated in Fig. 10(b), the sidelobes of the feed pattern are high, and it becomes necessary to waste an appreciable amount of power in spillover. Thus it is evident that the former shapes are more efficient than the latter; in addition, the excess spillover existing in the latter case may aggravate certain problems, as mentioned in Section III-B.

C. Antenna Pattern Characteristics

The final viewpoint, given in Fig. 11, presents quantitative values for a few particular properties of the antenna pattern. These properties are gain ratio in the sum mode, slope ratio in the difference mode, and the spillover ratios for both modes, for those particular feed sizes which yield maximum gains or slopes, as indicated. The values are given for a one-dimensional case; as before, two-dimensional results are obtainable by multiplying together the proper one-dimensional values.

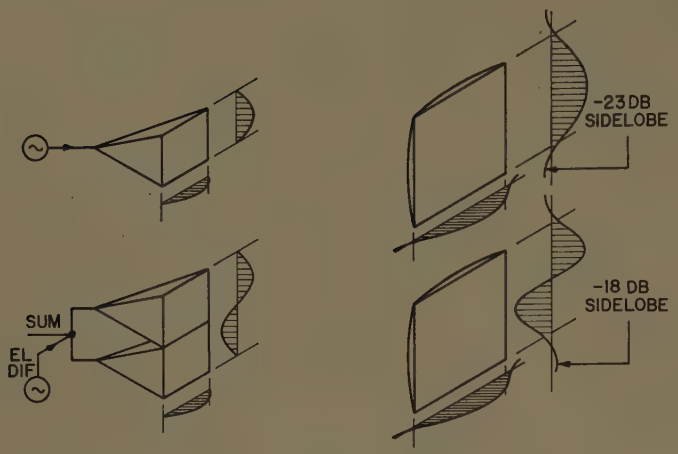

(a) An efficient set of shapes.

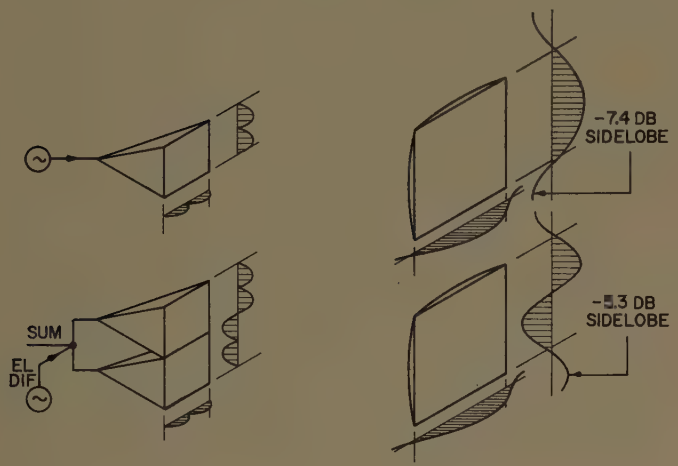

(b) An inefficient set of shapes.

Fig. 10.—Comparison of feed-excitation shapes; illumination viewpoint.

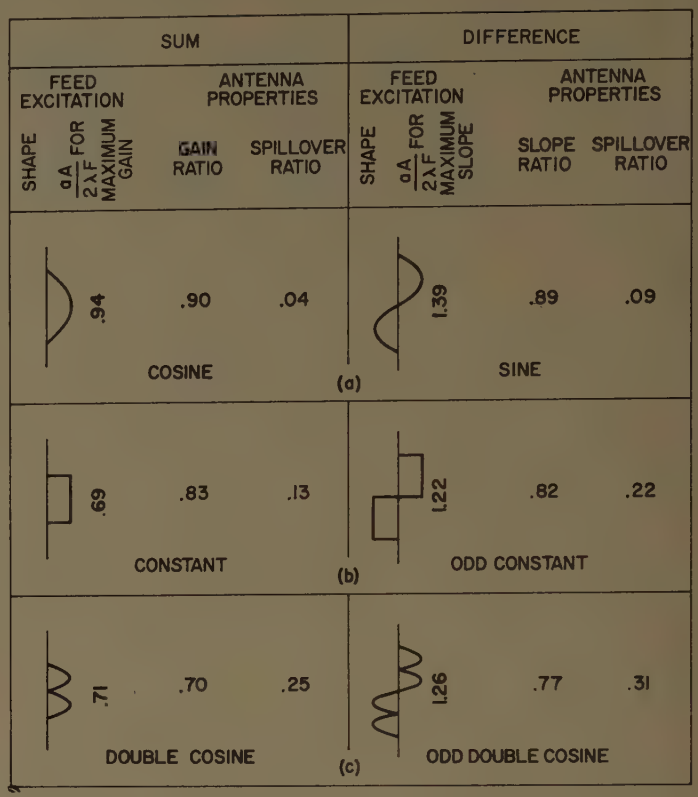

Fig. 11—Antenna-pattern characteristics for various shapes of feed excitation.

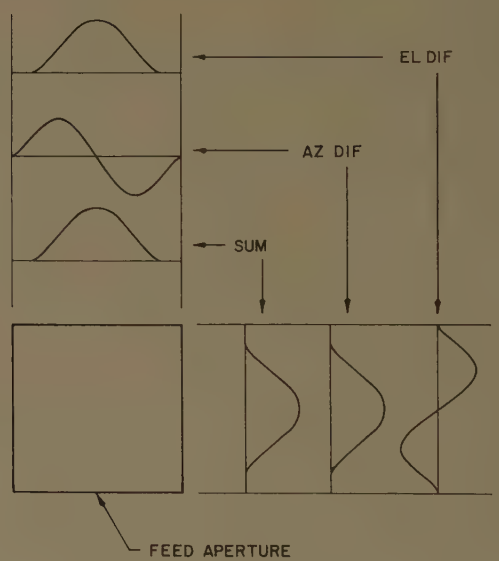

Fig. 12—An ideal feed excitation.

Three examples are chosen to illustrate the effect of shape of feed excitation; these are the single and double cosine and sine types mentioned just previously, plus the constant types. It is apparent that the single sine and cosine shapes (a) are the best and the double-cosine shapes (c) are the worst, while the constant shapes (b) are intermediate between these two. The differences among the various results are large enough to have a significant effect on antenna performance. For example, in going from the double shapes (c) to the single shapes (a), in only the one dimension, there is an increase of 1.1 db in sum gain (see also [2]) and 1.3 db in difference slope, and a reduction by a factor of 0.16 in sum spillover and 0.28 in difference spillover. These spillover reductions would be even more striking if a larger feed size had been chosen.

V. An Ideal Feed Excitation

In Fig. 12, an "ideal" feed excitation is shown in two dimensions, for all three modes. This is not to be regarded as a unique ideal, but rather as a typical one representing a kind of composite of the previously-discussed concepts. For example, the difference excitations are about twice as wide in the odd planes as are the effective sum excitations, and the shapes of the excitations are free of any avoidable irregularities. If a feed were designed to have all these features, the resulting antenna performance should be very close to optimum in all three modes of the monopulse antenna.

VI. Discussion

It is instructive to estimate the improved performance obtainable with a feed such as that shown in Fig.

12. Suppose that an ordinary feed had an effective normalized size of 0.80 in both planes and all three modes, and that with the new feed this size becomes 1.60 in the odd plane of the difference modes. Suppose further that the ordinary feed had shapes of excitation which were double cosine by constant for the even types and sine by odd constant for the odd. The curves and tables in this paper may now be employed to estimate the improvement, in terms of the complete two-dimensional quantities.

In the sum mode the gain should increase by about 1.4 db and the spillover ratio should (it is estimated) be reduced from about 0.3 to less than 0.03. These changes are a result of the improved excitation shape. In the difference modes the peak gains should be increased by an average of about 3.5 db and the slopes by an average of about 1.9 db, while the spillover ratio should (it is estimated) be reduced on the average from about 0.5 to less than 0.05. These changes are mainly a result of the doubled feed size in the odd planes.

The first sidelobe ratios in the difference modes should go from about 10.5 db to about 23.7 db, because of the doubled feed sizes. This 13-db improvement may be complemented by an improved suppression of the far sidelobes of about 10 db in all the modes, as a consequence of the spillover reduction. Finally, the criticalness of positioning the feed should be reduced to about $\frac{1}{4}$ in tilt and about $\frac{1}{2}$ in focusing, because of the doubled feed sizes.

The analysis in this paper has been confined to a rectangular or square main aperture. Although no calculations have been made for a circular aperture, it is believed that somewhat more improvement in difference gain, slope, and spillover, and somewhat less improvement in the near difference sidelobes, would be obtained. It is concluded, therefore, that for any amplitude-monopulse antenna involving a large feed and a focusing element, a feed excitation such as that shown in Fig. 12 should provide significantly better performance than can be obtained with an ordinary monopulse feed.

VII. Definitions

Gain Ratio:

For the sum mode, gain ratio is the on-axis antenna gain relative to the maximum possible gain. The latter, reference gain, is that gain which would be obtained if the main aperture were uniformly illuminated with no spillover. (An alternate term for gain ratio which is often used for microwave antennas is "efficiency".) Normally, the on-axis sum gain is also the peak gain; for the range of feed sizes where this is not true, the peak gain is also shown by means of a dashed addition to the curve in Fig. 5.

For the difference mode, gain ratio is the antenna gain at the peak of the difference pattern relative to the maximum possible sum gain. (The above definition of difference gain ratio employs the maximum possible sum gain as the reference quantity because this allows one to compare difference gain with sum gain directly on the graphs. It would also be possible to define difference gain ratio employing the maximum possible difference gain [16] as the reference quantity; in this case the difference gain ratio would be greater than that given on the curve in Fig. 6 by the factor 1/0.609, or 2.15 db.)

Spillover Ratio:

For each mode, spillover ratio is the ratio of power radiated by the feed into the region outside the edges of the main aperture, to total power radiated by the feed. (Spillover is likely to contribute to sidelobes in the antenna radiation pattern.)

Edge Taper:

For each mode, edge taper is the ratio of voltage at the edge of the main aperture to the maximum voltage on the main aperture, when the main aperture is illuminated by the feed. (In the case of the difference mode, a small feed may radiate a pattern whose peak is outside the edge of the main aperture; in this case the value of the edge voltage relative to the peak radiated voltage is indicated by the dotted portion of the curve in Fig. 6.)

Sidelobe Ratio:

For each mode, the sidelobe ratio is the ratio of voltage at the peak of the designated sidelobe of the antenna radiation pattern to the peak voltage of the main lobe of the same antenna pattern. The sidelobe ratios are calculated directly from the main aperture illumination without including any effect of spillover.

Beamwidth Ratio:

For the sum mode, the beamwidth ratio is the angle between half-power points of the antenna pattern with a specified feed size, relative to the angle with a very small feed (*i.e.*, uniform illumination of the main aperture). In the latter, reference case, the angle is $0.887\ \lambda/A$ radians.

For the difference mode, the beamwidth ratio is the angle between the outer half-power points of the antenna pattern with a specified feed size, relative to the angle with a very small feed (*i.e.*, odd, linear illumination of the main aperture). In the latter, reference case, the angle is $2.03\ \lambda/A$ radians.

Difference Slope:

Slope of the center of the antenna pattern in the difference mode, assuming no asymmetries. In other words, rate of change of the difference voltage with antenna angle, where the angle is small and the difference voltage contains no quadrature components.

Relative Difference Slope:

Difference slope relative to maximum possible sum voltage.

Difference Slope Ratio:

Ratio of the difference slope to the maximum possible difference slope. The latter could be obtained if the main aperture were illuminated by an odd, linear voltage pattern [17], [18] with no spillover; in this reference case the relative difference slope (see previous definition) would be $\pi A/\sqrt{3}\ \lambda$ voltage ratio per radian.

Feed-Tilt Ratio:

The rate of change of the on-axis difference signal with feed-tilt angle, where the amount of feed tilt is small, relative to the rate of change which would be obtained with any very small feed (*i.e.*, odd, linear illumination of the main aperture). In the latter, reference case, the rate of change of difference signal with feed-tilt angle, if taken relative to the difference slope, would be $6\lambda F/\pi A^2$.

Difference Defocus Ratio:

The rate of change of phase of the near-axis difference signal with axial displacement of the feed in wavelengths, where the phase change is caused only by the phase curvature across the main aperture resulting from a small amount of displacement of the feed from the focal point, relative to the rate of change which would be obtained with a very small feed (*i.e.*, odd, linear illumination of the main aperture). In the latter, reference case, the rate of change of difference phase with axial feed displacement in wavelengths is $3\pi A^2/20F^2$ radians.

Sum Defocus Ratio:

The rate of change of phase of the on-axis sum signal with axial displacement of the feed in wavelengths, where the phase change is caused only by the phase curvature across the main aperture resulting from a small amount of displacement of the feed from the focal point, relative to the rate of change which would be obtained with a very small feed operating in the difference mode (*i.e.*, odd, linear illumination of the main aperture). (The above definition employs the small-feed rate of change in the difference mode as the reference quantity because this simplifies the calculation of the hybrid monopulse angle. It would also be possible to define the sum defocus ratio employing the small-feed rate of change in the sum mode as the reference quantity; in this case the sum defocus ratio would be greater than that given on the graph by the factor 9/5, as indicated.

Round-Trip Sum Voltage Ratio:

The round-trip sum voltage ratio is the square of the on-axis sum-pattern voltage, relative to the maximum possible value. The latter, reference value, would be obtained if the main aperture were uniformly illuminated with no spillover. For the two-dimensional square case given in Fig. 8, the round-trip sum voltage ratio is equal to the square of the one-dimensional sum gain ratio given in Fig. 5.

Round-Trip Slope Ratio:

The round-trip slope ratio is the product of on-axis sum-pattern voltage and on-axis difference slope, relative to the maximum possible

value. The latter, reference value, could be obtained if the main aperture had uniform illumination with no spillover in the sum mode and in the even plane of the difference mode, and had odd, linear illumination with no spillover in the odd plane of the difference mode. For the two-dimensional square case given in Fig. 8, the round-trip slope ratio is equal to the 3/2 power of the one-dimensional sum gain ratio given in Fig. 5 times the difference slope ratio given in Fig. 8.

VIII. Acknowledgment

R. L. Mattingly has been principally responsible for the direction of this effort by Bell Telephone Laboratories, and the author would like to express his appreciation for the encouragement he has given it.

At Wheeler Laboratories, this work has been directed by H. A. Wheeler, D. Dettinger, N. A. Spencer, and P. A. Loth. The author would like to acknowledge the cooperation of the Wheeler staff in the preparation of this paper, especially H. A. Wheeler, H. W. Redlien, and D. S. Lerner for their helpful comments and suggestions, S. I. Warshaw and B. J. Karafin for their computational effort, and C. J. Stona for his work on the illustrations.

IX. Bibliography

[1] C. C. Cutler, "Parabolic-antenna design for microwaves," Proc. IRE, vol. 35, p. 1286; November, 1947.
[2] J. W. Crompton, "On the optimum illumination taper for the objective of a microwave aerial," *Proc. IEE*, vol. 101, Pt. 3, (also see ASTIA Doc. No. AD 12571); November, 1954.
[3] M. L. Kales, "Optimum Design Criterion for Simultaneous-Lobing Antennas," Naval Res. Lab., unpublished Rept. R-3451, ASTIA Doc. No. ATI 61934, pp. 18–24; April, 1949.
[4] D. R. Rhodes, "Introduction to Monopulse," McGraw-Hill Book Co., Inc., New York, N. Y., pp. 98–101; 1959.
[5] R. M. Page, "Monopulse Radar," 1955 IRE National Convention Record, pt. 8, pp. 132–134.
[6] J. F. P. Martin, Bell Telephone Labs., unpublished Memo. No. MM-47-2730-7; January, 1947.
[7] H. W. Redlien, "A Unified Viewpoint for Amplitude and Phase Comparison Monopulse Tracking Radars," Wheeler Labs., unpublished Rept. No. 845 to Bell Telephone Labs.; March 1959.
[8] P. A. Matthews and A. L. Cullen, "A study of the field distribution at an axial focus of a square microwave lens," *Proc. IEE*, vol. 103, Pt. C, pp. 449–456; July, 1956.
[9] P. W. Hannan, "Principles of Feed Design for Optimum Performance in All Three Modes of an Amplitude-Monopulse Radar Antenna," Wheeler Labs., unpublished Rept. No. 884; August, 1960.
[10] J. F. Ramsay, "Fourier transforms in aerial theory—part II, Fourier sine transforms," *Marconi Rev.*, vol. 10, pp. 17–22; January-March, 1947.
[11] B. Berkowitz, "Antennas fed by horns," Proc. IRE, vol. 41, pp. 1761–1765; December, 1953.
[12] H. W. Redlien, "Theory of Monopulse Operation—Introduction," Wheeler Labs., unpublished Rept. No. 434B to Bell Telephone Labs., (also ASTIA Doc. No. AD 305996); January, 1953.
[13] H. W. Redlien, "Theory of Monopulse Operation—Effects of a Defocused Antenna," Wheeler Labs., unpublished Rept. No. 495A to Bell Telephone Labs., (also ASTIA Doc. No. Ad 59288); August, 1953.
[14] J. H. Van Vleck and D. Middleton, "A theoretical comparison of visual, aural, and meter reception of pulsed signals in the presence of noise," *J. Appl. Phys.*, vol. 17, pp. 943–944; November, 1946.
[15] P. W. Hannan, "Reflections in microwave antennas and their harmful effects," 1954 IRE National Convention Record, pt. 1, pp. 39–45.
[16] P. W. Hannan, "Maximum gain in monopulse difference mode," IRE Trans. on Antennas and Propagation, vol. AP-9, pp. 314–315; May, 1961.
[17] G. M. Kirkpatrick, "Aperture illuminations for radar angle-of-arrival measurements," IRE Trans. on Aeronautical and Navigational Electronics, vol. AE-9, pp. 20–27; September, 1953.
[18] G. M. Kirkpatrick, General Electric Co., unpublished report, ASTIA Doc. No. AD 18458, pp. 13–15; August, 1952.

Optimum Feeds for All Three Modes of a Monopulse Antenna II: Practice*

PETER W. HANNAN†, SENIOR MEMBER, IRE

Summary—**In an amplitude-monopulse antenna whose main aperture is illuminated by a feed, it is desired to control the feed excitation independently in the sum, azimuth difference, and elevation difference modes. It is possible to describe a feed system, comprising an infinite array of radiators and hybrid junctions, which demonstrates the principle of complete independent control of the three modes.**

There are several practical feeds which approach a hypothetical ideal one in varying degrees. One representative type is the "twelve-horn feed;" although it has some disadvantages, it is versatile and quite useful. However the most attractive type for many applications appears to be one having a combination of multiple-horn excitation in one plane and multimode-waveguide excitation in the other. With a simple form of the "multihorn-multimode" feed, the ideal is substantially realized, and a major improvement in monopulse performance can be obtained.

* Received by the PGAP, November 22, 1960; revised manuscript received, March 27, 1961. The material in this paper is the result of antenna development work for the Bell Telephone Laboratories on Army Ordnance Corps projects. Preparation of this paper has been supported mainly by a subcontract with BTL in connection with prime contract No. DA-30-069-ORD-1955.

† Wheeler Labs., Smithtown, N. Y.

I. Introduction

In a previous paper [1] a study was made of the improved performance available in an amplitude-monopulse radar antenna comprising a feed and a focusing element. This improvement arises from the possibility of independently optimizing the feed in each of the three modes of operation, rather than compromising between them. There was presented a hypothetical "ideal" feed excitation which would essentially optimize all three modes, but no information was given regarding the attainment of such a feed. It is the purpose of this paper to discuss the means by which this theoretical feed may be reduced to practice.

Some early monopulse antennas have already obtained improved performance by reducing the amount of compromise between the modes. This has often occurred as a fortunate by-product of a feed design intended mainly to achieve some other benefit, such as shielding from nearby objects, a simple comparator structure, or a short focal length. As a result, the optimizing process has not usually been complete. Antennas known to the writer which belong in this category have been developed by Bell Telephone Laboratories [2], North American Aviation Company, Hughes Aircraft Corporation [3], and Radio Corporation of America [4].

About seven years ago, Wheeler Laboratories made an investigation of this problem, in connection with the design of a monopulse tracking antenna [5], [6], for Bell Telephone Laboratories. A principle was conceived and a number of design techniques were worked out for feeds which would give optimum performance in all three modes. The principle was subsequently applied in a study by Wheeler Laboratories, in which the basic merits of the amplitude and phase types of comparison were analyzed and compared [7].

An investigation of feeds for optimum monopulse performance has occupied the attention of several other groups. In the first published material known to the writer [8], the principle was recognized and experiments made with a particular technique which approaches optimum performance in more than one mode. A number of interesting techniques have been studied at Naval Research Laboratory and General Electric Company. A feed [9] for use in an operational antenna has been developed by Lincoln Laboratory which applies the principle to all three modes of operation.

Several additional monopulse tracking antennas have been designed by Wheeler Laboratories for Bell Telephone Laboratories. Some of these antennas [10] incorporate feeds which have achieved substantially optimum performance in all three modes of operation. While it is not proposed to describe the details of their design and measured performance in this paper, it is possible to present the basic methods which are involved. Various techniques will be discussed, and a comparison of their performance will be calculated.

II. Principle of Independent Control of Excitation in the Sum and Difference Modes

It is interesting to inquire whether an excitation of the ideal type is theoretically realizable. Ordinary methods of exciting a feed yield distributions which are limited to having the same width in all modes, and having shapes which are good for one mode but not for another. Upon consideration of the problem, it becomes evident that *independent control* of the excitation in the sum and difference modes is required to fulfill the objectives.

Fig. 1 presents a scheme which, in principle, is capable of achieving any degree of independent control which may be desired. As shown, the feed aperture is divided into many small sections, and each section is excited independently in the sum, azimuth difference, and elevation difference modes. The amplitude of each excitation is determined by the amount of coupling existing in the appropriate coupling element of the appropriate distribution network, while the necessary even or odd character of the excitation is provided by the series of hybrid junctions comprising the comparison network.[1]

It should be mentioned that any undesired irregularities or ripples in the excitation caused by a nonuniform field of an individual radiator can be effectively smoothed by making the spacings small compared to a wavelength. Of course the problems of impedance of the radiators, as well as coupling between radiators, would be very considerable. However, in principle, these problems could be solved.

Since the above scheme enables an ideal feed excitation to be approximated as closely as is desired, it may be stated that such an excitation is *theoretically realizable.*

Actually, the degree of independent control provided by the scheme of Fig. 1 is more extensive than that required to achieve the "ideal" excitation previously [1] indicated. In that case, the excitation was shown as being the product of the horizontal and vertical distributions, and the sum distribution was assumed to be utilized for the even plane of the difference mode. The scheme of Fig. 1, while capable of providing both these features, is not limited to doing so.

III. Practical Methods for Achieving Independent Control of Excitation

The scheme shown in Fig. 1 is theoretically able to provide independent control of excitation in the three

[1] This scheme demonstrates independent control not only for a feed in a focusing type of antenna, but also for an array type of antenna [7]; in the latter case independent control of the monopulse modes is also desirable. An alternate scheme for independent control of a practical array has been suggested by Mattingly [11].

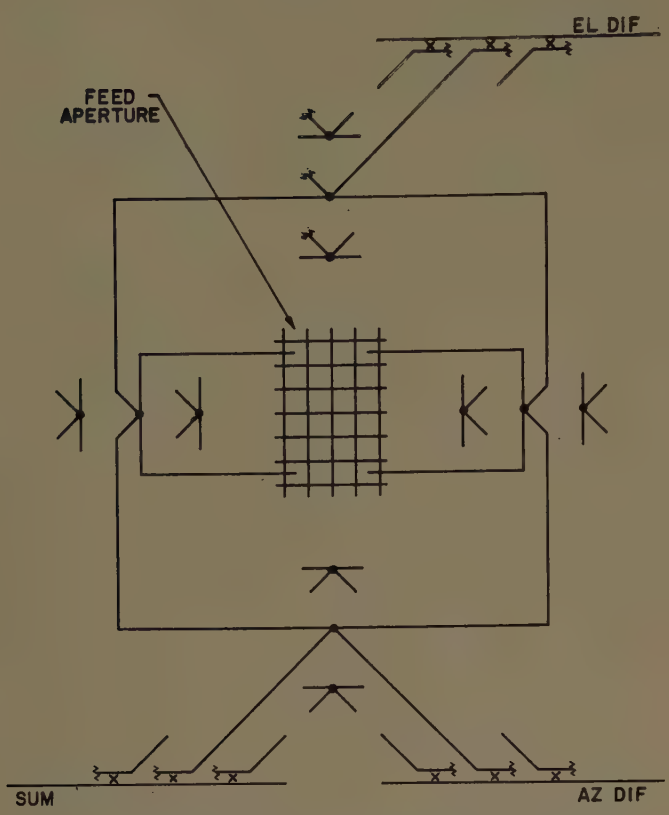

Fig. 1—A scheme for demonstrating complete independent control of the sum and both difference modes.

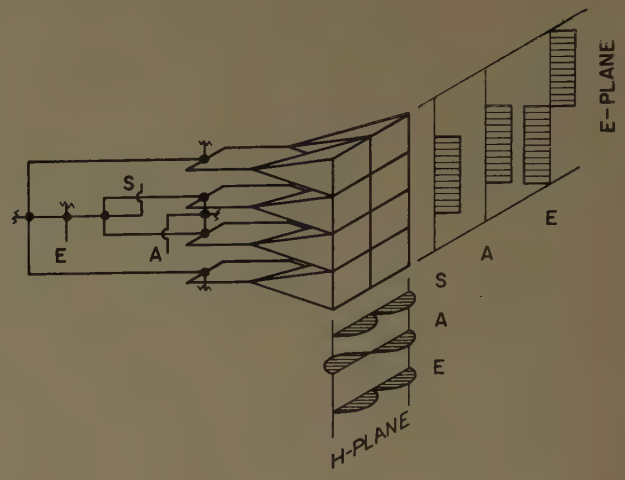

(a) Eight-horn feed for control in E plane.

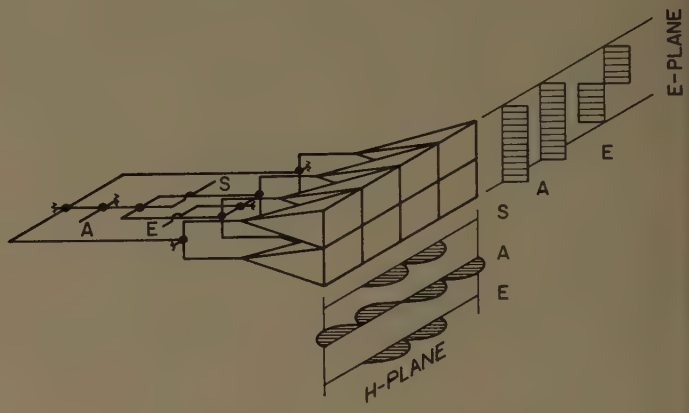

(b) Eight-horn feed for control in H plane.

Fig. 2—Single-plane multihorn feeds.

modes of operation. However, the large number of closely-spaced apertures and the multitude of circuits imply a low probability for achieving a satisfactory working design with a reasonable amount of effort. It is natural, therefore, to investigate some simpler schemes which may be more practical to develop, even though their feed excitations are not completely ideal.

There are two techniques which are considered here: one is termed the multihorn method and the other is called the multimode method. As an introduction, these techniques are first presented for the case in which independent control is the objective in the sum mode and *only one* difference mode, *i.e.*, control in only one plane. For simplicity, it will be assumed that the azimuth and elevation planes correspond to the H and E planes, respectively.

A. Single-Plane Multihorn Feeds

In Fig. 2, the multihorn method is illustrated, for either E-plane or H-plane control of 8 horns. Also shown is a network of hybrid junctions which would properly excite these horns. It is evident that in the plane of control, the desired two-to-one width of excitation is available. The shapes, however, are not ideal, particularly in the H plane. (This defect is also present in an ordinary four-horn cluster having no independent control.) Naturally, the two-to-one width cannot be obtained in the plane that lacks independent control, so that this feed would be far from optimum in a system requiring all three monopulse modes.

B. Single-Plane Multimode Feeds

Fig. 3 illustrates the multimode method, for either E-plane or H-plane control of two horns by means of three waveguide modes. (The terms "multimode method" and "waveguide modes" refer to the natural modes of propagation in a waveguide or horn; this should not be confused with the three so-called modes of operation, which are the sum, azimuth difference, and elevation difference modes.) Also shown in the figure are the two waveguide-mode combinations which in this case were chosen for the even excitation. As before, the desired two-to-one width of excitation is available in the plane of control. In addition, the shape of the sum mode in the plane of control is rather good. Some of the other shapes, however, are not ideal, especially those existing in the case of E-plane control. Again, of course, the two-to-one width cannot be obtained in the plane that lacks independent control, so that this feed would also be far from optimum in a system requiring all three modes of monopulse operation.

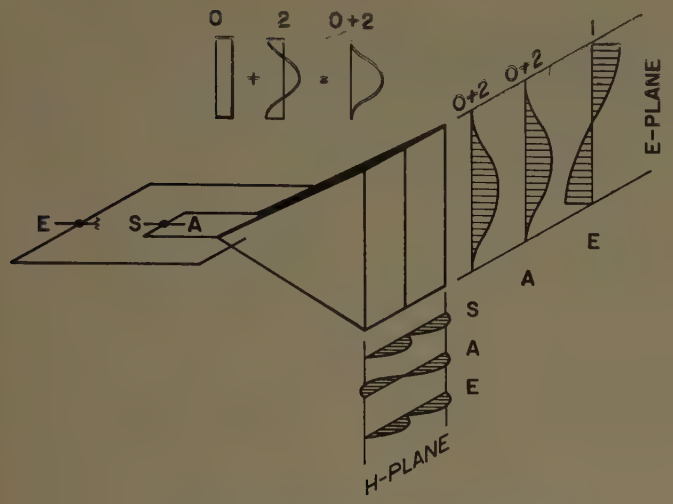

(a) Triple-mode feed for control in *E* plane.

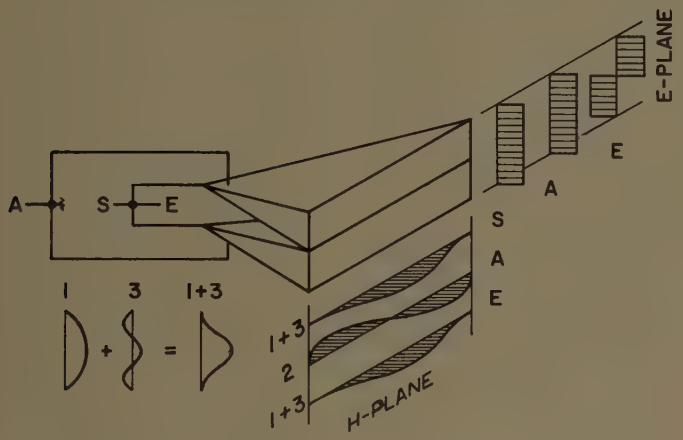

(b) Triple-mode feed for control in *H* plane.

Fig. 3—Single-plane multimode feeds.

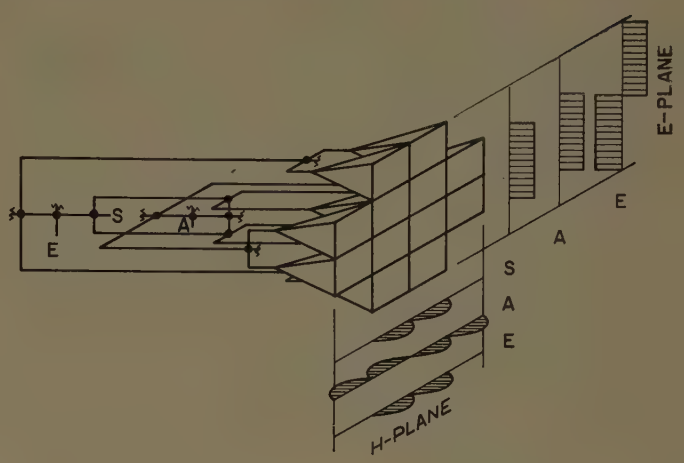

(a) Twelve-horn feed.

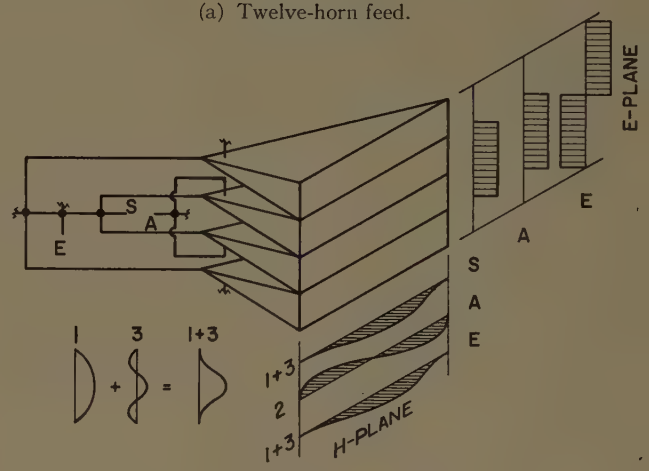

(b) Four-horn triple-mode feed.

Fig. 4—Dual-plane feeds.

C. Dual-Plane Multihorn Feed

Now consider the application of these methods towards obtaining independent control in the sum mode and *both* difference modes. Fig. 4(a) shows a multihorn method for the case of twelve horns, together with an appropriate network of hybrid junctions. In this case the desired two-to-one widths of excitation are available in both planes, but again, the shapes of excitation fall short of the ideal. It is interesting to note that this multihorn configuration is basically similar to the scheme of Fig. 1; however, the limited number of apertures and lack of amplitude control prevent complete optimization from being realized. On the other hand, a very substantial improvement in performance would be gained in comparison to the ordinary four-horn cluster; this will be illustrated quantitatively in a later section of this paper.

It should be realized that there are a number of other multihorn configurations available. For instance, the partitions in the outer eight horns of the twelve-horn feed may be removed to yield an eight-horn feed. This would give somewhat better performance in the elevation difference mode and would eliminate four hybrid junctions. However, these advantages would have to be weighed against the more complicated excitation shapes that would exist in such a feed. Another configuration would involve the addition of partitions or more horns to the twelve-horn feed. This would permit a closer approach to the scheme of Fig. 1, thereby allowing more complete optimization; however, the physical structure would become more complex.

D. Dual-Plane Multimode Feed

Having combined the single-plane multihorn methods of Fig. 2 into the dual-plane multihorn configuration of Fig. 4(a), it is natural to ask whether the multimode methods of Fig. 3 can be similarly combined. On investigation of this question, one concludes that, while there is no apparent theoretical limitation on such a process, it is quite unattractive because of the practical difficulties involved in properly controlling the many waveguide modes required. In addition, the elevation difference mode would still have a rather poor shape, unless even more waveguide modes were employed. However, it is of interest to note that a hypothetical

scheme employing an unlimited number of waveguide modes would provide an approach to complete independent control leading to the same theoretical conclusions as did the scheme of Fig. 1.

E. Dual-Plane Multihorn-Multimode Feed

There are still further combinations available among the methods presented in Figs. 2 and 3; these combinations involve a multihorn method in one plane and a multimode method in the other. Fig. 4(b) presents such a case, in which the better plane of each method has been retained. The result is a feed excitation in which not only are the desired two-to-one widths available in both planes, but the shapes are effectively ideal in the *H* plane and depart only a moderate amount from the ideal in the *E* plane.

The feed as shown comprises four identical horns, each utilizing three waveguide modes. As might be expected, there are a number of alternate multihorn-multimode configurations which might be considered. For instance, the outer two horns might be reduced in width and excited with only the 1-mode; this would reduce the physical size of the feed at the expense of a somewhat more complicated set of excitation shapes. Another example involves the use of more than the four horns shown, thereby permitting greater control of the excitation in the *E* plane. This would allow a closer approximation to the ideal shapes, at the expense of a more complex excitation network.

Returning to the simple configuration shown in Fig. 4(b), it is interesting to mention the factors relating to its usefulness in a real antenna system. As regards the practicability of this scheme, it may be noticed that the configuration of the hybrid network is less complex than that of Fig. 4(a), and is confined essentially to a single plane. The generation of the proper waveguide modes is certainly a problem of design; however, these modes lend themselves to techniques which are quite feasible, and can yield results very close to the ideal. Thus the "multihorn-multimode" method appears to be most attractive as a practical scheme for realizing almost completely the benefits obtainable with independent control of the sum and both difference modes.

IV. Comparison of Performance for Several Practical Feeds

It is instructive to compare a few practical feeds on a quantitative basis. Fig. 5 presents such a comparison, based on calculated values for three properties: sum gain ratio, difference slope ratio, and spillover ratio. For simplicity, the size and the mode ratio of each feed is chosen to yield maximum sum gain; as discussed in the previous paper [1], this is a somewhat smaller size

FEED EXCITATION WITH $\left(\frac{aA}{2\lambda F}\right.$ OR $\left.\frac{E_3}{E_1}\right)$ AND $\left(\frac{bB}{2\lambda F}\right)$ FOR MAXIMUM SUM GAIN	SUM		AZ DIF		EL DIF	
	GAIN RATIO	SPILLOVER RATIO	SLOPE RATIO	SPILLOVER RATIO	SLOPE RATIO	SPILLOVER RATIO
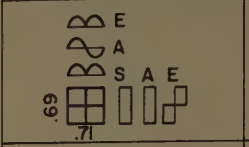	.58	.34	.52	.72	.48	.76
			(a) FOUR-HORN			
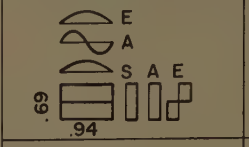	.75	.16	.68	.50	.55	.69
			(b) TWO-HORN DUAL-MODE			
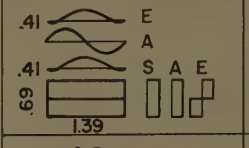	.75	.17	.81	.20	.55	.69
			(c) TWO-HORN TRIPLE-MODE			
	.58	.34	.71	.37	.67	.38
			(d) TWELVE-HORN			
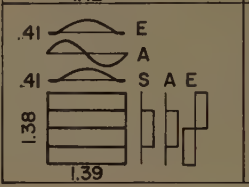	.75	.17	.81	.20	.75	.22
			(e) FOUR-HORN TRIPLE-MODE			

Fig. 5—Antenna-pattern characteristics for various practical feeds.

than that which might be chosen as an optimum when several properties are considered. As a result, the listed gains and spillovers are somewhat greater than they might be in a more typical case. Furthermore, the slopes turn out to be appreciably different from those which would be obtained with a larger feed. The assumptions made regarding a rectangular aperture, a large feed in wavelengths, etc.,[2] are the same as were made in the previous paper, and all the definitions and symbols are the same. The values listed are the complete two-dimensional quantities, as obtained by multiplying together the proper one-dimensional values. As before, it is assumed that the azimuth and elevation planes correspond to the *H* and *E* planes, respectively.[3]

[2] Since practical antenna defects (aperture blocking, reflections, cross-polarization, "space-attenuation," dissipation, tolerances, etc.) are neglected, the listed gains and slopes are likely to be higher than the values encountered in actual practice. On the other hand, the assumed large feed in wavelengths may have somewhat more spillover loss, and hence less gain, than one about a wavelength in size, particularly in those cases involving poor shapes of excitation.

[3] In the case of feeds giving lower spillover in the *H* plane than in the *E* plane, the harmful effects of the ground might be minimized by reversing this assumption.

A. Four-Horn Feed

The ordinary four-horn cluster is shown in Fig. 5(a). This has, of course, the defects associated with an excessively narrow difference excitation and the poor double-cosine shape for the H-plane even excitation. The main virtue of this feed appears to be its conceptual simplicity [5], [6], including its susceptibility to the historical lobing method of analysis. It also has a relatively small aperture size.

B. Two-Horn Dual-Mode Feed

In Fig. 5(b), another common feed is shown; in this type the E-plane partition, present in the four-horn cluster, has been removed. This allows two waveguide modes to propagate, and the H plane is characterized by a single cosine for the even excitation and a sine for the odd excitation. The single cosine is not only an efficient shape, but its effective width is narrower than that of a double cosine of the same over-all dimensions. As a consequence, the over-all feed-aperture size in the H plane can be increased, thereby allowing the azimuth-mode excitation to widen toward the desired value. However this width falls short of the ideal two-to-one difference-to-sum condition, and no further improvement can be made with only the two modes which are available. In addition, of course, the elevation-mode excitation remains too narrow. This type of feed [12] has found most use [3] in applications which place a premium on a simple mechanical structure and relatively short focal length.

C. Two-Horn Triple-Mode Feed

In Fig. 5(c) the feed shown in Fig. 3(b) is analyzed. Here the H-plane dimension of the feed has been set to maximize the difference slope, and then the mode ratio of the even excitation (E_3/E_1) has been set so that the sum gain is also maximized. While the performance in the sum and azimuth difference modes is excellent, that in the elevation difference mode, of course, remains poor. This type of feed is most helpful in applications [4] which require a very short focal length; it is believed that RCA was the first to incorporate the triple-mode technique in a monopulse antenna.

It is evident that the feeds of both Part B and Part C suffer from lack of independent control in the elevation plane. It should be noted that in certain antenna applications there may also be a problem caused by the different antenna patterns which would occur in the azimuth and elevation planes. These defects are virtually eliminated by the incorporation of independent control in both planes. The two practical feeds which achieve this are to be shown in Part D and Part E.

D. Twelve-Horn Feed

In Fig. 5(d) the feed shown in Fig. 4(a) is analyzed. Here the dimensions of every horn are chosen to be identical, for simplicity and ease of calculation. This happens to yield the two-to-one width condition, so with the size set to maximize sum gain, the difference slope is fairly close to the maximum value obtainable with this feed. As expected, the performance is good in all three modes, but is still somewhat less than optimum because of the inefficient shape of the feed excitation in the H plane. In many applications, this defect, together with the complexity of the circuitry, would tend to limit the attractiveness of the twelve-horn feed. On the other hand, it may be the only possible solution in some cases. One such case might be a diversity-polarization antenna using dual-polarized horns; perhaps another case is a low-frequency antenna in which a dipole feed array must replace the horn array. There are other, special uses for independent control in monopulse antennas where the twelve-horn method may be the most practical solution.[4] It is believed that the twelve-horn method was first employed by Lincoln Laboratory in a feed [9] developed for a versatile monopulse antenna.

E. Four-Horn Triple-Mode Feed

In Fig. 5(e) the feed shown in Fig. 4(b) is analyzed. Here the H-plane dimensions and mode ratios are set as they are in Part C, and the E-plane dimensions as in Part D. It is evident that this feed yields the best performance in all three modes when compared with any of the others. Furthermore, the performance is rather close to that obtainable with the "ideal" feed [1].

The numerical results given in Fig. 5 illustrate the advantages to be gained with a practical form of independent control. In going from the ordinary four-horn cluster to the four-horn triple-mode feed, for instance, the sum gain has increased by 1.1 db and the difference slopes have increased by 3.9 db, while the total sum spillover has decreased to about $\frac{1}{2}$ and the total difference spillovers to about $\frac{1}{4}$ of their original values. The reduction of difference spillover is particularly significant, since originally it was so great. Although not listed in Fig. 5, various other properties of the difference modes, such as gain, sidelobe level, and criticalness to misalignment are, as discussed in the previous paper [1], also greatly improved.

[4] For example, certain antenna systems obtain sequential lobing by combining the sum and difference signals of a monopulse antenna. Where independent control is available, the lobing performance may be greatly improved. With a twelve-horn feed and comparator, this feature is relatively straightforward to provide, as follows. Those ports of the comparator which would furnish even excitation of the outer horns in Fig. 4(a) are not terminated but are properly coupled to the difference ports, and these latter ports are combined alternately in-phase and out-of-phase with the sum ports in the proper manner. The result is a sequential lobing system having high crossover level and gain together with low sidelobes and spillover, compared with a lobing system using a four-horn feed. Lincoln Laboratory has worked out [9] some alternate schemes which instead provide independent channels for sequential lobing and communication.

V. Discussion

The analyses in these papers have assumed that the feed aperture is large compared with a wavelength. In many antennas this simplifying condition does not exist, and it is appropriate to ask whether the conclusions obtained herein would be significantly altered. It happens that when the feed aperture becomes small compared with a wavelength, one particular theoretical approach indicates that the main illumination would appear to resemble the optimum, regardless of the widths and shapes of the feed excitation. In such a case, therefore, one might be led to expect that a "simple" feed, not incorporating independent control, would yield good monopulse performance. While it is possible that some of the benefits of independent control could be obtained in this manner, the electrically small size of such a feed would introduce difficulties and defects which would considerably degrade the antenna performance. In the ordinary single-beam antenna, these problems are well-known; they include narrow bandwidth of impedance match, high-power limitations, and the likelihood of excessive cross polarization. For a monopulse antenna, these difficulties are usually aggravated, and additional feed problems, such as defocusing errors and coupling between radiators, are encountered. Thus it is believed that an electrically small feed should be avoided.

Another possibility exists for achieving the benefits of independent control without the additional circuits or waveguide modes described in this paper. Certain devices, when placed just in front of an ordinary monopulse feed, have the property of affecting the radiation of the feed differently for the various modes of operation. For example, a thin metal fin in the central H plane of a feed affects only the difference mode having odd symmetry about the fin. Such a fin was employed about seven years ago in a monopulse antenna [5], [6] designed by Wheeler Laboratories; it narrowed an excessively wide radiation from a four-horn feed in one difference mode, as well as improving the impedance match in this mode. However, it was found that the fin could not be designed to provide an effect equivalent to the ideal two-to-one feed size without introducing severe defects in various other properties of the nonopulse antenna. More recently, a similar limitation on the benefits of a fin was found in the case of a two-horn triple-mode feed. Although there may be some exceptions, it is probably fair to consider these experiences typical. Therefore it is believed that "parasitic" feed devices, while quite useful for certain limited purposes, are not a reliable means for designing an optimum monopulse feed.

Returning to the question of feed size, there remains to be considered the more common case, in which the feed aperture is neither large nor small compared with a wavelength. Under these conditions, the ordinary feed design may incorporate to some degree those desirable radiation properties obtainable with independent control. Nevertheless, when an independently controlled feed is designed, an improvement approaching that indicated in previous portions of this paper is likely to be obtained. About five years ago, for example, measurements were performed at Wheeler Laboratories with a monopulse antenna which initially utilized an ordinary four-horn cluster as the feed. The over-all aperture dimensions of this feed were about $3\lambda/2$, which was electrically just large enough to yield acceptable performance in a particular application, and the edge taper of the main illumination was about 11 db in the sum mode for maximum gain with a circular main aperture. Upon substitution of a feed having the same effective aperture size but a more efficient excitation shape, the antenna gain in the sum mode increased by about 1.0 db. When a further substitution was made in which one dimension of the feed aperture was increased to approach the desired two-to-one condition, the gain in the corresponding difference mode increased by more than 3.0 db and the sidelobe level changed from 12 db to 18 db below the difference peak. Thus the expectation that a wavelength-size feed aperture would encounter almost the full benefit from independent control has been experimentally confirmed for a particular case.

In some more recent antenna designs by Wheeler Laboratories, the multihorn-multimode technique has been applied to obtain simultaneous optimum performance in the sum and both difference modes. One case [10] involves a feed aperture very large compared with a wavelength, while another has over-all aperture dimensions of about 2 wavelengths. Both cases have yielded the benefits expected from independent control, and have proven satisfactory from a practical standpoint. It is concluded that the incorporation of a practical form of independent control in the feed of a monopulse antenna provides a worthwhile degree of improvement. In addition, the low spillover and noncritical nature of an antenna of this type suggests that independent control may permit some unusual antenna applications in which monopulse would ordinarily not be feasible.

VI. Acknowledgment

The author would like to thank R. L. Mattingly, who has been principally responsible for the direction of this effort by BTL, for the encouragement he has given it.

At Wheeler Laboratories, this work has been directed by H. A. Wheeler, D. Dettinger, N. A. Spencer, and P. A. Loth. The author would like to acknowledge the cooperation of the Wheeler staff in the preparation of this paper, especially H. A. Wheeler, H. W. Redlien, and D. S. Lerner for their helpful comments and suggestions, S. I. Warshaw and B. J. Karafin for their computational effort, and C. J. Stona for his work on the illustrations.

VII. Bibliography

[1] P. W. Hannan, "Optimum feeds for all three modes of a monopulse antenna I: Theory," IRE Trans. on Antennas and Propagation, vol. AP-9, pp. 444–454; September, 1961.
[2] H. W. Redlien, Wheeler Labs., unpublished Rept. No. 557, ASTIA No. AD 116472; October, 1952.
[3] W. A. Snyder, Hughes Aircraft Co., unpublished paper, *Abstracts of 5th Annual Symp. on USAF Res. and Dev.*, held at University of Illinois, ASTIA No. 90397; October, 1955.
[4] "Final Report on Instrumentation Radar AN/FPS-16 (XN-2)," Radio Corporation of America, unpublished Rept., ASTIA No. AD 250500, pp. 4-123, 4-125.
[5] P. A. Loth, Wheeler Labs., unpublished Rept. No. 686; September, 1959.
[6] P. W. Hannan, Wheeler Labs., unpublished paper, *Record of the 6th Ann. Radar Symp.*, held at University of Michigan, ASTIA No. AD 318072, pp. 165–194; June, 1960.
[7] H. W. Redlien, "A Unified Viewpoint for Amplitude and Phase Comparison Monopulse Tracking Radars," Wheeler Labs., unpublished Rept. No. 845 to Bell Telephone Labs.; March, 1959.
[8] J. P. Shelton, "Improved feed design for amplitude monopulse radar antenna," 1959 IRE National Convention Record, pt. 1, pp. 93–102.
[9] L. J. Ricardi and L. Niro, "Design of a twelve-horn monopulse feed," 1961 IRE International Convention Record, pt. 1, pp. 93–102.
[10] P. W. Hannan and P. A. Loth, "A monopulse antenna having independent optimization of the sum and difference modes," 1961 IRE International Convention Record, pt. 1, pp. 57–60.
[11] R. L. Mattingly, Bell Telephone Labs., unpublished Memo. No. 27495-42; August, 1959.
[12] P. G. Smith and C. E. Brockner, "Waveguide Hybrid Network for Monopulse Comparator," U. S. Patent No. 2,759,154; November, 1954- August, 1956.
[13] H. Jasik, "Antenna Engineering Handbook," McGraw-Hill Book Co., Inc., New York, N. Y., pp. 25–29, 25–30; 1961.

A New Way of Solving Maxwell's Equations*

V. H. RUMSEY†, fellow, ire

Summary—**A general solution of Maxwell's equations for a single frequency can be expressed as the combination of two types of solution, each of which is characterized by an electric vector which is equal to the magnetic vector times the intrinsic impedance of free space but a quarter cycle out of phase. These two types are mathematically orthogonal, and each can be conveniently expressed by means of a single scalar. The method leads to circularly polarized surface waves propagating along anisotropic sheets which are perfectly conducting in one tangential direction and perfectly transparent in the orthogonal tangential direction.**

I. Introduction

THE remarkable development of microwave technology in recent times depends to a great extent on a certain way of solving Maxwell's equations, namely the decomposition of the field into transverse electric (TE) and transverse magnetic (TM) parts. The importance of this technique rests on the fact that it is practically the only way of getting a complete set of solutions. In this paper we will work out an alternative way of solving Maxwell's equations which may be described roughly as a decomposition of the field into right-handed and left-handed circularly polarized parts (it is a rough description because it is not literally true, but for the present let it serve as a fairly meaningful name).

To understand how this compares with the TE, TM method, suppose we take the z axis as the reference so $E_z = 0$ for the TE part and $H_z = 0$ for the TM part. Thus the TM part can be considered as due to electric dipoles parallel to the z axis and the TE part as due to magnetic dipoles parallel to the z axis. From this point of view, the circularly polarized parts can be considered as due to right- and left-handed circularly polarized dipoles parallel to the z axis, a circularly polarized dipole consisting of a certain combination of an electric and a magnetic dipole. Hence, we can see in a rough way that the two methods are equivalent in generality. The choice between the two methods therefore depends on the nature of the problem at hand. It turns out that the circularly polarized method has the advantage in connection with problems involving propagation over sheets made of perfectly conducting filaments so that, at any point on the sheet, the conductivity is infinite in one direction but zero in the direction at right angles. The simplest example is a sheet made of parallel copper wires extremely close together, but not touching, so that the sheet would be "invisible" to an electric field parallel to the sheet but perpendicular to the wires.

II. Solutions for which $E = \pm j\eta H$

Let us begin with a statement of the classical technique (usually called the Hertz potential method). It says that Maxwell's equations, in the form

$$\nabla \times H = j\omega\epsilon E \quad \text{and} \quad \nabla \times E = -j\omega\mu H, \tag{1}$$

(assuming the $e^{j\omega t}$ time convention) are solved by putting

$$E = E_e + E_m \quad \text{and} \quad H = H_e + H_m, \tag{2}$$

$$E_e = \nabla \times \hat{z}U \quad \text{and} \quad H_m = \nabla \times \hat{z}V, \tag{3}$$

* Received by the PGAP, September 15, 1960; revised manuscript received January 25, 1961. The research described in this paper was sponsored by the U. S. Army Signal Corps under Contract DA 36-039 SC-84923.

† Dept. of Elec. Engrg., University of California, Berkeley.

where $\hat{z}$ is a unit vector parallel to the z axis and U and V satisfy the scalar wave equation

$$\nabla^2 f + \beta^2 f = 0 \qquad (\beta^2 = \omega^2 \mu\epsilon). \tag{4}$$

It can be shown that if U and V are general solutions of (4), the Hertz potential method gives a general solution of (1).[1,2]

As an alternative let us now consider solutions of (1) for which $E = CH$, C being some scalar constant. Substitution in (1) shows that this is possible if

$$C = \pm j\eta \tag{5}$$

where

$$\eta = \sqrt{\mu/\epsilon}. \tag{6}$$

Thus we get two types of solution denoted by E_1 and E_2:

$$E_1 = j\eta H_1 \quad \text{and} \quad E_2 = -j\eta H_2. \tag{7}$$

Note that the Poynting vector is expressed by

$$P = (\text{Re } Ee^{j\omega t}) \times (\text{Re } He^{j\omega t}), \tag{8}$$

which gives

$$P_1 = \eta H_r \times H_i \quad \text{and} \quad P_2 = -\eta H_r \times H_i, \tag{9}$$

H_r and H_i being the real and imaginary parts of H_1 or H_2, respectively. Thus the instantaneous Poynting vector is independent of time.

For a lossy medium with conductivity σ we have

$$\eta^2 = \frac{j\omega\mu}{j\omega\epsilon + \sigma}, \tag{10}$$

$$P_1 = \text{Re}\,(\eta) H_r \times H_i \quad \text{and} \quad P_2 = -\text{Re}\,(\eta) H_r \times H_i. \tag{11}$$

While (4) immediately gives us H_1 if we know E_1, it does not tell us how the three components of E_1 are related. Instead of working with the three scalar functions which constitute these three components, it is obviously much better to express the whole field by means of only one scalar function. This can be done by applying the Hertz potential technique to E_1. The results are as follows:

$$E_1 = \nabla \times \nabla \times \hat{z} U_1 - \beta \nabla \times \hat{z} U_1 \tag{12}$$

$$= \nabla\left(\frac{\partial U_1}{\partial z}\right) - \beta \nabla \times \hat{z} U_1 + \beta^2 \hat{z} U_1, \tag{13}$$

the formulas for E_2 being obtained by reversing the sign of β. The function U_1 from which E_1 is derived is any solution of (4). Now let us put

$$E = E_1 + E_2. \tag{14}$$

Then substitution for E_1 and E_2 from (12) gives

$$E = \nabla \times \nabla \times \hat{z}(U_1 + U_2) + \beta \nabla \times \hat{z}(U_2 - U_1). \tag{15}$$

We see that $(U_1 + U_2)$ and $(U_2 - U_1)$ are the TM and TE Hertz potential functions for E. Now it is evident that we can always find U_1 and U_2 to fit any such pair of Hertz potential functions and therefore in view of the generality of the Hertz potential method, we can represent any solution of (1) as a linear combination of solutions of types one and two. In short, the representation (14) is complete.

The orthogonality of the E_1 and E_2 types can be quickly demonstrated by means of the reaction method.[3] We consider the reaction (or coupling) between source a which radiates a field of type E_1 and source b which radiates a field of type E_2. The reaction, represented by the symbol $\langle ab \rangle$, is expressed by

$$\langle ab \rangle = \oint\!\!\oint_S (E_a \times H_b - E_b \times H_a) \cdot n dS, \tag{16}$$

where S is any closed surface separating sources a and b, n pointing from a to b. On putting

$$E_a = j\eta H_a \quad \text{and} \quad E_b = -j\eta H_b, \tag{17}$$

we see that $\langle ab \rangle = 0$, which says there is no coupling or reaction between the two sources. (The physical interpretation of $\langle ab \rangle = 0$ is this. If source a is a unit current generator connected to some antenna which radiates a field of type E_1, $\langle ab \rangle$ is the open circuit voltage this antenna receives from source b. Thus $\langle ab \rangle = 0$ means that the antenna which radiates type E_1 is "blind" to an incident field of type E_2.)

III. Sources of These Fields

We saw in (12) that we can express the field of type E_1 in the form

$$H_1 = \nabla \times \nabla \times \hat{z} U_1 - \beta \nabla \times \hat{z} U_1. \tag{18}$$

Now suppose

$$U_1 = \frac{e^{-j\beta r}}{4\pi r}, \tag{19}$$

which is the elementary source function. Then we find that the second term of H represents the field of an electric dipole of current moment

$$Il = -\hat{z}\beta, \tag{20}$$

and the first term represents a magnetic dipole of current moment

$$Ml = \hat{z} j\omega\mu. \tag{21}$$

[1] E. T. Whittaker, *Proc. London Math. Soc.*, vol. 1, pp. 367; 1903.
[2] P. M. Morse and H. Feshbach, "Methods of Theoretical Physics," McGraw-Hill Book Co., Inc., New York, N. Y.; 1953.
[3] V. H. Rumsey, "Reaction concept in electromagnetic theory," *Phys. Rev.*, vol. 94, pp. 1483–1491; June, 1954.

Thus (18) represents the field of the combination of an electric and a magnetic dipole at the same point, aligned in the same direction, with

$$(Ml) = -j\eta(Il). \tag{22}$$

By working out (18) it will be found that such a combination gives a circularly polarized field at every point on the sphere at infinity: it may therefore be called a circularly polarized dipole. Note, however, that it does not give circular polarization in the near field.

Now we can show that any field of type E_1 must be due to a collection of these circularly polarized dipoles. To do this we write Maxwell's equations for the field of an electric dipole density represented by J and a magnetic dipole density represented by K:

$$\nabla \times H = J + j\omega\epsilon E \tag{23}$$

$$-\nabla \times E = K + j\omega\mu H. \tag{24}$$

Substitution from (4) immediately gives

$$K = -j\eta J, \tag{25}$$

which is precisely the condition (22) for a circularly polarized dipole.

The Huygens source for a plane surface turns out very simply in terms of the scalar function U in (18). It can be derived by using the method described by Rumsey.[4] The result is this: If the source of some type E_1 field is on the left of the plane $z=0$, the field on the right is the same as would be generated by a density $2\beta(\partial U_1/\partial z)$ of normal circularly polarized dipoles spread over $z=0$, a unit circularly polarized dipole having $Il=1$ [see (22)].

IV. Application to Anisotropic Surfaces

The kind of application where a field of the type $E=j\eta H$ has advantages is obviously one for which the boundary conditions on E are the same as the boundary conditions on H. Such boundary conditions, although not common, occur in connection with propagation over anisotropic surfaces. For example, we may take the problem of reflection from a surface on which the normal components of E and H vanish, a problem which turns out to be a key point in connection with Huygens sources consisting of normal dipoles.[4] Propagation over a plane perfectly conducting anisotropic sheet is another example: a sheet of parallel insulated copper wires is a simple case, being perfectly conducting in the direction of the wires. In this case E parallel to the wires must be zero and H parallel to the wires must be at least continuous, since the discontinuity in tangential H is perpendicular to the current. Since the conditions on either side of the sheet are the same, tangential H on one side must be equal and opposite to the value on the other side. Now H parallel to the wires can only satisfy this condition and be continuous if it is zero, so here also the boundary conditions on E and H are the same.

To express this explicitly, suppose that we have a field which is of type E_1 for $z>0$ and of type E_2 for $z<0$, E_1 and E_2 being expressed in terms of the two scalars U_1 and U_2 according to (13). Let us make

$$U_1 = -U_2 \quad \text{and} \quad \frac{\partial U_1}{\partial z} = \frac{\partial U_2}{\partial z} \quad \text{at} \quad z = 0. \tag{26}$$

Then it will be found from (13) that this makes tangential E continuous but tangential H discontinuous by the amount J where

$$J = 2z \times H_1 = \frac{2z \times E_1}{j\eta}. \tag{27}$$

Therefore if

$$E \cdot l = 0 \quad \text{at} \quad z = 0, \tag{28}$$

where l is some vector in the xy plane, J must be parallel to l. The physical interpretation of these results is that there is an electric current sheet J on $z=0$ which flows along perfectly conducting filaments pointing in the direction of l. One application of this was given by Rumsey,[5] and a simpler application is described in the next paragraph.

To consider the simplest kind of waves that can be transmitted along an anistotropic sheet made of perfectly conducting filaments parallel to the x axis we take

$$U_1 = e^{\gamma_x x + \gamma_y y + \gamma_z z} \qquad (z > 0) \tag{29}$$

$$U_2 = -e^{\gamma_x x + \gamma_y y - \gamma_z z} \qquad (z < 0) \tag{30}$$

with

$$\gamma_x^2 + \gamma_y^2 + \gamma_z^2 = -\beta^2. \tag{31}$$

Note that this fits (26). From (13) we find that

$$j\eta H_1 = E_1 = (\bar{\gamma}\gamma_z + \hat{z} \times \bar{\gamma}\beta + \hat{z}\beta^2)U_1, \tag{32}$$

where the vector

$$\bar{\gamma} = \hat{x}\gamma_x + \hat{y}\gamma_y + \hat{z}\gamma_z. \tag{33}$$

From (32) we find $E \cdot E = 0$ which means that E (and of course H) is circularly polarized. The component of E parallel to the filaments is zero in this case if

$$0 = E_x = \gamma_x\gamma_z - \gamma_y\beta, \tag{34}$$

[4] V. H. Rumsey, "Some new forms of Huygens' principle," IRE Trans. on Antennas and Propagation, vol. AP-7, pp. S103–S116; December, 1959.

[5] V. H. Rumsey, "A solution to the equiangular spiral antenna problem" (Abstract), IRE Trans. on Antennas and Propagation, vol. AP-7, p. S117; December, 1959.

which gives on substitution in (31) and (32)

$$\begin{cases}\gamma_x = \pm j\beta \\ \gamma_z = \pm j\gamma_y\end{cases} \quad \text{and} \quad \begin{cases}E_z = (\beta^2 - \gamma_y^2)U_1 \\ E_y = \pm jE_z\end{cases}. \tag{35}$$

Thus the solution is fixed by γ_y, which may therefore be considered to represent the mode in which the anisotropic sheet is excited.

Now Re (E) and Im (E) represent the instantaneous fields at $t=0$, and at $\omega t = -\pi/2$. From (29) and (35) with

$$\gamma_y = j\beta_y, \tag{36}$$

we find

$$\pm \text{ Im } E_y = \text{Re } E_z$$

$$= (\beta^2 + \beta_y^2) \cos (\beta_y y \pm \beta x) e^{+\beta_y z} \quad \text{with} \quad z > 0, \tag{37}$$

$$\mp \text{ Re } E_y = \text{Im } E_z = (\beta^2 + \beta_y^2) \sin (\beta_y y \pm \beta x) e^{\pm\beta_y z}, \tag{38}$$

from which it can be shown that the instantaneous electric field is tangential to the curves

$$\beta_y z \pm \log \sin (y\beta_y \pm \beta x) = \text{constant}. \tag{39}$$

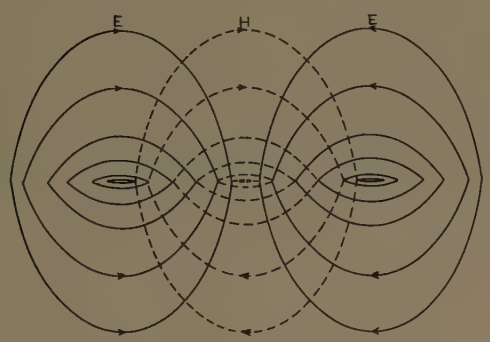

Fig. 1—The instantaneous field of a circularly polarized surface wave traveling over a sheet of wires.

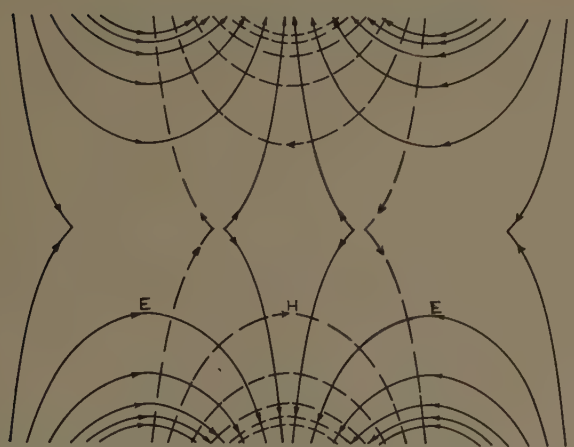

Fig. 2—The field of a circularly polarized wave which increases exponentially with distance from the anisotropic sheet.

These are plotted in Figs. 1 and 2 for $x=0$. A three-dimensional picture is shown in Fig. 3. Note that the "phase vector" (the vector normal to planes of constant phase) lies in the (x, y) plane, having components $(\pm\beta, \beta_y)$, but the electric vector lies in the (y, z) plane, and consequently the waveform moves obliquely over the anisotropic sheet with a phase velocity less than c (the velocity of light) by the factor $(1+\beta_y^2/\beta^2)$. Note also that the Poynting vector is along the x axis:

$$P = \pm \hat{x}(\beta^2 + \beta_y^2)^2 e^{\pm 2\beta_y z}. \tag{40}$$

Thus if we always adopt that choice of the signs in (37) to (40) which makes the field decrease exponentially with distance from the anisotropic sheet, reversing the sign of β_y reverses the phase vector and the Poynting vector but does not change the sense of polarization with reference to the direction of the Poynting vector, as illustrated in Fig. 4.

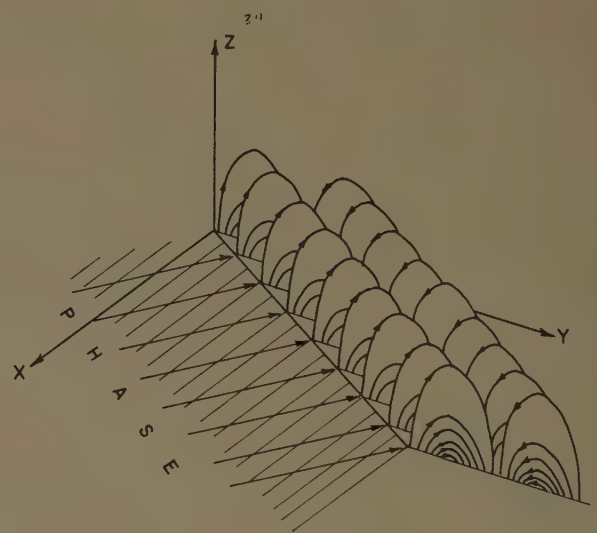

Fig. 3—The waveform moves obliquely over the sheet of wires in the direction of the phase vector.

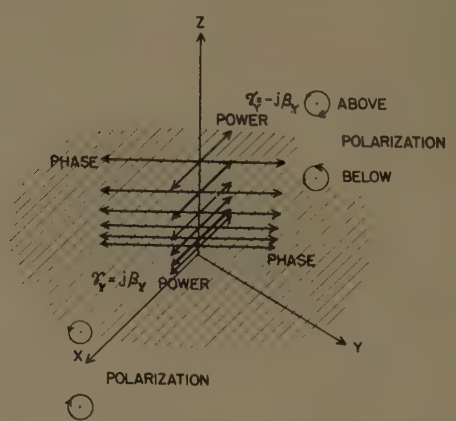

Fig. 4—The Poynting vector is inclined to the phase vector, and the polarization is right-handed about the Poynting vector for $z>0$.

When γ_y is real, corresponding to an exponential driving voltage distribution, the solution is essentially similar if we interchange the y and z axes. However, the results look quite different as we can see from Figs. 5 and 6. Note that the waveform shown in Fig. 6 now moves away from the sheet, but still the Poynting vector is parallel to the wires and the phase velocity along the wires is c. These limitations also apply to the more general case where γ_y is complex. In all these cases we get slow waves, circularly polarized in the plane normal to the wires, and traveling along the wires with the velocity of light.

Turning now to a different kind of example let us consider a conical surface which is perfectly conducting along its generators and perfectly nonconducting in the perpendicular direction. Here we can use the radial type of Hertz potential. Thus if $\hat{r}$ is the unit vector in the radial direction, let us try

$$E_1 = \nabla\left(\frac{\partial U_1}{\partial r}\right) + \beta\hat{r} \times \nabla U_1 + \beta^2 \hat{r} U_1 \tag{41}$$

outside the cone and

$$E_2 = \nabla\left(\frac{\partial U_2}{\partial r}\right) - \beta\hat{r} \times \nabla U_2 + \beta^2 \hat{r} U_2 \tag{42}$$

inside. These formulas also give

$$E_1 = j\eta H_1 \quad \text{and} \quad E_2 = -j\eta H_2,$$

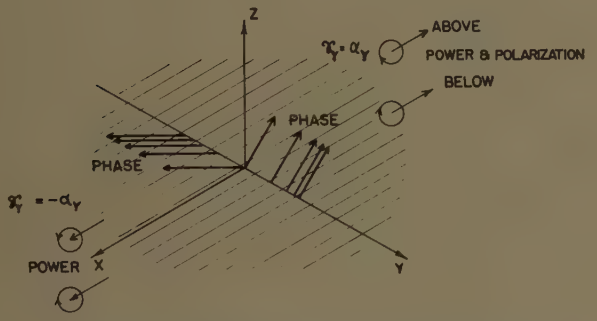

Fig. 5—For an exponential distribution of driving voltage, the phase vector is inclined to the wire sheet.

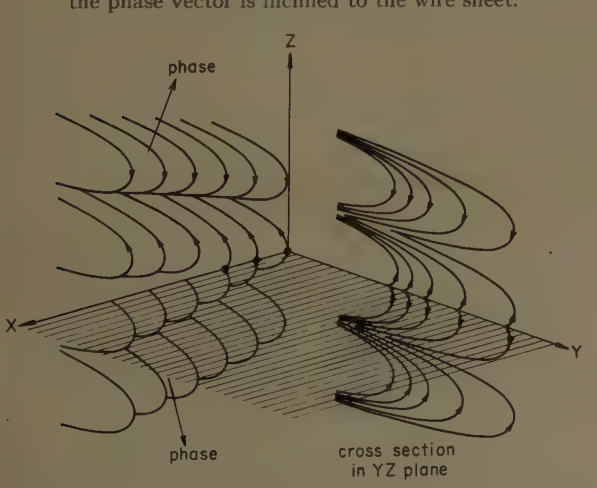

Fig. 6—The waveform moves away from the sheet for an exponential excitation along the y axis.

when U_1 and U_2 satisfy

$$\nabla^2 \frac{U}{r} + \beta^2 \frac{U}{r} = 0. \tag{43}$$

Now if we take (using conventional spherical coordinates)

$$U_1 = e^{-j\beta r}\left[\frac{\tan\frac{\theta}{2}}{\tan\frac{\theta_0}{2}}\right]^n e^{jn\phi}, \tag{44}$$

$$U_2 = e^{-j\beta r}\left[\frac{\tan\frac{\theta_0}{2}}{\tan\frac{\theta}{2}}\right]^n e^{jn\phi}, \tag{45}$$

we find that the radial components of E and H vanish everywhere, that E_ϕ is continuous and that there is a sheet of current flowing in the radial direction on the cone $\theta = \theta_0$ of density

$$\frac{-4jn\beta}{\eta r \sin\theta_0}. \tag{46}$$

Thus we obtain a set of circularly polarized TEM waves traveling along the anisotropic conical surface with a phase velocity less than c being equal to c in the radial direction.

V. Conclusion

The purpose of this paper is to introduce a new way of solving Maxwell's equations which is more than merely an alternative to the classical method, as the examples show. Although these examples are simple, indeed they are the most elementary of all, they give us an interesting class of circularly polarized surface waves, which are in some respects strikingly different from familiar types of electromagnetic waves. This approach suggests a number of further applications, the case of lossy media being one of the more obvious. Although the mathematics for this case are much the same, the physical implications are much different. Another application with extensive ramifications is that mentioned at the beginning of Section IV. The application to frequency independent antennas is not discussed in this paper, because it requires explanation at great length, but it is perhaps the most interesting, as well as being the original, motivation for this investigation.

Acknowledgment

The author wishes to thank B. Cheo and W. J. Welch for their helpful discussions.

Correlation of Wind Shear with Tropospheric Scatter Signals*

LOUIS H. BAUER†, MEMBER, IRE

Summary—**Examination of the hourly values of the 10–90 per cent fading range of selected 915 Mc tropospheric scatter records of a 400-mile path have shown unusual behavior which correlates well with wind shear through the scatter volume. Although the meteorological data were of a gross nature and were collected at a point at least 70 miles from the common volume, correlation coefficients of 0.76 to 0.8 were obtained. The data indicate that the fading range (10–90 per cent in this case) increases by 1.4 db per meter/sec/km increase in average wind shear through the scatter volume.**

Introduction

EXPERIENCE and experiment have proved that radio signals at frequencies of 100 Mc and above can be transmitted, reliably, to receiving stations located far beyond the horizon. This beyond-the-line-of-sight communication, known as tropospheric scatter, is a field in which a large amount of time has been devoted to experiment and study during the past ten years. The phenomenon was observed much earlier but could not be explained satisfactorily.[1–3] However, as the quantity of experimental data increased, it was learned that the reception of these signals was not due to fleeting, isolated events, and that the signals, covering a wide frequency range, could be transmitted and received, at will, provided that a transmitting and receiving system with sufficient power and sensitivity was used.

In 1950, Booker and Gordon[4] published a theory to explain the scatter process by postulating that the electromagnetic waves were scattered from irregularities of the index of refraction in the atmosphere. The theory was based on the premise that there are random variations (eddies) of refractive index which cause energy to be scattered out of the line of sight toward the receiver. Since most of the experimental data could be explained by this theory it has gained wide acceptance, although additional theories have been advanced at various times.[5]

After the Booker-Gordon theory was published, scientists tried to correlate meteorological parameters with median signal level or fading frequency of the received scattered signal. In this effort, measures of turbulence (such as Richardson's number) were studied and analyzed but conclusive results were not produced. Some favorable results were obtained when changes in refractive index[6] were correlated with the scattered signal. Ringwalt, *et al.*,[7] and Ament[8] have reported correlation of signal level and wind shear at the path midpoint at 1250 Mc over a 262-nautical-mile link.

In this paper, an experiment that produced data which show correlation of a measure of turbulence (wind shear) with the 10–90 per cent fading range[9] of the scattered signal is described. This effort was motivated by the desire to explain unusual behavior of the received signal for several periods of operation. Although the meteorological data were of a gross nature, conclusive results were obtained. These results should provide the impetus for further study and experimentation.

Path Geometry and Equipment

The data in this paper were obtained on an experimental tropospheric scatter link directed by the Propagation Laboratory of the Electronics Directorate of the Air Force Cambridge Research Center, Bedford, Mass. The link was an East-West 400-mile path extending from Bedford to Wilson, N. Y., with the midpoint at Utica, N. Y. Based on the 3-db points of the free-space antenna patterns of the transmitting and receiving antennas (28-foot dishes), the common volume extended from an altitude of about 20,000 feet (6.0 km) to about 40,000 feet (12.0 km) over Utica. Fig. 1 shows the pertinent path parameters. From the geometry of the path, the scattering angle θ was calculated to be approximately 2°.

AFCRC operated and maintained the transmitting station which was located at the Bedford airport. The transmitter, comprising a temperature controlled crystal oscillator with a stability of 1 part in 10^8 per day,

* Received by the PGAP, December 28, 1960; revised manuscript received, March 15, 1961. The work discussed in this report was performed under Contract AF 19(604)-1835 for the Propagation Lab. of the Electronics Directorate of the AF Cambridge Research Center, Bedford, Mass., by Cornell Aeronautical Lab., Buffalo, N. Y.

† Radiation, Inc., Orlando, Fla. Formerly with the Cornell Aeronautical Lab., Buffalo, N. Y.

[1] A. B. Crawford, C. R. England, and W. W. Mumford, *Bell Sys. Tech. J.*, vol. 17, pp. 489–519; October, 1938.

[2] R. Hull, *QST*, vol. 21, pp. 16; May, 1937.

[3] G. Marconi, "Radio communication by means of very short electric waves," *Proc. Roy. Inst. Great Britain*, December, 1932.

[4] H. G. Booker and W. E. Gordon, "A theory of radio scattering in the troposphere," PROC. IRE, vol. 38, pp. 401–412; April, 1950.

[5] T. J. Carroll and R. M. Ring, "Propagation of short radio waves in a normally stratified troposphere," PROC. IRE, vol. 43, pp. 1384–1390; October, 1955.

[6] M. H. Latour, N. E. Rosier, and W. E. Zetroner, "Some Results from an Over-Water Tropospheric Propagation Study," presented at URSI Meeting, Washington, D. C.; April 23–26, 1958.

[7] D. L. Ringwalt, W. S. Ament, and F. C. MacDonald, "Measurements of 1250 Mc scatter propagation as function of meteorology," IRE TRANS. ON ANTENNAS AND PROPAGATION, vol. AP-6 (Communication), pp. 208–209; April, 1958.

[8] W. S. Ament, "Airborne radiometeorological research," PROC. IRE, vol. 47, pp. 756–761; May, 1959.

[9] The 10–90 per cent fading range is defined as the difference in signal levels at which the received signal is equalled or exceeded 10 and 90 per cent of the time.

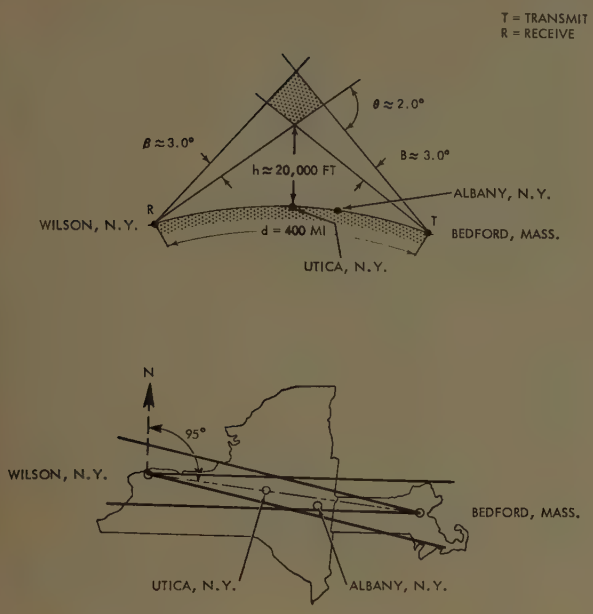

Fig. 1—Plan and side view for Bedford, Mass.-Wilson, N. Y., troposphere scatter link.

was operated at a frequency of 915 Mc CW. Output power of this equipment, 10 kw ±1 db, was fed into a 28-foot dish antenna, the center of which was about 25 feet above ground and oriented toward the western end of the scatter link.

The receiving station located at Wilson was operated by Cornell Aeronautical Laboratory under Contract AF 19(604)-1835. Equipment in this station included a conventional heterodyne-type receiver with an over-all bandwidth of 100 cps and a measured noise figure of 9 db. The local oscillator of the receiver was a frequency standard of the same model as the one used in the transmitter. Consequently, its frequency stability was also 1 part in 10^8 per day. The resultant drift rate between the transmitter and receiver was approximately 10 cycles per day. Input to the receiver was obtained from a 28-foot dish antenna, the center of which was 35 feet above ground and oriented toward Bedford. Output of the receiver was calibrated with the known power output of a signal generator.

The scatter link operated forty-eight hours each week. During this time, two types of data were recorded at the receiving site. The first consisted of Esterline-Angus records which provided a qualitative measure of the character of the signal, and the second consisted of records from a ten-level totalizer which produced data suited to statistical analysis.

Reduction of Scatter Data

The totalizer consisted of ten counters which recorded the time that the signal equalled or exceeded preset signal levels. Once each hour the counters were photographed and this information was transferred to IBM cards for processing on a digital computer. The computer determined the percentage of time the signal equalled or exceeded each level and then plotted these values on a probability scale from which the median, 10 and 90 per cent values were obtained. The total error due to receiver calibration and method of determining the median, 10 and 90 per cent values was estimated to be no greater than ±3 db.

The Esterline-Angus records of the received signal were used to indicate any unusual signal behavior such as large amplitude peaks of short duration (generally less than five minutes). These peaks were believed to be due to aircraft in or near the common volume. Other phenomena such as fading frequency and signal enhancement due to lightning strokes[10] were obtained from the Esterline-Angus charts.

Wind Shear

The source of wind shear data was that available in Northern Hemisphere Data Tabulations obtained from the U. S. Department of Commerce. These tabulations report wind speed and direction at 1000-meter altitude intervals four times each day. The nearest weather station to the common volume was at Albany, N. Y., about 70 miles to the east. This situation imposed a handicap on correlation of the data because weather data were not collected in the common volume.

The measure of wind shear used for this comparison was the mean square value of the average of the wind shear where the altitude interval was taken at 1000-meter increments for the levels from 7 km to 11 km. The altitude interval was limited to this range because data outside the 7 to 11-km region showed poor correlation for some periods while good correlation was always obtained for the 7 to 11-km interval. For each 1-km layer the shear was found by resolving the vector into North-South and East-West components and then adding these components vectorially. The value of shear for the four levels (7–8 km, 8–9 km, 9–10 km, 10–11 km) was then averaged to obtain a single value. For comparison, this value was plotted to the same time scale as the fading range. No attempt was made to take into account the time delay due to difference in location of common volume and weather station.

Correlation of Scatter Signal and Wind Shear

Three sets of data containing significant changes in fading range are presented. These samples do not, however, represent the major portion of the data which has been collected since the receiving site has been in operation. The major portion of the total data collected on this link exhibited normal scatter characteristics with the 10–90 per cent fading range values occurring at about 13 db. Thus, these samples are unusual and are not representative of the majority of the data.

Wind shear and fading range are shown in Figs. 2–4.

[10] L. H. Bauer and W. A. Flood, "UHF forward scatter from lightning strokes," Proc. IRE (Correspondence), vol. 45, p. 1743; December, 1957.

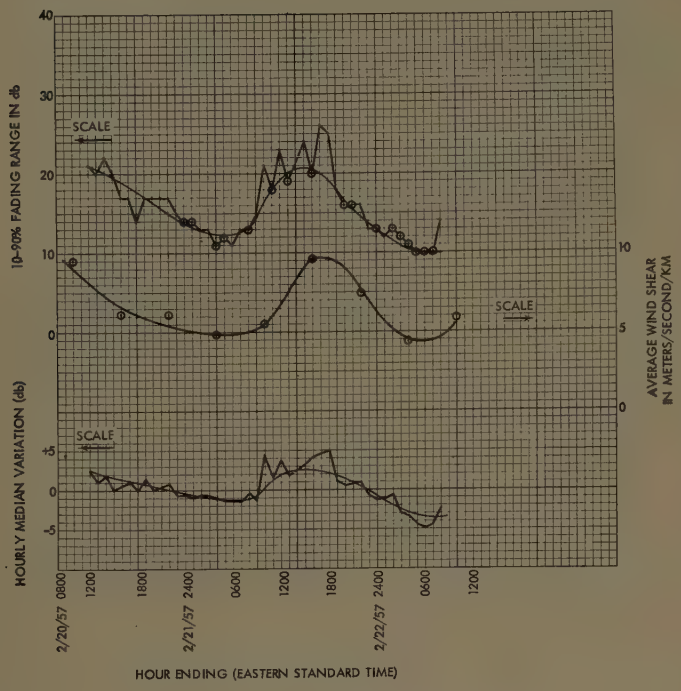

Fig. 2—Data for February 20–22, 1957.

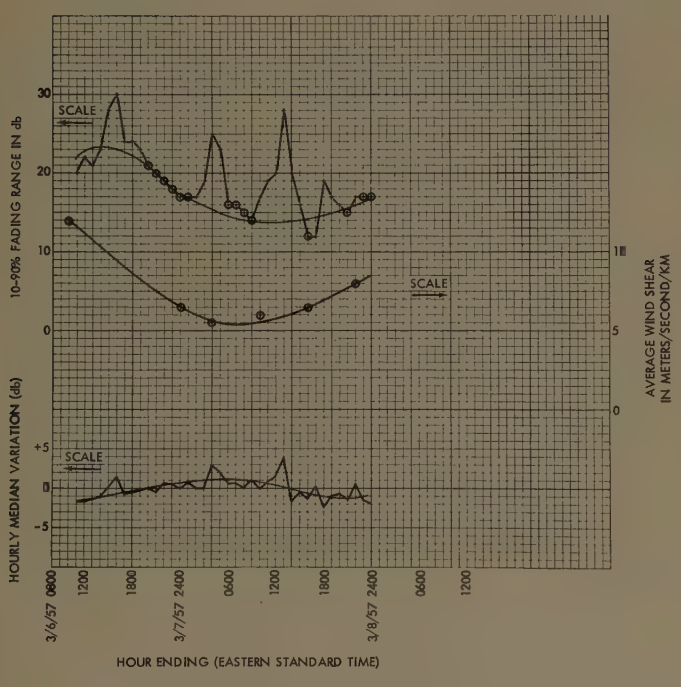

Fig. 3—Data for March 6–7, 1957.

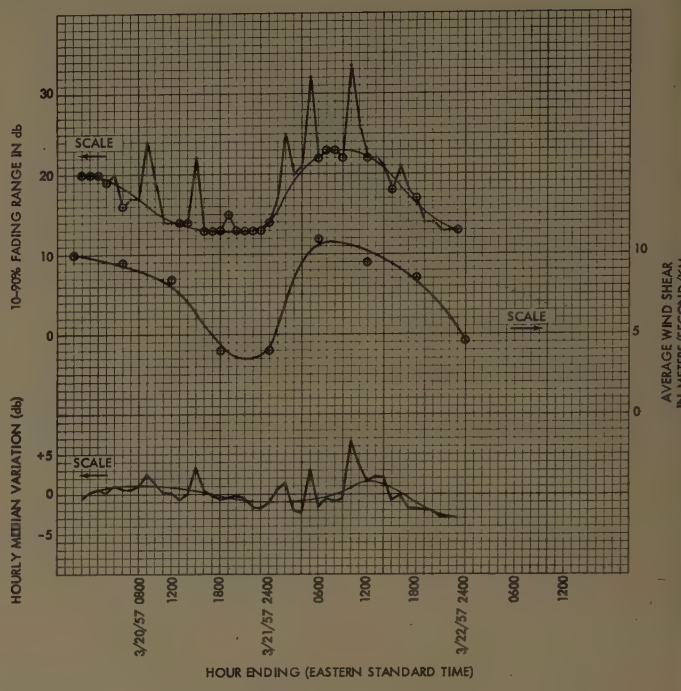

Fig. 4—Data for March 20–22, 1957.

On each graph the hours that are free of peak activity due to aircraft have been denoted by circling the point. This does not mean that all other hours are worthless, because the peaks may be contributing only a small amount to the fading range (1 or 2 db). On the other hand, the very large increase in fading range for some hours is due to excessive peak activity and should not be considered because of the difficulty in removing the effects of aircraft. The same behavior is found in the plot of hourly median values.

It can be seen from the graphs that there is good correlation between the two quantities, fading range and wind shear. To obtain a measure of the correlation, the data were analyzed statistically to obtain the correlation coefficient for each period. Briefly, a smooth curve was drawn through both wind shear and fading range as shown by the line on the plots. Then the corresponding values of wind shear and fading range were picked off at two hour intervals. The correlation coefficient was then computed for these values using

$$r = \frac{n(\sum xy) - (\sum x)(\sum y)}{\sqrt{[n(\sum x^2) - (\sum x)^2][n(\sum y^2) - (\sum y)^2]}},$$

where

r = correlation coefficient,
x = value of one of the variables,
y = value of the other variable,
n = number of xy pairs.

No effort was made to compensate for time lag between the two sets of data.

Values of correlation coefficient of 0.8, 0.76, 0.78 for February 20–22, 1957, March 6–8, 1957, and March 20–22, 1957, respectively, were computed. It is apparent that the correlation is quite good. Confidence in the correlation coefficient is contingent on the number of independent samples and the accuracy of the data. The matter of independent samples is somewhat hard to define. The rule used here is that the wind speeds

encountered for these data would surely flush the common volume in two hours; thus, two-hour intervals produce independent samples. If the time constant of the mechanism is greater than two hours the choice is, of course, too small. In the absence of adequate information the choice seems reasonable.

To obtain the behavior of the hourly median value the variation of the median was subjected to the same technique as the fading range. That is, a smooth curve was drawn through the data, and the correlation coefficient was computed using two-hour intervals. The values of correlation coefficient were 0.79, −0.79, and 0.46 for February 20–22, 1957, March 6–8, 1957, and March 20–22, 1957. When these values are compared to those of fading range for these three samples, it is obvious that the wind shear does not correlate as well with the median as it did with fading range. This result tends to contradict the results of Ringwalt[7] and Ament[8]; however, additional samples with shear data collected at the path midpoint may make the median variation compatible with their data.

From the smoothed data of Figs. 2–4, the values of hourly fading range were plotted against the corresponding value of wind shear as shown in Fig. 5. By the method of least squares the trend of the data was established and is indicated by the solid line. The plot shows that the fading range increases by 1.4 db per meter/sec/km increase in wind shear. It is interesting to note that the value of fading range does not go below about 12–13 db, which was also true for the majority of all data collected on this link.

The recordings of scatter data during the periods of large wind shear were insufficient to determine accurately the spectra of fading frequencies. However, by comparison with samples of known fading characteristics estimates of the range of fading frequencies were obtained. For the three samples, frequencies from zero to 5–10 cps were present. This is in contrast to a nominal range of zero to about 2 cps. Examination of the meteorological data showed that the winds were primarily from the west, ranging from about 25 to 50 meters/sec.

An additional plot of fading and wind shear is shown in Fig. 6. For this day (July 3, 1957) a thunderstorm moved into the common volume between 1400 and 1500 hours. Evidence of the thunderstorm activity was contained in the Esterline-Angus record by spikes due to forward scatter from lightning strokes. From the figure it can be seen that the fading range abruptly increased by about 13 db between 1400 and 1500 hours. Likewise, the average wind shear abruptly increased during this same time. Due to rapid change in the data, the correlation of wind shear and fading range is graphically depicted in the plot. The figure also indicates why use of meteorological data at shorter time intervals would be most desirable.

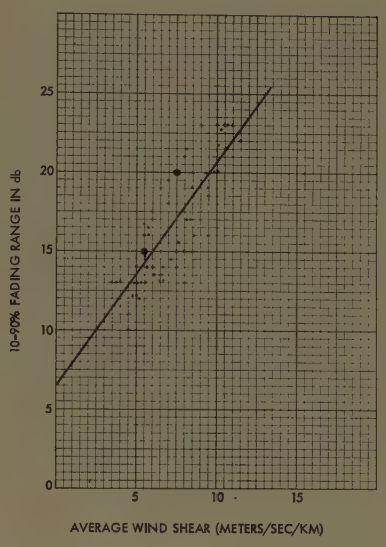

Fig. 5—Variation in fading range with wind shear.

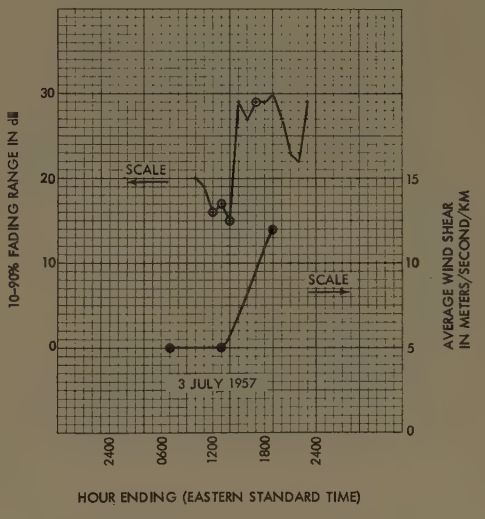

Fig. 6—Data for July 3, 1957.

Conclusion

The data presented in this paper contain two items for consideration. One is the correlation of fading range and wind shear; the second, the large departure from the expected 13.4 db for the 10–90 per cent fading range. The explanations for these two results are not readily apparent. One would expect the increased wind shear to result in increased turbulence, thus producing Rayleigh fading characteristics. However, analysis of additional data collected over this link[11] indicate that signal statistics are seldom stationary over a 15-minute interval and almost never for hourly periods. Accordingly, because of the nonstationary nature of the hourly values, sequentially adding several Rayleigh distributions of different mean value would be expected to in-

[11] W. K. Klemperer, "Tropospheric Scatter Propagation Investigation," Aeronautical Lab., Cornell University, Buffalo, N. Y., Rept. No. C-1074-P-1, Final Rept. on Contract No. AF 19(604)-1835; February 19, 1960.

crease the fading range to a value greater than that expected from a Rayleigh distribution. One might also argue, on this basis, that the 10–90 per cent fading range for all hourly data would be greater than the Rayleigh range of 13.4 db. Such was not the case.[11]

The physical mechanism which produced the correlation between fading range and wind shear is not readily apparent from these data. One might speculate that during these periods of high wind shear the viscous cutoff of the spectrum of mean square refractive index fluctuations is located at lower wave numbers as discussed by Bolgiano.[12] Under this condition scattering from large eddy sizes could be postulated leading to a quasi-coherent scattering mechanism. Whether a model of this type is valid can only be determined from additional data samples and better meteorological data.

The results show that additional data of short term statistics are required. These are summarized in the following list:

1) Obtain meteorological data in the scatter volume and at a number of locations removed from the scatter volume. (These data would be useful in determining the horizontal extent of the effects of wind shear.)
2) Collect meteorological data at least at hourly intervals, and more often if possible, to reduce the gross features of present scheduled radiosonde data.
3) Employ refractometer sounding in and near the common volume. This would furnish small-scale data.
4) Include fading frequency spectra in the analysis.

Inclusion of the above items would remove the gross features of the data of this report and would provide data from which the mechanisms of scatter in the troposphere may be specified.

It is hoped that the results presented here will provide the stimulus for further analysis of troposcatter data to specify the dependence of scatter signals on meteorological parameters, particularly wind shear.

ACKNOWLEDGMENT

The assistance of Dr. Walter A. Flood in interpreting the data presented in this paper is gratefully acknowledged.

[12] R. Bolgiano, "A theory of wavelength dependence in ultra-high frequency transhorizon propagation based on meteorological considerations," *J. Res.*, vol. 64D, pp. 231–237; May–June, 1960.

Coherent and Incoherent Scattering of Microwaves from the Ocean*

C. I. BEARD†, SENIOR MEMBER, IRE

Summary—This report, the third in a series,[1,2] summarizes experimental studies of microwave over-ocean propagation on line-of-sight paths. Measurements at 5.3, 3.2, and 0.86 cm wavelength in 1955, in the Gulf of Mexico, between two oil drilling platforms one mile apart are compared with the results of the phenomenological model developed earlier. The total field was measured at maxima, and minima of the interference patterns using a sequence of receiver beam widths. The scattered field alone was measured by means of a narrow beam. The 1955, Gulf of Mexico data, are consistent with the previous 1953, Golden Gate data, in regions of overlap of certain parameters, and provide extended coverage for other values under different conditions.

Specifically, some of the new findings are: a) The experimental values of the coherent reflected field are larger than exp $[-2(2\pi h\psi/1000\lambda)^2]$ for values of "apparent ocean roughness" ($h\psi/\lambda$) greater than 110 milliradians. h = standard deviation of water surface, ψ = grazing angle in milliradians, and λ = electromagnetic wavelength. b) After rising from zero, the incoherent scattered power exhibits a downtrend for $h\psi/\lambda$ greater than 110. The incoherent power divided by the square of the smooth sea reflection coefficient shows no polarization dependence. c) The distribution along the surface as measured by the narrow-beam antenna shows that the coherent and incoherent power are markedly peaked in the specular direction. d) The ratios of coherent-to-incoherent power (m^2) obtained from the shapes of the probability distributions agree with the power ratios obtained by measurements of the magnitudes of the signals. e) Total signal spectra broaden with increasing $h\psi/\lambda$ as found at the Golden Gate; the relative shapes of spectra agree with those from the Golden Gate. Horizontally- and vertically-polarized total signal spectra are the same.

* Received by the PGAP, February 27, 1961. This work, completed under Signal Corps Contract DA 36-039 SC-85402, was begun under Contract NOrd 7386, Bureau of Ordnance, Dept. of the Navy, while the writer was with the Appl. Phys. Lab., The Johns Hopkins University, Silver Spring, Md.

† Sylvania Electronic Defense Labs., Mountain View, Calif.

[1] C. I. Beard, I. Katz, and L. M. Spetner, "Phenomenological vector model of microwave reflection from the ocean," IRE TRANS. ON ANTENNAS AND PROPAGATION, vol. AP-4, pp. 162–167; April, 1956. Published version of Rept. CM-846, Appl. Phys. Lab., The Johns Hopkins Univ., Silver Spring, Md.; July, 1955.

[2] C. I. Beard and I. Katz, "The dependence of microwave radio signal spectra on ocean roughness and wave spectra," IRE TRANS. ON ANTENNAS AND PROPAGATION, vol. AP-5, pp. 183–191; April, 1957.

I. Introduction

THIS work is a continuation of previous studies of microwave propagation on line-of-sight paths over water. As in earlier work[1,2] the procedure of Rice,[3] essentially as developed by Lawson and Uhlenbeck[4] and Goldstein[5] and others, is used to analyze the measured received fields into coherent ("steady signal") and incoherent ("noise") components. These components, so isolated, are then plotted against $h\psi/\lambda$, the "apparent ocean roughness." h is the standard deviation of the water surface, ψ is the grazing angle (milliradians in this report), and λ is the electromagnetic wavelength. It is found that the data points cluster around smooth curves. The Gaussian curve obtained for the coherent field by the theoretical treatment of Pekeris, Macfarlane, Davies,[6] Goldstein and Goldmuntz,[7] Ament,[8] and others, fits the measured field data only up to $h\psi/\lambda = 100$. More complete theories which treat both the coherent and incoherent scattering simultaneously[9] still have to be applied to the Gaussian distribution of ocean surface height. The spectral widths of the total received field were experimentally[2] and theoretically[10] shown to be related to $h\psi/\lambda$.

The reduced data for the 1953 Golden Gate experiments on forward scatter from the ocean indicated a relationship between the fields (coherent as well as incoherent) and $h\psi/\lambda$. However, more data were desirable to determine how specific the results were to the conditions of the Golden Gate, and how dependent the fields are on other variables such as ocean-wave direction, the number of swells in the first Fresnel zone, wave spectra, illumination, polarization, etc. Accordingly, experiments were planned at the Applied Physics Laboratory of The Johns Hopkins University, and were performed by the Electrical Engineering Research Laboratory (EERL) of the University of Texas in 1955, in the Gulf of Mexico. The results of these investigations have appeared in a series of reports.[11–16]

The wealth of original data obtained in the course of the Gulf of Mexico measurements, and the cooperation of individuals at EERL in making data records available to the writer, motivated the additional detailed analysis[17] reported in the present paper. In order to sketch the state of the subject, the results of F. E. Brooks[16] and the present study are summarized as follows:

1) Vertical polarization Gulf data are given[16] which indicate that the coherent field follows $\exp[-2(2\pi h\psi/1000\lambda)^2]$ up to $h\psi/\lambda$ of 80 mils. The coherent term was extracted from the data by the approximate equation (7) (to be given shortly). The present work, using the exact equation (6), shows there is a well-founded experimental "curve" formed by both the Gulf and Golden Gate data for $h\psi/\lambda > 100$ which is not accounted for by the simple Gaussian theoretical coherent expression $\exp[-2(2\pi h\psi/1000\lambda)^2]$. Shadowing appears to be negligible for the data points in this "curve" for $h\psi/\lambda$ above 100. Horizontal and vertical polarization data agree in certain cases. Discussion and evidence are given of the pronounced effects of surf beats and changes of index of refraction gradients on the determination of the coherent term from Q-band data.

2) Vertical polarization Gulf data given[16] for the incoherent field for $h\psi/\lambda < 80$ fill a gap in the earlier Golden Gate results.[1] In the present paper this treatment is extended, and more Gulf data points for both vertical and horizontal polarization are given for $80 < h\psi/\lambda < 275$. For the incoherent field the principal result is to show that as a function of $h\psi/\lambda$ the combined Golden Gate and Gulf data points cluster in a smooth band that rises from zero, reaches a peak at $h\psi/\lambda \sim 100$, and then decreases gradually to the highest value of $h\psi/\lambda$ of 275. The peak of the incoherent "curve" occurs

[3] S. O. Rice, "Mathematical analysis of random noise," *Bell Sys. Tech. J.*, vol. 23, pp. 282–332, 1944; and vol. 24, pp. 46–156, 1945. See (3.10)–(11) and (4.2)–(3).

[4] J. L. Lawson and G. E. Uhlenbeck, "Threshold Signals," M.I.T. Rad. Lab. Ser., vol. 24, chs. 3 and 6, McGraw-Hill Book Co., Inc., New York, N. Y.; 1950.

[5] See D. E. Kerr, "Propagation of Short Radio Waves," M.I.T. Rad. Lab. Ser., vol. 13, pp. 550–562, McGraw-Hill Book Co., Inc., New York, N. Y.; 1951.

[6] H. Davies, "The reflection of electromagnetic waves from a rough surface," *Proc. IEE*, pt. 4, Monograph No. 90, pp. 1–6; January, 1954.

[7] H. Goldstein and L. A. Goldmuntz, "Mean Square Signal Computation," Nuclear Development Associates, White Plains, N. Y., Rept. NDA-18-2; August 18, 1952.

[8] W. S. Ament, "Toward a theory of reflection by a rough surface," Proc. IRE, vol. 41, pp. 142–146; January, 1953.

[9] V. Twersky, "On scattering and reflection of electromagnetic waves by rough surfaces," IRE Trans. on Antennas and Propagation, vol. AP-5, pp. 81–90; January, 1957. Also, "On scattering and reflection of sound by rough surfaces," *J. Acoust. Soc. Am.*, vol. 29, pp. 209–225; February, 1957.

[10] L. M. Spetner, "A statistical model for forward scattering of waves off a rough surface," IRE Trans. on Antennas and Propagation, vol. AP-6, pp. 88–94; January, 1958.

[11] F. E. Brooks, Jr., G. P. DuBose, Jr., and C. W. Tolbert, "Preliminary Survey Report of the 1955 Gulf of Mexico Propagation Tests," Elec. Engrg. Res. Lab., Univ. of Texas, Austin, Tex., Rept. EERL 3-17; January, 1956.

[12] F. E. Brooks, Jr., G. P. DuBose, Jr., and C. W. Tolbert, "Preliminary Summary Report of Radio, Meteorological and Oceanographic Data Obtained During 1955 Gulf of Mexico Propagation Tests," Elec. Engrg. Res. Lab., Univ. of Texas, Austin, Tex., Rept. EERL 3-18; January, 1956.

[13] C. I. Beard and F. E. Brooks, Jr., "Comparison of Predictions of Vector Model of Microwave Reflection from the Ocean with Experimental Results," Appl. Phys. Lab., The Johns Hopkins Univ., Silver Spring, Md., Rept. CF-2526; June, 1956.

[14] F. E. Brooks, Jr., N. K. Wagner, and J. R. Gerhardt, "Supplementary Data Report for 1955 Gulf of Mexico Propagation Tests," Elec. Engrg. Res. Lab., Univ. of Texas, Austin, Tex., Rept. EERL 3-20; March, 1957.

[15] N. K. Wagner and J. R. Gerhardt, "Final Report of Meteorological and Oceanographic Results for 1955 Gulf of Mexico Propagation Tests," Elec. Engrg. Res. Lab., Univ. of Texas, Austin, Tex., Rept. EERL 3-22; March, 1957.

[16] F. E. Brooks, Jr., "Final Report of Radio Results for 1955 Gulf of Mexico Propagation Tests," Elec. Engrg. Res. Lab., Univ. of Texas, Austin, Tex., Rept. EERL 3-21; March, 1957.

[17] C. I. Beard, "Coherent and Incoherent Scattering of Microwaves from the Ocean," Sylvania Electronic Defense Labs., Mountain View, Calif., Rept. EDL-E53; July, 1960.

at the same value of $h\psi/\lambda$ (100) at which the experimental coherent "curve" departs from the Gaussian theory; thus, a common mechanism is indicated—most probably multiple scattering. Horizontal and vertical polarization data are shown to be the same within the band of uncertainty. The shape of the incoherent curve obtained in this paper is different from the earlier work[1] in which the incoherent term was drawn as a constant for $h\psi/\lambda > 50$. Elementary considerations are used to show that the initial slope of the curve should be zero rather than finite.

3) The effect of decreasing the receiver illumination on the coherent and incoherent terms is small until the illumination of the first Fresnel zone is appreciably decreased.[16] In this paper, the trends of the "effective" coherent terms are compared with the theoretical curve.

4) The coherent and incoherent field magnitudes obtained from a narrow 0.3° beam pointing in the specular direction[16] (the 0.3° beam subtends the first Fresnel zone) generally fall no farther below the average coherent and incoherent curves than do some of the lower data points obtained with antennas that fully illuminate the water. From this it is concluded that most of the coherent and incoherent energies come from the first Fresnel zone.

5) The present paper develops and analyzes the distribution of the coherent and incoherent fields along the water surface as seen by the narrow (0.3°) beam. For low $h\psi/\lambda$ the coherent field is sharply peaked in the specular direction, but the coherent "image" spreads out for greater roughness (larger $h\psi/\lambda$). The incoherent power relative to that in the specular direction is also peaked in the specular direction, but the surface distribution does not change over the range of $h\psi/\lambda$ measured (21 to 78). From these data the differential scattering cross section can be computed.

6) By pointing the 0.3° beam in azimuth, it is shown[16] that the scattered energy must be concentrated in a narrow band ($\sim$0.3°) along the path.

7) Curves of m^2 (the ratio of coherent to incoherent power) vs $h\psi/\lambda$ are computed from the magnitudes of the coherent and incoherent data of the combined Golden Gate and Gulf results. These new calculated curves fit the data values of m^2 (obtained from the shapes of the probability distributions) at an interference maximum more closely than the earlier curves.[18] Horizontal and vertical polarization values of m^2 are shown to agree in general in the plot at a maximum. The results of m^2 vs $h\psi/\lambda$ for the reflected signal alone show some agreement. Within the experimental error, we infer from the plots of m^2 that the Rice model applies.

8) EERL has developed a ten-antenna array at Q band with a waveguide switch for rapid sampling of each antenna.[16] The signals from nine of the antennas are resolved into a direct wave, a coherent wave, and an incoherent wave. The arrival directions of the incoherent waves are presented as sources in the water called "glitter diagrams"; these apparent sources jump about in time. However, in the present paper, the ten-antenna array is exploited as a source of horizontal polarization data; the coherent and incoherent magnitudes and the total field spectra are compared with vertical polarization data.

9) Cross correlation of the ten-antenna signals indicates that the orthogonal components of the incoherent component (to be discussed) are uncorrelated.[16]

10) Many examples of the power spectra of the Gulf received signals are given.[16] In the present paper an analysis is made of the radio signal spectral widths vs $h\psi/\lambda$ following our earlier procedure.[2] The resulting plots and those of the earlier work[2] show similar trends; the present results extend the curves to values of $h\psi/\lambda < 100$. Horizontally and vertically polarized total signal spectra are shown to be the same. The amount of spectral broadening with $h\psi/\lambda$ is much less than at the Golden Gate, and this may be the result of the equipment's attenuating the higher frequencies. The relative shapes of the Golden Gate and Gulf of Mexico total signal spectra are shown to agree, however.

II. Vector Model Relations

The nomenclature and vector diagram have been given previously in Fig. 1 of Beard, *et al.*,[1] The envelope of the instantaneous total field (of magnitude T) at the receiver is the sum of the assumed constant[18] direct field D, a time-average coherent reflected field (of magnitude C and phase ϕ), and a random incoherent scattered field (of magnitude I). It is assumed that the incoherent field I arises from a large number of independent random scatterers and that it is Rayleigh distributed with an equiprobable phase. For convenience, a steady signal vector S is introduced as $S = |\boldsymbol{D} + \boldsymbol{C}|$.

The coherent field C and the incoherent power $\overline{I^2}$ are extracted from the recordings vs time of the envelope of the total field T as follows:

For this probability distribution, Rice[3] gives:

$$\overline{T}/\sigma = (\sqrt{\pi/2})[(1 + m^2)I_0(m^2/2) + m^2 I_1(m^2/2)] \exp(-m^2/2), \quad (1)$$

where

$$I_0(x) = J_0(ix), \qquad I_1(x) = iJ_1(-ix),$$

[18] If necessary, the effects of atmospheric inhomogeneities can be taken into account by the meteorological results of these Gulf of Mexico experiments and other studies. See for example, R. B. Muchmore and A. D. Wheelon, "Line-of-sight propagation phenomena—I. Ray treatment," Proc. IRE, vol. 43, pp. 1437–1449; October, 1955; J. W. Herbstreit and M. C. Thompson, "Measurements of the phase of radio waves received over transmission path with electrical lengths varying as a result of atmospheric turbulence," Proc. IRE, vol. 43, pp. 1391–1401; October, 1955.

and

$$m^2 = S^2/2\sigma^2$$
$$= \text{sine wave power/average incoherent power}$$
$$= S^2/\overline{I^2}. \quad (2)$$

Substituting

$$\overline{T^2} = 2\sigma^2(1 + m^2) \quad (3)$$

into

$$T_{sd}^2 = \overline{T^2} - \overline{T}^2 \quad (4)$$

yields

$$T_{sd}/\sigma = [2(1 + m^2) - (\overline{T}/\sigma)^2]^{1/2}. \quad (5)$$

From (1) and (5), $T_{sd}/\overline{T}$ can now be computed as a function of m^2. (See Appendix.)

Since the cumulative distribution analyzer of EERL obtains the median of T rather than the mean, one uses the results of Norton, *et al.*,[19] which tabulate T_{med}/S in terms of $1/m^2$ (using our notation). Then by use of (2) and (5), one obtains values of T_{sd}/T_{med} vs m^2. (See Appendix.)

By means of curves drawn from the values in the Appendix one can find the magnitude of the vector signal $S_{\min}=(D-C)$ at a minimum of the interference pattern simply from the measured ratio of T_{sd}/T_{med} or $T_{sd}/\overline{T}$. The same procedure can also be used to find $S_{\max}=(D+C)$ at a maximum. Then C/D is obtained from

$$C/D = (S_{\max} - S_{\min})/(S_{\max} + S_{\min}). \quad (6)$$

Note that (6) is not the same as the commonly used approximation

$$C/D \cong (\overline{T}_{\max} - \overline{T}_{\min})/(\overline{T}_{\max} + \overline{T}_{\min}), \quad (7)$$

obtained directly from the data.

The incoherent power $\overline{I^2}=2\sigma^2$ is obtained from the Appendix for the measured ratio T_{sd}/T_{med} (at a maximum for best accuracy).

Although (1)–(5) have been expressed in terms of total field T, they are equally applicable to R, the reflected field alone. In this case, the steady signal S is only C, the parameter m^2 equals $C^2/2\sigma^2$, and R replaces T. With these substitutions, the Appendix can be used to solve for C and σ and thus $\overline{I^2}$.

Cumulative distributions for the Rice model,[3] obtained by numerically integrating[16] the probability density function, are plotted in Fig. 1 as a function of m^2.

[19] K. A. Norton, L. E. Vogler, W. V. Mansfield, and P. J. Short, "The probability distribution of the amplitude of a constant vector plus a Rayleigh-distributed vector," PROC. IRE, vol. 43, pp. 1354–1361; October, 1955.

For the total field data, m^2 may be expressed in terms of measurements at a maximum or a minimum by

$$m^2 = (D \pm C)^2/2\sigma^2 = [(1/r) \pm (C/Dr)]^2/2(\sigma/Dr)^2, \quad (8)$$

where the plus sign is for a maximum, the minus sign is for a minimum, and r is the smooth sea reflection coefficient. Empirical curves of C/Dr and σ/Dr vs $h\psi/\lambda$ (to be given later) together with (8) enable one to plot m^2 vs $h\psi/\lambda$ with r as a parameter. Factors setting r are the grazing angle, polarization, wavelength, and conductivity as influenced by temperature and salinity. Thus the plots of m^2 at maxima and minima (to be given later) will apply to a wide variety of conditions through the parameter r.

If the "reflected" field R is measured solely, then instead of (8) one has

$$m^2 = C^2/2\sigma^2 = (C/Dr)^2/2(\sigma/Dr)^2. \quad (9)$$

Again using the empirical curves of C/Dr and σ/Dr vs $h\psi/\lambda$, one can plot m^2 as a function of $h\psi/\lambda$.

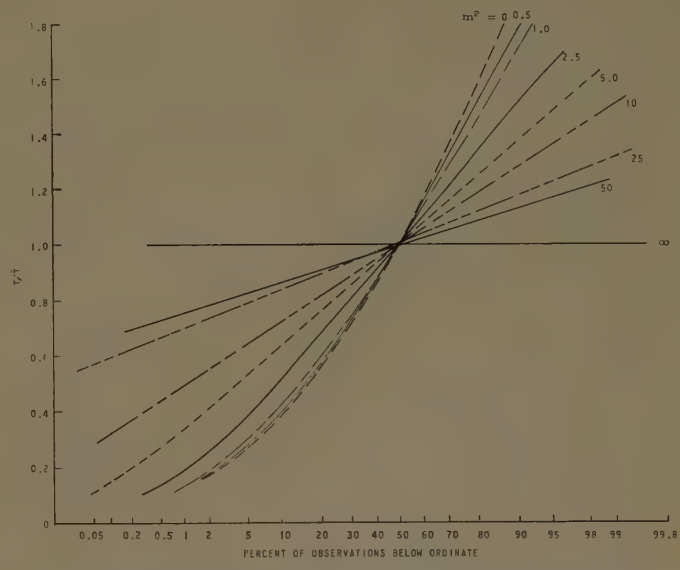

Fig. 1—Normalized cumulative amplitude distributions of a constant vector (coherent signal) plus a Rayleigh-distributed vector (noise). m^2=ratio of coherent power to incoherent power.

III. Description of Gulf Experiments

The site selected was the farthest offshore "pair" of oil drilling platforms along the United States coastline. The platforms, 5425 feet apart, are located 20 miles off the Louisiana coast in the Gulf of Mexico. The large offshore distance minimizes the disruptive effect of land masses on the uniformity of oceanographic and meteorological conditions over the path area. The path length is chosen short to minimize meteorological effects, yet long enough to include at least several swells so that the statistical assumptions of the model (Section II) will apply. The water depth of about 35 feet

is "deep water"[20] for wave periods of less than 4 seconds. For map and photographs, see Beard.[17] Measurements were made from April 19 through May 2, 1955.

Three wavelengths, C band (5.3 cm), X band (3.2 cm), and Q band (0.86 cm), were used to give a wide range of apparent surface roughness ($h\psi/\lambda$). The transmitting antennas were square 20-db horns for C and X bands (with beam widths of about 20° in the vertical plane) and a circular 27-db horn for Q band. The receiving horns for C and Q bands were the same as their transmitting horns. At X band, receiving antennas of five different beam widths were used.

For total field interference pattern measurements, the transmitter height was first adjusted for minimum average received signal and then a 10-minute recording was made; the transmitter was then raised or lowered to a position giving maximum average received signal and another 10-minute recording made.

Complete details of the radio measurements are available.[11,12,14,16,17] Extensive oceanographic and meterological measurements[12,14,15] were coordinated with the radio measurements.

IV. Experimental Results

A. Coherent Field vs Apparent Ocean Roughness

In Fig. 2 are plotted the values of the normalized coherent field C/Dr obtained in the Gulf of Mexico experiment (except those in Section IV-C) along with the three values from the Golden Gate experiment. (In the earlier work[1] only five points were available; two of these were airplane runs of considerable uncertainty and, hence, are not repeated here.) For the Gulf data essentially only h/λ of $h\psi/\lambda$ is varying since ψ changes only 1 or 2 mils[17] about a value of 13 mils.[21] The values of C/D were extracted from the data by using curves drawn from the table in the Appendix to obtain the values for (6). The measured field, from which the coherent field was extracted, is listed in the caption of Fig. 2.

Difficulty was experienced with the quantity h since the step guage was damaged by a floating log at the beginning of the experiment. A detailed analysis of the wave data has been made together with correction for the errors introduced.[11,15] It is estimated that the wave heights are now within 10 per cent of their correct values, and thus, the values of $h\psi/\lambda$ are within 10 per cent of their correct values.

The discussion of Fig. 2 is divided naturally into two parts depending upon whether the roughness parameter ($h\psi/\lambda$) is less or greater than 100.

For $h\psi/\lambda < 100$, the Gaussian theoretical curve[6–8] given in Fig. 2 generally forms an upper envelope of the Gulf experimental points. This theoretical curve is given by the expression

$$C/Dr = \exp[-2(2\pi h\psi/1000\lambda)^2],$$

with ψ in milliradians. The most likely source of error is to be off the true minimum. Whichever way the transmitter is off the minimum, the measured value of C will be less than the true value. Hence, the upper envelope of the experimental points (in the absence of other errors) would be closest to the true values.

The result obtained by Rice[22] for slightly rough surfaces is (in the notation used here):

$$C/Dr = 1 - 2(2\pi h\psi/1000\lambda)^2.$$

This expression fits the data of Fig. 2 up to $h\psi/\lambda$ of 70 as well as the Gaussian, since it is the first two terms of the expansion of the Gaussian.

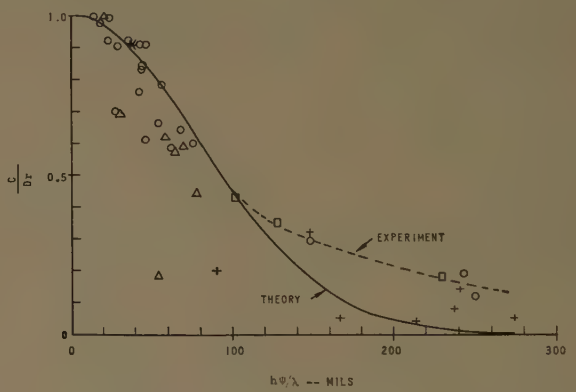

Fig. 2—Coherent field vs apparent ocean roughness.

As an example of the errors encountered near a minimum, the surf beat guage records show that the combination of surf beat[23] plus tide caused water level[24] variations during the 10-minute recordings at minima of up to 1 inch (an average value was 0.6 inch). For Q band, a one-inch change in water level over the 900-foot length of the first Fresnel zone changes the relative phase between C and D by 30° for this path. The mean total signal for the full 10-minute recording, which is the quantity used to compute C/D, is consequently higher than it would otherwise be, and the computed C/D is smaller.

The index of refraction gradient measured between

[20] Deep water is defined as the depth greater than half the water wavelength. $\lambda_w = (g/2\pi)T^2 \tanh(2\pi D/\lambda_w)$ where λ_w is the wavelength, T is the period, g is the acceleration of gravity, and D is the depth.

[21] For $\psi = 13$ mils, the values of the smooth sea, vertical polarization reflection coefficient r, used in calculating C/Dr, are 0.81, 0.82, and 0.88 for wavelengths of 5.3, 3.2, and 0.86 cm, respectively. See J. A. Saxton and J. A. Lane, "Electrical properties of sea water," *Wireless Engrg.*, vol. 29, pp. 269–275; October, 1952. For the three Golden Gate points, ψ is 27 mils.

[22] S. O. Rice, "Reflection of electromagnetic waves from slightly rough surfaces," *Commun. Pure Appl. Math.*, vol. 4, pp. 351–378; August, 1951.

[23] W. H. Munk, "Surf beats," *Trans. Amer. Geophys. Union*, vol. 30, pp. 849–854; December, 1949.

[24] For "shallow water" waves (depth$\ll\lambda_w/2$), $\lambda_w \approx T\sqrt{gD}$. For the 35-foot depth and $T = 60$ seconds (for surfbeats), $\lambda_w = 2000$ feet, a sizable fraction of the path.

the two heights (of 9.5 feet and 35.4 feet) contained swings of 0.4 to 0.8 N unit[25] even when averaged over periods of 2 to 3 minutes.[15] If these large-scale refractive-index fluctuations are assumed to travel with the mean wind speed, their horizontal dimensions range from one to two miles. A change of 0.5 N unit corresponds to 5.6°, 9.3°, and 34.7° at C, X, and Q bands, respectively, if one assumes that this change occurs between the entire specular and direct "ray" paths.

The over-all result of these two effects is that the measurements were probably made within $\pm 10°$ error of a minimum at C and X bands. At $h\psi/\lambda = 50$, the 10° error at a minimum corresponds to the measured value of C/D being only 4 per cent low. This is a satisfactory tolerance. However, the Q-band measurements could have varied within $\pm 35°$ of a minimum. At $h\psi/\lambda = 90$, a 30° error corresponds to the measured value of C/D being 16 per cent low; at $h\psi/\lambda = 250$, the 30° error causes only an 8 per cent error in C/D.

That the interference pattern is in motion at times is demonstrated by taking selected one-minute averages from the two Q-band total field recordings made at a one-foot height interval (180)° on April 29; the highest and lowest values of C/D are computed from these averages by (7) in Table I.

TABLE I

Run	$\overline{T}$ 1-Min. Averages		C/D From 1-Min. Averages		C/D 5-Min. Average
	Highest	Lowest	Highest	Lowest	
Q-I-29a	0.240	0.217	0.21	0.07	0.09
Q-I-29b	0.187	0.156			

The 3-to-1 variation in C/D shows how the antennas are "sliding up and down" the interference pattern. In addition, the comparison shows how the 5-minute average loses most of the interference pattern.

An attempt was made to see if there was any dependence of C/Dr on swell direction. The plot of C/Dr vs $h\psi/\lambda$ for swell direction in a 45° sector centered from the south was found to agree with another plot for swell direction in a 45° sector centered from the southeast. Thus with the limited quantity of data available, no clear-cut effect exists.

Fig. 2 also contains the values of C/Dr determined from the reflected signal alone (measured by the 0.3°-beam width X-band antenna). Five of these seven points are near the total signal points; the sixth is not, although it is next to a total signal point; the seventh is in complete disagreement. Since this 0.3° beam subtends just the first Fresnel zone, it appears that the first Fresnel zone contributes the major part of the coherent term in five out of seven cases. (The only extremely low point at $C/Dr = 0.18$ is suspected of misorientation as discussed later in Section IV-D.)

All of the C/Dr points discussed so far are for vertical polarization. One X-band horizontal polarization point was obtained when the 0.3°-beam width antenna was turned on its side. (The vertical plane beam width is now approximately 2°.) With the antenna pointed at the transmitter in azimuth, the measured $C/Dr = 0.91$ ($r = 1$). With the antenna pointed one beamwidth (0.3°) off in azimuth, $C/Dr = 0.90$, a good check. These values, plotted as one point (at $h\psi/\lambda = 38$) in Fig. 2, fall on the theoretical curve.

In contrast to the Gaussian theoretical curve following the upper envelope of the experimental points for $h\psi/\lambda < 100$, it falls markedly below the experimental for $h\psi/\lambda > 100$. The experimental "curve" in Fig. 2 for $h\psi/\lambda > 100$ is formed by a total of seven points: five vertical polarization points (two X band from the 1953, Golden Gate tests and three Q band from the 1955, Gulf of Mexico tests) and two horizontal polarization points (from the Q-band 10-antenna data).

One obvious possibility for the failure of the simple Gaussian for $h\psi/\lambda > 110$ might be shadowing. That is, the ocean waves block the microwaves from illuminating the troughs of the waves and thus the actual scatterer height, say H, is less than the measured height h. Of these seven data points, however, four have no shadowing of the total wave height and two others have negligible shadowing (91 per cent of the total wave height is seen)[26]; only one point has large shadowing.[17]

Other data for horizontal polarization were obtained by the Q-band 10-antenna system.[27] Plots of the median signal at each of nine vertically spaced antennas are shown in Fig. 3 for three of the days on which pronounced interference patterns were observed. Values of C/Dr for all of the seven days of data are plotted in Fig. 2. Only two of these seven values agree with the other data, and these two also agree with the departure of the experimental "curve" above the Gaussian theoretical curve for $h\psi/\lambda > 100$.

Some possible reasons for the 10-antenna values of C/Dr being low are as follows: For the geometry used, the discrete antenna spacing is one-sixth of a lobe. Thus it is possible to be off a minimum by half this spacing, or 30 electrical degrees. There appears to be no relation between the low values of C/Dr and the swell and wind wave directions. Also, shadowing does not seem to be a factor since only two of the ten antenna points have any appreciable shadowing; *i.e.*, more than 11 per cent of

[25] $N = (n-1)10^6$, where n is the index of refraction.

[26] B. L. Hicks, "Elementary Theory of Shadowing by a Rough Surface," Control Sys. Lab., Univ. of Illinois, Urbana, Ill., Rept. R-81; March, 1956.

[27] A. W. Straiton and C. W. Tolbert, "Measurement and analysis of instantaneous height-gain curves at 8.6 millimeters over rough surfaces," IRE Trans. on Antennas and Propagation, vol. AP-4, pp. 346–351; July, 1956.

Measured Field	Polarization	Location
□ total field	vertical	Golden Gate
○ total field	vertical	Gulf of Mexico
△ reflected field alone	vertical	Gulf of Mexico
* total field	horizontal	Gulf of Mexico
+ total field (10-antenna)	horizontal	Gulf of Mexico

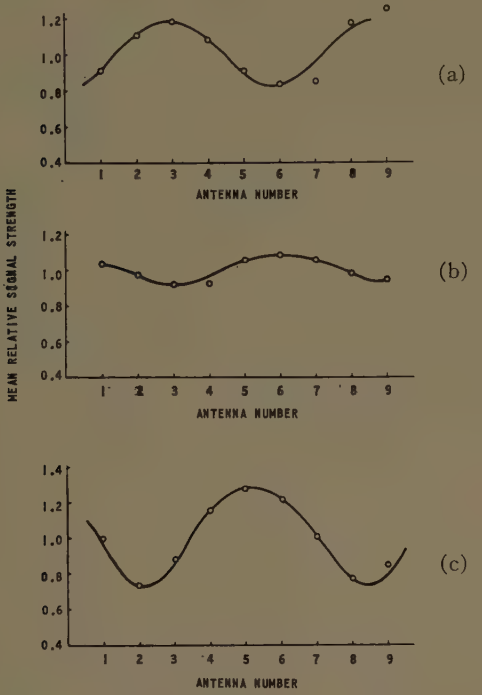

Fig. 3—Sample time average height-gain runs with the 10-antenna, Q-band, horizontal-polarization array. (a) April 29, 1955, fitted $C/D=0.184$, $h\psi/\lambda=90$; (b) April 30, 1955, fitted $C/D=0.08$, $h\psi/\lambda=237$; (c) May 1, 1955, fitted $C/D=0.274$, $h\psi/\lambda=148$.

the wave height is obscured.[28] The fact that the X-band horizontal polarization point for $h\psi/\lambda=38$, discussed previously, agrees with the other data shows that there is nothing peculiar to horizontal polarization; rather, it also points a finger at the extreme sensitivity of the Q-band measurements to water level and meteorological changes washing out the interference pattern over a several minute time average, as shown previously.

B. Incoherent Field vs Apparent Ocean Roughness

The normalized values of the incoherent term σ/Dr as found from the standard deviation of the fields (Section II) are plotted in Fig. 4 for both the 1953, Golden Gate data and the 1955, Gulf data. A smooth curve has been drawn through the aggregate of the points with a band showing generally the upper and lower limits of the data.

The Gulf total signal data have supplied information on the rising part of the curve below $h\psi/\lambda=50$, not available in the Golden Gate data. In addition, the seven reflected signal points (from the 0.3°-beam antenna) lie in the region $20<h\psi<80$. About five out of the seven points lie within the band, although six of the seven points lie below the "average curve." Thus in this range of $h\psi/\lambda$ a small area of water around the specular direction (approximately the first Fresnel zone) appears to be the main contributing area to the incoherent term. (Section IV-D also supports this deduction.) One might expect a greater surface area to be contributing to the incoherent term than to the coherent term. Possibly the reason such was not found here is the restricted range of $h\psi/\lambda$ encountered for the reflected signal alone.

[28] These two are the runs at $h\psi/\lambda=274$ and 237, both with 40 per cent of the wave height shadowed.

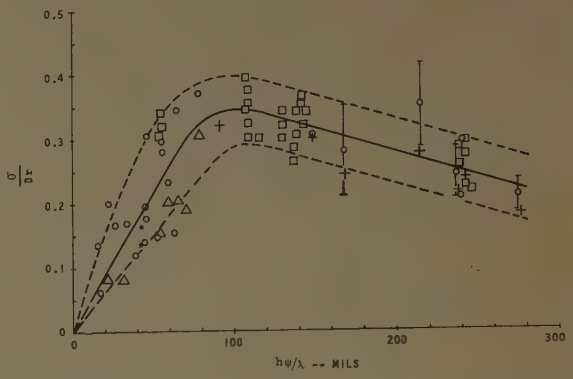

Fig. 4—Incoherent field vs apparent ocean roughness. Incoherent power $=2\sigma^2$.

In the Gulf data, the higher values of $h\psi/\lambda$ (above 148) were obtained at Q band. The three vertical polarization Q-band points, taken at maxima in the interference pattern (for $h\psi/\lambda\geqq148$), fall in and near X-band Golden Gate data. Four other Q-band vertical-polarization points taken at unknown positions in the interference pattern were treated in the following way:[17] Since D was not known, T_{sd} was divided by $\overline{T}$ instead of D and then multiplied by $[1\pm(C/D)]$ to give the uncertainty range. The value of C/D was obtained by picking C/Dr from the experimental curve in Fig. 2 and multiplying it by r. The uncertainty range is shown by the vertical lines on these four points in Fig. 4.

All of the points just discussed are for vertical polarization. The X-band horizontal polarization points also fall near the average curve. Q-band horizontal-polarization data from the 10-antenna system are available on seven other days. Of these seven points shown on Fig. 4, six fall inside the band and one falls slightly below.

The accumulation of data at both X and Q bands, at different values of h and ψ, and with both vertical and horizontal polarization, supports a downtrend in σ/Dr for $h\psi/\lambda>120$. The earlier results[1] indicated that after $h\psi/\lambda$ had reached a certain value of roughness, greater roughness had no more effect, and σ/Dr remained constant. The results of m^2 vs $h\psi/\lambda$ to be given later also favor the downtrend of σ/Dr. It is interesting to note that σ/Dr begins to decrease from its maximum at $h\psi/\lambda$ of 100 to 120, which is the same region at which the

experimental values of C/Dr depart upwards from the Gaussian theoretical curve. Thus a common mechanism may be responsible for this behavior. Again, application of multiple scattering[9] to this problem is needed.

Although the spread of the experimental data precludes the determination of the initial slope of the σ/Dr curve as $h\psi/\lambda \to 0$, this slope can be arrived at by substituting limiting values of the quantities into (8). For the values of parameters involved, the magnitude of the smooth sea reflection coefficient r behaves as $(1-a\psi)$ as $\psi \to 0$. For C/Dr the first two terms of the expansion of the Gaussian expression are used. Assume that σ/Dr can be expressed as a function of $(h\psi/\lambda)^n$, where n is some power, as $h\psi/\lambda \to 0$; then

$$m \to \frac{[1/(1-a\psi)] \pm [1-2(2\pi h\psi/1000\lambda)^2]}{\sqrt{2}\, f(h\psi/\lambda)^n} \quad \text{as } h\psi/\lambda \to 0. \quad (10)$$

The limit of m^2 as $h\psi/\lambda \to 0$ is ∞ (see Figs. 10 and 11). Eq. (10) at a maximum (the plus sign) satisfies this condition if $n \geqq 1$, and is thus not productive. At a minimum (the minus sign) if $h\psi/\lambda \to 0$ by $h \to 0$ or $\lambda \to \infty$, again $n \geqq 1$. However, at a minimum, if $h\psi/\lambda \to 0$ by $\psi \to 0$, then n must be equal to or greater than 2 as $m^2 \to \infty$. Hence, the initial slope of the σ/Dr curve instead of being finite, as drawn previously, should be zero by this argument.

C. *Effect of Illumination on C and σ*

To look into the effect of reducing the illumination of the water surface on C and σ, antennas of various beam widths in the vertical plane were used (Table II). (The axes of the antenna beams are horizontal.) The results for antenna No. 1 have been given in Figs. 2 and 4. The results for antennas No. 2–4 are given in Fig. 5. All data in Fig. 5 are for X band, vertical polarization, and an approximately constant grazing angle. The abscissa variation is caused primarily by the wave height.

In the plots of the coherent term, the Gaussian theoretical function from Fig. 2 is plotted along with reduced values of this function which are considered to approximate the data. The fractional reduction is denoted on the plots. The four low points in the plot for antenna No. 3 are ascribed tentatively to not finding the full depth of the interference minimum.

In the plots of the incoherent term in Fig. 5, the solid line is the average line of Fig. 4. In the plots for antennas No. 3 and 4, the ordinates of this line are reduced by the same factors found for the coherent terms for comparison only and not to indicate any fit with the data points. (Even with all the data in Fig. 4, only a band can be drawn.)

The following qualitative conclusions, however, may be drawn from the limited data of Fig. 5:

Measured Field	Polarization	Location
□ total field	vertical	Golden Gate
○ total field	vertical	Gulf of Mexico
△ reflected field alone	vertical	Gulf of Mexico
* total field	horizontal	Gulf of Mexico
+ total field (10-antenna)	horizontal	Gulf of Mexico

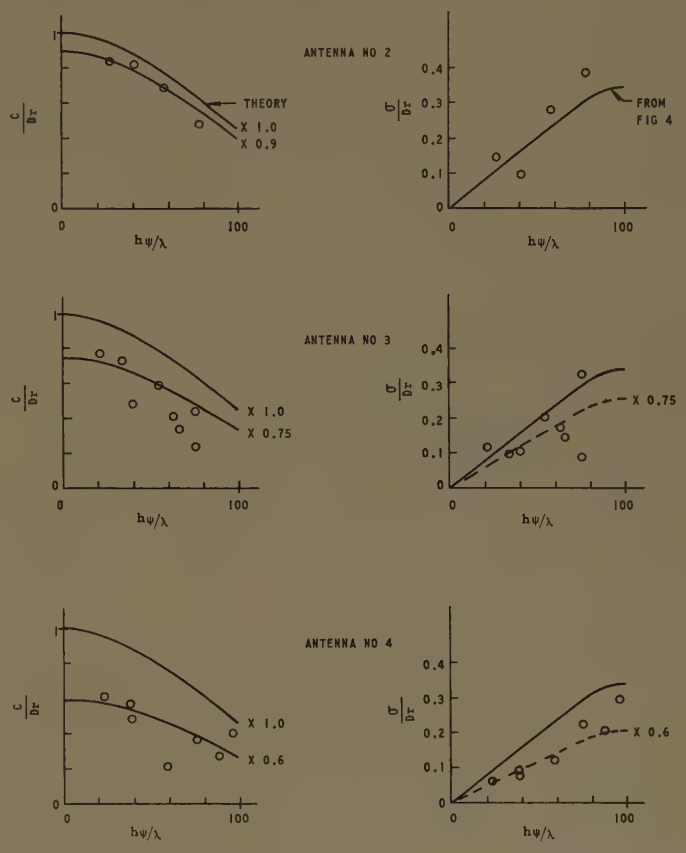

Fig. 5—Effect of illumination on coherent and incoherent scattered fields. Illumination in specular direction is down <0.2 db, 1 db, and 5 db, for antennas 2, 3, and 4, respectively.

1) The coherent term decreases progressively as the illumination decreases. The quantitative decrease, however, cannot be described by the quantitative illumination decrease at the specular point. Consider Table II. Thus, for only one antenna (No. 4) is the coherent term cut experimentally by approximately the same amount as the beam strength in the specular direction is reduced. However, even this appears to be a coincidence, since the point on the water at which the illumination is down by the same amount that $C(\text{expt})/C(\text{theo})$ is down is moving continually toward the transmitter as the receiver beam width is narrowed. This is because the portions of the Fresnel zones between the receiver and the specular point are less effective as they are under-illuminated in comparison to the Fresnel zone area between the specular point and the transmitter (*e.g.*, with antenna No. 4, the specular point illumination is down 5 db, but the receiver end of the first Fresnel zone is down 12 db, while the transmitter end is down only 3 db).

TABLE II

COMPARISON OF ILLUMINATION WITH DECREASE OF COHERENT FIELD

Receiver Antenna	Vertical Beamwidth	Beam Strength at Specular Point. db down	$\frac{C(\text{expt})}{C(\text{theo})}$ from Fig. 5. db down	Point on Water at which Illumination is down by the Ratio $C(\text{expt})/C(\text{theo})$
1	20°	<0.2	0	
2	11°	<0.2	0.9	receiver end of 12th–15th Fresnel zones
3	2.3°	~1	2.5	receiver end of first Fresnel zone
4	1.2°	~5	4.4	vicinity of specular region

2) The shape of C/Dr vs $h\psi/\lambda$ *approximately* follows the Gaussian theoretical shape regardless of illumination.

3) The incoherent term is also reduced as the illumination is decreased.

4) The effect of decreasing the illumination from the antenna at one path terminal is relatively small until the illumination of the first Fresnel zone is appreciably affected.

D. Distribution of Coherent and Incoherent Fields Along the Water Surface

The narrow 0.3°-beam width X-band, vertical polarization receiving antenna scanned the water surface (by steps) to see how the scattered field was distributed along the water path. From the 5-minute recording at each pointing angle both median and standard deviation of the reflected field R were obtained. Either the coherent field or the directly measured median value shows a strong 0.6°-width peak in the specular direction (0.8° pointing angle below direct path) followed by a gradual decrease to approximately 30 db below direct signal at a pointing angle of −7.5°. There seem to be no apparent trends in either the median values or the coherent fields at angles other than the specular angle. However, when the coherent fields (or medians) are divided by their values at the specular angle, a trend does appear (Fig. 6). First, one notices that at all depression angles greater than 1.1° the relative values decrease in the order of April 27, 28, 29, and 19, May 1, and April 30 (with April 21 not fitting). This sequence follows the trend of $h\psi/\lambda$ values (Table III) with the exception of April 27. Table III shows that the sequence corresponds to increasing values of C/D in the specular direction. Values of the relative medians at one angle (−3.5°) are given directly under the C/D values in Table III to show that the inverse relation holds for every day (except April 21).

One type of error requires mention. (For more detail, see Beard.[17]) All the curves in Fig. 6 should have a

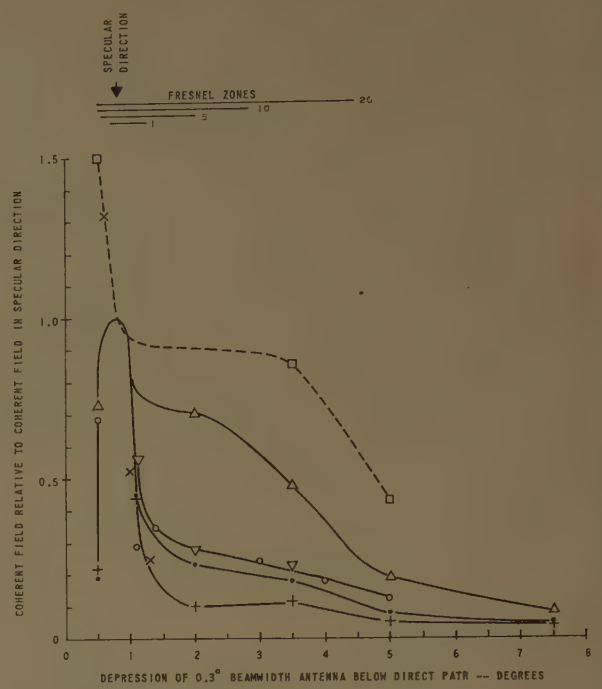

Fig. 6—Distribution along the path of the relative coherent field received by a 3.3°-beam width antenna. April, 1955: ○=19, ×=21, □=27, ▽=28, ▽=29, +=30. May, 1955: • =1.

TABLE III

REFLECTED SIGNAL DATA FROM 0.3°-BEAM WIDTH ANTENNA (NO. 5)

Item	Apr. 27	Apr. 28	Apr. 29	Apr. 19	Apr. 21	May 1	Apr. 30
T_{med}/D at −0.8°*	0.200	0.458	0.499	0.506	0.535	0.570	0.821
T_{sd}/D at −0.8°	0.101	0.219	0.162	0.151	0.161	0.066	0.068
σ/D at −0.8°	~0.13	0.250	0.167	0.155	0.165	0.066	0.068
C/D at −0.8°	~0.15	0.364	0.467	0.480	0.506	0.565	0.816
$\frac{T_{med}(-3.5°)}{T_{med}(-0.8°)}$	0.665	0.394	0.222	(0.22)†		0.184	0.122
$h\psi/\lambda$ (mils)	54	78	65	70	59	31	21

* The specular angle is −0.8° below the direct path.
† The value in parentheses is interpolated from Fig. 6.

maximum of unity at −0.8°. The two days of April 21 and 27 which have maxima at −0.6° and −0.5°, respectively, lead one to suspect that the 0.3°-beamwidth antenna was misoriented by 0.2° and 0.3°, respectively. (The data of April 26 had to be discarded because of a 0.2° misorientation.) However, even if the curve of April 27 is reduced by the ratio of peaks of 1/1.5, the points at −3.5° and −5° are still higher than the respective points for the next-lower curve of April 28.

These results mean that for large values of C/D (low $h\psi/\lambda$) the coherent field is sharply peaked and comes from the specular direction predominantly. As $h\psi/\lambda$ becomes larger, more and more of the path contributes a larger proportion of the coherent field compared to that in the specular direction. Stated in other words, as $h\psi/\lambda$ becomes larger, the coherent "image" spreads out.

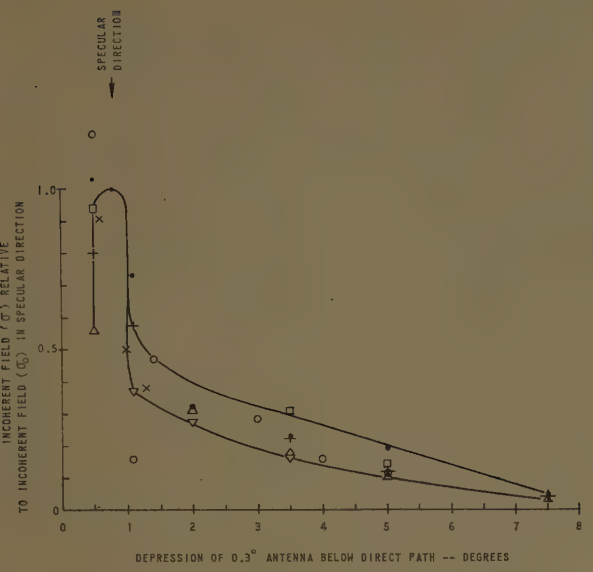

Fig. 7—Distribution along the path of the relative incoherent field received by a 0.3°-beam width antenna. April 1955: ○=19, ×=21, □=27, △=28, ▽=29, +=30. May 1955: •=1.

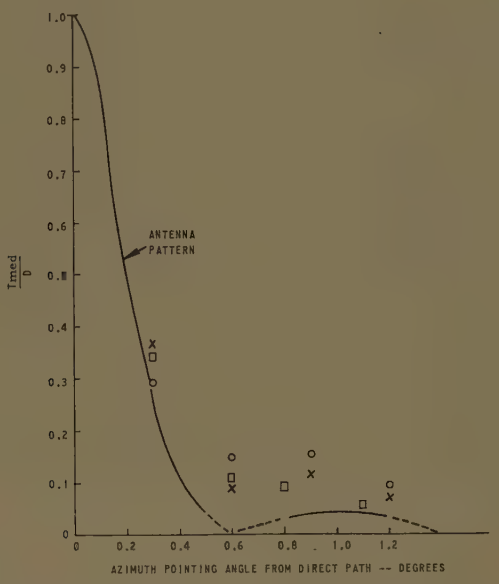

Fig. 8—Azimuthal variation of median signal received by a 0.3°-beam width antenna. Receiver position in interference pattern: ×=at maximum; ○=at minimum; □=unknown.

The standard deviations of the signals received with the 0.3°-beam width antenna at various depression angles are divided by the standard deviations (σ_0) in the specular direction and are plotted in Fig. 7. These *relative* standard deviations do not spread out with smaller C/D, or larger $h\psi/\lambda$, as does the relative coherent field. Instead they all seem to have the same distribution along the path between the specular point and the 0.3°-beam antenna (within a band of uncertainty given by the lines in Fig. 7, the order of points within this band shows no trend with C/D or $h\psi/\lambda$).

Thus the incoherent scattered energy, represented by $2\sigma^2$, is also sharply peaked in the specular direction. If the ordinates of Fig. 7 are squared and replotted, the area under the specular peak is found to be roughly 60 per cent of the total area. The remaining 40 per cent in the "tail" is distributed in the same angular fashion independent of $h\psi/\lambda$ over the narrow range of $h\psi/\lambda$ covered (21–78).

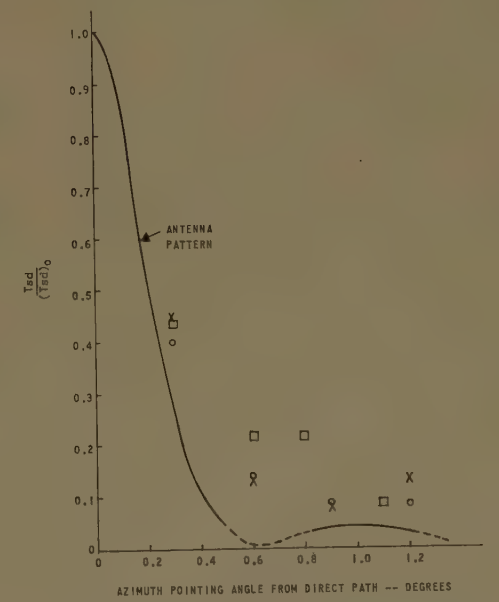

Fig. 9—Azimuthal variation of the standard deviation of the signal received by a 0.3°-beam width antenna. Receiver position in interference pattern: ×=at maximum; ○=at minimum; □=unknown.

E. Azimuthal Distribution of Signal[16]

The azimuthal distribution of the received signal was investigated by turning the 16-foot receiving antenna on its side to put its narrow 0.3° beam in the azimuth plane. If the scattered signal from the water surface is distributed over an appreciable angle, there should be an apparent broadening of the antenna pattern as the beam is swung in azimuth. Plots of the median and the standard deviation of the received signal are compared to the radiation pattern of the antenna in Figs. 8 and 9. All values are normalized to unity at 0° when the 16-foot antenna is pointed at the transmitter. The filling in of the null shows a background of azimuth scattering some 15-to-20 db down. The standard deviations show the same thing in general, although for 0.6° and greater off the path the standard deviation values contain only one significant figure. For these conditions (3.2 cm, horizontal polarization, $\psi=13$, $h\psi/\lambda=40$) it is concluded that both the C and I signals come principally from a narrow band along the path (less than 0.3° off axis on either side of the center line). It would be interesting to have similar data for large values of $h\psi/\lambda$ and various ocean wave directions to see if the apparent antenna pattern broadens significantly.

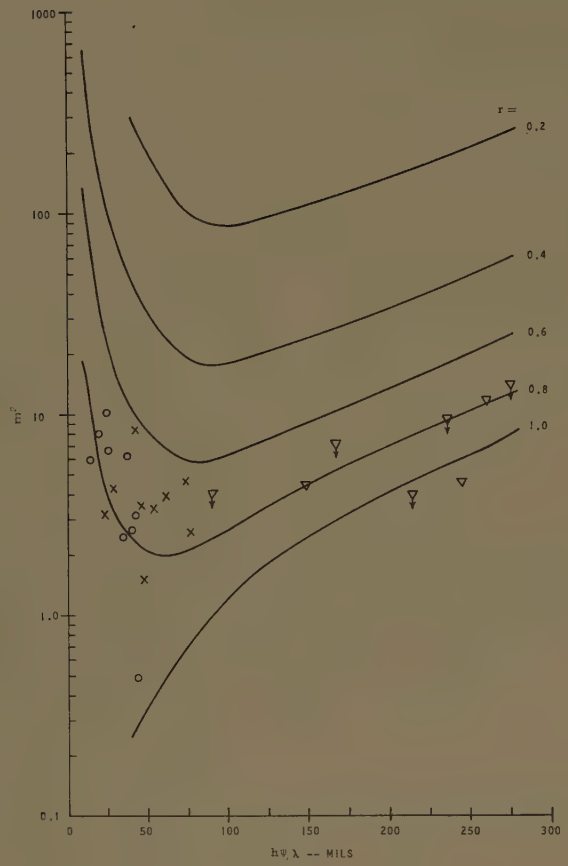

Fig. 10—m^2 vs $h\psi/\lambda$ at a minimum in the interference pattern. Vertical polarization: ○ = C band, × = X band, and ▽ = Q band.

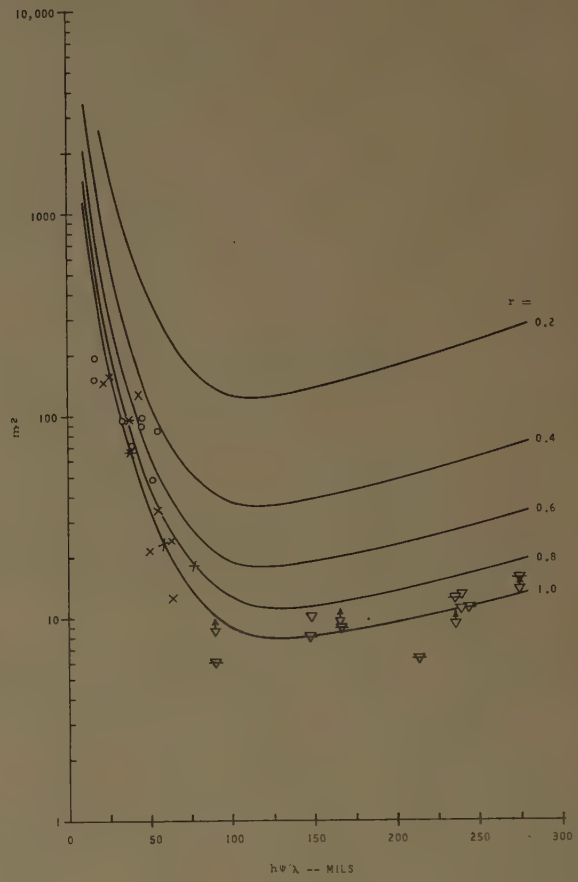

Fig. 11—m^2 vs $h\psi/\lambda$ at a maximum in the interference pattern. Vertical polarization: ○ = C band, × = X band, and ▽ = Q band. Horizontal polarization: * = X band and ▽ = Q band.

F. First Probability Distribution Shapes vs $h\psi/\lambda$

In the previous sections, the magnitudes of C^2 and $\overline{I^2}$ have been obtained by assuming that the Rice probability distribution holds. As a check let us compare the shapes of the experimental probability distributions with those of the Rice model. A measure of the shape is given by the parameter m^2 and is found by matching the experimental plots to the cumulative distributions of the Rice model in Fig. 1. Figs. 10–12 show the results of this comparison of the values of the shape parameter m^2 with curves computed from the magnitudes of Figs. 2 and 4 [the solid and dashed curves of Fig. 2 and the solid curve of Fig. 4 by means of (8) and (9)]. On several days, an interference pattern at Q band was not detected by the procedure used.[17] These points are marked with arrows showing the direction of the correction that should be made in case the transmitter was not at a maximum or a minimum.

The points at a minimum (Fig. 10) exhibit too much scatter for any conclusions to be drawn. The points should lie between $r=0.81$ and $r=0.88$ for vertical polarization at the frequencies used. The higher m^2 values in the region of $h\psi/\lambda<75$ can be partially accounted for by assuming that the measurements were not made at the exact minima. (For a 20° error off the minimum in this region of $h\psi/\lambda$, m^2 can be twice as great.)

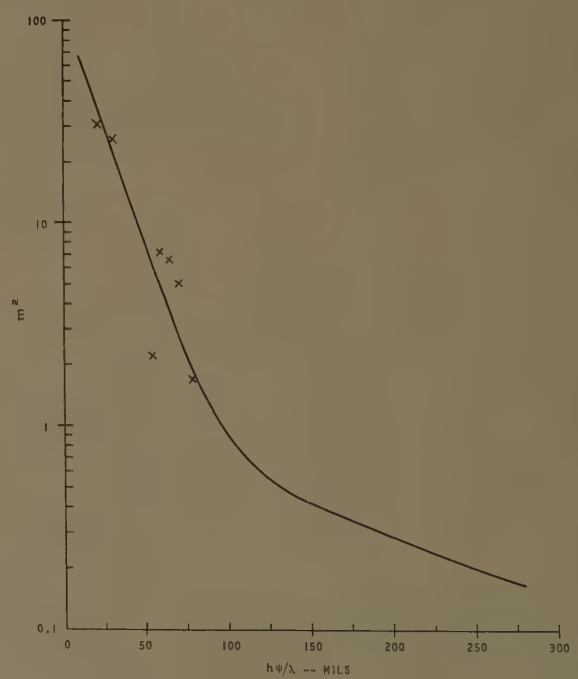

Fig. 12—m^2 vs $h\psi/\lambda$ for reflected field only. Vertical polarization at X band.

The experimental behavior at a maximum (Fig. 11) is more reassuring. Scatter at low $h\psi/\lambda$ values could be partially a result of wave-height errors since the curves slope steeply in this region.

The fact that the Q-band points for $h\psi/\lambda \geq 100$ fall in a band between the $r=0.8$ and 1.0 curves lends independent support to the downtrend of σ/Dr for $h\psi/\lambda > 110$ in Fig. 4. The independence arises from determining m^2 entirely by the shapes of the probability distributions. Curves of m^2 vs $h\psi/\lambda$ drawn earlier[13] by taking σ/Dr as a constant[1] for $h\psi/\lambda > 100$, sloped downward since the numerator of (8) was continually decreasing. Thus, the plot of experimental points, which slopes upward, did not fit. The downtrend of σ/Dr for $h\psi/\lambda > 110$ in Fig. 4 is sufficient to compensate for the numerator of (11) and to produce the agreement of Fig. 11.

X- and Q-band horizontal polarization data are also plotted in Fig. 11 and should lie along the $r=1$ curve. Except for two low Q-band points the agreement is good, showing that the presentation of Fig. 11 is general.

The results for reflected signal alone are given in Fig. 12. Since only X band was used, the data do not extend over a large range in $h\psi/\lambda$. More extensive coverage in $h\psi/\lambda$ would be valuable since this curve offers one of the most critical tests of the model. Except for the low point (at $h\psi/\lambda=54$) belonging to April 27, 1955 (which run has previously shown pecularities possibly due to misorientation), the data show correspondence with the predicted curve. Note that m^2 vs $h\psi/\lambda$ appears to be insensitive to polarization from (9) since σ/Dr has been shown to be independent of polarization and C/Dr also appears to be insensitive.

G. Cross Correlation of Signals from 10-Antenna Array[16]

The phenomenological model[1] assumes that the I_x and I_y components of the incoherent field are independent. If this is true, the cross-correlation function of these signals should be zero. Although the I_x and I_y signals are not available for cross-correlation computations, cross correlation between the 10-antenna total signals may reveal interesting information.

Antennas separated by only a slight distance would be expected to have high correlation. Antennas separated by a quarter of a height gain lobe would be expected to have no correlation. Data from three days, April 29, April 30, and May 1, were chosen for this analysis because these data showed pronounced height-gain curves (Fig. 3). For each day cross-correlation functions were computed for adjacent antennas, antennas at a maximum and a minimum, antennas spaced a lobe spacing, and antennas at a maximum and at 90°.

For all cases the cross-correlation coefficient seems to be small, being a maximum of 0.4 for adjacent antennas on the 29th. (The highest other peaks are 0.3.) Correlation is positive for adjacent antennas, slightly negative for an antenna at a maximum and at a minimum in the height-gain curve, and very small for antennas separated by a lobe spacing or by a quarter of a lobe spacing (90°). This would tend to confirm the assumption that I_x and I_y are independent functions.

H. Relation of Radio Signal Spectra to $h\psi/\lambda$

So far only the amplitude statistics of the radio signal have been described. Power spectra of the total signal and of the water surface variations have been made[12,29,30] for comparison with each other in the manner of a previous investigation.[2]

The spectra of vertically polarized signals are obtained from total signals recorded at the maxima of the interference patterns. It has been shown previously[1,2] for $I_x^2/|\boldsymbol{D}+\boldsymbol{C}|^2 \ll 1$, which is near a maximum, that, to a first approximation, the fluctuating part of T is that of I_y. The results are summarized by Beard.[17]

Spectra of horizontally polarized signals are obtained from the 10-antenna, Q-band system. The nine individual spectra are plotted together on one graph for each run.[16] Fig. 13 shows one example.

The fluctuating part of the signal of each of the nine antennas (I_n) at the various positions in the interference pattern is obtained as follows:

From the vector diagram of Fig. 1 of Beard, *et al.*:[1]

$$T^2 = (D + C\cos\phi + I_y\cos\phi - I_x\sin\phi)^2 + (C\sin\phi + I_y\sin\phi + I_x\cos\phi)^2.$$

$$S = (D^2 + 2DC\cos\phi + C^2)^{.1/2}$$

$$T - S = S[1 + (1/S^2)(2CI_y + 2DI_y\cos\phi - 2DI_x\sin\phi + I_x^2 + I_y^2]^{1/2} - S.$$

If

$$(I_x, I_y, I_x^2, I_y^2) \ll S:$$

$$I_n = T_n - S_n \cong (1/S_n)\,|\,I_y(D\cos\phi + C) - I_xD\sin\phi\,| + \cdots.$$

The spectrum of I_n is the sum of the spectrum of I_y and the spectrum of I_x in general. For $\phi=0°$, only the spectrum of I_y is involved; for $\phi=90°$ and $C \ll D$ the spectrum of I_x is primarily involved. Hence, if the spectra of I_x and of I_y are the same in shape, then the spectra of I_n for all nine antennas at a particular time will be similar. Fig. 13 is fairly representative in that some runs show more variation and others show less.[16] (For six-minute runs with 57 degrees of freedom, there is 80 per cent confidence that the true value lies between 0.8 and 1.3 times the actual value.[30]) An average is made of the nine separate spectra of one run before the $\frac{1}{2}$, $\frac{1}{4}$, and $\frac{1}{10}$ power points are determined. (See Beard[17] for a summary.)

[29] F. E. Brooks, Jr. and H. W. Smith, "Data Reduction Facilities at the Electrical Engineering Research Laboratory," Elec. Energy, Res. Lab., University of Texas, Austin, Rept. EERL-81; April, 1956.
[30] R. B. Blackman and J. W. Tukey, "The Measurement of Power Spectra," Dover Publications, Inc., New York, N. Y.; 1959.

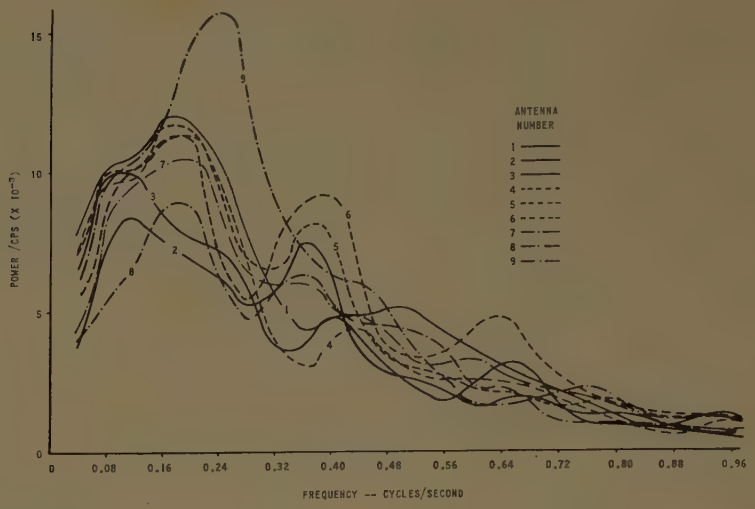

Fig. 13—Example of power spectrum of total field at nine vertically-spaced antennas. April 21, 1955; $C/D=0.04$; $T_{sd}/D=0.26$; $h\psi/\lambda=214$.

As has been found before, in all but a few cases, the peak of the radio spectrum coincides with the peak frequency of the ocean wave spectrum. The $\frac{1}{2}$, $\frac{1}{4}$, and $\frac{1}{10}$ power frequencies of the radio spectra are therefore divided by the peak wave frequencies and plotted as in Fig. 14. There are several comparisons to be made between Fig. 14 and the similar plot of the previous work.[2]

For the first time both horizontally and vertically polarized total signal spectra are plotted together (Fig. 14), and the results indicate that they are the same.

The Gulf data have filled in the region of $h\psi/\lambda<100$ which previously was essentially vacant. As $h\psi/\lambda\rightarrow 0$ the $\frac{1}{2}$, $\frac{1}{4}$, and $\frac{1}{10}$ power frequency ratios (f_r/f_w) seem to be leveling off at 1.35, 1.7, and 2.2, respectively. As $h\psi/\lambda\rightarrow 0$, one would expect the radio spectrum to shrink into the ocean wave spectrum. For the Neumann ocean wave power spectrum,[31] the ratios of $\frac{1}{2}$, $\frac{1}{4}$, and $\frac{1}{10}$ power frequencies to the peak frequency are 1.47, 1.77, and 2.18, respectively. These are to be compared with the limiting ratios of the radio spectra given above.

Within the range of $h\psi/\lambda$ encountered (up to 275) the ratios f_r/f_w are qualitatively consistent with the linear trend found earlier[2] up to $h\psi/\lambda=600$. However, the slopes of the Gulf data in Fig. 14 are only 20 per cent of those of the Golden Gate data.[2] This situation is thought to be a result of the equipment attenuating the higher frequencies. (See Beard[17] for a detailed discussion.) The numerical value of the ordinate scale, therefore, has been omitted from Fig. 14.

Although the magnitudes of the slopes in Fig. 14 do not agree with the Golden Gate data, the *relative* shapes of the spectra do agree as shown in Table IV. This fact lends considerable support to the basic trends, pointing further to equipment limiting the scale factor of Fig. 14.

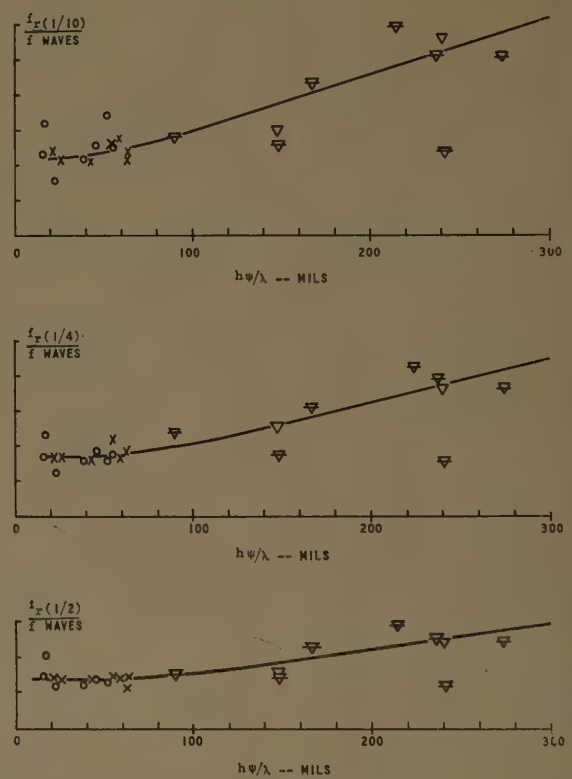

Fig. 14—Total field power spectral widths vs $h\psi/\lambda$. $f_r(0.1)$ = frequency of 1/10 power point of total field spectrum, etc. f_{waves} = frequency of maximum of ocean wave spectrum. Vertical polarization: ○ = C band, × = X band, and ▽ = Q band. Horizontal polarization: ▽ = Q band.

TABLE IV

RELATIVE SPECTRAL SHAPES

$h\psi/\lambda$	250		200		150		100	
Ratios	GG*	Gulf	GG	Gulf	GG	Gulf	GG	Gulf
$f_r(0.1)/f_r(0.25)$	1.46	1.34	1.5	1.34	1.43	1.36	1.33	1.37
$f_r(0.25)/f_r(0.5)$	1.49	1.55	1.48	1.52	1.40	1.45	—	1.35
$f_r(0.1)/f_r(0.5)$	2.18	2.08	2.22	2.04	2.00	1.98	—	1.85

* Golden Gate data of Beard and Katz.[2]

[31] G. Neumann, "On Ocean Wave Spectra and New Method of Forecasting Wind-Generated Sea," Beach Erosion Board, U. S. Army Corps of Engrs, Washington, D. C., Tech. Memo. No. 43; 1953.

Appendix

TABLE V

PARAMETERS OF A PROBABILITY DISTRIBUTION OF A CONSTANT SIGNAL VECTOR (S) PLUS A RAYLEIGH-DISTRIBUTED VECTOR (NOISE)*

$m^2=S^2/2\sigma^2$	$\bar{T}/\sigma$	T_{sd}/σ	$T_{sd}/\bar{T}$	$S/\bar{T}$	T_{med}/S†	$K=10\cdot\log 1/m^2$†	T_{sd}/T_{med}
0.00000	1.2533	0.6551	0.5227	0.00000			0.5564
0.10000	1.3152	0.6857	0.5214	0.34018	2.7653	10	0.5542
0.15849	1.3507	0.7019	0.5196	0.41682	2.2586	8	0.5520
0.25119	1.4060	0.7249	0.5156	0.50406	1.8724	6	0.5463
0.39811	1.4911	0.7568	0.5075	0.59840	1.5860	4	0.5348
0.63096	1.6205	0.7974	0.4921	0.69320	1.3817	2	0.5138
1.00000	1.8129	0.8446	0.4659	0.78008	1.2437	0	0.4802
1.5849	2.0912	0.8925	0.4268	0.85133	1.1546	− 2	0.4342
2.5112	2.4802	0.9333	0.3763	0.90360	1.0981	− 4	0.3793
3.9811	3.0062	0.9616	0.3199	0.93858	1.0622	− 6	0.3208
6.3095	3.6963	0.9778	0.2645	0.96079	1.0394	− 8	0.2649
10.0000	4.5854	0.9869	0.2152	0.97528	1.0249	−10	0.2153
15.848	5.7194	0.9920	0.1734	0.98437	1.0157	−12	0.1735
25.113	7.1579	0.9955	0.1391	0.99010	1.0100	−14	0.1391
39.809	8.97		0.111		1.0063	−16	0.111
63.091	11.27		0.0887		1.0040	−18	0.0887
100.00	14.19		0.0704		1.0025	−20	0.0704

* m^2=signal/noise power.
† Reference 19.

Acknowledgment

The author wishes to acknowledge the large part that Dr. F. E. Brooks, Jr., played in the entire program. He co-authored or authored all of the radio data reports which EERL/UT issued on the 1955 Gulf of Mexico tests. EERL/UT also kindly made available the original data recordings and copies of Figs. 1, 3, and 13. Much credit belongs to the many members of the staff of EERL/UT who contributed to carrying out the field trip and to reducing the data. We wish to thank the Magnolia-Continental-Newmont Oil Companies for permission and assistance in using their two platforms.

Electromagnetic Propagation in an Exponential Ionization Density*

LEONARD S. TAYLOR†, MEMBER, IRE

***Summary*—The propagation of a plane electromagnetic (TE) wave into a plane stratified medium in which the ionization density varies as exp (z/z_0) is investigated. The solution of the wave equation appears as a combination of Bessel functions of imaginary order and complex argument, but the magnitude of the reflection coefficient (taken at $z=-\infty$) is given by the simple expression exp $\{-(4\pi z_0 \cos\theta_i/\lambda)\tan^{-1}(\nu_c/\omega)\}$, where θ_i is the angle of incidence, λ is the free-space wavelength and (ν_c/ω) is the ratio of electron collision frequency to the frequency of the field. In general, the field components must be obtained from a complex series, but at depths beyond the critical density asymptotic forms are given which display the rapid decay of the evanescent field in terms of elementary functions.**

Introduction

INTEREST in the propagation of an electromagnetic wave in an ionized gas with an exponential variation of electron density has been aroused by the presence of ionization profiles resembling this variation in the vicinity of reentry and other high-speed bodies in the atmosphere. Although numerical solutions of the wave equation are sufficient to determine the field quantities to any desired accuracy, such calculations are not very useful when scaling laws or other general results are desired. In the present instance, an extensive numerical investigation has already been made for the TM case.[1] We shall show that an "exact" solution is possible for the TE case and that the quantity of principal interest, the reflection coefficient, may be expressed quite generally in elementary terms. Although the evaluation of the field amplitudes generally requires the evaluation of a complex series, at reasonable depths in the plasma asymptotic forms may be used which reduce the series to simple forms, displaying the rapid reduction of the evanescent wave.

The Solution of the Wave Equation

We consider an electrically neutral medium in which the electron density $N(z)$ varies exponentially in the z-direction, passing through the critical value $m\omega^2/4\pi e^2$ (Gaussian Units) at the origin (see Fig. 1). Here m and $-e$ are the electronic mass and charge, and $\omega/2\pi$ is the frequency of the incident electromagnetic wave. The index of refraction in the medium is given by

$$n^2 = 1 - 4\pi\gamma e^2 N(z)/m\omega^2 = 1 - \gamma \exp(z/z_0), \qquad (1)$$

where z_0 is the "e-folding distance" which characterizes the electron density gradient $(z_0 \geq 0)$, and

$$\gamma = (1 - i\nu_c/\omega)^{-1}. \qquad (2)$$

* Received by the PGAP, March 15, 1961. This work was supported by AF Contract 30(602)-1968.
† Missile and Space Vehicle Dept., General Electric Co., Valley Forge, Pa.

[1] M. Klein, *et al.*, "Interaction of a Non-Uniform Plasma with Microwave Radiation," General Electric Tech. Information Ser., No. R 59SD467; November 23, 1959.

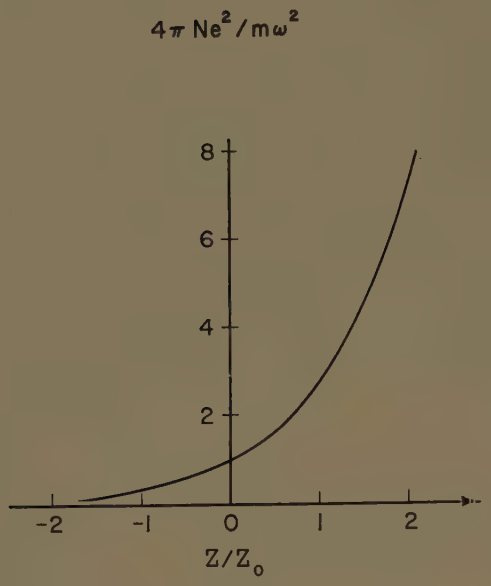

Fig. 1.

ν_c is the quantity usually described as the collision frequency. The negative sign appears in (2) by virtue of the choice of the positive exponential for the time dependence.

Assuming a TE wave incident at $-\infty$ in the yz-plane, it may be shown from Maxwell's equations[2] that

$$E_x(y, z, t) = u(z) \exp [i(k_0 \sin\theta_i y + \omega t)], \tag{3}$$

where $k_0 = \omega/c$ and

$$\frac{d^2u(z)}{dz^2} + k_0^2[n^2(z) - \sin^2\theta_i]u(z) = 0. \tag{4}$$

In these expressions θ_i is the angle of incidence. Eq. (3) is the result of a separation of variables; the form of the y-dependence is an expression of the generalized Snell's Law, $k \sin\theta = \text{const}$. Combining (1) and (4) we obtain

$$\frac{d^2u(z)}{dz^2} + k_0^2[\cos^2\theta_i - \gamma \exp (z/z_0)]u(z) = 0. \tag{5}$$

We now observe that (5) resembles the standard form[3]

$$\frac{d^2u}{d\xi^2} - [k_0^2 \exp (2\xi) + \zeta^2]u = 0 \tag{6}$$

with solution

$$u(\xi) = \mathfrak{F}_\zeta(k_0 e^\xi), \tag{7}$$

where $\mathfrak{F}$ is the cylinder function of imaginary argument. Eq. (7) suggests the transformations

$$\nu = 2z_0 k_0 \cos\theta_i \tag{8}$$

$$\alpha = 2z_0 k_0 \sqrt{-\gamma} \exp (z/2z_0), \tag{9}$$

which reduce (5) to the Bessel equation

$$\alpha^2 \frac{d^2u}{d\alpha^2} + \alpha \frac{du}{d\alpha} + (\alpha^2 + \nu^2)\mu = 0. \tag{10}$$

We write, therefore,

$$u(\alpha) = AJ_{i\nu}(\alpha) + BJ_{-i\nu}(\alpha). \tag{11}$$

Eq. (11) represents more than just a formal solution of the problem. Although it is true that the Bessel functions of imaginary order are not tabulated, the theory of Bessel functions (or at least that part of the theory which is independent of the nature of the order) may be applied to the problem. As shall be demonstrated shortly, this procedure leads to elementary expressions for some important quantities of interest.

The Reflection Coefficient

We adopt the normalization associated with the Bessel functions and write the series solution of (11),[3]

$$u(\alpha) = A \sum_{m=0}^{\infty} \frac{(-1)^m(\alpha/2)^{i\nu+2m}}{m!\Gamma(m + 1 + i\nu)} + B \sum_{m=0}^{\infty} \frac{(-1)^m(\alpha/2)^{-i\nu+2m}}{m!\Gamma(m + 1 - i\nu)}. \tag{12}$$

It will be simplest, henceforth, to use a coordinate scale in which $z_0 = 1$. Then with this convention, from (8) and (9), we have

$$u(z) = A \exp (izk_0 \cos\theta_i) \sum_{m=0}^{\infty} \frac{(-1)^m(k_0\sqrt{-\gamma})^{i\nu+2m}}{m!\Gamma(m + 1 + i\nu)} \exp (mz) + B \exp (-izk_0 \cos\theta_i) \cdot \sum_{m=0}^{\infty} \frac{(-1)^m(k_0\sqrt{-\gamma})^{-i\nu+2m}}{m!\Gamma(m + 1 - i\nu)} \exp (mz). \tag{13}$$

For large negative z, we have only the first term of each series, so that

$$u(z) = A \exp (izk_0 \cos\theta_i)[(k_0\sqrt{-\gamma})^{i\nu}/\Gamma(1 + i\nu)] + B \exp (-izk_0 \cos\theta_i)[(k_0\sqrt{-\gamma})^{-i\nu}/\Gamma(1 - i\nu)]. \tag{14}$$

Thus, at the low density limit, the wave resolves into the forward and backward components as required. Since we have taken the positive exponential for the time dependence, the second term in (14) is the incident wave. Normalizing to unity, we take

$$B = (k_0\sqrt{-\gamma})^{i\nu}\Gamma(1 - i\nu). \tag{15}$$

Thus, writing

$$A = R(k_0\sqrt{-\gamma})^{-i\nu}\Gamma(1 + i\nu), \tag{16}$$

we have for $z \ll 0$

$$u(z) \approx \exp (-izk_0 \cos\theta_i) + R \exp (izk_0 \cos\theta_i). \tag{17}$$

[2] M. Born and E. Wolf, "The Principles of Optics," Pergamon Press, New York, N. Y., pp. 50–54; 1959.

[3] G. N. Watson, "Theory of Bessel Functions, 2nd ed.," Cambridge University Press, Cambridge, England; 1952.

Therefore, R is the (complex) voltage reflection coefficient, and (11) becomes

$$u(z) = (k_0\sqrt{-\gamma})^{i\nu}\Gamma(1-i\nu)J_{-i\nu}(\alpha) + R(k_0\sqrt{-\gamma})^{-i\nu}\Gamma(1+i\nu)J_{i\nu}(\alpha). \quad (18)$$

We now assume that the plasma is bounded to the right by a perfect reflector at $z=z_w$. Then

$$R = (k_0\sqrt{-\gamma})^{2i\nu}\Gamma(-i\nu)J_{-i\nu}(\alpha_w)/\Gamma(i\nu)J_{i\nu}(\alpha_w), \quad (19)$$

where use has been made of the relation $\Gamma(\xi+1)=\xi\Gamma(\xi)$ and

$$\alpha_w = \alpha(z=z_w). \quad (20)$$

We now move the boundary out to large positive z_w, so that $|\alpha_w| \gg 1$. Then noting

$$|\arg \alpha_w| = \tfrac{1}{2}|\arg \gamma| = \tfrac{1}{2}\tan^{-1}(\nu_c/\omega) < \pi, \quad (21)$$

we may employ the asymptotic forms[3]

$$J_{\mp i\nu}(\alpha_w) = (2/\pi\alpha_w)^{1/2}\cos(\alpha_w - \pi/4 \mp i\pi\nu/2). \quad (22)$$

Thus, (19) may be written as

$$R \approx (k_0\sqrt{-\gamma})^{2i\nu}\Gamma(-i\nu)\cos(\alpha_w - \pi/4 + i\pi\nu/2)/\Gamma(i\nu) \cdot\cos(\alpha_w - \pi/4 - i\pi\nu/2). \quad (23)$$

But,

$$\frac{\cos(\alpha_w - \pi/4 + i\pi\nu/2)}{\cos(\alpha_w - \pi/4 - i\pi\nu/2)} = \frac{\exp(-\pi\nu/2+i\alpha_w-i\pi/4)+\exp(\pi\nu/2-i\alpha_w+i\pi/4)}{\exp(\pi\nu/2+i\alpha_w-i\pi/4)+\exp(-\pi\nu/2-i\alpha_w+i\pi/4)}. \quad (24)$$

Thus, since for $\mathrm{Im}(\alpha_w)>0$, we have for z_w sufficiently large

$$\frac{\cos(\alpha_w - \pi/4 + i\pi\nu/2)}{\cos(\alpha_w - \pi/4 - i\pi\nu/2)} \approx \exp(\pi\nu), \quad (25)$$

therefore, for distant positions of the reflecting wall

$$R \approx [(k_0\sqrt{-\gamma})^{2i\nu}\Gamma(-i\nu)/\Gamma(i\nu)]\exp(\pi\nu), \quad (26)$$

and z_w does not appear in the expression for R. Thus the wall has "disappeared" back into the plasma, as expected.

We are interested in the main only in the absolute value $|R|$. From (26)

$$|R| = |(k_0\sqrt{-\gamma})^{2i\nu}|\exp(\pi\nu). \quad (27)$$

But $|(\rho e^{i\phi})^{2i\nu}| = e^{-2\phi\nu}$, whence

$$|R| = \exp(\pi\nu - 2\nu\arg\sqrt{-\gamma}). \quad (28)$$

Eq. (2) and (8) now yield the principal result of this analysis

$$|R| = \exp[-(4\pi\cos\theta_i/\lambda)\tan^{-1}(\nu_c/\omega)]. \quad (29)$$

Eq. (29) is a general expression for the reflection coefficient. The only approximations used in its derivation involved the position of the reflecting wall in the plasma; (29) will be accurate whenever the wall is sufficiently deep in the plasma.

In Fig. 2, the power reflection coefficient $|R|^2$ is plotted vs $\cos\theta_i/\lambda$ for various values of ν_c/ω. (It should be recalled that λ will be measured in multiples of z_0.) Since the TE and TM waves are identical for normal incidence, (29) provides a check on numerical calculations previously made[1] for the TM wave. In these calculations the wave equation was integrated numerically, assuming that the field could be taken as zero slightly forward of $z=0$. The results are in agreement to within 2 or 3 per cent, confirming the adequacy of the assumption. We also note in passing that the reflection coefficient is unity at $\omega=0$ and decreases monotonically with increasing ω, assuming $\nu_c=$ constant. The limiting forms are

$$|R| \approx \exp(-4\pi\cos\theta_i/\lambda), \qquad \nu_c/\omega \gg 1 \quad (30)$$

$$|R| \approx \exp(-2\nu_c\cos\theta_i/z_0c), \qquad (\nu_c/\omega)^2 \ll 1 \quad (31)$$

where $c=3\times10^{10}$ cm sec^{-1}.

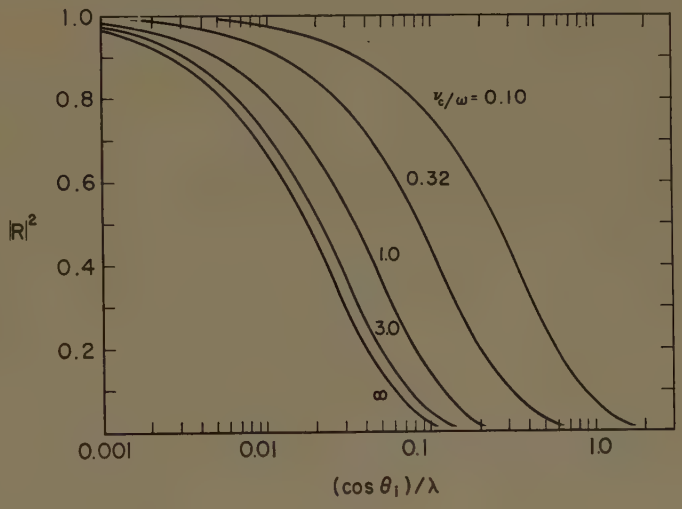

Fig. 2.

Finally, we notice that since

$$\alpha = 2^{1/2}k_0\exp(z/2)\times[1+(\nu_c/\omega)^2]^{-1/2} \cdot\{-[\sqrt{1+(\nu_c/\omega)^2}-1]^{1/2} + i[\sqrt{1+(\nu_c/\omega)^2}+1]^{1/2}\}, \quad (32)$$

the condition which assured the disappearance of the reflecting wall, $\mathrm{Im}(\alpha_w)\gg1$, is given by

$$z_w \gg 2\ln(\lambda/\pi), \qquad (\nu_c/\omega)^2 \ll 1 \quad (33)$$

and

$$z_w \gg 2\ln[2^{-3/2}(\nu_c/\omega)^{-1/2}\lambda/\pi], \quad (\nu_c/\omega)^2 \gg 1. \quad (34)$$

Eqs. (33) and (34) might be regarded as "probes" which determine the limits of penetration of the radiation field, *viz.*, we regard the reflecting wall as

a probe which we insert from $+\infty$. When (33) or (34) is fulfilled, an approximate measurement of the reflected field amplitude at $-\infty$ will not detect the presence of the reflecting wall, so that we might assert that the field does not penetrate to the depth of the wall. For $(\nu_c/\omega)^2 \ll 1$, the measurement would not be very sensitive to the presence of the perfect reflector in the nearly perfectly reflecting medium, but in the lossy case $(\nu_c/\omega)^2 \gg 1$, however, the assertion does appear reasonable. We notice then that for $(\nu_c/\omega)^2 \gg 1$, the field does not appreciably penetrate even up to $z=0$ for wavelengths which are very short compared to z_0.

The phase of the reflection coefficient may be calculated from (26) if the phase of the gamma function of imaginary argument is known. This is a tabulated function.[4] Moreover, for short wavelengths, the approximation[5]

$$\arg\{\Gamma(i\nu)\} \approx 3\pi/4 + \nu[\ln \nu - 1] - 1/12\nu, \quad \nu \gg 1 \tag{35}$$

may be employed. For long wavelengths, the expression[6]

$$\Gamma(z) = \operatorname*{Lim}_{n\to\infty} \frac{1\cdot 2\cdot\cdots\cdot(n-1)}{z(z+1)\cdot\cdots\cdot(z+n-1)}\, n^z \tag{36}$$

leads to

$$\arg\{\Gamma(i\nu)\} = \pi/2 + \nu \operatorname*{Lim}_{n\to\infty}\left\{\ln n - \nu^{-1}\sum_{m=1}^{n}\tan^{-1}(\nu/m)\right\}. \tag{37}$$

Thus, we have upon expansion of the arc tangent and regrouping

$$\arg\{\Gamma(i\nu)\} = \pi/2 - \gamma'\nu + \sum_{m=1}^{\infty}\frac{(-1)^m\nu^{2m+1}}{2m+1}\zeta(2m+1), \quad \nu < 1, \tag{38}$$

where $\gamma' =$ Euler's number ≈ 0.5772, and ζ is the Riemann Zeta function. Thus, ignoring terms in ν^3 or higher, we have from (26)

$$\arg R \approx \pi + 2\nu(\gamma' + \ln k_0), \qquad \nu < 1. \tag{39}$$

It is apparent that in the limit $\nu = 0$, $\arg R = \pi$, correctly. We point out that (37) may readily be applied to reasonably large values of ν. Thus the foregoing, plus the relation[6]

$$|\Gamma(i\nu)| = (\pi/\nu \sinh \pi\nu)^{1/2}, \tag{40}$$

may be combined with (26), (16), and (15) to evaluate the series (12). We forego this general calculation in the present work and restrict our attention in the next section to the evanescent fields beyond the critical density level.

[4] E. J. Gumbel, "Tables of the Gamma Functions for Complex Argument," Natl. Bur. of Standards Publication 9-34; 1954.
[5] E. Jahnke and F. Emde, "Tables of Functions, 4th ed.," Dover Publications, Inc., New York, N. Y., pp. 10–11; 1945.
[6] E. T. Whittaker and G. N. Watson, "A Course of Modern Analysis, 4th ed.," Cambridge University Press, Cambridge, England, pp. 237–239; 1958.

Energy Absorption

Further knowledge of the local details of the field may be obtained by considering the rate of energy absorption in the plasma as a function of z. Since from Maxwell's equations (with $\mu = 1$)

$$ik_0 H = \nabla \times \boldsymbol{E} = \hat{\jmath}\frac{\partial E_x}{\partial z} - \hat{k}\frac{\partial E_x}{\partial y}, \tag{41}$$

the rate of energy absorption is given by

$$\nabla\cdot\boldsymbol{S} = (c/8\pi)\nabla\cdot \operatorname{Re}\{\boldsymbol{E}^* \times \boldsymbol{H}\} = -(c/8\pi k_0)\nabla\cdot \operatorname{Im}\left\{\hat{\jmath}E_x^*\frac{\partial E_x}{\partial y} + \hat{k}E_x^*\frac{\partial E_x}{\partial z}\right\}. \tag{42}$$

From (3)

$$\nabla\cdot\boldsymbol{S} = -(c/8\pi k_0)\nabla\cdot \operatorname{Im}\left\{\hat{\jmath}ik_0 \sin\theta_i u^* u + \hat{k}u^*\frac{du}{dz}\right\}. \tag{43}$$

The first term on the right now drops out as expected, and we have

$$\nabla\cdot\boldsymbol{S} = -(c/8\pi k_0)\frac{d}{dz}\operatorname{Im}\left\{u^*\frac{du}{dz}\right\}. \tag{44}$$

Employing (1), (2), and (4), we may now show that for any general electron number density variation

$$\nabla\cdot\boldsymbol{S} = -\frac{e^2}{32\pi^2 m\omega}\left[\frac{(\nu_c/\omega)}{1+(\nu_c/\omega)^2}\right]N(z)\,|u(z)|^2. \tag{45}$$

We observe that for $|\alpha| \gg 1$, it is possible to employ the asymptotic forms for the Bessel functions and write the solution of the wave equation in terms of elementary functions. Thus in this case, which is of practical interest, the field a few e-folding distances beyond the critical density may be derived in a simple manner from our previous results.

Combining (18), (22), and (26), we have after some recombinations,

$$u(z) \approx i\nu(2/\pi)^{1/2}(k_0\sqrt{-\gamma})^{i\nu}\Gamma(-i\nu)\sinh\pi\nu \cdot\{\alpha^{-1/2}\exp[i(\alpha - \pi/4) + \pi\nu/2]\}. \tag{46}$$

Thus, making use of (32) we find

$$\nabla\cdot\boldsymbol{S} = -\frac{c}{8\pi^2}\left[\frac{(\nu_c/\omega)}{1+(\nu_c/\omega)^2}\right]\left[\left|(-\gamma)^{i\nu}\right|(\pi\nu)e^{\pi\nu}\sinh\pi\nu\right] \cdot\exp(z/2 - 2\operatorname{Im}\alpha). \tag{47}$$

Therefore, the z-dependence of $\nabla\cdot\boldsymbol{S}$ is given by the factor

$$\exp\left\{z/2 - 2^{3/2}k_0[1+\sqrt{1+(\nu_c/\omega)^2}]^{1/2}e^{z/2}\right\}. \tag{48}$$

The very rapid decrease with increasing z is in accordance with our expectations. For $(\nu_c/\omega)^2 \ll 1$, (47) becomes

$$\nabla \cdot \mathbf{S} \approx -\frac{c}{8\pi^2}(\nu_c/\omega)[(\pi\nu)e^{\pi\nu}\sinh \pi\nu] \cdot \exp(z/2 - 4k_0e^{z/2}). \quad (49)$$

The bracketed expression yields the θ_i-dependence of $\nabla \cdot \mathbf{S}$. At grazing angles, the variation is proportional to $\cos^2 \theta_i$.

The formula (49) is not valid when ν is large. The reason for this discrepancy is that the asymptotic forms for the Bessel functions which were employed are not valid unless the argument of the functions is large compared to the order. In this instance, we must employ the more recondite forms,

$$J_{i\nu}(i\nu \sec \beta) \approx (2/\pi i\nu \tan \beta)^{1/2} \cos [i\nu(\tan \beta - \beta) - \pi/4], \quad (50)$$

$$J_{-i\nu}(i\nu \sec \beta) \approx (2/\pi i\nu \tan \beta)^{1/2} \cos [i\nu(\tan \beta - \beta + \pi) - \pi/4]. \quad (51)$$

We justify the use of these expressions on the basis of the Meissel expansions[3]

$$J_\nu(\nu \sec \beta) = (2/\pi\nu \tan \beta)^{1/2} e^{-P_\nu} \cos (Q_\nu - \pi/4), \quad (52)$$

$$Y_\nu(\nu \sec \beta) = (2/\pi\nu \tan \beta)^{1/2} e^{-P_\nu} \sin (Q_\nu - \pi/4), \quad (53)$$

where

$$P_\nu = \frac{\cot^6 \beta}{16\nu^2}(4 \sec^2 \beta + \sec^4 \beta) - \frac{\cot^{12} \beta}{128\nu^4}(32 \sec^2 \beta + \cdots) \cdots \quad (54)$$

$$Q_\nu = \nu(\tan \beta - \beta) - \frac{\cot^3 \beta}{24\nu}(2 + 3 \sec^2 \beta) - \frac{\cot^6 \beta}{5760\nu^3}(16 - \cdots) \cdots . \quad (55)$$

The variables in these expansions are not restricted to real quantities. In the present instance we take in (48),

$$\sec \beta = \alpha/i\nu = \sqrt{\gamma} \sec \theta_i \exp (z/2). \quad (56)$$

We note that in order to employ (52) and (53) successfully, β must be large. Then, as with (46), we now find

$$u(z) = \nu(2/\pi)^{1/2}(k_0\sqrt{-\gamma})^{i\nu}\Gamma(-i\nu)e^{\pi\nu}\sinh \pi\nu \cdot \left\{\frac{\exp [\nu(\beta - \tan \beta)]}{(\nu \tan \beta)^{1/2}}\right\}. \quad (57)$$

Some Propagation Characteristics of High UHF Signals in the Immediate Vicinity of Trees*

A. H. LaGRONE†, FELLOW, IRE, AND C. W. CHAPMAN†

Summary—**Results are reported of measurements made at very low angles of 2880-Mc vertically-polarized signals over wooded areas, with the elevation angle to the transmitter the principal variable. The effects of one tree and of many trees on the apparent location of a signal source, as determined with a narrow-beam antenna, are reported. A hypothetical direction-finding system is assumed and its pointing characteristics determined.**

I. Introduction

THE operation of radio and radar systems at frequencies in the 3000-Mc range is often limited or greatly influenced by the presence of vegetation on the path. This is particularly true of a field-tracking radar system. This system must, at times, be expected to operate effectively under conditions considerably less than ideal. Thus, any advance knowledge of the effect of vegetation on the path on the performance of the tracking system is highly desirable.

This paper presents measurements of signal strength and antenna patterns for various receiver locations behind trees and for various transmitter elevation angles. The effects caused by local vegetation are deduced and reported. A hypothetical direction-finding system is assumed and its pointing characteristics determined. All measurements were made at 2880 Mc using vertical polarization.

II. Signal Strength Measurements

Vertically-polarized signal-strength measurements were made with trees on the path very close to the receiving antenna. The geometry of the two paths used in making measurements is shown in Fig. 1. The Balcones path employed a 280-foot tower to lower a transmitter behind a small grove of live oak and cedar trees. The transmitting antenna was a wide-angle horn. The receiving antenna was a 4-foot parabolic dish having a

* Received by the PGAP, March 24, 1961; revised manuscript received, June 7, 1961. This work was done under the sponsorship of the AF Research Div., Air Research and Dev. Command, Bedford, Mass., Contract AF 19(604)-5504, Task No. 36015.

† Dept. of Elec. Engrg., University of Texas, Austin, Tex.

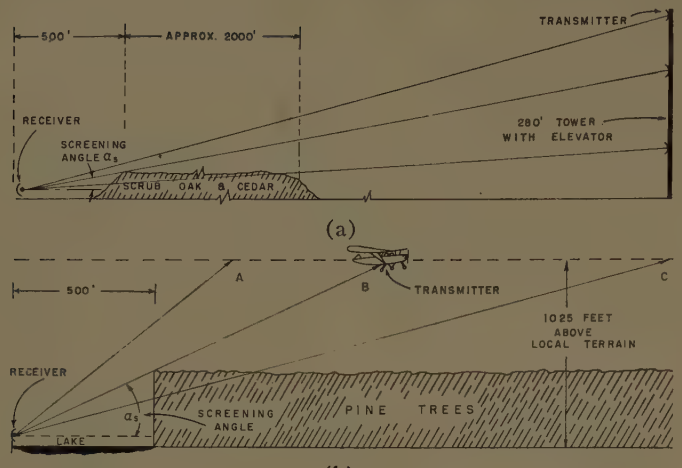

Fig. 1—Field-measurement paths. (a) Two-mile path at Balcones Research Center, Austin, Tex. (b) Path at Bastrop State Park, Bastrop, Tex.

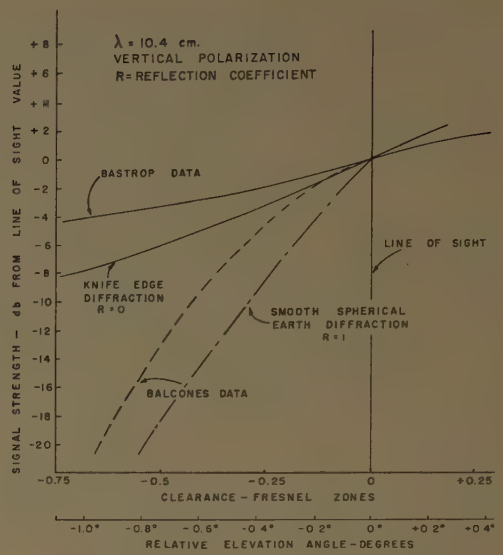

Fig. 2—Signal-strength comparison.

beam angle of $3\frac{1}{2}°$. The receiving antenna was located 8 feet above ground, approximately 500 feet from the edge of the grove, and was fixed in elevation pointing at the center of the tower. The trees were about 20 feet tall. The Bastrop path employed an airplane carrying the transmitter with a wide-angle horn mounted on the landing gear. The receiving equipment was the same as used at the upper path except for a tracking mechanism, added to keep the receiving antenna pointed toward the airplane. Tracking was accomplished optically to the line-of-sight. For one degree below line-of-sight, tracking was accomplished by decreasing the antenna elevation angle at the same angular rate as obtained at line-of-sight. The airplane flew at an elevation of 1025 feet above local terrain. The pine trees on this path were 50-to-60 feet tall.

It should be noted that the tall trees at Bastrop result in a much larger line-of-sight angle α_s than at Balcones. This larger line-of-sight angle, hereafter called screening angle, apparently makes a significant difference in the signal-strength level when the transmitter is below line-of-sight. This is discussed further in a later paragraph.

The results of the signal-strength measurements at Balcones and at Bastrop are shown in Fig. 2. Theoretical knife-edge diffraction[1,2] and smooth-sphere diffraction curves[3] are shown for comparison. All curves have been normalized to their line-of-sight value, and the distance factor[4] in the Bastrop data has been removed.

It will be noted that the signal at Balcones has about the same slope as the theoretical smooth-sphere diffraction curve, Fig. 2. This is in general agreement with signal-strength measurements made by other researchers at different frequencies but under similar circumstances.[5] Trees are found not to present an opaque diffracting edge at the optical line-of-sight, but rather an effective diffracting surface somewhere below the optical line-of-sight, the depth depending on the density of the foliage and limbs, and the screening angle.

The signal-strength curve at Bastrop is found to be considerably stronger at the same relative elevation angle than that at Balcones and significantly stronger than the theoretical knife-edge diffraction curve. The difference in the screening angle at the two sites is believed to be the principal difference in the two cases. At Balcones, the propagation path is almost parallel to the tops of the trees, while at Bastrop this is not so. At Balcones, for example, a path from the receiver to the transmitter, 1° below the line-of-sight path, passes through approximately 1000 feet of oak and cedar trees while a similar path at Bastrop passes through only 87 feet of pine trees. By this comparison one does not mean to imply that the received signal actually travels the above paths between the transmitter and the receiver, but rather that the diffraction problem is different in the two cases. It appears that the effective diffracting edge at Bastrop may be well below the visual line-of-sight path, while at Balcones it may be very near the visual line-of-sight path. More measurements of the type reported here would have to be made before the interrelationship of the variables could be put on an empirical basis.

The time characteristics of the vertically-polarized signal at Balcones for different elevation angles of the transmitter are shown in Fig. 3. The average wind speed was recorded at 10 mph at tree-top level during the

[1] A. Sommerfeld, "Optics," Academic Press, Inc., New York, N. Y., pp. 249–253; 1954.

[2] "Summary Technical Report of the National Defense Research Committee," U. S. Gov't. Printing Office, Washington, D. C., vol. 1, pp. 125–131; 1946.

[3] K. Bullington, "Radio propagation fundamentals," *Bell Sys. Tech. J.*, vol. 36, pp. 593–626; May, 1957.

[4] H. R. Reed and C. M. Russell, "Ultra High Frequency Propagation," John Wiley and Sons, Inc., New York, N. Y., pp. 81–82; 1953.

[5] H. Head, "The influence of trees on television field strengths at ultra-high frequencies," Proc. IRE, vol. 48, pp. 1016–1020; June, 1960.

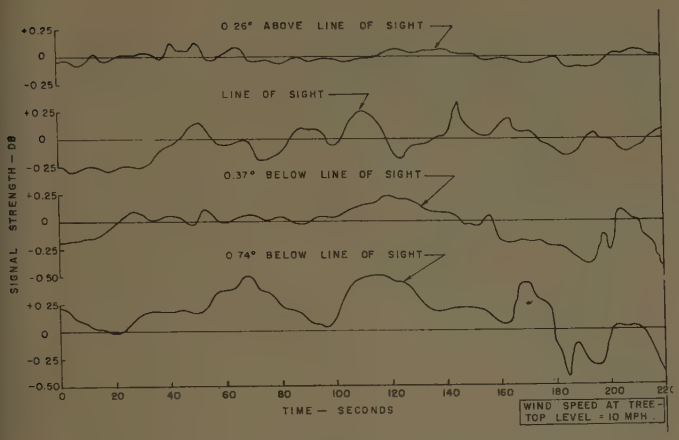

Fig. 3—Time characteristics of signal at Balcones.

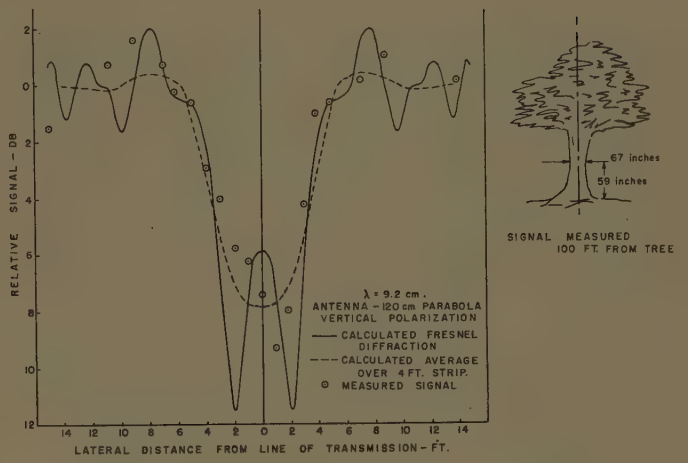

Fig. 4—Diffraction study of a narrow opaque obstacle. After J. S. McPetrie and L. H. Ford, "Experiments on propagation of 9.2 cm-wavelengths, especially on the effects of obstacles," *J. Inst. Elec. Engrs. (London)*, vol. 93, pt. 3-A, pp. 531–543; March–May, 1946.

measurements. The curves show the signal-strength variations to increase as the transmitter drops further below line-of-sight. The variations are observed to be relatively slow and in the order of 1-to-6 cycles per minute.

III. Receiving Antenna Radiation Patterns on the Balcones Path

Receiving antenna radiation patterns in the horizontal plane were made at Balcones for the same transmitter elevation angles shown on the time-characteristics study in Fig. 3. It was felt that any deterioration in the approximate point source, caused by the trees, would be detected in the patterns by the beamwidth broadening, the signal maximum shifting, and the nulls filling in.

The beamwidth was found to be somewhat greater as the transmitter dropped deeper behind the trees, but not a significant amount. The signal maximum appeared, as nearly as could be determined, to come from the same point for all cases. No significant fill-in in the nulls was observed.

IV. Absorption and Diffraction Study of a Single Tree

It was decided that a detailed study of a single tree be made to see what could be learned about the diffraction and absorption of radio signals for such an obstacle. A preliminary search of the literature revealed little information on the subject; however, one significant paper by McPetrie and Ford[6] was found.

Fig. 4 is a diffraction study of a narrow opaque obstacle made by McPetrie and Ford. As indicated in the sketch of the tree, shown on the figure, the signal-strength measurements were made laterally from a path passing through the center of the tree, 59 inches above ground and approximately 100 feet behind the tree. The principal path did not at any time pass through the branches of the tree. The trunk was 5 feet 7 inches in diameter. The Fresnel diffraction curve,[6] shown as a solid line, was computed on a point basis for a very long, opaque strip of the same width as the tree. The dotted curve is an integrated curve and represents the signal received in a 4-foot strip normal to the axis of the tree. This curve should approximate the signal received by a 120-cm parabolic antenna. The measured signals, using the 120-cm parabolic antenna, are shown as circles. A reasonable agreement with the theoretical curve is obtained. McPetrie and Ford made similar measurements at other distances behind the tree with comparable results.

No lateral signal-strength measurements were found in the literature where the path passed directly through the foliage of the tree. Since this seemed to be important to the present study, such measurements were made.

The diffraction and absorption characteristics of a signal passing through a large live oak tree, dubbed Montopolis oak, is shown in Fig. 5. The oak tree was approximately 30 feet tall and had a foliage spread of about 50 feet. The trunk was 5.4 feet in diameter, 3 feet above ground. Three lateral runs were made behind the tree at distances of 300, 600, and 900 feet. The approximate transmission paths through the branches of the tree are shown on the tree insert. The approximate shape of the foliage is also shown.

It will be noted that the signal drops a surprising amount when directly behind the Montopolis oak and considerably more than would be predicted by absorption alone. At a frequency of 2880 Mc, the average absorption should be approximately 0.18 db/foot, giving 9 db for the thickest part of the foliage.[7]

[6] J. S. McPetrie and L. H. Ford, "Experiments on propagation of 9.2 cm wavelengths, especially on the effects of obstacles," *J. Inst. Elec. Engrs. (London)*, vol. 93, pt. 3-A, pp. 531–543; March–May, 1946.

[7] A. H. LaGrone, "Forecasting television service fields," Proc. IRE, vol. 48, pp. 1009–1016; June, 1960.

The signal strength is observed to rise sharply about 18-to-20 feet to the left of the tree trunk. This is due to the thinness of the foliage in this part of the tree. The transmitter was actually visible through the leaves.

The terrain behind the Montopolis oak was not table top level, hence the height at which the path passes through the tree on the various lateral runs was different. A calibrating run, not shown, was made in front of the tree and showed no serious variations in signal strength.

Antenna patterns in the horizontal plane taken directly behind the Montopolis oak at distances of 300, 600, and 900 feet are shown in Fig. 6. The free-space pattern of the antenna is included to show the extent of pattern distortion. The approximate point at which the transmitter would be found if the tree were removed is shown on the tree insert.

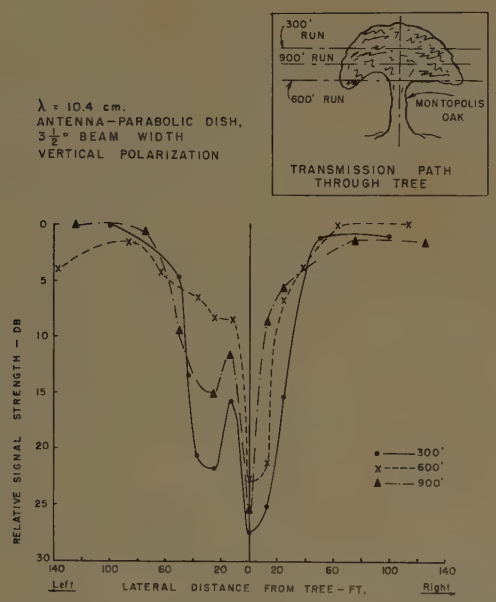

Fig. 5—Diffraction and absorption study at various distances behind a live oak tree.

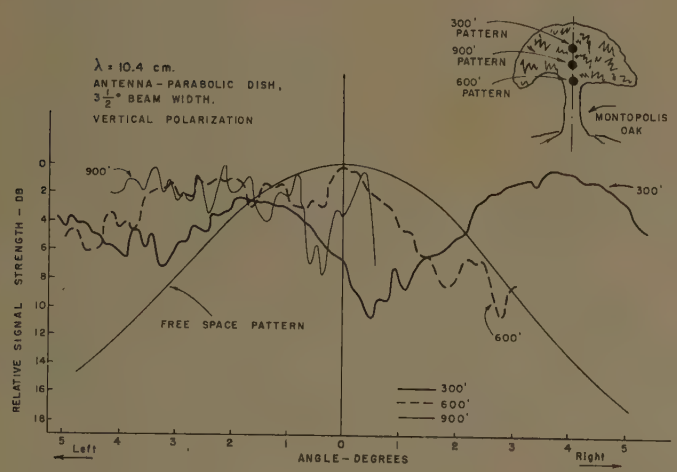

Fig. 6—Antenna patterns directly behind Montopolis oak.

The deterioration of the approximate point source is clear. The antenna beam patterns are no longer recognizable, and pointing for a signal maximum would be meaningless insofar as indicating the true direction of the transmitter.

The Montopolis oak patterns were all taken with the transmitter at a fixed height. No facilities were available at this site for raising or lowering the transmitter more than a few feet at most. In order to vary the height of the transmitter, a tree near the 280-foot tower at Balcones was selected.

The Balcones tree, a hackberry, was much smaller than the Montopolis oak, but perhaps more nearly represented average field conditions than the Montopolis oak. The geometry of the path is shown in Fig. 7.

Antenna patterns in the horizontal plane taken behind the hackberry tree at Balcones are shown in Fig. 8. The patterns were separated in preparing the drawing, for the sake of clarity, and their relative positions do not indicate their relative amplitudes.

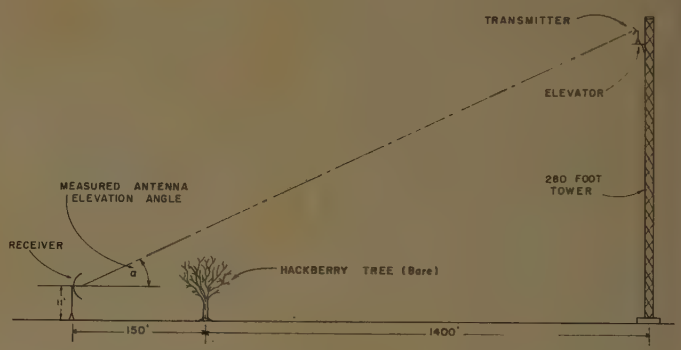

Fig. 7—Path geometry for hackberry tree measurements.

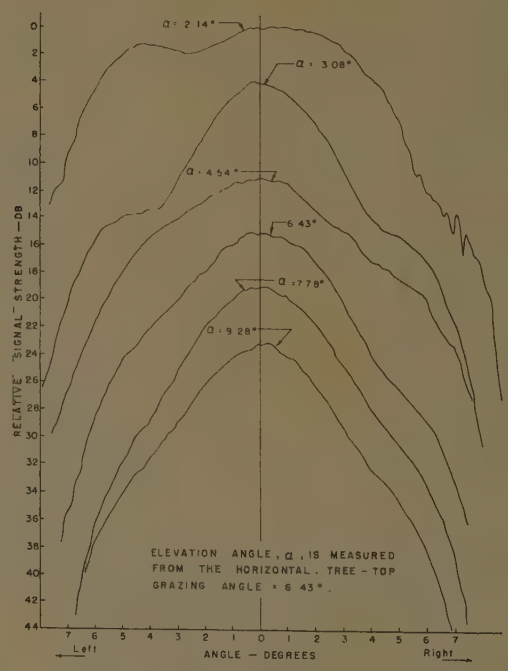

Fig. 8—Antenna patterns behind leafless hackberry tree at various elevation angles.

In these patterns, the deterioration of the approximate point source is again evident though not to the extent found behind the Montopolis oak (Fig. 6). At the highest-elevation angle, $\alpha = 9.28°$, the shape of the beam is reasonably close to the free-space shape, although some deterioration is observable here. At $\alpha = 9.28°$, the center of the main beam is approximately 2.85° above the top of the tree. At the lowest-elevation angle, $\alpha = 2.14°$, the beamwidth is $9\frac{1}{4}°$ between half-power points. This, compared to the $3\frac{1}{2}°$-beam angle for the free-space pattern, indicates the distortion taking place in the approximate point source. The remaining curves show the pattern constantly changing as the transmitter moves up the tower.

V. Pointing Error Signal Analysis

The effect of pattern distortion, as observed in Figs. 6 and 8, on direction-finding radar equipment is severe. Add to this the absorption due to transmission through the branches and foliage of the trees, if any, and the problem of low-angle tracking is even more difficult. Ordinary search radar tracking an airplane through a tree would see a distorted picture of the target echo. The echo would change with elevation angle of the target and would be very broad at times. It would be difficult to get a true bearing on such a target.

Radars that employ a lobe-comparison technique for improving their pointing accuracy must have lobe patterns that are of a known shape and patterns that do not change under operating conditions. Such radars employ narrow beams and frequently do their lobe switching by employing a nutating feed. A discussion of the lobe-switching techniques employed, of course, is beyond the scope of this paper.

While it is not desirable to discuss a particular radar, an analysis can be made of a hypothetical radar employing the $3\frac{1}{2}°$ pattern of the receiving antenna used in these measurements. Let it be assumed, for example, that the antenna beam can be switched continuously and rapidly in azimuth through an angle of $\pm 2\frac{1}{2}°$. "On Target" conditions would be indicated by equal echo signal amplitudes with the beam in the left- and right-azimuth positions. With this hypothetical antenna system, the direction of the transmitter was determined for each of the antenna patterns taken at Balcones.

Fig. 9 shows the theoretical pointing error for four patterns measured behind the grove of scrub oak and cedar trees on the Balcones path shown in Fig. 1. The antenna patterns used in this study are discussed in Section III.[8] The pointing error for $\alpha = +0.26°$ was assumed to be zero, and the other pointing errors were determined relative to this reference.

Fig. 10 shows the theoretical pointing errors determined for the hackberry tree at Balcones. The direction obtained from the pattern taken at the highest elevation angle ($\alpha = 9.28°$) was assumed to be correct, and the other pointing errors were determined relative to it. The error curve is observed to be S-shaped, in that it shifts from one side to the other as the transmitter moves down the tower. This pointing error would, of course, be different for another tree, and in all probability, quite unpredictable.

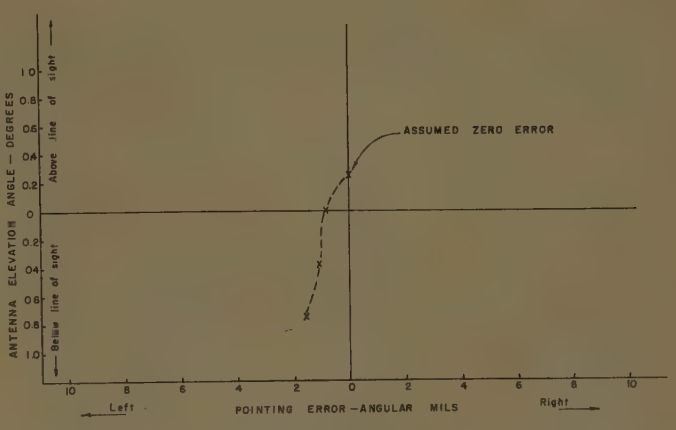

Fig. 9—Theoretical pointing error behind grove of live oak and cedar trees at Balcones.

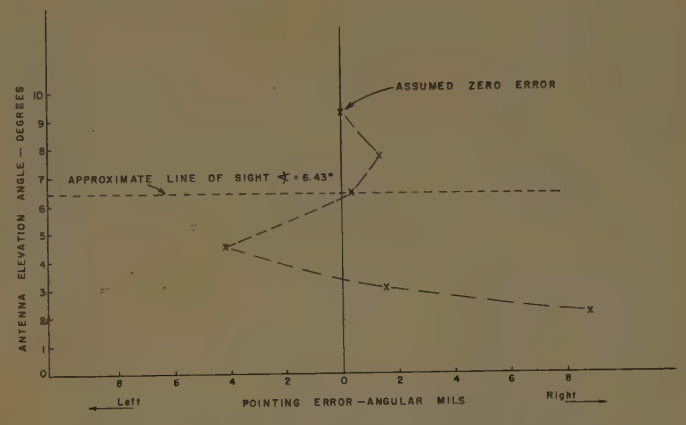

Fig. 10—Theoretical pointing error behind leafless hackberry tree at Balcones.

VI. Conclusions

1) The signal strength for vertical polarization behind an obstruction of trees is found to vary with the screening angle, and for small screening angles, to approach the theoretical curve for diffraction over a spherical surface.

2) Time variations in the vertically-polarized signal are observed to be relatively slow and of the order of 1-to-6 cycles per minute.

3) An approximate point source is distorted when a tree or a portion of a tree is intercepted by the main beam of the receiving antenna.

4) Radars employing beam-comparison techniques are subject to significant pointing errors when a tree or a portion of a tree is intercepted by the main beam of the tracking antenna.

[8] A. H. LaGrone and C. W. Chapman, "Some Effects of Trees on Low Angle Propagation at a Wavelength of 10.4 Centimeters," Elec. Engrg. Res. Lab., The University of Texas, Austin, Tex., Rept. No. 6-36, pp. 8–9; July, 1960.

Tropospheric Scatter Propagation and Meteorological Conditions in the Caribbean*

R. E. GRAY†, MEMBER, IRE

Summary—**Results are given of radio propagation measurements which have recently been made in the Caribbean. The transmission loss on beyond-the-horizon paths in this region was found to be considerably less than that measured over paths of similar length in temperate climates.**

The fact that the path loss is, in general, relatively low in the Caribbean is believed to be chiefly due to the large gradient of the refractive index of the atmosphere which normally prevails in the first few hundred feet above the earth's surface in that area.

Introduction

During the last few years a study has been made of the radio propagation and meteorological conditions in the Caribbean area. More than 6000 hours of transmission loss measurements have been made in the UHF band over eighteen beyond-the-horizon paths in this region. This study showed that, in general, the median transmission loss was about 14 db less over typical paths in the Caribbean than on overland paths in temperate climates.

Beyond-the-horizon radio propagation in the Caribbean is influenced by a slow vertical sinking of air from anticyclonic areas, and particularly from that area known as the Bermuda High, by warm dry air from land masses blowing over a cooler sea, and by the relatively large decrease of the refractive index of the atmosphere with height, a condition which normally prevails in the first few hundred feet above the earth's surface in this region.

It is shown that the relatively low path loss measured in the Caribbean may be explained by the large refractive index gradient normally existing near the earth's surface in that area. The geometry of typical tropospheric scatter paths, and the nonlinear nature of the normal refractive index gradient, indicates that it is the gradient in the first few hundred feet, rather than in the more usual first kilometer, which determines the modified radius of the earth for tropospheric scatter transmission.

Measurements show that a single empirical curve may be drawn representing the transmission loss as a function of the effective distance for both the Caribbean and temperate climate areas.

I. Path Loss Measurements

Transmission Paths Measured

This paper describes the results of UHF transmission loss measurements made on thirteen beyond-the-horizon paths between islands in the West Indies, and on five such paths between Florida and neighboring islands.[1,2] These transmission paths varied in length from 80 to 540 statute miles.

Conditions of Test

All transmission loss tests were made on frequencies between 800 and 1000 Mc, except those between Florida and Nassau,[2] where a frequency of 1970 Mc was employed. Ten-foot in diameter paraboloid antennas were used for transmitting and receiving for all tests except those on a path longer than 500 miles where a 28-foot in diameter paraboloid was used for transmitting; the usual 10-foot antenna was employed for receiving.

Tests on each path were conducted continuously, 24 hours per day, for periods ranging from two weeks to several months; however, the median path loss figures referred to in this paper were determined from tests lasting a total of between 300 and 800 hours on each path.

The measurements were carried out at various times of the year; however, the received carrier level during two years of operation on the Florida-Cuba link showed that the change in the monthly median path loss in this area was only a few db. Summer and winter tests made on a longer path in the eastern Caribbean showed a seasonal change of 8 db. It is believed, therefore, that the measured median loss for all paths may be considered to be within about ± 4 db of the annual median value.

The recorded level of the received carrier on each path was divided into 15-minute intervals, and the median carrier level was determined from the distribution of the 15-minute medians. It is believed that the over-all accuracy of all path loss measurements was of the order of ± 2 db.

Results of Path Loss Measurements

The value of the median scatter loss measured on each path has been plotted as a function of the effective distance.

By scatter loss is meant the measured median path loss in excess of the computed free space loss. The effective distance in statute miles is defined as the angular distance in radians (angle of intersection of the antenna beams) multiplied by the radius of the earth modified

* Received by the PGAP, April 19, 1961; revised manuscript received, May 25, 1961.

† IT & T Labs., Inc., Nutley, N. J.

[1] K. P. Stiles, "Report on over-the-horizon radio transmission tests between Florida and Cuba," 1956 IRE Convention Record, pt. 8, pp. 212–215.

[2] K. P. Stiles, "Tropospheric scatter path loss tests Florida-Bahamas," IRE Trans. on Communication Systems, vol. CS-7 (no. 3.), pp. 205–208; September, 1959.

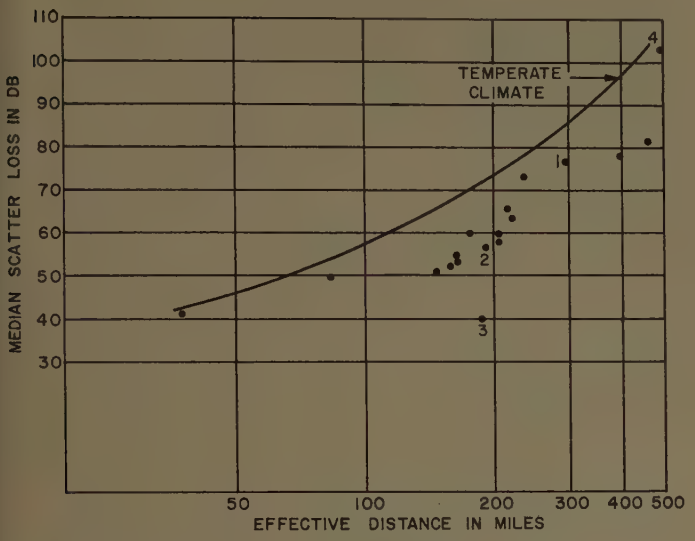

Fig. 1—Scatter loss in the Caribbean area as a function of the effective distance computed for a value of K of 1.33.

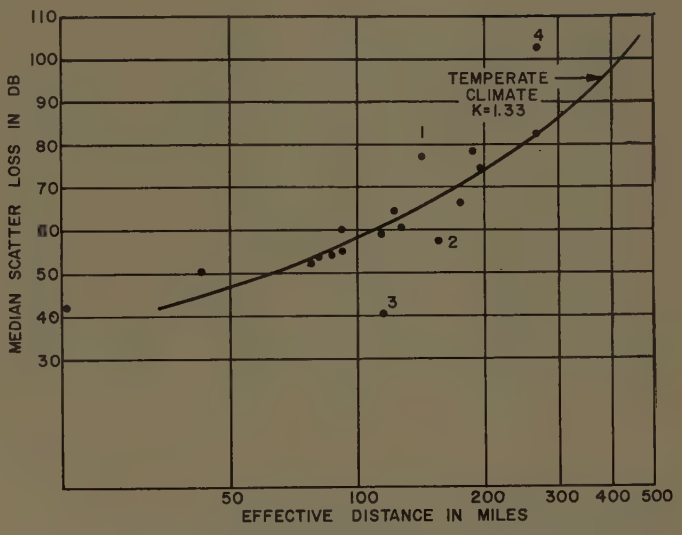

Fig. 2—Scatter loss in the Caribbean area as a function of the effective distance computed for a value of K of 2.4.

for normal refraction, which is usually taken as 5280 miles. The effective distance of a transmission path is thus the distance on the surface of a smooth earth of radius 5280 miles which subtends an angle at the center of the earth equal to the angle of intersection of the antenna beams as computed for the actual transmission path. It should be noted, however, that the computed angular distance for a particular path is a function of the value assumed for the earth's radius modified for atmospheric refraction.

The value of the median scatter loss measured between Florida and Nassau has been reduced by 3 db to correct for the fact that this path was measured on approximately twice the frequency employed for tests on the other paths.

Scatter Loss and Effective Distance with $K=1.33$: The values of scatter loss have been plotted in Fig. 1 as a function of the effective distance. This distance has been computed from the profile of each path, and assumes a modified earth radius of 4/3 the true radius, or a value of K of 1.33. In Fig. 1 there is also shown an empirical curve of the annual median loss at 900 Mc derived from the average of a large number of path loss measurements made on overland paths in temperate climates.

Scatter Loss and Effective Distance with $K=2.4$: In Fig. 2 the scatter loss values have been plotted as before, as a function of effective distance, but in this case the distance has been computed assuming the ratio of the modified to real radius of the earth (K) to be 2.4 instead of 1.33. In Fig. 2, the empirical path loss curve for temperate climates is again shown, the effective distance in this case corresponding to a value of K of 1.33. It will be seen that the scatter loss values, with the exception of the four points numbered 1–4, now lie close to the temperate climate curve.

In the case of path No. 1, both horizons were on land and it is seen that the measured loss corresponds to an effective distance of approximately 220 miles, which is equivalent to a value of K for this path of about 1.7 instead of 2.4.

On path No. 2, a 4000-foot mountain formed a common horizon from each end of the path, and it is believed that some obstacle gain was obtained on this path.

In the case of path No. 3, a 4000-foot peak on an island near the middle of the path formed a common horizon from the two terminals, and considerable obstacle gain was no doubt obtained.

Path No. 4 showed an exceptionally high transmission loss, about equivalent to an effective distance corresponding to a value of K of 1.4. The reason for the high loss measured on this path is not known, but it is suggested that it may have resulted from the fact that one end of the path was only about 60 feet above sea level, whereas the other was at an elevation of 2000 feet.

II. Meteorological Conditions

Refraction of Radio Waves[3]

If there were no atmosphere, radio waves would travel in straight lines, and the curvature of the rays, relative to the earth's surface, would be $1/R$ where R is the radius of the earth. Refraction in the atmosphere causes a bending of the rays, and with a constant refractive index gradient the curvature is equal to the variation in the refractive index n with height, that is to dn/dh. With a constant refractive index gradient, we may consider the radio rays to be straight lines with the earth having an effective radius R_1, where

$$\frac{1}{R_1} = \frac{1}{R} + \frac{dn}{dh}.$$

[3] D. E. Kerr, "Propagation of Short Wave Radio Waves," M.I.T. Rad. Lab. Ser., McGraw-Hill Book Co., Inc., New York, N. Y., vol. 13; 1951.

If the ratio of R_1 to R is denoted by K, then

$$K = \frac{1}{1 + R\dfrac{dn}{dh}}.$$

The Gradient of the Refractive Index

If one assumes the usual value of K of 1.33 for land paths in temperate climates, then transmission loss measurements show that the scatter loss on beyond-the-horizon paths in the Caribbean area corresponds to an effective value of K of 2.4 for oversea paths, and about 1.7 for overland paths. Actual measurements of the refractive index gradient in this region, however, indicate that the value of K is considerably lower, being approximately between 1.45 and 1.65. Fig. 3 shows the average value of K at San Juan, Puerto Rico; very similar values are also obtained at Swan Island, some 400 miles west of Jamaica. At Miami, Fla., the average monthly value of K varies from approximately 1.41 to 1.65. The figures quoted above were derived from the difference in the refractive index of the atmosphere measured at the surface of the earth and at 1 km above the surface.[4]

The values of K derived in this way are thus in fair agreement with the value of 1.7 estimated from path loss tests of an overland path, but are much lower than the value of 2.4 estimated for oversea paths in the Caribbean. This lack of agreement is believed to be due to the fact that the values of K quoted above for San Juan and Miami were derived from the gradient of the refractive index measured over land for the first km of height, and do not, therefore, correspond to the much larger gradients which are likely to exist in the first few hundred feet above the surface of the sea.

The Geometry of Transmission Paths

From profiles of typical beyond-the-horizon oversea paths, it is seen that a large percentage of the transmission path is relatively close to the surface of the sea. If one assumes a smooth earth with a linear refractive index gradient and with antenna elevations of only 30 feet, then Fig. 4 shows the percentage of the transmission path which is below 500 feet for path lengths of from 100 to 400 miles and with values of K of 2.4 and 1.33. If the heights of the antennas are increased to 500 feet, then the percentage of the path which is below 500 feet is also increased. For example, if one assumes a value of K of 2.4, a path length of 200 miles and the terminals 500 feet above sea level, then 84 per cent of the transmission path will be below 500 feet. Thus, from the geometry of typical beyond-the-horizon transmission paths, it is seen that if the refractive index gradient is not linear, then it is the average gradient, not in the first few thousand feet but in the first few hundred feet, that is likely to be of chief importance.

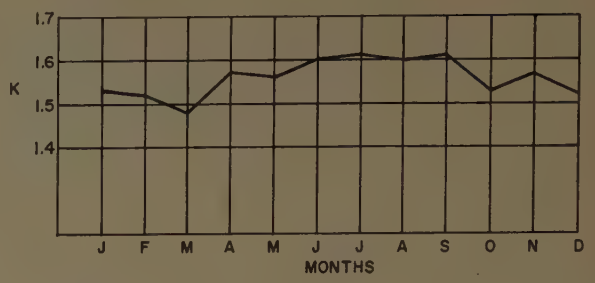

Fig. 3—Modified Earth's radius factor K for San Juan, Puerto Rico.

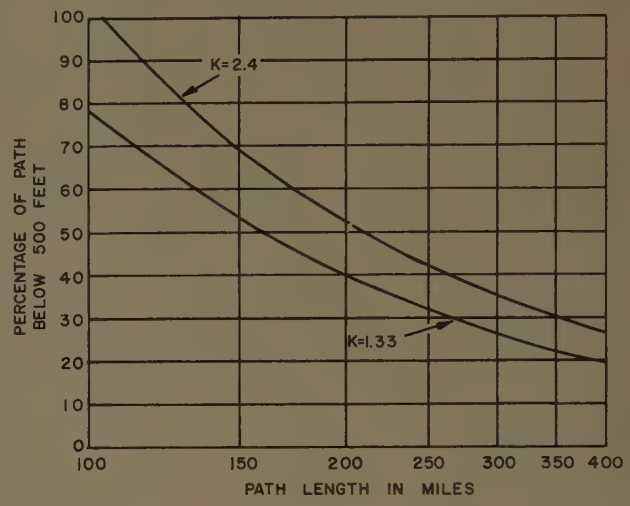

Fig. 4—Percentage of a transmission path below 500 feet with antennas 30 feet above a smooth earth.

It can be shown that if the variation in refractive index with altitude is parabolic, then the effective gradient of the refractive index on a beyond-the-horizon transmission path is given by[5]

$$G = \frac{2G_1 + G_2}{3}$$

where

G = effective gradient,
G_1 = gradient at the lowest point on the path,
G_2 = gradient at the base of the common volume.

Refractive Index Gradients Near the Surface of the Sea

The refractive index gradient near the sea surface is likely to be high on oversea paths particularly in warm

[4] Private Communication from B. R. Bean, Natl. Bur. of Standards, Boulder, Colo.

[5] P. Misme, "Influence Radioclimatiques Sur Les Liasons Trans Horizon," *L'Onde Electrique*, vol. 394, pp. 116–123; January, 1960.

climates. This is so because of the large gradient of the relative humidity near the surface of a warm sea, and because of the temperature inversion which is often caused by warm dry air from neighboring land masses blowing over a cooler sea.[6]

Measurements made of the refractive index gradient over the Irish Sea in the summer of 1944[7] showed that this gradient was greater than normal below 1000 feet for wind speeds less than about 18 miles per hour, and under conditions of low wind speed ducting conditions often occurred below about 500 feet.

Measurements reported by Katzin and by Bean of the refractive index gradient near the sea surface in the Caribbean have shown a high percentage of surface ducting conditions.[8,9] Further measurements made in that area by Fitzsimmons and Stephenson[10] have shown that on the Caribbean side of the Panama Canal Zone the large lapse rates of temperature and specific humidity, observed in the lowest 50 feet above the Caribbean, result from the high water temperature of 80° to 83°F, and from the steady trade winds blowing spray into the lower air. Soundings showed that the refractive index gradient in the first 300 feet above the surface of the sea often showed the existence of a surface duct within the first 100 feet with an effective value of K, for the first 300 feet, of about 2.4.

Misme reports measurements made on the south coast of France by observing radar echos from the island of Corsica. These showed the following seasonal values of K:[11]

Season	K
Spring	2.7
Summer	2.6
Fall	1.8
Winter	1.4
Annual	2.1

Thus, measurements of the refractive index near the sea surface in warm climates indicate that the average value of K is likely to lie between 2 and 3.

Refractive Index Gradient Near the Surface of the Land

It has been shown by Bean and Thayer[12] that the average value of the surface refractivity is well correlated with the refractive index gradient as measured at 45 U. S. weather stations. Fig. 5, taken from N.B.S. Rept. No. 6025, shows the relation found between the surface value of refractive index N_s, and ΔN, the difference between the value of the refractive index at the earth's surface and at 1 km above the surface. Since the surface value of the refractive index in the Caribbean is usually between 350 and 380, the corresponding value of ΔN would be expected, from Fig. 5, to lie between 50 and 60, corresponding to a value of K of between 1.5 and 1.65.

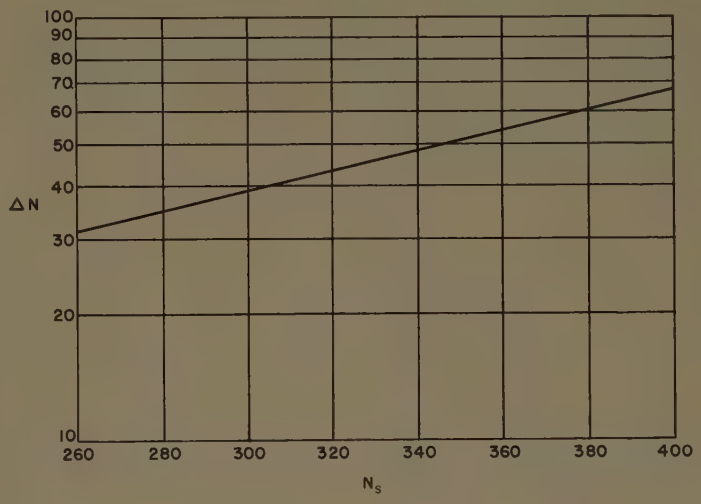

Fig. 5—Refractive index gradient in the first km of height (ΔN) as a function of the surface value of the refractive index (N_s).

It has, however, been shown by Misme[13] that the gradient of the refractive index within the first 1000 feet of the atmosphere may in general be higher than the value obtained from Fig. 5. For example, measurements made at Trappes, near Paris, showed that the value of ΔN at the 0.35-km level varied from 44 in February to 66 in August, the corresponding values of N_s being about 310 and 340. It is probable, therefore, that for overland paths in the Caribbean—that is, for paths where the two radio horizons are land areas more than about five miles from the coast—the average effective value of K is somewhat greater than 1.6. This agrees with the figure of 1.7 estimated from transmission loss measurements made over path No. 1 which had land horizons.

[6] R. B. Montgomery and R. H. Borgoyne, "Modified Index Distribution Close to the Ocean Surface," M.I.T. Rad. Lab., Cambridge. Mass., Rept.; February 16, 1945.

[7] P. A. Sheppard, "The Structure and Refractive Index of the Lower Atmosphere," presented at the Conf. on Meteorological Factors in Radio Wave Propagation, London, Eng.; 1946.

[8] M. Katzin, R. W. Bauchman, and W. Binnian, "3 and 9 centimeter propagation in low ocean ducts," PROC. IRE, vol. 35, pp. 891–905; September, 1947.

[9] B. R. Bean, "Climatology of ground-based radio ducts," *J. R. Natl. Bur. of Standards*, pp. 29–34; July–August, 1959.

[10] K. E. Fitzsimmons and S. T. Stephenson, "Low Level Meteorological Soundings and Radar Correlations for the Panama Canal Zone," N.D.R.C., Ottawa, Can., project no. PDRC 647; June, 1944.

[11] P. Misme, "Le Gradient Equivalent, Measure Directs et Calcul Theorique," *Annales des Telecommunication*, vol. 15, pp. 92–99; March–April, 1960.

[12] B. R. Bean and G. D. Thayer, "On Models of the Atmospheric Radio Refractive Index," Natl. Bur. of Standards, Rept. No. 6025; November, 1959.

[13] P. Misme, "Essai De Radioclimatologie D'Altitude Dans le Nord de la France," Annals des Telecommunications, vol. 13, pp. 303–310; November–December, 1958.

Conclusions

Transmission loss measurements made on beyond-the-horizon paths in the Caribbean have shown that in general the path loss in that area is considerably less than that found in temperate climates. These measurements indicate that if the appropriate values of the earth's radius factor K are assumed, then a single empirical curve can be drawn, for both Caribbean and temperate climate areas, representing the annual median scatter loss for effective distances of between 50 and 300 miles.

The effective values of K for overland and oversea paths are estimated in Table 1. The values of K given above for oversea paths are greater than have been generally assumed. It is believed, however, that such high effective values may be explained by the geometry of typical beyond-the-horizon paths, and by the relatively large refractive index gradient normally found near the sea surface.

TABLE I

	Value of K	
	Caribbean	Temperate Climate
Overland paths	1.7	1.33
Oversea paths	2.4	1.90

Transmission loss and meteorological measurements indicate that it is the effective length of the path, corresponding to the refractive index gradient in the first few hundred feet of the earth's atmosphere, and not in the first km, which chiefly determines the median scatter loss on typical beyond-the-horizon transmission paths.

communications

Comments on "Scatter Communications with Radar Chaff"*

The recent paper by Hessemer[1] proposes the novel use of (radar) chaff for the purpose of scattering electromagnetic energy for non-line-of-sight communication links. While inventive in its approach, this paper makes no reference to several well-known papers of particular importance to the problem considered.

The omitted references have particular bearing on 1) the considerations of scattering from an ensemble of chaff dipoles randomly oriented in space, and 2) the evaluation of the energy scattered from a short chaff dipole. These references should be made in order to verify (or refute) the formulas and data presented by Hessemer.

Van Vleck, Bloch, and Hamermesh[2] have written the first definitive paper concerned with the scattering of electromagnetic energy from thin wires (chaff). The Van Vleck work gives the first evaluation of scattering by an individual dipole and also evaluates the back-scattering cross section averaged over all angles of orientation of the dipole. The peak (resonant) value of $\bar{\sigma}$ (back-scattering cross section for normal incidence averaged over polarization angles) obtained by Van Vleck, *et al.*, is about $0.32\lambda^2$, measurably more than the $0.27\lambda^2$ obtained by Hessemer when his angles are specified to correspond to the back-scattering case.

Further work reported in the open literature relating to the cross sections of individual thin wires,[3-8] for lengths near the first resonance, bear an even greater importance on the Hessemer paper. Hessemer uses a heuristic approach to this problem, involving antenna-dipole input impedances for which no terminals are defined. It has been shown that reliable results are obtained for scattering from thin wires only when a thorough treatment of the boundary-value problem is made.

Tai[3] published the first paper using the variational technique for treating the boundary-value problem posed by the thin-conducting wire less than 4.0λ in length. Tai also discusses the current distributions on the wires[3] and the validity of the thin wire approximation.[4] Kouyoumjian[5] uses a similar technique and compares the results favorably with experiment. Sevick[6] obtains excellent agreement with experiment, using the variational technique with the Morita[7] current distributions and making corrections for end conditions. The writers[8,9] have extended the above results to include effects of loss, obtaining good comparison between theory and experimental results.

An example indicating the error of the approximate method of Hessemer may be drawn from the authors' work.[8] A dipole of length 0.4λ has a back-scattering cross section (per unit length of dipole) which is reduced by a factor of 1.74 from that of a resonant dipole. This dipole is a circular cylinder about 0.02λ in diameter, which is comparable to the flat strip of a length-to-width ratio of 20 to 35 given by Hessemer. Hessemer obtains a reduction of 6.5 for his 0.4λ dipole.

E. S. Cassedy
Microwave Research Inst.
Polytechnic Inst. of Brooklyn
Brooklyn, N. Y.
J. Fainberg
Radiation Lab.
The Johns Hopkins University
Baltimore, Md.

Author's Reply[10]

The comments of Cassedy and Fainberg are well taken but need to be put into proper perspective with reference to the work under discussion.

The author was well aware of the work of Van Vleck, Bloch, Hamermesh, and Phillips[11-12] and made reference to it in an

* Received by the PGAP, April 25, 1961.

[1] R. A. Hessemer, Jr., "Scatter communications with radar chaff," IRE TRANS. ON ANTENNAS AND PROPAGATION, vol. AP-9, pp. 211–217; March, 1961.

[2] J. H. Van Vleck, F. Bloch, and M. Hamermesh, "Theory of radar reflection from wires or thin metallic strips," *J. Appl. Phys.*, vol. 18, pp. 274–294; March, 1947.

[3] C. T. Tai, "Electromagnetic back scattering from cylindrical wires," *J. Appl. Phys.*, vol. 23, pp. 909–916; August, 1952.

[4] C. T. Tai, "A new interpretation of the integral equation formulation of cylindrical antennas," IRE TRANS. ON ANTENNAS AND PROPAGATION, vol. AP-3, pp. 125–127; July, 1955.

[5] R. C. Kouyoumjian, "The Calculation of the Echo Areas of Perfectly Conducting Objects by the Variational Method," Antenna Lab., The Ohio State University, Columbus, Tech. Rept. No. 444-13; November, 1953.

[6] J. Sevick, "Experimental and Theoretical Results on the Back Scattering Cross Section of Coupled Antennas," Cruft Lab., Harvard University, Cambridge, Mass., Tech. Rept. No. 150; May, 1952.

[7] T. Morita, "The measurement of current and charge distributions on cylindrical antennas," PROC. IRE, vol. 38, pp. 898–904; August, 1950.

[8] E. S. Cassedy and J. Fainberg, "Back scattering cross sections of cylindrical wires of finite conductivity," IRE TRANS. ON ANTENNAS AND PROPAGATION, vol. AP-8, pp. 1–7; January, 1960.

[9] E. S. Cassedy and J. Fainberg, "Electromagnetic Cross Sections of Cylinders of Finite Conductivity," Rad. Lab., The Johns Hopkins University, Baltimore, Md., Tech. Rept. No. AF-81; August, 1960.

[10] Received by the PGAP, May 24, 1961.

[11] F. Bloch, M. Hamermesh, and M. Phillips, "Return Cross-Sections From Random Oriented Resonant Half-Wave Length Chaff," Radio Research Lab., Harvard University, Cambridge, Mass., 411-TM-127; June 19, 1944.

[12] J. H. Van Vleck, F. Bloch, and M. Hamermesh, "Theory of radio reflection from wires or thin metallic strips," *J. Appl. Phys.*, vol. 18, pp. 274–294; March, 1947.

earlier[13] report. However, the sophisticated method that they used does not lend itself to a rotation of coordinates, which is the central point of the paper in question. In fact, very little work is reported in the literature for the case where the transmitter and receiver are at different locations. As to the values for the singular back-scatter case, Mentzer[14] shows values ranging from a low of $0.24\lambda^2$ to a high of $0.37\lambda^2$, depending on the method of analysis. It is rather significant that a direct "antenna" approach yields an answer in this same range as well as the very important "bistatic" data.

The second point seems to be more a matter of interpretation. A half-wave resonant dipole actually resonates at a length slightly less than 0.5λ depending on the antenna geometry. The data presented by the author assumed the resonant point at 0.5λ; thus the 0.4λ data represent a point 0.1λ down from resonance. With this interpretation, the work of Cassedy and Fainberg[15] gives a value of about 5.5 rather than 1.74. Considering the differences in length-to-width ratio plus the fact that the numerical values given by this author were merely approximations used to demonstrate a result, it is difficult to compare the values of 5.5 and 6.5.

R. A. Hessemer, Jr.
Elec. Engrg. Dept.
University of Arizona
Tucson, Ariz.

[13] R. A. Hessemer, Jr., "Scatter Communications with Radar Chaff," Appl. Research Lab., University of Arizona, Tucson, S-5-80146; March, 1959.
[14] J. R. Mentzer, "Scattering and Diffraction of Radio Waves," Pergamon Press, Inc., New York, N. Y., p. 98; 1955.
[15] E. S. Cassedy and J. Fainberg, "Back scattering cross sections of cylindrical wires of finite conductivity," IRE Trans. on Antennas and Propagation, vol. Ap-8, pp. 1–7; January, 1960.

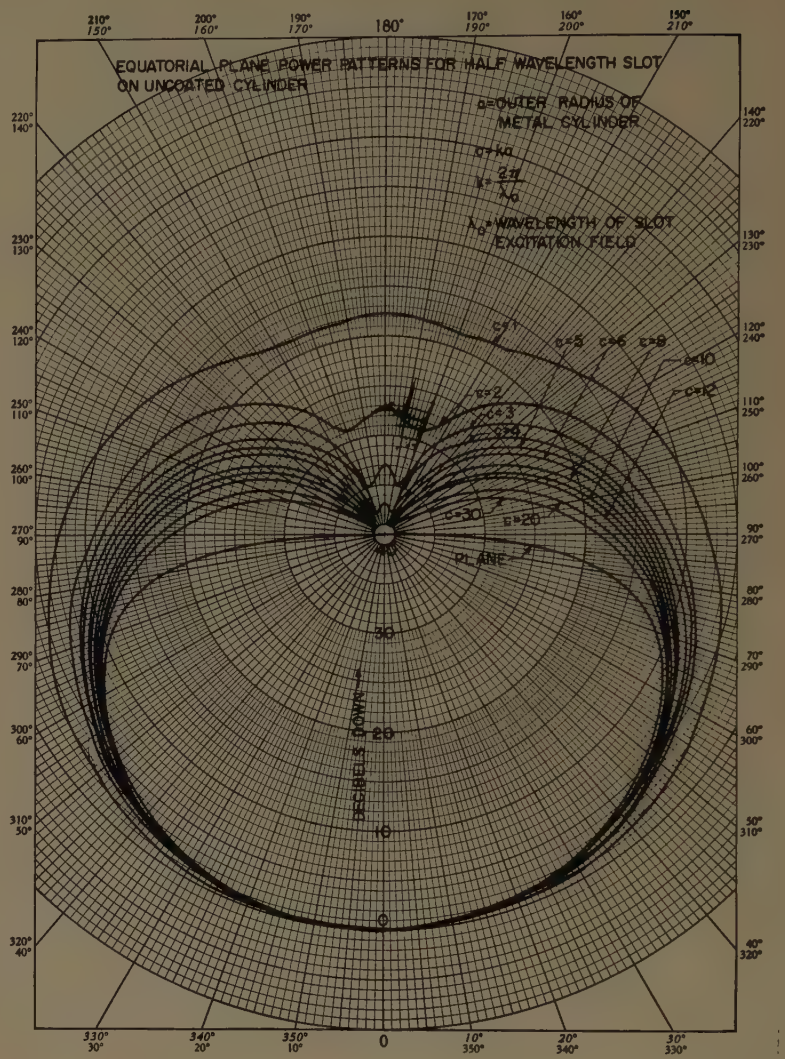

Fig. 1.

Calculated Equatorial Plane Radiation Patterns Produced by a Circumferential Slot on a Cylinder*

***Summary*—The equatorial plane radiation fields produced by a sinusoidal distribution of axial electric field along a half wavelength circumferential slot on a metallic cylinder of radius a have been computed by means of an IBM-704 electronic computer. Radiation patterns in this plane are given for sizes of cylinder from $1 \leq ka \leq 30$. It is believed that these computations are the most accurate made to date for these patterns. From these patterns it is seen that as the cylinder increases in size, for a given wavelength, the patterns sharpen, and in the limit of infinite cylinder radius the patterns approach that from a slot on an infinite plane.**

Recent work involving the determination of the radiation fields produced by a circumferential slot on a dielectric coated cylinder[1] considers, as a special case, the noncoated cylinder. It is believed that the calculations made for this special case are the most accurate made to date since they were performed by means of an IBM-704 computer. Although some of these calculations were manually performed in the past by others and have been reported,[2] it seems worthwhile to report these more accurate results here in a concise form over a large range of cylinder radii. The field calculated E_θ is given by (131) p. 44 of Wait[2] for the equatorial plane $\theta = \pi/2$ with the slot centered at $\phi_0 = 0$.

Power radiation patterns in decibels, plots of

$$20 \log_{10} \left[\frac{|f(0)|}{|f(\phi)|} \right],$$

are shown in Fig. 1, where $f(\phi)$ is defined by

$$f(\phi) \equiv \left. \frac{+E_\theta}{V_0 \dfrac{e^{-jkr}}{r}} \right|_{\theta=\pi/2},$$

TABLE I
On Axis Field Strength Values
$f(\phi) \equiv |f(\phi)| e^{j\theta_f}$

$c \equiv ka$	$\lvert f(\phi)\rvert_{\phi=0}$	$\theta_f\rvert_{\phi=0}$	Terms
1	0.31677	296.90	5
2	0.32480	6.7027	10
3	0.32349	69.231	15
4	0.32214	129.39	12
5	0.32118	188.50	15
6	0.32052	247.05	18
7	0.32005	305.25	21
8	0.31972	3.2459	18
9	0.31947	61.090	27
10	0.31927	118.82	30
12	0.31901	234.09	30
14	0.31884	349.16	38
16	0.31872	104.12	42
18	0.31864	219.00	46
20	0.31858	333.82	50
22	0.31854	88.605	54
24	0.31850	203.35	58
26	0.31847	318.08	62
28	0.31845	72.78	66
30	0.31843	187.47	70
∞	0.31831	−90.000	Plane Solution

[1] C. M. Knop, "The Radiation Fields from a Circumferential Slot on a Metal Cylinder Coated with a Lossy Dielectric," Res. Lab., Bendix Systems Division, Bendix Corp., Ann Arbor, Mich. Research Note No. 21; October 5, 1960.
[2] J. R. Wait, "Electromagnetic Radiation from Cylindrical Structures," Pergamon Press, New York, N. Y., p. 3; 1959.

* Received by the PGAP, May 1, 1961.

and where V_0 = voltage across the center of the slot, $k = 2\pi/\lambda_0$, and λ_0 = free space wavelength of wave exciting slot. In the equatorial plane

$$H_\phi = \frac{E_\theta}{\sqrt{\mu_0/\epsilon_0}},$$

and all other radiation fields are zero.

Tabulations of the magnitude and phase of $f(\phi)$ for $\phi = 0$, *i.e.*, of the on axis fields are given in Table I which also gives the number of terms taken in the summation of (131). It is believed that with this number of terms, five significant figure accuracy is obtained in both the magnitude and phase of $f(\phi)$. Computations[3,4] were made for $1 \leq c \leq 30$ in increments of 1 up to $c = 10$ and in increments of 2 for $10 \leq c \leq 30$, where $c = ka$. Not all patterns for these cases are shown in Fig. 1 for the sake of clarity. The angular increments in ϕ were in 5 degrees for $0 \leq \phi \leq 90$ and 2 degrees for $90 \leq \phi \leq 180$. All the patterns are symmetrical with respect to ϕ. Tabulation of all these calculations should appear in a forthcoming report. From these calculated power patterns, it is seen that as the cylinder becomes larger the patterns sharpen.

The equatorial plane radiation pattern for the case of a half wavelength slot in an infinite metallic plane is also shown in Fig. 1. For this slot

$$f(\phi) = -j\frac{\cos\left(\frac{\pi}{2}\sin\phi\right)}{\pi\cos\phi}.$$

The radiation fields from this slot have been obtained in the past by using the magnetic current concept,[5,6] but can also be obtained as a special case of the radiation fields produced by an aperture in an infinite plane coated with a dielectric-magnetic slab.[7] It is seen that the pattern for a large cylinder approaches that from the plane. In particular, for cylinders of size $c \geq 30$, the patterns are identical within approximately $\frac{1}{2}$ db for angles off the axis of ± 65 degrees. In addition, from Table I it is seen that for cylinders of $c \geq 30$, the absolute magnitudes of the on axis field strength from the plane and from these large cylinders are identical within three significant figures.

C. M. Knop
A. R. Battista
Hallicrafters Co.
Chicago, Ill.

[3] Basically, the program for computation utilized the following methods: SHARE NUBES-3 and the technique of Goldstein and Thaler.[4] The technique employed in the electronic computation was to output the results after each sum, where a sum was formed for each value of ϕ used. Each sum was then examined, and when it was evident (as ascertained by inspection of future sums) that any more summing would not affect the seventh significant figure of $|f(\phi)|$ the process was stopped. The time required for the IBM-704 computer to process each case was approximately 20 seconds to one minute depending on the size of the cylinder. This program is currently available.

[4] M. Goldstein and R. M. Thaler, "Recurrence techniques for the calculation of Bessel functions," Mathematical Tables and Other Aids to Computation, vol. 13, pp. 102–108; April, 1959.

[5] Wait, *op. cit.*, pp. 190–193.

[6] J. D. Kraus, "Antennas," McGraw-Hill Book Co., Inc., New York, N. Y., p. 358; 1950.

[7] C. M. Knop, "The Radiation Fields Produced by a Specified Tangential Electric Field Distribution Over an Aperture in a Perfectly Conducting Infinite Plane Coated with a Dielectric-Magnetic Slab," Res. Lab., Bendix Systems Div., Bendix Corp., Ann Arbor, Mich., Research Note No. 30; February 1, 1961.

Dielectric Lens for Second-Mode Spiral*

The operation of a double Archimedes spiral antenna in the second mode was described recently.[1] For a particular application its omnidirectional pattern and horizontal polarization were suitable, but the vertical beamwidth was too large. An attempt was made to reduce the vertical beamwidth while increasing the antenna gain.

It had been suggested[2] that one type of horizontally polarized omnidirectional antenna of small vertical beamwidth could be obtained by embedding a small horizontal-loop antenna in the center of a flat disc of a dielectric material. This same idea has been applied to the second-mode spiral with the results that are given here.

Our double spiral is similar to that of Donellan[1] except that the central feed section is a $\frac{1}{8}$-inch-thick sandwich transmission line between two ground planes instead of being microstrip. The outer diameter of the spiral is $1\frac{3}{4}$ inches, and the ground plane is $\frac{7}{8}$ inch in diameter. The whole spiral is embedded in a dielectric material with $\epsilon = 2.56$. The dielectric is one-half inch thick at the center and tapers to a line at 8 inches in diameter. The assembled view is given in Fig. 1 and the parts are shown in Fig. 2.

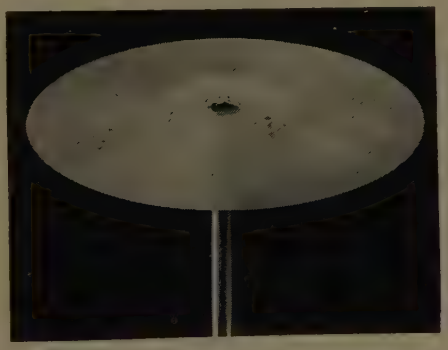

Fig. 1.

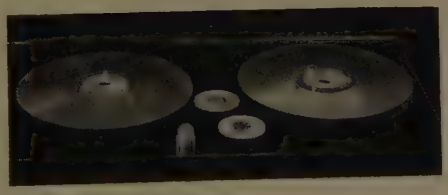

Fig. 2.

The vertical radiation pattern of the antenna has a beamwidth of about 50° over the frequency range 4000–5600 Mc (essentially the bandwidth of the basic spiral). A typical pattern is shown in Fig. 3. By the application of the lens, the vertical beamwidth has been reduced by a factor of about 3, with a consequent increase in gain of between 4 and 5 db.

* Received by the PGAP, May 3, 1961.

[1] J. R. Donellan, "Second-mode operation of the spiral antenna," IRE Trans. on Antennas and Propagation, vol. AP-8, p. 637; November, 1960.

[2] C. Ducot, "Omnidirectional dielectric aerials for ultra short waves," *Le Recherche Aeronaut.*, no. 9, pp. 33–36; May–June, 1949. Ministry of Supply, Royal Aircraft Establ., Farnborough, Eng., RAE Translation No. 546.

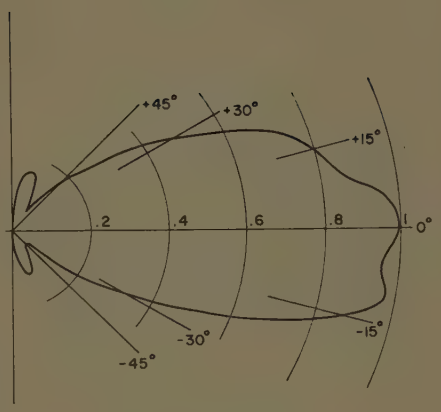

Fig. 3—Antenna power pattern—vertical plane, no reflector.

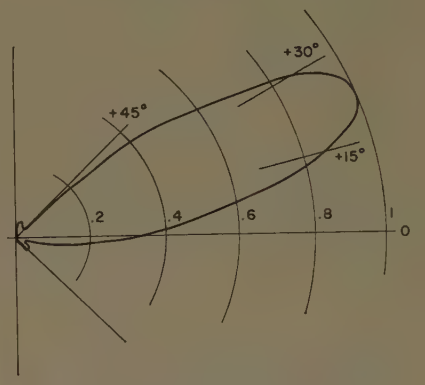

Fig. 4—Antenna power pattern—vertical plane, reflector spacing 1.25 inches.

Incidental to the development of this antenna, patterns were also taken of the double spiral with dielectric lens mounted at different spacings from a large ground plane. A spacing of $1\frac{1}{4}$ inches from the center of the spiral to the ground plane gave the pattern shown in Fig. 4.

J. H. Craven
Radio and Elec. Engrg. Div.
Natl. Research Council
Ottawa, Can.

Comments on "Diffraction of Scalar Waves by a Circular Aperture"*

The authors would like to call attention to an error in sign and an omission of a crucial sentence in the above paper.[1] Both the error and the omission occur in the uniqueness proof which appears on page S17, column 1. As the proof stands, the reader may be left with the impression that the uniqueness of the solution follows from the equation

$$\int_D (|\nabla v|^2 + k^2|v|^2)dV = 0.$$

* Received by the PGAP, May 4, 1961.

[1] J. Bazer and A. Brown, Inst. Math. Sci., New York University, N. Y., IRE Trans. on Antennas and Propagation, vol. AP-7, pp. S12–S20; December, 1959.

However, this equation is incorrect and should, in fact, be

$$\int_D (|\nabla v|^2 - k^2|v|^2)dV = 0.$$

To conclude uniqueness from this corrected equation, it is sufficient to require that k have a small positive imaginary part and a sentence to this effect should have been included at the beginning of the proof. For a uniqueness proof which does not make use of this added assumption, we refer the reader to the forthcoming report by Levine.[2]

J. Bazer
A. Brown
Inst. Math. Sci.
New York University, N. Y.

[2] L. Levine, "Some Uniqueness Theorems for the Reduced Wave Equation," Inst. Math. Sci., Div. of Electromagnetic Res., New York University, N. Y., Res. Rept. No. BR-33.

On the Determination of the Disk Temperature and the Flux Density of a Radio Source Using High-Gain Antennas*

Introduction

One of the major observational tasks in radio astronomy is the determination of the disk temperature and flux density of radio sources. A highly directive, pencil beam antenna is often used in the observations. The power output available from the antenna is used to calculate the disk temperature and flux density of radio sources. When the beamwidth of the antenna is very large compared with the angular extent of a radio source under observation, the disk temperature T_d and the flux density F of the radio source are related to the observed antenna temperature T_A by[1]

$$T_d = \frac{T_A}{\eta_r}\frac{\Omega_A}{\Omega_d} \tag{1}$$

and

$$F = \frac{2kT_A}{A_{eM}}, \tag{2}$$

where Ω_d is the solid angle subtended by the source, Ω_A is the antenna solid angle, k is Boltzmann's constant and A_{eM} is the maximum effective aperture of the antenna.

The antenna solid angle Ω_A is given by

$$\Omega_A = \iint_{4\pi} f(\theta, \Phi)d\Omega = \frac{4\pi}{D_M}, \tag{3}$$

where $f(\theta, \Phi)$ is the radiation power pattern of the antenna normalized with respect to the maximum radiation intensity. Thus, $f(\theta, \Phi) \leq 1$. D_M is the maximum directivity of the antenna. It is well known in antenna theory[2] that $A_{eM}\Omega_A = \eta_r\lambda^2$, where λ is the wavelength and η_r is the radiation efficiency of the antenna.

In order to detect weaker radio sources, an antenna of larger effective aperture must be used which also provides a narrower beam. As the beamwidth of the antenna becomes comparable with the diameter of the radio source, (1) and (2) are no longer valid. The purpose of this communication is to show the accurate relations which exist between the observed values and the physical quantities of the radio source. Conversion factors are derived for three typical antenna patterns. These are useful in calculating the disk temperature and flux density of extended radio sources from their observed antenna temperature.

Disk Temperature and Flux Density

Let us consider a highly directive, pencil beam antenna pointing at the center of a radio source. It is assumed that the radio source is a circular disk with an angular diameter θ_d, having a uniform brightness temperature T_d across the disk. The radiation is randomly polarized and the source is located against a background of zero brightness. The antenna temperature due to the radio source is then given by

$$T_A = \eta_r \frac{\iint_{\text{source}} T_d f(\theta, \Phi)d\Omega}{\iint_{4\pi} f(\theta, \Phi)d\Omega} = \eta_r T_d \Omega_d \frac{\iint_{\text{source}} f(\theta, \Phi)d\Omega}{\Omega_d \Omega_A},$$

or

$$T_d = \frac{T_A}{\eta_r}\frac{\Omega_A}{\Omega_d}\left[\frac{\Omega_d}{\iint_{\text{source}} f(\theta, \Phi)d\Omega}\right]. \tag{4}$$

The flux density of the radio source is given by

$$F = \iint_{\text{source}} \frac{2kT_d}{\lambda^2}d\Omega = \frac{2kT_d}{\lambda^2}\Omega_d.$$

Substituting (4), we have

$$F = \frac{2kT_A\Omega_A}{\lambda^2\eta_r}\frac{\Omega_d}{\iint_{\text{source}} f(\theta, \Phi)d\Omega} = \frac{2kT_A}{A_{eM}}\left[\frac{\Omega_d}{\iint_{\text{source}} f(\theta, \Phi)d\Omega}\right]. \tag{5}$$

Comparisons of (1) and (2) with (4) and (5) show that a correction factor inside the brackets in (4) and (5) is required to obtain the accurate disk temperature and flux density. This correction factor becomes unity when the source is so small that $f(\theta, \Phi) = 1$ across the source. Then (4) and (5) reduce to (1) and (2).

The correction factor may be readily computed if the antenna power pattern and the angular diameter of the radio source are known. In order to compute the correction factor, it is sufficient to know the antenna power pattern for the regions of the major lobe and its immediate vicinity.

Correction Factors

Three mathematical functions are selected for computing their correction factors. These functions represent typical shapes of the antenna major lobe encountered in practice. The correction factors are derived in terms of the ratio of the angular diameter θ_d of the source and the half-power beamwidth θ_H of the antenna. The antenna beams are assumed to have a circular symmetry with respect to its axis of maximum directivity.

Case 1: Let $f(\theta, \Phi) = e^{-(p\theta)^2}$, where p is a constant. If θ_H is the angle between the half-power points of the antenna main lobe, $f(\theta, \Phi) = \frac{1}{2}$ at $\theta = \theta_H/2$, from which $p = 2\sqrt{\ln 2}/\theta_H$. Thus we have

$$\iint_{\text{source}} f(\theta, \Phi)d\Omega = \int_0^{2\pi}\int_0^{\theta_d/2}[e^{-(p\theta)^2}]\sin\theta d\theta d\Phi = \frac{\pi}{p^2}[1 - e^{-(p\theta_d/2)^2}]$$

assuming $\sin\theta = \theta$ for small angles.

The correction factor K_1 becomes[3]

$$K_1 = \frac{\Omega_d}{\iint_{\text{source}} f(\theta, \Phi)d\Omega} = \frac{(\ln 2)(\theta_d/\theta_H)^2}{1 - [e^{-(\ln 2)(\theta_d/\theta_H)^2}]}.$$

Case 2: Let

$$f(\theta, \Phi) = \left[\frac{\sin(p\sin\theta)}{p\sin\theta}\right]^2,$$

where p is a constant. At $\theta = \theta_H/2$, $f(\theta, \Phi) = \frac{1}{2}$, from which we obtain $p = 1.392/\sin(\theta_H/2) = 2.784/\theta_H$ assuming $\sin\theta = \theta$ for small angles. Thus we have

$$\iint_{\text{source}} f(\theta, \Phi)d\Omega = \int_0^{2\pi}\int_0^{\theta_d/2}\left[\frac{\sin(p\sin\theta)}{p\sin\theta}\right]^2\sin\theta d\theta d\Phi.$$

Substituting $u = p\sin\theta$ and $\sin\theta = \theta$, the above integral becomes

$$\frac{2\pi}{p^2}\int_0^{p\theta_d/2}\frac{\sin^2 u}{u}du = \frac{\pi}{p^2}\int_0^{p\theta_d}\frac{1-\cos u}{u}du = \frac{\pi}{p^2}\text{Cin}(p\theta_d),$$

* Received by the PGAP, May 18, 1961. This work was carried out under Contract AF 19(604)-4079 of the AF Cambridge Res. Labs., Electronics Res. Directorate through The Ohio State University Res. Foundation.

[1] J. L. Pawsey and R. N. Bracewell, "Radio Astronomy," The Clarendon Press, Oxford, England; 1955.

[2] J. D. Kraus, "Antennas," McGraw-Hill Book Co., Inc., New York, N. Y.; 1950.

[3] H. C. Ko, "On the Analysis of Radio Astronomical Observations Made With High Resolution Radio Telescope Antennas," The Ohio State University, Columbus, Radio Observatory Rept. No. 21; February, 1961.

where Cin $(p\theta_d)$ is the modified cosine-integral whose values are tabulated in the literature.[2,4,5]

The correction factor K_2 becomes

$$K_2 = \frac{\Omega_d}{\pi[\text{Cin}\,(p\theta_d)]/p^2} = \frac{(2.784\theta_d/\theta_H)^2}{4\,\text{Cin}\,(2.784\theta_d/\theta_H)}.$$

Case 3: Let

$$f(\theta, \Phi) = \left[\frac{2J_1(p\sin\theta)}{p\sin\theta}\right]^2,$$

where J_1 is the Bessel function of the first kind of order one and p is a constant. At $\theta=\theta_H/2$, $f(\theta, \Phi)=\frac{1}{2}$, from which we obtain $p=1.616/\sin(\theta_H/2)=2\times1.616/\theta_H$. Substituting $u=p\sin\theta$ and $\sin\theta=\theta$, we have

$$\begin{aligned}\iint_{\text{source}} f(\theta,\Phi)d\Omega &= \frac{1}{p^2}\int_0^{2\pi}\int_0^{p\theta_d/2}\frac{4J_1^2(u)}{u^2}\,u\,du\,d\Phi \\ &= \frac{8\pi}{p^2}\int_0^{p\theta_d/2}\frac{J_1^2(u)}{u}\,du \\ &= \frac{4\pi}{p^2}\left[1 - J_1^2(p\theta_d/2) - J_0^2(p\theta_d/2)\right],\end{aligned}$$

where J_1 and J_0 are the Bessel functions of the first kind of order one and zero, respectively.

Thus the correction factor K_3 becomes

$$\begin{aligned}K_3 &= \frac{\Omega_d}{\iint_{\text{source}} f(\theta,\Phi)d\Omega} \\ &= \frac{\Omega_d p^2}{4\pi[1 - J_1^2(p\theta_d/2) - J_0^2(p\theta_d/2)]} \\ &= \frac{(1.616\theta_d/\theta_H)^2}{4[1 - J_1^2(1.616\,\theta_d/\theta_H) - J_0^2(1.616\,\theta_d/\theta_H)]}.\end{aligned}$$

It can be shown that when θ_d/θ_H becomes very small, all these factors reduce to unity as expected. The order of corrections required may be seen by the following numerical examples. Thus, for $\theta_d=\theta_H$, $K_1=1.39$, $K_2=1.38$, and $K_3=1.38$; for $\theta_d=2\theta_H$, $K_1=2.96$, $K_2=3.19$, and $K_3=3.15$.

H. C. Ko
Radio Observatory
Dept. of Elec. Engrg.
The Ohio State University
Columbus, Ohio

[4] C. T. Tai, "Table of Modified Cosine-Integral," Stanford Research Institute, Menlo Park, Calif., Tech. Rept. No. 15, SRI Project No. 188; January, 1951.

[5] "Tables of Generalized Sine- and Cosine-Integrals," Harvard University Press, Cambridge, Mass.; 1949.

Operators for Wave Equations in General Linear Media*

This communication presents some linear vector and scalar operators for electromagnetic waves in stationary, isotropic, and linear media. Commutability of two linear operators are discussed in deriving wave equations. These waves are directly obtained from a set of Maxwell's equations:

$$\text{curl}\,\bar{E}(q,t) = L_1\bar{H}(q,t), \quad (1)$$

$$\text{curl}\,\bar{H}(q,t) = \bar{J}(q,t) + L_2\bar{E}(q,t), \quad (2)$$

$$\bar{E}\cdot\text{grad}\,\epsilon(q,t) + \epsilon(q,t)\,\text{div}\,\bar{E} = \rho(q,t) \quad (3)$$

$$\bar{H}\cdot\text{grad}\,\mu(q,t) + \mu(q,t)\,\text{div}\,\bar{H} = 0, \quad (4)$$

where linear operators L_1 and L_2 stand for $-\mu_t - \mu(\partial/\partial t)$ and $\epsilon_t + \epsilon(\partial/\partial t)$; the subscript t stands for the partial derivative with respect to time; the symbol q designates the magnitude of a general position vector $\bar{q}$; the current density vector $\bar{J}$ can be either $\sigma(q,t)\bar{E}$ or $\rho\bar{v}(q,t)$, where σ is a linear isotropic conductivity and $\bar{v}$ is the electron velocity. The four equations above are combined to give

$$\begin{pmatrix} L_e & l_e \\ l_m & L_m \end{pmatrix}\begin{pmatrix}\bar{E}\\ \bar{H}\end{pmatrix} = \begin{pmatrix}\bar{S}_e\\ \bar{S}_m\end{pmatrix}, \quad (5)$$

where L_e is $\nabla^2 - (\epsilon_t\mu)_t - [\epsilon_t\mu + (\epsilon\mu)_t](\partial/\partial t) - \mu\epsilon(\partial^2/\partial t^2) + \nabla(\nabla\epsilon\cdot/\epsilon)$ and the last term produces $(\nabla\epsilon\cdot\bar{E}/\epsilon)$. l_e is used for $-(\nabla\mu\times)_t$, and source terms $\bar{S}_e$ and $\bar{S}_m$, respectively, represent $\text{grad}(\rho/\epsilon) + (\mu\bar{J})_t$ and $-\text{curl}\,\bar{J}$. Indicated interchanges between ϵ and μ provide L_m and l_m, such as $L_m = L_e(\epsilon\to\mu, \mu\to\epsilon)$ and $l_m = l_e(\mu\to\epsilon)$, respectively.

If may be hard, if not impossible, to obtain a matrix of inverse operators so that

$$\begin{pmatrix} N_e & n_e \\ n_m & N_m \end{pmatrix}\begin{pmatrix} L_e & l_e \\ l_m & L_m \end{pmatrix} = \begin{pmatrix} 1 & 0 \\ 0 & 1 \end{pmatrix}. \quad (6)$$

If this N matrix is determined, the premultiplication by N matrix gives $\bar{E}$ and $\bar{H}$ explicitly. This process has been shown later for restricted cases. In the past, the identical forms for linear scalar operators, L_e and L_m, have been widely treated for homogeneous media. However, other media can assume the identical form for L_e and L_m; this is realized if $(\epsilon/\mu)_t$ is zero.

The restricted class of source-free ($\rho=0$, $\bar{J}=0$) physical systems assumes the propagation of waves in the z direction, as along a cylinder parallel to the z axis having arbitrary cross-sectional geometry. Let the subscripts s and z stand for the transverse and z-direction parts. Eqs. (1) and (2) are rewritten as

$$\begin{pmatrix} L_1 & -\nabla_z\times \\ -\nabla_z\times & L_2 \end{pmatrix}\begin{pmatrix}\bar{H}_s\\ \bar{E}_s\end{pmatrix} = \nabla_s\times\begin{pmatrix}\bar{E}_z\\ \bar{H}_z\end{pmatrix}. \quad (7)$$

The problem here is how to derive linear vector wave equations for $\bar{H}_s(q,t)$ and $\bar{E}_s(q,t)$ when the z-direction field components are given in general forms as $\bar{E}_z(q,t)$ and $\bar{H}_z(q,t)$. This problem will be discussed for four medium types separately.

A homogeneous medium, i.e., ϵ and μ are independent of q and t

The inverse matrix is readily obtained, giving[1]

$$L_3\begin{pmatrix}\bar{E}_s\\ \bar{H}_s\end{pmatrix} = \begin{pmatrix} -\nabla_z\times\nabla_s\times & \mu\nabla_s\times\dfrac{\partial}{\partial t} \\ -\sigma\nabla_s\times\dfrac{\partial}{\partial t} & -\nabla_z\times\nabla_s\times \end{pmatrix}\begin{pmatrix}\bar{E}_z\\ \bar{H}_z\end{pmatrix}, \quad (8)$$

where L_3 is for $\{\nabla_z\times\nabla_z\times + \epsilon\mu(\partial^2/\partial t^2)\}$.

A Medium of $\epsilon(t)$ and $\mu(t)$

In this case the N matrix for (7) is obtained, resulting in

$$L_4\begin{pmatrix}\bar{E}_s\\ \bar{H}_s\end{pmatrix} = -\begin{pmatrix}\nabla_z\times\nabla_s\times & L_1\nabla_s\times \\ L^2\nabla_s\times & \nabla_z\nabla_s\times\end{pmatrix}\begin{pmatrix}\bar{E}_z\\ \bar{H}_z\end{pmatrix}, \quad (9)$$

where L_4 is for $\{\nabla_z\times\nabla_z\times - L_1L_2\}$.

A medium of $\epsilon(q)$ and $\mu(q)$, and a medium of $\epsilon(q,t)$ and $\mu(q,t)$

Equations similar to (8) and (9) are not easily derived. Because operators ∇_z and L_1 do not commute each other,

$$(L_1\nabla_z\times - \nabla_z\times L_1)\bar{H}_s = (\mu_z\bar{q}_0\times\bar{H}_s)_t, \quad (10)$$

where μ_z designates the partial derivative of μ with respect to z and $\bar{q}_0$ is a unit position vector. For this reason $\bar{E}_s(q,t)$ is not derivable from general functions, $\bar{E}_z(q,t)$ and $\bar{H}_z(q,t)$. Similarly, the noncommutability between ∇_z and L_2 is shown by

$$(L_2\nabla_z\times - \nabla_z\times L_2)\bar{E}_s = (\epsilon_z\bar{q}_0\times\bar{E}_s)_t. \quad (11)$$

An Exceptional Case of $\epsilon(q,t)$ and $\mu(q,t)$ for Harmonic Fields

If $\bar{E}_z$ and $\bar{H}_z$ vary with a specified time-dependence, *e.g.*, a harmonic variation of $\exp(j\omega t)$, the separability of field quantities between the time-dependent and the position-dependent parts requires that the time dependence of $\epsilon(q,t)$ and $\mu(q,t)$ be the same as the time-dependence of $\bar{E}_z$ and $\bar{H}_z$. Suppose $\bar{E}_z$ and $\bar{H}_z$ vary like $\exp(j\omega t)$; the inverted matrix of this exceptional case presents

$$\begin{pmatrix} L_5 & \bar{E}_s(q) \\ L_6 & \bar{H}_s(q)\end{pmatrix} = \begin{pmatrix} -\nabla_z\times\dfrac{1}{\mu}\nabla_s\times & -2j\omega\nabla_s\times \\ 2j\omega\nabla_s\times & \nabla_z\times\dfrac{1}{\epsilon}\nabla_s\times\end{pmatrix}\begin{pmatrix}\bar{E}_z(q)\\ \bar{H}_z(q)\end{pmatrix}, \quad (12)$$

where L_5 is for an operator $(\nabla_z\times 1/\mu\nabla_z\times - 4\omega^2\epsilon)$ and $L_6 = L_5(\epsilon\to\mu, \mu\to\epsilon)$.

The association between the commutator and the simultaneous measurements of two physical quantities corresponding to two linear operators has a sound basis for the quantum mechanics, whereas macroscopic experimental facts (Maxwell's equations) yield physical quantities which are always measured simultaneously. Eqs. (10) and (11) only say that if μ_z and ϵ_z are nonvanishing, linear wave equations for $\bar{E}_s$ and $\bar{H}_s$ are not simply related to $\bar{E}_z(q,t)$ and $\bar{H}_z(q,t)$, as in (8) and (9).

A few things taken for granted in homogeneous media are not directly applicable to other medium types. For instance, Ohm's law and Maxwell's equations are valid in isotropic linear media, yet the

[1] W. K. H. Panofsky and M. Phillips, "Classical Electricity and Magnetism," Addison-Wesley Publishing Co., Inc., Reading, Mass., pp. 192–193; 1955.

* Received by the PGAP, May 19, 1961.

relaxation time of the medium, which is a combined result of the law and equations, is subject to examination, as in:

$$(\partial\rho/\partial t) + (\sigma\rho/\epsilon) + \bar{D}\cdot\text{grad}\,(\sigma/\epsilon) = 0. \quad (13)$$

Hoffman[2] studied the case of $\sigma(q)$, $\epsilon(q)$, and a harmonic field for $\bar{E}$.

Phenomena of a nonlinear system include those of its linearized system as a special case. Physical facts encountered in electromagnetic wave propagation through media of $\epsilon(q, t)$ and $\mu(q, t)$ embrace many specialized cases, such as equations[3] of Mathieu for periodic variations of medium parameters and nonuniform transmission line problems.[4,5] Although Maxwell's equations may not be separable in general, those interested in problems of satellite communications and controlled inhomogeneous devices (like plasma-filled waveguides) would find useful aproximate numerical solutions. Vector linear operators presented here may also be of some use in these problems.

I. Sugai
ITT Federal Labs.
Nutley, N. J.

[2] W. C. Hoffman, "A possible mechanism for radiation and reflection from ionized gas clouds," Proc. IRE, (Correspondence), vol. 47, pp. 1274–1275; July, 1959.
[3] A. M. Markovkin, "Some properties of media with periodically time-varying parameters ϵ and μ," *Radiotekh. i Elektron*, vol. 4, pp. 785–791; May, 1959.
[4] H. Osterberg, "Propagation of plane electromagnetic waves in inhomogeneous media," *J. Opt. Soc. Am.*, vol. 48, pp. 513–521; August, 1958.
[5] L. M. Brekhovskikh, "Waves in Layered Media," Academic Press, Inc., New York, N. Y., pp. 168–189; 1960.

On the Transposed Radiating Systems in an Anisotropic Medium*

It has been known for some time[1,2] that the Lorentz form of reciprocal theorem, or the Rayleigh-Carson form of reciprocal theorem, can be generalized to two sets of fields in an anisotropic medium provided that one of the fields is defined in a medium which is transposed to the other. Let us consider, for example, the case of a magneto-ionic medium with a dielectric tensor medium represented by $[\epsilon]$. If we denote the two sets of fields by $(\boldsymbol{E}_1, \boldsymbol{H}_1)$ and $(\boldsymbol{E}_2, \boldsymbol{H}_2)$ and assume that they are harmonically varying with respect to time, then they satisfy

$$\nabla \times \boldsymbol{E}_1 = -j\omega\mu\boldsymbol{H}_1 \quad (1)$$

$$\nabla \times \boldsymbol{H}_1 = \boldsymbol{J}_1 + j\omega[\epsilon]\boldsymbol{E}_1 \quad (2)$$

and

$$\nabla \times \boldsymbol{E}_2 = -j\omega\mu\boldsymbol{H}_2 \quad (3)$$

$$\nabla \times \boldsymbol{H}_2 = \boldsymbol{J}_2 + j\omega[\bar{\epsilon}]\boldsymbol{E}_2, \quad (4)$$

where $[\bar{\epsilon}]$ denotes the transposed tensor of $[\epsilon]$. The currents $\boldsymbol{J}_1$ and $\boldsymbol{J}_2$ are the ones not of magneto-ionic origin. Applying the technique used in deriving the ordinary Lorentz theorem one finds that

$$\iiint_V \nabla\cdot[\boldsymbol{E}_1 \times \boldsymbol{H}_2 - \boldsymbol{E}_2 \times \boldsymbol{H}_1]dv = \iiint_V (\boldsymbol{J}_1\cdot\boldsymbol{E}_2 - \boldsymbol{J}_2\cdot\boldsymbol{E}_1)dv \quad (5)$$

or

$$\iint_S (\boldsymbol{E}_1 \times \boldsymbol{H}_2 - \boldsymbol{E}_2 \times \boldsymbol{H}_1)\cdot d\boldsymbol{S} = \iiint_V (\boldsymbol{J}_1\cdot\boldsymbol{E}_2 - \boldsymbol{J}_2\cdot\boldsymbol{E}_1)dv. \quad (6)$$

If in the region of integration $\boldsymbol{J}_1$ and $\boldsymbol{J}_2$ are zero then one obtains the Lorentz form of the reciprocal theorem, that is,

$$\iint_S (\boldsymbol{E}_1 \times \boldsymbol{H}_2 - \boldsymbol{E}_2 \times \boldsymbol{H}_1)\cdot d\boldsymbol{S} = 0. \quad (7)$$

If we let S go to infinity in (6), then the Rayleigh-Carson form of the reciprocal theorem is obtained, that is,

$$\iiint_V (\boldsymbol{J}_1\cdot\boldsymbol{E}_2 - \boldsymbol{J}_2\cdot\boldsymbol{E}_1)dv = 0. \quad (8)$$

Eq. (8), when interpreted in a more sophisticated manner, forms the basis of Rumsey's reaction concept.

We apply now (8) to the problem of relating the transmitting and the receiving properties of an antenna. Assume that the axis of the medium, corresponding to the direction of the stationary magnetic field B_0, is in the direction of the z-axis as shown in Fig. 1(a). Let $(\boldsymbol{E}_1, \boldsymbol{H}_1)$ be the field created by a transmitting antenna T_A with the receiving antenna R_B placed at the central region of the coordinate system. The receiving antenna R_B is represented schematically by three heavy lines. For field $(\boldsymbol{E}_2, \boldsymbol{H}_2)$, we interchange the role of transmitting and receiving as shown in Fig. 1(b). The stationary magnetic field is reversed so that the medium would correspond to the transposed tensor $[\bar{\epsilon}]$. Applying (8), one obtains

$$V_B I_B = V_A I_A. \quad (9)$$

Eq. (9) is the reciprocal relation as applied to two antennas in an anisotropic medium. So far we have merely repeated the expositions which are already known.

Now suppose that the B_0 field in Fig. 1(a) is a fixed field which could not be reversed, the system in Fig. 1(b) would then be impractical to reproduce. In order to remedy this difficulty a *transposed radiating system* can be formed that is shown in Fig. 1(c). The system is created by rotating the entire structure in Fig. 1(b), including the B_0 field, around the x-axis by 180°. Electromagnetically, the transposed radiating system has the same property as the one before rotation. The medium in Fig. 1(c), however, is not transposed. In fact it has the same characteristic as the one in Fig. 1(a) if $[\epsilon]$ is symmetric with respect to the x-y plane. The reciprocal relation as stated by (9) now can be interpreted as the one between Fig. 1(a) and 1(c). The above demonstration can be illustrated by a more complicated system shown in Fig. 2, where the circle represents a spherical body upon which an antenna B is mounted. It is obvious that the receiving property of B is now directly related to the transmitting property of the same antenna mounted at the opposite side of the sphere.

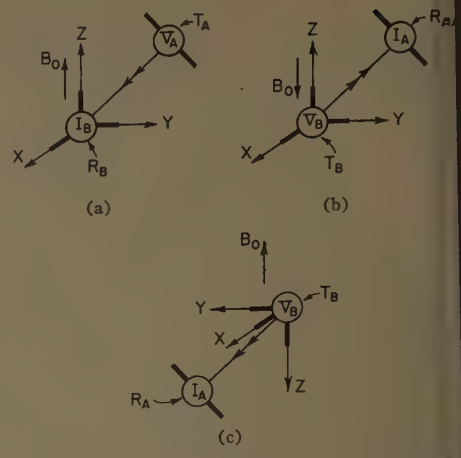

Fig. 1—(a) A transmitting antenna and a receiving antenna in an anisotropic medium. (b) The role of transmitting and receiving being changed as well as the direction of the B_0 field. (c) The transposed radiating system with the same B_0 field as in (a).

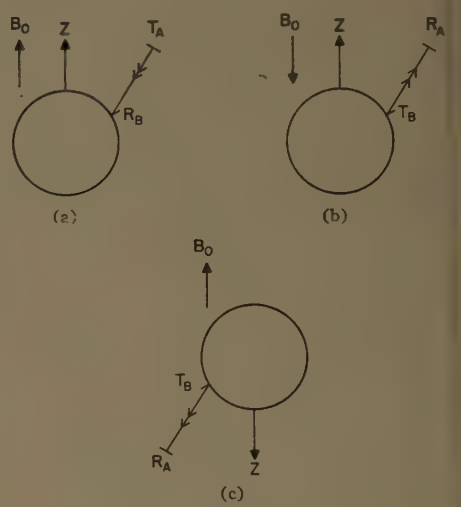

Fig. 2—A more complicated system where (a), (b), and (c) have the same significance as those in Fig. 1.

The application of the transposed radiating systems to some specific problems will be reported later in a subsequent paper.

The author acknowledges the valuable discussions which he had with Dr. R. G. Kouyoumjian and Dr. H. C. Ko on this problem.

Chen To Tai
Antenna Lab.
Dept. of Elec. Engrg.
The Ohio State University
Columbus, Ohio

* Received by the PGAP, May 29, 1961. This research was supported in part by Aeronautical Systems Div., Air Force Systems Command, Wright-Patterson Air Force Base, Ohio, under Contract No. AF 33 (616)6782, and The Ohio State University Research Foundation.
[1] M. H. Cohen, "Reaction Concept for Electromagnetic Field in an Anisotropic Medium," The Ohio State University, Columbus, Antenna Lab. Informal Rept., 1954; see also V. H. Rumsey, "Reaction concept in electromagnetic theory," *Phys. Rev.*, vol. 94, pp. 1483–1491; June, 1954.
[2] R. F. Harrington and A. T. Villeneuve, "Reciprocal Relationships for Gyrotropic Media," IRE Trans. on Microwave Theory and Techniques, vol. 6, pp. 308–310; July, 1958.

Contributors

Louis H. Bauer (S'52–A'54–M'61) was born in Jonesboro, Ill., on March 6, 1925. He received the B.S.E.E. degree in 1953 from Utah State University, Logan, and did graduate work at the University of Buffalo, Buffalo, N. Y., from 1953 to 1955.

L. H. Bauer

In 1953, he joined the Physics Department of Cornell Aeronautical Laboratory, Buffalo, where he remained for five years. For one year, he was concerned with the design of ground based computers for aircraft intercept systems. Simulation of intercept problems was an integral part of this effort. Also during his employment at Cornell Aeronautical Laboratory, he spent one and a half years developing and evaluating passive countermeasures for employment against tracking radars. For approximately six months he worked on the analysis of drone data link systems for battlefield surveillance. The last one and a half years at Cornell were spent on experimental and theoretical studies of tropospheric scattered signals. Included were variations in the spectra, amplitude distribution, and power level of the signal resulting from meteorological factors. In 1958 he joined the staff of the Research Division of Radiation Inc., Orlando, Fla., He has investigated the effects of atmospheric and ionospheric anomalies as they relate to range, pointing, and Doppler errors in guidance and tracking systems. Additional effort has been concerned with analysis of aircraft control in limited war and development of a system to maintain coherent signals between widely separated receiving sites. He is presently engaged in a program to determine the cause of missile induced ionization which is characteristic of missiles during transit through the ionosphere.

Mr. Bauer is a member of Phi Kappa Phi.

❖

Charles I. Beard (SM'56) was born in Ambridge, Pa., on November 30, 1916. He received the B.S.E.E. degree in 1938 from Carnegie Institute of Technology, Pittsburgh, Pa.

C. I. Beard

After a year at Westinghouse Research Laboratories on dielectrics, he spent two years at Massachusetts Institute of Technology, Cambridge, as a Teaching Fellow in physics. From 1941 to 1946, he served as a Signal Corps radar officer. He obtained the Ph.D. in physics from M.I.T., in 1948, where he performed his research in microwave spectroscopy. From 1948 to 1950, he was at the Field Research Laboratories of Magnolia Petroleum Company, where he conducted experiments in the propagation of electromagnetic waves in conducting media. In 1950, he joined the Applied Physics Laboratory of Johns Hopkins University and did research in microwave spectroscopy and in the propagation of microwaves over the ocean.

Since 1956, he has been at Sylvania Electronic Defense Laboratories, Mountain View, Calif., where he is a Senior Engineering Specialist. His research is in the scattering of microwaves, particularly scattering from random distributions.

Dr. Beard is a member of Commission II of URSI, the American Physical Society, Tau Beta Pi, and Sigma XI (RESA).

❖

Carrol W. Chapman was born in Austin, Tex., on July 22, 1933. He received the B.S.E.E. degree in 1959 from The University of Texas, Austin, Tex.

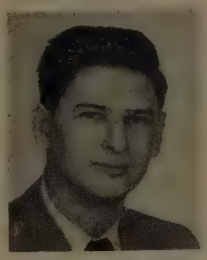

C. W. Chapman

He is presently employed as a research engineer at the Electrical Engineering Research Laboratory of The University of Texas while working toward the M.S. degree in electrical engineering.

❖

Kun-Mu Chen was born in Taipei, Formosa, on February 3, 1933. He received the B.S.E.E. degree from the National Taiwan University, Formosa. He received the M.S. and Ph.D. degrees in applied physics, from Harvard University, Cambridge, Mass., in 1958 and 1960, respectively. He was a C. T. Loo Fellow and a Gordon McKay Fellow at Harvard.

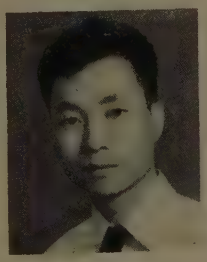

K.-M. Chen

In 1956–1957, he was a teaching assistant at the National Taiwan University. Since 1960, he has been a Research Associate at the Radiation Laboratory of the University of Michigan, Ann Arbor.

Dr. Chen is a member of Sigma Xi.

Robert S. Elliott (S'51–A'52–SM'54–F'61) was born in Brooklyn, N. Y., on March 9, 1921. After receiving the B.A. degree in English literature from Columbia University, New York, N. Y., he transferred to engineering and received the B.S.E.E. degree in 1943. After the war's end, he returned to graduate school, receiving the M.S. and Ph.D. degrees in 1952, both from the University of Illinois, Urbana.

R. S. Elliott

For three years during the war, he worked on the proximity fuze, radar, and the early Bumblebee missile at the Applied Physics Laboratory. Afterwards, while completing his graduate studies, he served as Assistant Professor and entered the antenna profession via summer employment at Sperry, New York, and North American, Los Angeles, Calif. Upon completion of the Ph.D., he served a year of active duty in the Navy during the Korean war, being associated with a missile program undertaken by the Naval Ordnance Laboratory. Three years of employment at Hughes Aircraft Company, Culver City, Calif., followed, during which time he was principally engaged in research on surface wave antennas.

In 1956, he left Hughes Aircraft Company to participate in the formation of Rantec Corporation, in Calabasas, Calif., serving as its first Vice President and Technical Director. In 1958, he returned to teaching and is now Professor of Engineering at the University of California, Los Angeles. He offers a four-semester graduate sequence in electromagnetic theory and its applications, and shares with Prof. Hershberger the responsibility of directing a plasma research program.

Dr. Elliott is a member of Sigma Xi and Tau Beta Pi.

❖

Warren L. Flock (S'42–A'44–M'54) was born in Kellogg, Idaho, on October 26, 1920. He received the B.S.E.E. degree from the University of Washington, Seattle, in 1942, the M.S.E.E. degree from the University of California, Berkeley, in 1948, and the Ph.D. degree in engineering from the University of California, Los Angeles, in 1960.

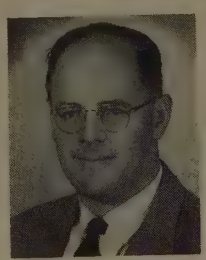

W. L. Flock

From 1942 to 1945, he was a staff

member of the Radiation Laboratory, Massachusetts Institute of Technology, Cambridge. In 1946–1947, he worked at the Sandia branch of the Los Alamos Scientific Laboratory, and in 1948–1950, he was a Research Assistant at the Institute of Geophysics, UCLA. From 1950 to 1960, he was with the Department of Engineering, UCLA, where he held the positions of Associate Research Engineer and Lecturer and worked in the areas of radiowave propagation, plasma studies, and natural resources. At present, he is an Associate Professor of geophysics at the Geophysical Institute, University of Alaska. He has also served as a consultant to the Rantec Corporation, Calabasas, Calif., and is at present a consultant to the RAND Corporation, Santa Monica, Calif.

Dr. Flock is a member of AIEE, Tau Beta Pi, Sigma Xi, and the American Geophysical Union.

❖

Richard E. Gray (A'26–VA'39–M'55) was born in Wynford, Dorset, England, on February 15, 1902, and graduated from Faraday House, an electrical engineering college in London, England.

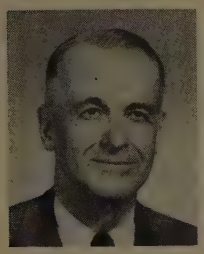

R. E. Gray

He joined Standard Telephones and Cables in 1924. From 1927 to 1929, he was with the laboratories of Le Material Telephonique in Paris, France. In 1940, he was on leave of absence to the Royal Aircraft Establishment at Farnborough, England, and in 1943 to the Telecommunication Research Establishment at Malvern, England. He has been with IT & T Laboratories, Inc., in Nutley, N. J., since 1946, where he is now a Senior Scientist engaged in radio propagation studies.

Mr. Gray is a member of the IEE.

❖

Peter W. Hannan (S'49–A'49–M'55–SM'59), for a photograph and biography, please see page 231 of the March, 1961, issue of these Transactions.

❖

Ronold W. P. King (A'30–SM'43–F'53), for a photograph and biography, please see page 232 of the March, 1961, issue of these Transactions.

❖

Louis A. Kurtz (S'44–A'46–M'55) was born in Long Beach, Calif., on March 13, 1923. He received the B.S.E.E. and M.S.E.E. degrees from the University of California, Berkeley, in 1945 and 1951, respectively.

From 1947 to 1949, he was at the University of California as a Teaching Assistant and Research Engineer, doing research on a U. S. Navy antenna project. In 1949, he joined the Dalmo Victor Company, San Carlos, Calif., as a Research Engineer in the design and development of radar antennas. From 1949 to 1956, he worked in the Microwave Laboratory Antenna Department of Hughes Research Laboratories, Culver City, Calif., where he was a research engineer in the design and development of two-dimensional slot array antennas.

L. A. Kurtz

In 1956, he joined the Rantec Corporation, Calabasas, Calif., where he is Manager of the Microwave Antenna Department. His current fields of activity include two-dimensional arrays of slots and dipoles with applications to search and tracking in the fields of telemetering, airborne fire control, reconnaissance and missile guidance, as well as tracking feeds for large reflector antennas for use in radio astronomy and space communications.

❖

Alfred H. LaGrone (M'48–SM'51–F'61) was born in Panola County, Tex., on September 25, 1912. He received the B.S., M.S., and Ph.D. degrees from The University of Texas, Austin.

A. H. LaGrone

From 1938 to 1942, he was a Distribution Engineer with the San Antonio Public Service Company, San Antonio, Tex. From 1942 to 1946, he was on active duty with the U. S. Navy. In 1946, he worked as Radio Engineer with the Electrical Engineering Research Laboratory at The University of Texas. In 1954, he joined the faculty of The University of Texas and is presently Professor of Electrical Engineering.

Dr. LaGrone received the Scott Helt Memorial award given by the IRE Professional Group on Broadcasting in 1959. He is a member of Sigma Xi, Tau Beta Pi and Eta Kappa Nu. He is a Registered Professional Engineer.

❖

Victor H. Rumsey (SM'50–F'60) Was born in Devizes, England, on November 22, 1919. He received the B.A. Cantab. degree with distinction in Part III of the Mathematical Tripos in 1941.

V. H. Rumsey

From 1941 to 1948, he was engaged in research on radar and atomic energy for the United Kingdom government, and from 1948 to 1954, he was head of the Ohio State University Antenna Laboratory, Columbus. He became a professor of electrical engineering at the University of Illinois, Urbana, in 1954, and in 1957 he joined the University of California, Berkeley, as a Professor of electrical engineering.

❖

Leonard S. Taylor (A'54–M'56) was born in New York, N. Y., on December 28, 1928. He received the A.B. degree in physics from Harvard University, Cambridge, Mass., in 1951, and the M.S. and Ph.D. degrees in physics from New Mexico State University, University Park, in 1956 and 1960, respectively.

L. S. Taylor

From 1951 to 1954, he was employed by the Raytheon Manufacturing Co., Bedford, Mass., where he worked in microwave component development and guided missile flight test analyses. From 1955 to 1959, he was at White Sands Missile Range where he was engaged in the development of special microwave telemetry equipment and communications system analysis.

During 1959 and 1960, he was a Research Fellow at New Mexico State University, investigating the index of refraction of ionized gases (his Ph.D. dissertation). Since August, 1960, he has been with the Advanced Aerodynamics Operation of the General Electric Space Sciences Laboratory, Valley Forge, Pa., where he has been engaged in research on the interaction of electromagnetic waves and plasmas.

Dr. Taylor is a member of the American Physical Society and Sigma Pi Sigma.

❖

Stanley L. Wehn (S'58) was born in Los Angeles, Calif., on August 11, 1930. He received the B.S.E. degree from the University of California, Los Angeles, in 1959, and is presently continuing his studies toward the M.S.E.E. degree.

S. L. Wehn

During the Korean conflict, he served in AC & W units in Korea and the United States. He joined the Rantec Corporation, Calabasas, Calif., in 1957, working first in the Antenna Group and later in the Ferrite and Microwave Component Development Group. He has made significant contributions to mutual-impedance effects in large scanning arrays, ferrite scanned two-dimensional slot arrays and antenna feed systems. In addition, he has contributed to the development of microwave components, including ferrite devices, for waveguide and coaxial lines.

Mr. Wehn is a member of Tau Beta Pi.

PAPERS TO BE PUBLISHED IN FUTURE ISSUES

Some Remarks on Green's Dyadic for Infinite Space ..... *J. Van Bladel*

A Reaction Theorem and Its Application to Antenna Impedance Calculations ..... *J. H. Richmond*

Scattering by a Periodically Apertured Conducting Screen ..... *R. B. Kieburtz and A. Ishimaru*

ELF Waves in the Presence of Exponential Ionospheric Conductivity Profiles ..... *J. Galejs*

Apparent Temperatures of Smooth and Rough Terrain ..... *S. Chen and W. H. Peake*

Single Channel Direction Finding in a Multicomponent Field ..... *W. M. Sherrill and D. N. Travers*

A Solution to the Frequency-Independent Antenna Problem ... *B. Ru-Shao Cheo, V. H. Rumsey and W. J. Welch*

Radiation from a Radial Electric Dipole near a Long Finite Circular Cylinder ..... *H. H. Kuehl*

The Radiation Fields from a Circumferential Slot on a Metal Cylinder Coated with a Lossy Dielectric .. *C. M. Knop*

Diffraction of a Plane Wave by a Perfectly Conducting Sphere with a Concentric Shell ..... *M. A. Plonus*

Array Factors with Nonuniform Spacing Parameter ..... *A. L. Maffett*

Linear Arrays with Variable Interelement Spacings ..... *M. G. Andreasen*

On the Mapping of Extended Sources with Nonlinear Correlation Antennas ... *C. J. Drane and G. B. Parrent, Jr.*

Antennas and Data Processing ..... *R. N. Bracewell*

Electromagnetic Radiation from a Cylindrically Capped Bi-Wedge ..... *M. A. Plonus*

INSTITUTIONAL LISTINGS

The IRE Professional Group on Antennas and Propagation is grateful for the assistance given by the firms listed below, and invites application for Institutional Listing from other firms interested in the field of Antennas and Propagation.

AERO GEO ASTRO CORP., 1200 Duke St., Alexandria, Va.
Space Instrumentation; Antennas; Transponders; Command Receivers; Augmenters; Telemetry; Radar

ANDREW CORPORATION, P.O. Box 807, Chicago 42, Ill.
Antennas, Antenna Systems, Transmission Lines, Development and Production

THE BOEING COMPANY, Antenna Dept., P. O. Box 3976, Seattle 24, Wash.
Development, Fabrication & Installation; Precision Airborne & Ground Antennas & Systems

DEVELOPMENTAL ENGINEERING CORP., Leesburg, Va.; Boston, Mass.; Boulder, Colo.; Washington, D.C
Antenna Research, Design & Evaluation-Propagation Studies & Communications Systems Engineering

DORNE & MARGOLIN, INC., 29 New York Ave., Westbury, L. I., N. Y.
Research, Development and Manufacture—Antenna and Microwave Technology

FXR, Inc., 25–26 50th St., Woodside 77, N. Y.
Precision Microwave Test Equip., High Power Microwave Electronics, Microwave Components & Instrumentatio

JANSKY & BAILEY, A Div. of Atlantic Research Corp., Shirley Highway & Edsall Rd., Alexandria, Va.
Complete Engineering Services for Antennas and Propagation Programs

SCIENTIFIC-ATLANTA, INC., 2162 Piedmont Rd., N.E., Atlanta 9, Ga.
Antenna Pattern Ranges, R & D, RF Components, Telemetry Tracking Systems, Fourier Computer & Computati

TECHNICAL APPLIANCE CORP., 1 Taco St., Sherburne, N. Y.
Des., Dev., & Mfg.: Antennas & Antenna Systems for Communications, Telemetry, & Tracking

WHEELER LABORATORIES, INC., Great Neck, N. Y.; Antenna Lab., Smithtown, N. Y.
Consulting Services, Research and Development, Microwave Antennas and Waveguide Components

WEINSCHEL ENGINEERING COMPANY, INC., Kensington, Md.
Antenna Pattern Receivers; Bolometer Amplifiers; Microwave Sources; Insertion Loss Measuring Systems

The charge for Institutional Listing is $50 for one issue or $200 for six consecutive issues (one year). Application may be made to the Professional Groups Secretary, The Institute of Radio Engineers, Inc., 1 East 79 Street, New York 21, N. Y.